

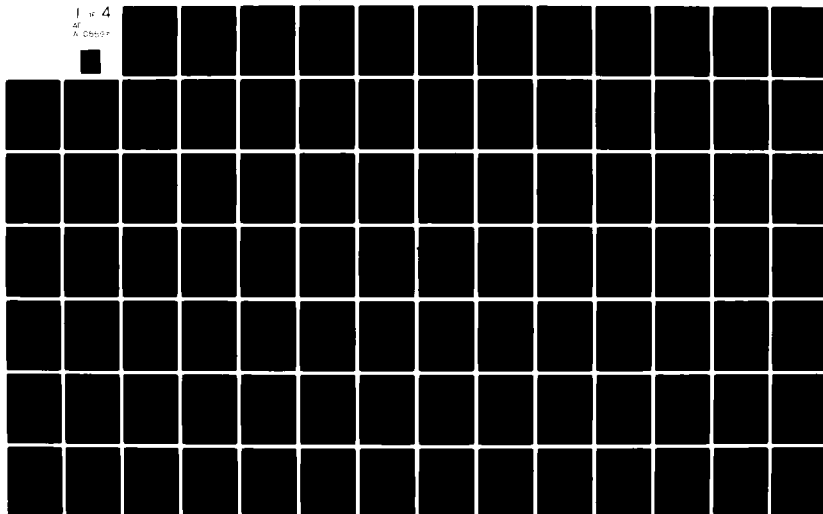
AD-A105 593

PENNSYLVANIA STATE UNIV UNIVERSITY PARK APPLIED RESE--ETC F/6 20/1  
A SCATTERING FUNCTION APPROACH TO UNDERWATER ACOUSTIC DETECTION--ETC(U)  
OCT 81 L J ZIOMEK  
N00024-79-C-6043  
ARL/PSU/TN-81-144 NL

UNCLASSIFIED

1 of 4

AD  
A000000



AD A105593

A SCATTERING FUNCTION APPROACH TO UNDERWATER ACOUSTIC  
DETECTION AND SIGNAL DESIGN

Lawrence J. Ziomek

Technical Memorandum  
File No. TM 81-144  
October 7, 1981  
Contract No. N00024-79-C-6043 ✓

Copy No. 6

The Pennsylvania State University  
Intercollege Research Programs and Facilities  
APPLIED RESEARCH LABORATORY  
Post Office Box 30  
State College, PA 16801

APPROVED FOR PUBLIC RELEASE  
DISTRIBUTION UNLIMITED

NAVY DEPARTMENT

NAVAL SEA SYSTEMS COMMAND

DTIC FILE COPY

DTIC

A

UNCLASSIFIED

SECURITY CLASSIFICATION OF THIS PAGE (When Data Entered)

REPORT DOCUMENTATION PAGE		READ INSTRUCTIONS BEFORE COMPLETING FORM
1. REPORT NUMBER 81-144	2. GOVT ACCESSION NO. AD-A105593	3. RECIPIENT'S CATALOG NUMBER
4. TITLE (and Subtitle) A Scattering Function Approach to Underwater Acoustic Detection and Signal Design.		5. TYPE OF REPORT & PERIOD COVERED Ph.D. Thesis, November 1981
7. AUTHOR(s) Lawrence J. Ziomek		6. PERFORMING ORG. REPORT NUMBER 81-144
9. PERFORMING ORGANIZATION NAME AND ADDRESS The Pennsylvania State University Applied Research Laboratory, P.O. Box 30		8. CONTRACT OR GRANT NUMBER(s) N00024-79-C-6043
11. CONTROLLING OFFICE NAME AND ADDRESS Naval Sea Systems Command Department of the Navy Washington, DC 20362		10. PROGRAM ELEMENT, PROJECT, TASK AREA & WORK UNIT NUMBERS
14. MONITORING AGENCY NAME & ADDRESS (if different from Controlling Office)		12. REPORT DATE 7 October 1981
15. SECURITY CLASS. (of this report) Unclassified, Unlimited		13. NUMBER OF PAGES 286 pages & figures
16. DISTRIBUTION STATEMENT (of this Report) Approved for public release, distribution unlimited, per NSSC (Naval Sea Systems Command), 8/7/81		15a. DECLASSIFICATION/DOWNGRADING SCHEDULE
17. DISTRIBUTION STATEMENT (of the abstract entered in Block 20, if different from Report)		
18. SUPPLEMENTARY NOTES		
19. KEY WORDS (Continue on reverse side if necessary and identify by block number) underwater, acoustic, detection, signal, interference, thesis		
20. ABSTRACT (Continue on reverse side if necessary and identify by block number) In this dissertation, the design of transmit and processing waveforms is used to maximize the signal-to-interference ratio (SIR) to improve the detectability of a doubly spread target return in the presence of volume and/or surface reverberation plus white Gaussian noise. The SIR is dependent upon target and reverberation scattering functions and the cross-ambiguity function of the transmit and processing waveforms. Volume reverberation, target, and surface reverberation scattering functions are derived. Volume reverberation is modelled		

DD FORM 1 JAN 73 1473

EDITION OF 1 NOV 65 IS OBSOLETE

UNCLASSIFIED

SECURITY CLASSIFICATION OF THIS PAGE (When Data Entered)

UNCLASSIFIED

SECURITY CLASSIFICATION OF THIS PAGE(When Data Entered)

as the spatially uncorrelated scattered field from randomly distributed point scatterers in deterministic plus random translational motion. A single scattering approximation is used and general, frequency dependent transmit and receive arrays are included in all derivations. The doubly spread target is modelled as a linear array of discrete highlights in deterministic translational motion. A target scattering function is obtained from the general bistatic volume reverberation scattering function by appropriately specifying the volume density function of the discrete point scatterers for a monostatic geometry. A surface reverberation scattering function dependent upon the directional wave number spectrum is derived for a bistatic geometry using a generalized Kirchhoff approach. This approach uses a Fresnel corrected Kirchhoff integral and the Rayleigh hypothesis that a scattered field can be represented as a sum of plane waves travelling in different directions. No small slope approximation is made. All three scattering functions predict spreading in both time delay and frequency.

Three optimization problems concerning the maximization of the SIR for a doubly spread target are formulated. Each problem is expressed in terms of an equivalent nonlinear programming problem defined on a real space by restricting the transmit and processing waveforms to be complex weighted, uniformly spaced pulse trains. Each subpulse can be different in shape and can occupy the entire interpulse spacing interval. The first two optimization problems involve maximization with respect to the complex weights. The third problem involves maximization with respect to the subpulse parameters (for example, frequency deviation, swept bandwidth, etc.). Of the three optimization problems, maximization with respect to the subpulse parameters is the most interesting and significant one. However, even with several simplifying assumptions, it is shown to be a difficult nonlinear programming problem. No numerical results are obtained for the various optimization problems.

A

UNCLASSIFIED

SECURITY CLASSIFICATION OF THIS PAGE(When Data Entered)



## ABSTRACT

In this dissertation, the design of transmit and processing waveforms is used to maximize the signal-to-interference ratio (SIR) to improve the detectability of a doubly spread target return in the presence of volume and/or surface reverberation plus white Gaussian noise. The SIR is dependent upon target and reverberation scattering functions and the cross-ambiguity function of the transmit and processing waveforms. Volume reverberation, target, and surface reverberation scattering functions are derived. Volume reverberation is modelled as the spatially uncorrelated scattered field from randomly distributed point scatterers in deterministic plus random translational motion. A single scattering approximation is used and general, frequency dependent transmit and receive arrays are included in all derivations. The doubly spread target is modelled as a linear array of discrete highlights in deterministic translational motion. A target scattering function is obtained from the general bistatic volume reverberation scattering function by appropriately specifying the volume density function of the discrete point scatterers for a monostatic geometry. A surface reverberation scattering function dependent upon the directional wave number spectrum is derived for a bistatic geometry using a generalized Kirchhoff approach. This approach uses a Fresnel corrected Kirchhoff integral and the Rayleigh hypothesis that a scattered field can be represented as a sum of plane waves travelling in different directions. No small slope approximation is made. All three scattering functions predict spreading in both time delay and frequency.

Three optimization problems concerning the maximization of the SIR for a doubly spread target are formulated. Each problem is expressed in terms of an equivalent nonlinear programming problem defined on a real space by restricting the transmit and processing waveforms to be complex weighted, uniformly spaced pulse trains. Each subpulse can be different in shape and can occupy the entire interpulse spacing interval. The first two optimization problems involve maximization with respect to the complex weights. The third problem involves maximization with respect to the subpulse parameters (for example, frequency deviation, swept bandwidth, etc.). Of the three optimization problems, maximization with respect to the subpulse parameters is the most interesting and significant one. However, even with several simplifying assumptions, it is shown to be a difficult nonlinear programming problem. No numerical results are obtained for the various optimization problems.

## TABLE OF CONTENTS

	<u>Page</u>
ABSTRACT . . . . .	iii
LIST OF TABLES . . . . .	viii
LIST OF FIGURES . . . . .	ix
ACKNOWLEDGMENTS . . . . .	xi
Chapter	
I. INTRODUCTION . . . . .	1
II. FUNDAMENTALS OF LINEAR TIME-VARYING FILTERS . . . . .	10
2.1 Introduction . . . . .	10
2.2 Linear Time-Varying Deterministic Filters . . . . .	11
2.2.1 Impulse response and transfer functions . . . . .	11
2.2.2 Additional filter functions . . . . .	17
2.2.3 Output power spectrum . . . . .	21
2.3 Linear Time-Varying Random Filters . . . . .	25
2.3.1 Filter autocorrelation functions . . . . .	25
2.3.2 Uncorrelated spreading - the scattering function . . . . .	31
2.3.3 The scattering function and its Fourier transforms . . . . .	37
2.3.4 Input-output relations - output power spectral density . . . . .	41
2.3.5 Channel characterization via the scattering function . . . . .	45
III. DETECTION IN THE PRESENCE OF REVERBERATION . . . . .	50
3.1 Introduction . . . . .	50
3.2 A Binary Hypothesis Testing Problem . . . . .	51
3.2.1 Complex envelope notation . . . . .	51
3.2.2 The signal-to-interference ratio for a doubly spread target . . . . .	58
3.2.3 The signal-to-interference ratio for a slowly fluctuating point target . . . . .	64
3.3 Optimum and Sub-Optimum Receivers . . . . .	66
3.3.1 Optimum receivers for detecting a slowly fluctuating point target . . . . .	66
3.3.2 Sub-optimum receiver for detecting a slowly fluctuating point target . . . . .	71
3.3.3 Sub-optimum receiver for detecting a doubly spread target . . . . .	73

## TABLE OF CONTENTS (continued)

<u>Chapter</u>	<u>Page</u>
IV. VOLUME REVERBERATION AND TARGET SCATTERING FUNCTIONS . .	75
4.1 Introduction . . . . .	75
4.2 Volume Reverberation Scattering Function . . . . .	76
4.3 Target Scattering Function . . . . .	101
4.4 Example Problem Calculations . . . . .	107
4.4.1 Volume reverberation scattering function . .	107
4.4.2 Target scattering function . . . . .	120
V. SURFACE REVERBERATION SCATTERING FUNCTION . . . . .	125
5.1 Introduction . . . . .	125
5.2 Surface Reverberation Transfer Function . . . . .	126
5.2.1 Background discussion . . . . .	126
5.2.2 Analysis . . . . .	137
5.3 Second Order Functions . . . . .	179
5.3.1 Two-frequency correlation function . . . . .	179
5.3.2 Surface reverberation scattering function .	182
VI. MAXIMIZATION OF THE SIGNAL-TO-INTERFERENCE RATIO FOR A DOUBLY SPREAD TARGET: PROBLEMS IN NONLINEAR PROGRAMMING . . . . .	191
6.1 Introduction . . . . .	191
6.2 Mathematical Preliminaries - Problem Formulation .	202
6.3 Maximization of the SIR for a Slowly Fluctuating Point Target . . . . .	211
6.3.1 The optimum processing waveform for a given transmit signal . . . . .	211
6.3.2 The optimum transmit-processing waveform pair - an iterative technique . . . . .	214
6.4 Maximization of the SIR for a Doubly Spread Target . . . . .	221
6.4.1 The optimum processing waveform for a given transmit signal . . . . .	221
6.4.2 The optimum transmit-processing waveform pair . . . . .	228
6.4.3 Maximization of the SIR for a doubly spread target with respect to the subpulse parameters . . . . .	233
VII. SUMMARY AND CONCLUSIONS . . . . .	241
VIII. RECOMMENDATIONS FOR FUTURE RESEARCH . . . . .	251

## TABLE OF CONTENTS (continued)

	<u>Page</u>
REFERENCES . . . . .	254
APPENDIX A: Derivation of the Return Signal from a Slowly Fluctuating Point Target . . . . .	260
APPENDIX B: Derivation of the Probability Density Function of the Random Doppler Shift $\phi_{\text{RND}}$ . . . . .	267
APPENDIX C: Derivation of the Normal Partial Derivative of the Total Acoustic Pressure Field on the Ocean Surface . . . . .	270
APPENDIX D: Functional Dependence of the Transmit and Receive Directivity Functions and Vectors $\vec{a}(x,y)$ and $\vec{b}(x,y)$ on the $(x,y)$ Coordinates . .	275
APPENDIX E: The Relationship Between $R_F(\Delta x, \Delta y, \Delta t')$ , $R_F(\Delta x, \Delta y, \Delta t)$ and the Directional Wave Number Spectrum of the Ocean Surface . . . . .	283

## LIST OF TABLES

<u>Table</u>	<u>Page</u>
1. Normalized Target Scattering Function . . . . .	122
2. Round-Trip Time Delay Calculations . . . . .	123
3. Values of the Binomial Expansion Factor $ b_T $ for Different Combinations of Beamwidth $\epsilon$ and Grazing Angle $\gamma$ . . . . .	154

## LIST OF FIGURES

<u>Figure</u>	<u>Page</u>
1. Linear time-varying filter . . . . .	12
2. Two different representations of linear, time-varying filters: (a) the more common representation, and (b) an alternate representation . . . . .	18
3. Interdependence amongst the four filter functions that characterize linear, time-varying channels . . . . .	22
4. Interdependence amongst the four filter autocorrelation functions that characterize linear, time-varying, random channels . . . . .	32
5. The scattering function and its Fourier transforms . . . . .	40
6. Receiver structure for processing $\tilde{r}(t)$ . . . . .	60
7. Geometry for calculation of scattered field from a single particle undergoing translational motion . . . . .	78
8. Scatter in the direction $\hat{n}_R$ from several moving particles occupying an elemental volume $dV$ when insonified in the direction $\hat{n}_T$ . . . . .	84
9. Orientation of line target with respect to the transmit and receive arrays . . . . .	103
10a. Probability density function of the random Doppler shift for a monostatic transmit/receive array geometry, $\sigma = 0.1$ m/sec . . . . .	110
10b. Probability density function of the random Doppler shift for a monostatic transmit/receive array geometry, $\sigma = 1.0$ m/sec . . . . .	111
11. Normalized Doppler profile of volume reverberation scattering function, $\theta_o = 0^\circ$ , $\psi_o = 0^\circ$ . . . . .	113
12. Normalized Doppler profile of volume reverberation scattering function, $\theta_o = 30^\circ$ , $\psi_o = 0^\circ$ . . . . .	114
13. Normalized Doppler profile of volume reverberation scattering function, $\theta_o = 45^\circ$ , $\psi_o = 0^\circ$ . . . . .	115

## LIST OF FIGURES (continued)

<u>Figure</u>		<u>Page</u>
14a.	Normalized Doppler profile of volume reverberation scattering function. Relative deterministic motion only ( $\theta_o = 45^\circ$ , $\psi_o = 0^\circ$ ) . . . . .	116
14b.	Normalized Doppler profile of volume reverberation scattering function. Relative deterministic motion only ( $\theta_o = 45^\circ$ , $\psi_o = 0^\circ$ ) . . . . .	117
15a.	Normalized Doppler profile of volume reverberation scattering function. Relative deterministic plus random motion ( $\theta_o = 45^\circ$ , $\psi_o = 0^\circ$ ) . . . . .	118
15b.	Normalized Doppler profile of volume reverberation scattering function. Relative deterministic plus random motion ( $\theta_o = 45^\circ$ , $\psi_o = 0^\circ$ ) . . . . .	119
16.	Transmit array T, receive array R, and ocean medium being enclosed by the closed surface $S' = S + S''$ . . . . .	127
17.	Bistatic geometry for surface-scatter communication channel . . . . .	131
18.	Geometry for example calculation of the radius of curvature criterion and the shadow prevention criterion in the incident direction. By definition, the angles $\varphi$ , $\theta_i$ , and $\beta$ are all positive . . . . .	141
19.	Geometry for example calculation of the shadow prevention criterion in the scatter direction. By definition, the angles $\varphi$ and $\theta_s$ are positive, while the angle $\beta'$ is negative . . . . .	147
20.	Spherical angles $\theta_1$ , $\psi_1$ and $\theta_2$ , $\psi_2$ of the unit vectors $\hat{r}_1$ and $\hat{r}_2$ , respectively . . . . .	151
21.	Geometry for the calculation of the binomial expansion criterion. The angle $\epsilon$ is the beamwidth of the directivity pattern and $\gamma$ is the grazing angle . . . . .	153
C1.	Scatter geometry for locally plane surface area element $dS$ . . . . .	272
D1.	Orientation of the $X_T Y_T Z_T$ coordinate system with respect to the $XYZ$ reference coordinate system . . . . .	276
D2.	Orientation of the $X_B Y_B Z_B$ coordinate system with respect to the $XYZ$ reference coordinate system . . . . .	280



#### ACKNOWLEDGMENTS

I would like to express my gratitude to my thesis adviser, Dr. Leon H. Sibul, for introducing me to the very interesting topic of scattering functions. I would also like to thank my committee members, Dr. John L. Brown, Jr., Dr. Suzanne T. McDaniel, and Dr. Richard E. Zindler, for their help in ensuring a successful completion of this dissertation. Dr. Brown's sequence of electrical engineering courses proved invaluable. The helpful discussions, advice, and support from Drs. McDaniel and Zindler are very much appreciated. In addition, I especially acknowledge the contributions of one of my original committee members, the late Dr. Francis H. Fenlon, who died shortly before the completion of this dissertation. His advice, support, and friendship will be greatly missed.

And finally, Mrs. Dorothy Tindal's expert typing is sincerely appreciated.

This research was supported by the Applied Research Laboratory of The Pennsylvania State University under contract with the Naval Sea Systems Command.

## CHAPTER I

### INTRODUCTION

The purpose of this introductory chapter is threefold: (1) to state the problem considered in this dissertation, (2) to highlight the contents and assumptions in each chapter, and (3) to summarize the significance of the results contained herein. Since this dissertation includes several unique (although related) topics, detailed discussion of relevant literature is reserved to the individual chapters themselves.

This dissertation is concerned with the detection of a doubly spread target return in the presence of volume and/or surface reverberation plus white Gaussian noise. The particular approach taken is to maximize the signal-to-interference ratio (SIR) via design of the transmit and processing waveforms. Previous research efforts have been devoted mainly to either the slowly fluctuating point target or singly spread target problems. The basic philosophy adopted is to treat both the ocean medium and the target as linear, time-varying, random filters.

Accordingly, Chapter II discusses the fundamentals of linear, time-varying, deterministic and random filters. Throughout this dissertation, the terms filter, system, and channel are used interchangeably. Four system functions which are used to characterize linear, time-varying filters are introduced. These functions are (1) the time-varying impulse response, (2) the time-varying frequency response or transfer function, (3) the spreading function, and (4)

the bi-frequency function. It is shown that these four system functions and their corresponding autocorrelation functions are related to one another via Fourier transformations. In addition to various input-output relationships, expressions for the output power spectrum for both deterministic and random systems are derived. The important channel property of uncorrelated spreading is also discussed. The discussion on uncorrelated spreading introduces the concepts of the wide-sense stationary uncorrelated spreading (WSSUS) communication channel and the scattering function along with its various Fourier transforms. The scattering function determines the average amount of spread that an input signal's power will undergo as a function of round-trip time delay (range) and frequency.

A brief discussion of two different ways of characterizing a time-varying channel via its scattering function concludes Chapter II. The first method involves interpreting the scattering function as a joint density function since it is real, non-negative, and can be normalized to integrate to unity. Thus, first and second order moments of the round-trip time delay (range) and frequency spread can be computed. The second method is concerned with the finite extent of the scattering function in the range-frequency plane. As a result of this approach, the concepts of an underspread and an overspread channel are defined. Criteria for avoiding spreading in range and/or frequency are formulated in terms of the duration and bandwidth of the transmit signal and the extent of the scattering function in the range-frequency plane.

Chapter III introduces the problem of detecting a doubly spread target return in the presence of reverberation and noise. A

doubly spread target return is one which exhibits a spread in both round-trip time delay and Doppler shift values. Chapter III begins with a brief discussion of the complex envelope notation for bandpass signals since the binary hypothesis testing problem is formulated in terms of the complex envelopes of the target, reverberation, and noise signals. Both the target and reverberation returns are modelled as the outputs from linear, time-varying, random filters which are assumed to be WSSUS communication channels.

The particular receiver structure used is a correlator followed by a magnitude squared operation. The magnitude squared output from the correlator is tested against a threshold determined from a probability of false alarm constraint in a Neyman-Pearson test.

Having specified both the binary hypothesis testing problem and the receiver, the signal-to-interference ratio (SIR) for a doubly spread target is derived. It is shown to be dependent upon the target and reverberation scattering functions and the cross-ambiguity function of the transmit signal and the processing waveform. It is also demonstrated that the more familiar SIR expression for a slowly fluctuating point target can be obtained from the general SIR expression for a doubly spread target.

The final discussion in Chapter III is devoted to the question of receiver optimality, i.e., when is our choice of receiver an optimum or sub-optimum receiver for detecting either a slowly fluctuating point target or a doubly spread target. The discussion on optimality introduces the performance measure  $\Delta$  which is shown to be equal to the SIR. The performance measure determines the probability of detection

for a given probability of false alarm in the important case of Gaussian statistics. In the case of Gaussian statistics, maximizing  $\Delta$  is equivalent to maximizing the probability of detection and it is noted that this can be achieved by proper signal design.

In order to maximize the SIR for a doubly spread target via signal design, one must be able to specify both the target and reverberation scattering functions. In general, the reverberation return is a composite of volume, surface, and bottom reverberation returns. However, only volume and surface reverberation are considered.

In Chapter IV, both a volume reverberation and a target scattering function are derived. In the past, assumed functional forms for the reverberation (clutter) scattering function were used in order to calculate the SIR.

Volume reverberation is modelled as the scattered acoustic pressure field from randomly distributed discrete point scatterers in deterministic plus random translational motion. The point scatterers are distributed in space according to an arbitrary volume density function with dimensions of number of scatterers per unit volume.

The two-frequency correlation function representing the volume reverberation communication channel is derived for a bistatic transmit/receive planar array geometry. A single scattering approximation is used and frequency dependent attenuation of sound pressure amplitude due to absorption is included. The scattered fields from different regions within the scattering volume are assumed to be uncorrelated. The relationships between the two-frequency correlation function, coherence time, coherence bandwidth, and frequency and time spreading

are also discussed. The volume reverberation scattering function is obtained from the two-frequency correlation function via a two-dimensional Fourier transformation. The volume reverberation scattering function derived in Chapter IV is shown to include explicitly all the important system functions and physical parameters as opposed to having them lumped together and accounted for by a single random variable as was common practice in the past. A probability density function of random Doppler shift due to the random motion of the scatterers is also derived. In addition, the average received energy from volume reverberation is computed from the volume reverberation scattering function. Using several simplifying assumptions, it is shown to reduce to the sonar equation for reverberation level.

The doubly spread target is modelled as a linear array of discrete highlights in deterministic translational motion. The target scattering function is obtained from the monostatic form of the volume reverberation scattering function by appropriately specifying the volume density function of the highlights.

Computer simulation results for both the volume reverberation and target scattering functions are presented as examples involving a monostatic transmit/receive array geometry. Computer plots of the probability density function of the random Doppler shift are also presented for a monostatic geometry as a function of the standard deviation of the random motion of the scatterers.

Chapter V is devoted to the derivation of a surface reverberation scattering function. The underwater acoustic propagation path between

transmit and receive arrays via the surface of the ocean is treated as a linear, time-varying, random WSSUS communication channel. The random, time-varying surface reverberation transfer function is derived for a general bistatic geometry using a generalized Kirchhoff approach. The generalized Kirchhoff approach uses a Fresnel corrected Kirchhoff integral and the Rayleigh hypothesis that the scattered acoustic pressure field can be represented as a sum of plane waves travelling in many different directions. Also, no small slope approximation is made.

The transfer function obtained in Chapter V is shown to be greater in magnitude than those transfer functions previously derived by the classical Kirchhoff approach, especially for the specular and backscatter geometries. This is encouraging since results based upon a classical Kirchhoff approach have predicted values for the scattering coefficient that were smaller than experimental values. In addition, a Gaussian functional form for the projected transmit beam pattern was commonly assumed for mathematical convenience. The fact that the actual projected transmit and receive beam patterns are not likely to be Gaussian when doing experimental work leads to a major source of error when comparing theoretical predictions with experimental results. As a result, the transmit and receive directivity functions included in the derivation of the transfer function in Chapter V are kept as general, frequency dependent expressions. The necessary transformation equations which will project both directivity functions exactly are provided.

Two second order functions are derived from the surface reverberation transfer function by assuming that the randomly rough, time-

varying ocean surface is a zero mean, wide-sense stationary, Gaussian random process. They are the two-frequency correlation function and the surface reverberation scattering function. These second order functions are shown to be dependent upon the directional wave number spectrum of the ocean surface. Previously published expressions for the ocean surface reverberation scattering function were based upon a Fresnel corrected Kirchhoff integral and a small slope approximation. They pertain only to a specular geometry. In addition, these expressions do not include a receive directivity function and a Gaussian functional form for the projected transmit beam pattern was assumed. And furthermore, very specific models for the ocean surface were used rather than the general form of the directional wave number spectrum.

The optimization problem of maximizing the SIR for a doubly spread target via signal design is considered in Chapter VI. Both the transmit and processing waveforms are restricted to be pulse trains. Each subpulse of the transmit pulse train is allowed to be arbitrary in shape and can occupy the entire interpulse spacing interval if desired. This represents a generalization of earlier approaches. The processing waveform is a time and frequency shifted replica of the transmit pulse train. Each subpulse of both the transmit and processing pulse trains is complex weighted. Restricting the transmit and processing waveforms to be complex weighted pulse trains allows the integral expression of the SIR to be transformed into an equivalent vector-matrix form.

Before the various optimization problems concerning the doubly spread target are discussed, the slowly fluctuating point target case



is considered. Although the point target problem is not of primary concern in Chapter VI, it is an important and interesting problem in its own right and is included for completeness since substantial research effort has been devoted to it in the past. Two different optimization problems concerning the maximization of the SIR for a slowly fluctuating point target are discussed. The first problem is to find the optimum, unit-energy, complex processing weighting vector that maximizes the SIR when the complex transmit weighting vector and the parameters of the subpulses are given. The second problem is to find the optimum, transmit-processing, complex weighting vector pair that maximizes the SIR when the parameters of the subpulses are given. The maximization is subject to unit-energy constraints on both the transmit and processing waveforms.

Three different optimization problems concerning the maximization of the SIR for a doubly spread target are discussed. The first problem is to find the optimum complex processing weighting vector that maximizes the SIR when the complex transmit weighting vector and the parameters of the subpulses are given. The maximization is subject to a unit-energy constraint on the processing weighting vector and a constraint on the desired amount of reverberation to be removed by the processing weighting vector. The second problem is to find the optimum, transmit-processing, complex weighting vector pair that maximizes the SIR when the parameters of the subpulses are given. The maximization is subject to a dynamic range constraint on the transmit weighting vector, a unit-energy constraint on the processing weighting vector, and a constraint on the desired amount of reverberation to be removed by the processing weighting vector.

And finally, the third problem is to maximize the SIR for a doubly spread target with respect to the parameters of the subpulses. For this particular optimization problem, it is assumed that both the transmit and processing weighting vectors are equal and given, and that the maximization is subject to a constraint on the desired amount of reverberation to be removed by the processing waveform and constraints on the subpulse parameters themselves.

Since all three optimization problems for the doubly spread target are originally defined on a complex space, the approach taken in Chapter VI is to formulate the optimization problems into equivalent nonlinear programming problems defined on a real space.

The significance of this dissertation can be summarized by stating that all the information required to solve the problem of detecting a doubly spread target return in the presence of reverberation and noise by maximizing the SIR via signal design is furnished; namely, the receiver structure; target, volume reverberation, and surface reverberation scattering functions; and the formulation of the various SIR optimization problems into equivalent nonlinear programming problems defined on a real space.

## CHAPTER II

### FUNDAMENTALS OF LINEAR TIME-VARYING FILTERS

#### 2.1 Introduction

The purpose of this chapter is to introduce some of the basic mathematical relationships, terminology, and concepts that are part of linear, time-varying, filter theory. This chapter is divided into two major sections. Section 2.2 is devoted to deterministic filters, and Section 2.3 is devoted to random filters. Throughout this chapter and the remainder of this dissertation, the terms filter, system, and channel will be used interchangeably.

Section 2.2 introduces four filter functions which are used to characterize linear, time-varying filters. These functions are (1) the time-varying impulse response, (2) the time-varying frequency response or transfer function, (3) the spreading function, and (4) the bi-frequency function. It is shown that these four system functions are related to one another via Fourier transformations. In addition to various input-output relationships, an expression for the output power spectrum is derived which demonstrates the frequency spreading property of linear, time-varying filters.

Since Section 2.3 is devoted to random filters, the discussion begins by defining the autocorrelation functions of the four system functions. It is shown that the system autocorrelation functions are also related to one another via Fourier transformations. The important channel property of uncorrelated spreading is considered next. The discussion on uncorrelated spreading introduces the concept

of the scattering function and its various Fourier transforms. In addition to various input-output relationships, expressions for the output autocorrelation function and the output power spectral density are also derived. Analogous to the deterministic results, the expression for the output power spectral density also predicts frequency spreading. And finally, there is some discussion on two different ways of characterizing a time-varying channel via its scattering function. The first method involves interpreting the scattering function as a density function from which first and second order moments can be computed, and the second method is concerned with the finite extent of the scattering function itself.

## 2.2 Linear Time-Varying Deterministic Filters

2.2.1 Impulse response and transfer functions. A linear, time-varying filter is commonly depicted as in Figure 1, where it is characterized by its corresponding time-varying impulse response function  $h(t, \tau)$ . The function  $h(t, \tau)$  describes the response of the filter at time  $t$  due to the application of a unit impulse at time  $\tau$ . The relationship between the input signal  $x(t)$  and the output signal  $y(t)$  is given by:<sup>1-3</sup>

$$y(t) = \int_{-\infty}^{\infty} x(\alpha)h(t, \alpha)d\alpha \quad . \quad (2.2-1)$$

Note that if we let  $x(t) = \delta(t - \tau)$  in Equation (2.2-1), where  $\delta(\cdot)$  is the Dirac delta function, then:

$$\int_{-\infty}^{\infty} \delta(\alpha - \tau)h(t, \alpha)d\alpha = h(t, \tau) \quad , \quad (2.2-2)$$

where use has been made of the sifting property of the Dirac delta function.

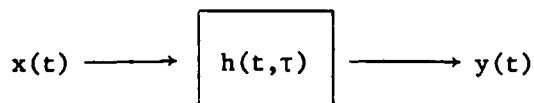


Figure 1. Linear time-varying filter.

The causality condition for a time-varying filter is:

$$h(t, \tau) = 0 \quad \text{for } t < \tau \quad (2.2-3)$$

which states that the filter cannot respond before the application of an input signal. Using the causality condition of Equation (2.2-3) and assuming that the input signal  $x(t)$  is zero for  $t < t_0$ , Equation (2.2-1) becomes:

$$y(t) = \int_{t_0}^t x(\tau) h(t, \tau) d\tau \quad (2.2-4)$$

Both Equation (2.2-1) and (2.2-4) are equivalent representations of the output if the time-varying filter is causal. The output of a linear, time-invariant, causal filter can also be obtained from Equations (2.2-1) and (2.2-4). In this case,  $h(t, \tau)$  becomes  $h(t - \tau)$ , where  $h(t - \tau) = 0$  for  $t < \tau$ ; and Equation (2.2-4) reduces to the well known convolution integral

$$y(t) = \int_{t_0}^t x(\tau) h(t - \tau) d\tau \quad (2.2-5)$$

Analogous to the frequency response or transfer function  $H(f)$  of linear, time-invariant systems is the time-varying frequency response or transfer function  $H(f, t)$  of linear, time-varying systems. It is defined by Zadeh<sup>1,2</sup> as:

$$H(f,t) \triangleq \int_{-\infty}^{\infty} h(t,\tau) \exp[-j2\pi f(t - \tau)] d\tau \quad , \quad (2.2-6)$$

where  $t$  is considered to be a parameter. Note that Equation (2.2-6) will reduce to  $H(f)$  when the filter under consideration is in fact time-invariant. When this is the case,  $h(t,\tau) = h(t - \tau)$  and Equation (2.2-6) becomes:

$$H(f,t) = \int_{-\infty}^{\infty} h(t - \tau) \exp[-j2\pi f(t - \tau)] d\tau \quad . \quad (2.2-7)$$

If we let  $\alpha = t - \tau$ , then  $d\alpha = -d\tau$  and Equation (2.2-7) becomes:

$$H(f) = \int_{-\infty}^{\infty} h(t) \exp(-j2\pi ft) dt \quad (2.2-8)$$

which is the Fourier transform of  $h(t)$ . A very important observation to make at this time is that  $h(t,\tau)$  and  $H(f,t)$ , as defined by Equation (2.2-6), do not form a direct Fourier transform pair as  $h(t)$  and  $H(f)$  do.<sup>3</sup> It will be shown later that if an alternate form of the time-varying impulse response is used, a direct Fourier transform pair can be formed between it and its corresponding time-varying transfer function.

An equally important result is the fact that a complex exponential input signal can be used to define the frequency response of both linear time-invariant and linear time-varying systems.<sup>1</sup> This can easily be shown by representing a linear, time-varying filter by the linear operator  $L(\cdot)$  which operates on input time functions. The output of the filter  $y(t)$  can then be expressed as:

$$y(t) = L[x(t)] \quad . \quad (2.2-9)$$

If we now let  $x(t) = \exp(+j2\pi f_0 t)$ , where  $f_0$  is some arbitrary constant frequency, then from Equations (2.2-1) and (2.2-9):

$$L[\exp(+j2\pi f_0 t)] = \int_{-\infty}^{\infty} \exp(+j2\pi f_0 \tau) h(t, \tau) d\tau, \quad (2.2-10)$$

and using the definition of  $H(f, t)$  given by Equation (2.2-6),

$$L[\exp(+j2\pi f_0 t)] = H(f_0, t) \exp(+j2\pi f_0 t), \quad (2.2-11)$$

where  $L[\exp(+j2\pi f_0 t)]$  is the response of the filter to  $\exp(+j2\pi f_0 t)$  and  $H(f_0, t)$  is the time-varying frequency response of the filter evaluated at  $f = f_0$ .

As was mentioned previously,  $h(t, \tau)$  and  $H(f, t)$ , as defined by Equation (2.2-6), do not form a direct Fourier transform pair. However, if we follow the development of Kailath<sup>3</sup> and introduce the alternate form of the time-varying impulse response  $h(t, t - \tau)$ , then it can be shown that  $h(t, t - \tau)$  and  $H(f, t)$ , as defined by Equation (2.2-6), do form a direct Fourier transform pair, i.e.,

$$h(t, t - \tau) \xleftrightarrow[\tau]{} H(f, t) \quad (2.2-12)$$

with  $t$  as a parameter. The function  $h(t, t - \tau)$  describes the response of the filter at time  $t$  due to the application of a unit impulse at time  $t - \tau$ . The time domain parameter  $\tau$  corresponds to the "age" of the application of the unit impulse, i.e.,  $t - \tau$  seconds ago.

Equation (2.2-12) can be verified by starting with the definition of  $H(f, t)$ , i.e.,

$$H(f,t) = \int_{-\infty}^{\infty} h(t,\alpha) \exp[-j2\pi f(t - \alpha)] d\alpha \quad , \quad (2.2-13)$$

where  $t$  can be considered as a fixed constant. If we let  $\alpha = t - \tau$ , then  $d\alpha = -d\tau$  and Equation (2.2-13) becomes:

$$H(f,t) = \int_{-\infty}^{\infty} h(t,t - \tau) \exp(-j2\pi f\tau) d\tau \quad (2.2-14)$$

which is the Fourier transform of  $h(t,t - \tau)$  with respect to  $\tau$ .

As a result,

$$h(t,t - \tau) = \int_{-\infty}^{\infty} H(f,t) \exp(+j2\pi f\tau) df \quad , \quad (2.2-15)$$

where  $h(t,t - \tau)$  is the inverse Fourier transform of  $H(f,t)$ .

The relationship between the input and output signals when  $h(t,t - \tau)$  is used to describe a linear, time-varying filter can be obtained from Equation (2.2-1), i.e.,

$$y(t) = \int_{-\infty}^{\infty} x(\alpha) h(t,\alpha) d\alpha \quad . \quad (2.2-16)$$

If we let  $\alpha = t - \tau$  as before, then  $d\alpha = -d\tau$ , where  $t$  is considered to be a fixed constant. Substituting these relations into Equation (2.2-16) yields the desired result:<sup>3</sup>

$$y(t) = \int_{-\infty}^{\infty} x(t - \tau) h(t,t - \tau) d\tau \quad . \quad (2.2-17)$$

The causality condition for  $h(t,t - \tau)$  is:

$$h(t,t - \tau) = 0 \quad \text{for } \tau < 0 \quad . \quad (2.2-18)$$



Note that this condition depends only on  $\tau$  and not upon an inequality relationship between  $t$  and  $\tau$ .

If the filter described by  $h(t, t - \tau)$  is in actuality time-invariant, then  $h(t, t - \tau) = h[t - (t - \tau)] = h(\tau)$ . As a result, Equation (2.2-14) reduces to  $H(f) = F\{h(\tau)\}$ , where  $F\{\cdot\}$  indicates a forward Fourier transform. And furthermore, Equation (2.2-17) reduces to the familiar convolution integral

$$y(t) = \int_{-\infty}^{\infty} x(t - \tau)h(\tau)d\tau, \quad (2.2-19)$$

where  $h(\tau) = 0$  for  $\tau < 0$  for a causal filter.

And finally, if we let  $x(t) = \exp(+j2\pi f_0 t)$  in Equation (2.2-17), then,

$$L[\exp(+j2\pi f_0 t)] = H(f_0, t)\exp(+j2\pi f_0 t), \quad (2.2-20)$$

where  $H(f_0, t)$  is the time-varying transfer function of the filter given by Equation (2.2-14) evaluated at  $f = f_0$ , and where use of Equation (2.2-9) was made. Hence, a complex exponential input signal can be used to define the frequency response of a linear, time-varying filter characterized by either  $h(t, \tau)$  or  $h(t, t - \tau)$ .<sup>3</sup>

In order to be consistent with the underwater acoustic signal processing literature (e.g., see References 4-7), the time-varying impulse response  $h(t, t - \tau)$  will hereafter be denoted as  $h(\tau, t)$ , i.e.,

$$h(\tau, t) \equiv h(t, t - \tau), \quad (2.2-21)$$

where  $h(\tau, t)$  denotes the response of the filter at time  $t$  due

to the application of a unit impulse at time  $t - \tau$ . This notation is more succinct and convenient, especially when dealing with Fourier transform pairs. Figure 2 summarizes the important relationships established so far. Figure 2a is the more common representation of a linear, time-varying filter, and Figure 2b is the alternate representation which will be used for the remainder of this dissertation.

2.2.2 Additional filter functions. Two filter functions have already been presented which characterize linear, time-varying filters. They are the time-varying impulse response and transfer functions. Two additional filter functions will now be introduced; namely, the spreading function and the bi-frequency function. The spreading function will be discussed first.

The spreading function  $S(\tau, \phi)$  is defined as the Fourier transform of  $h(\tau, t)$  with respect to  $t$ ,<sup>4-7</sup> i.e.,

$$h(\tau, t) \xleftrightarrow[t]{} S(\tau, \phi) , \quad (2.2-22)$$

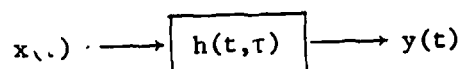
where

$$S(\tau, \phi) \triangleq \int_{-\infty}^{\infty} h(\tau, t) \exp(-j2\pi\phi t) dt \quad (2.2-23)$$

and

$$h(\tau, t) = \int_{-\infty}^{\infty} S(\tau, \phi) \exp(+j2\pi\phi t) d\phi . \quad (2.2-24)$$

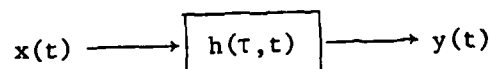
The frequency variable,  $\phi$  (in Hz), corresponds to the rate of change of the filter's impulse response. The spreading function is a frequency domain measure of the time variation of the filter. If the spectrum  $S(\tau, \phi)$  is confined to low values of  $\phi$ , then this would be an



$$y(t) = \int_{-\infty}^{\infty} x(\tau) h(t, \tau) d\tau$$

$$H(f, t) = \int_{-\infty}^{\infty} h(t, \tau) \exp[-j2\pi f(t - \tau)] d\tau$$

(a)



$$y(t) = \int_{-\infty}^{\infty} x(t - \tau) h(\tau, t) d\tau$$

$$h(\tau, t) \xleftrightarrow[\tau]{} H(f, t)$$

$$H(f, t) = \int_{-\infty}^{\infty} h(\tau, t) \exp(-j2\pi f\tau) d\tau$$

$$h(\tau, t) = \int_{-\infty}^{\infty} H(f, t) \exp(+j2\pi f\tau) df$$

(b)

Figure 2. Two different representations of linear, time-varying filters: (a) the more common representation, and (b) an alternate representation.

indication that the characteristics or properties of the system are changing slowly with time. However, if  $S(\tau, \phi)$  occupied the region of high  $\phi$  values, then this would be an indication that the filter's properties are varying rapidly with time.

It has already been shown that the output of a linear, time-varying filter can be represented as

$$y(t) = \int_{-\infty}^{\infty} x(t - \tau)h(\tau, t)d\tau, \quad (2.2-25)$$

where Equation (2.2-21) was substituted into Equation (2.2-17). An alternate representation of  $y(t)$  can now be obtained by substituting Equation (2.2-24) into Equation (2.2-25). Doing so yields:

$$y(t) = \int_{-\infty}^{\infty} \int x(t - \tau)\exp(+j2\pi\phi\tau)S(\tau, \phi)d\tau d\phi, \quad (2.2-26)$$

where the integrand term  $x(t - \tau)\exp(+j2\pi\phi\tau)$  is a time and frequency shifted version of the input signal. The output, as given by Equation (2.2-26), can be interpreted as being equal to the sum of time and frequency shifted components of the input weighted by the spreading function  $S(\tau, \phi)$ . Therefore, the spreading function determines the amount of spread in round-trip time delay  $\tau$  and frequency  $\phi$  that an input signal will undergo as it passes through the time-varying channel.<sup>4-6</sup>

The last filter function to be discussed is the bi-frequency function  $B(f, \phi)$ . It is defined as being the Fourier transform of  $H(f, t)$  with respect to  $t$ ,<sup>4-7</sup> i.e.,

$$H(f, t) \xleftrightarrow[t]{\quad} B(f, \phi) \quad (2.2-27)$$

where

$$B(f, \phi) \triangleq \int_{-\infty}^{\infty} H(f, t) \exp(-j2\pi\phi t) dt \quad (2.2-28)$$

and

$$H(f, t) = \int_{-\infty}^{\infty} B(f, \phi) \exp(+j2\pi\phi t) d\phi \quad (2.2-29)$$

Just as the spreading function gives an indication of how rapidly  $h(\tau, t)$  changes with time, the spectrum  $B(f, \phi)$  gives an indication of how rapidly  $H(f, t)$  changes with time.<sup>5,6</sup> If  $B(f, \phi)$  is confined to large values of  $\phi$ , then this would be an indication that  $H(f, t)$  varies rapidly with time. However, if  $B(f, \phi)$  is concentrated mainly in the region of low  $\phi$  values, then this would be an indication that  $H(f, t)$  varies slowly with time.

The bi-frequency function can also be found by taking the Fourier transform of  $S(\tau, \phi)$  with respect to  $\tau$ , i.e.,

$$S(\tau, \phi) \xleftrightarrow[\tau]{\quad} B(f, \phi) \quad , \quad (2.2-30)$$

where

$$B(f, \phi) = \int_{-\infty}^{\infty} S(\tau, \phi) \exp(-j2\pi f\tau) d\tau \quad (2.2-31)$$

and

$$S(\tau, \phi) = \int_{-\infty}^{\infty} B(f, \phi) \exp(+j2\pi f\tau) df \quad (2.2-32)$$

In addition,  $h(\tau, t)$  and  $B(f, \phi)$  form a two-dimensional Fourier transform pair, i.e.,

$$h(\tau, t) \xleftrightarrow[\tau, t]{} B(f, \phi) \quad , \quad (2.2-33)$$

where

$$B(f, \phi) = \int_{-\infty}^{\infty} \int_{-\infty}^{\infty} h(\tau, t) \exp[-j2\pi(f\tau + \phi t)] d\tau dt \quad (2.2-34)$$

and

$$h(\tau, t) = \int_{-\infty}^{\infty} \int_{-\infty}^{\infty} B(f, \phi) \exp[+j2\pi(f\tau + \phi t)] df d\phi \quad . \quad (2.2-35)$$

The interdependence which exists amongst the four filter functions is depicted in Figure 3. Any one of these functions may be used to define completely the time-varying channel.<sup>7</sup> The forward Fourier transforms with respect to  $\tau$  and  $t$  are denoted by the appearance of  $\tau$  and  $t$ , respectively, beside the lines in Figure 3.

**2.2.3 Output power spectrum.** Let us now compute the complex frequency spectrum of the output signal  $y(t)$ . We begin by expressing the input in terms of its inverse Fourier transform, i.e.,

$$x(t) = \int_{-\infty}^{\infty} X(f) \exp(+j2\pi ft) df \quad . \quad (2.2-36)$$

If  $x(t)$ , as represented by Equation (2.2-36), is passed through a linear, time-varying filter, then,

$$y(t) = \int_{-\infty}^{\infty} X(f) L[\exp(+j2\pi ft)] df \quad (2.2-37)$$

or

$$y(t) = \int_{-\infty}^{\infty} X(f) H(f, t) \exp(+j2\pi ft) df \quad , \quad (2.2-38)$$

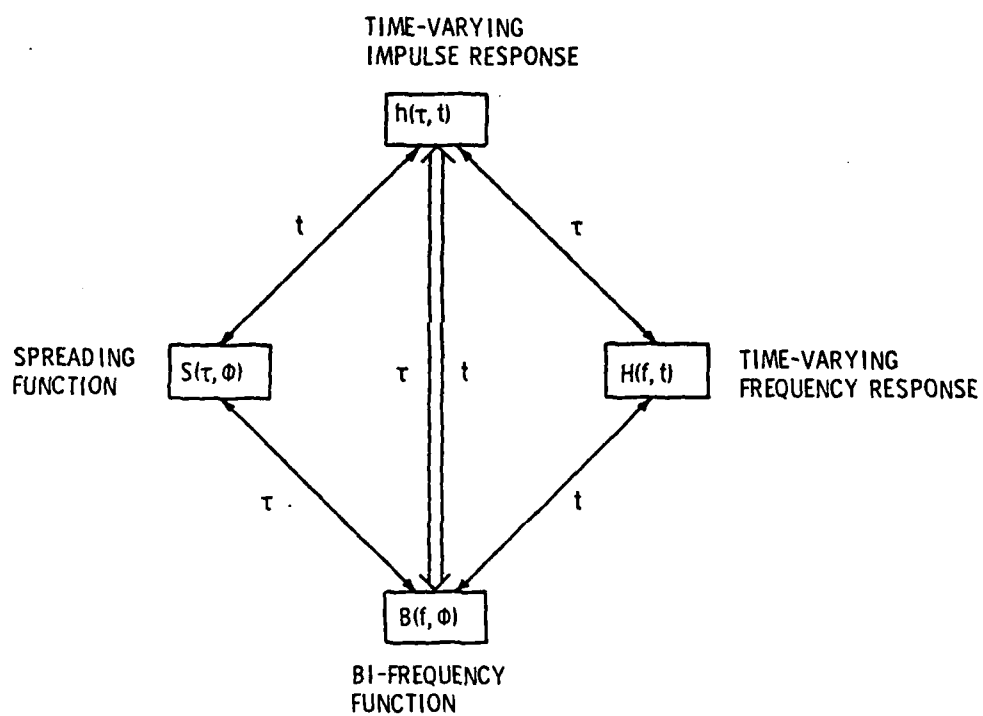


Figure 3. Interdependence amongst the four filter functions that characterize linear, time-varying channels.

where use was made of Equations (2.2-9) and (2.2-20). Note that Equation (2.2-38) is not the inverse Fourier transform of  $X(f)H(f,t)$ .<sup>5</sup> By definition, the output spectrum  $Y(\eta)$  is equal to:

$$Y(\eta) \triangleq \int_{-\infty}^{\infty} y(t) \exp(-j2\pi\eta t) dt \quad (2.2-39)$$

and upon substituting Equation (2.2-38) into Equation (2.2-39), one obtains:

$$Y(\eta) = \int_{-\infty}^{\infty} X(f) \int_{-\infty}^{\infty} H(f,t) \exp[-j2\pi(\eta - f)t] dt df \quad (2.2-40)$$

From Equation (2.2-28), it can be seen that the inner integral appearing in Equation (2.2-40) is equal to  $B(f, \eta - f)$  so that:<sup>1</sup>

$$Y(\eta) = \int_{-\infty}^{\infty} X(f) B(f, \eta - f) df \quad (2.2-41)$$

which is in the form of a frequency domain convolution integral.

Referring back to Equations (2.2-28) and (2.2-41), note that  $\phi \equiv \eta - f$  or  $\eta \equiv f + \phi$ . In other words, the output frequencies  $\eta$  are equal to the sum of the input frequencies  $f$  and the filter variation frequencies  $\phi$ .<sup>3</sup> Equation (2.2-41) demonstrates that one of the properties of linear, time-varying filters is the frequency spreading of the input spectrum due to the system variation frequencies  $\phi$ . As Kailath<sup>3</sup> points out, the frequency behavior of linear, time-varying channels is usually evidenced by a frequency spread, frequency shift, or both. The amount of frequency spreading produced may depend upon the frequency components of the input.



Since  $y(t)$  is a deterministic signal, the output power spectrum can be obtained directly from Equation (2.2-41) by computing  $|Y(\eta)|^2$ .

As a concluding example, let us use Equation (2.2-41) to compute the relationship between the input and output power spectrums for linear, time-invariant, deterministic filters subject to deterministic inputs. If a linear, time-varying filter is in fact time-invariant, then  $H(f,t) = H(f)$  and Equation (2.2-28) reduces to:

$$B(f,\phi) = H(f) \int_{-\infty}^{\infty} \exp(-j2\pi\phi t) dt \quad (2.2-42)$$

or

$$B(f,\phi) = H(f)\delta(\phi) \quad (2.2-43)$$

since

$$1 \xleftrightarrow[t]{} \delta(\phi) \quad (2.2-44)$$

Substituting Equation (2.2-43) into Equation (2.2-41) yields the familiar expression:

$$Y(\eta) = X(\eta)H(\eta) \quad (2.2-45)$$

and as a result,

$$S_y(\eta) = S_x(\eta) |H(\eta)|^2, \quad (2.2-46)$$

where  $S_x(\eta) = |X(\eta)|^2$  and  $S_y(\eta) = |Y(\eta)|^2$  are the input and output power spectrums, respectively, since  $x(t)$  and  $y(t)$  are both deterministic signals.

## 2.3 Linear Time-Varying Random Filters

2.3.1 Filter autocorrelation functions. In Section 2.2, four system functions were introduced which are used to characterize linear, time-varying, deterministic filters. These system functions are: (1) the time-varying impulse response,  $h(\tau, t)$ ; (2) the time-varying frequency response,  $H(f, t)$ ; (3) the spreading function,  $S(\tau, \phi)$ ; and (4) the bi-frequency function,  $B(f, \phi)$ . However, if the filter is random, then each of these channel functions must be considered as a random function of two variables. In this section, we will derive the various Fourier transform pairs which exist amongst the four filter autocorrelation functions. But first, let us define the autocorrelation and autocovariance functions as they are to be used in this dissertation.

Consider a random process  $x(r, s)$  which is a function of the two variables  $r$  and  $s$ . The autocorrelation function of  $x(r, s)$ , denoted by  $R_x(r, r', s, s')$ , is defined as:

$$R_x(r, r', s, s') \triangleq E\{x(r, s)x^*(r', s')\} \quad , \quad (2.3-1)$$

where  $E\{\cdot\}$  is the linear, expectation operator and the asterisk denotes complex conjugation. The average instantaneous power of  $x(r, s)$  can be found from Equation (2.3-1) by setting  $r' = r$  and  $s' = s$ , i.e.,

$$R_x(r, s) = E\{|x(r, s)|^2\} \quad . \quad (2.3-2)$$

The autocovariance function of  $x(r, s)$ , denoted by  $C_x(r, r', s, s')$ , is defined as:

$$C_x(r, r', s, s') \triangleq E\{[x(r, s) - \mu_x(r, s)] \cdot [x(r', s') - \mu_x(r', s')]^*\} \quad , \quad (2.3-3)$$

where

$$\mu_x(r,s) = E\{x(r,s)\} \quad . \quad (2.3-4)$$

Upon expanding the right-hand side of Equation (2.3-3), one obtains:

$$C_x(r,r',s,s') = R_x(r,r',s,s') - \mu_x(r,s)\mu_x^*(r',s') \quad . \quad (2.3-5)$$

It can be seen from Equation (2.3-5) that if  $x(r,s)$  is zero mean, then the autocovariance and autocorrelation functions are equal. Also, the variance of  $x(r,s)$  can be obtained from Equation (2.3-5) by setting  $r' = r$  and  $s' = s$ , i.e.,

$$\text{Var}\{x(r,s)\} = C_x(r,s) = E\{|x(r,s) - \mu_x(r,s)|^2\} \quad . \quad (2.3-6)$$

$$= E\{|x(r,s)|^2\} - |\mu_x(r,s)|^2 \quad , \quad (2.3-7)$$

where use has been made of Equation (2.3-2). From Equation (2.3-7), it can be seen that if  $x(r,s)$  is zero mean, then the variance of  $x(r,s)$  is equal to the average instantaneous power of  $x(r,s)$ .

Now that the autocorrelation and autocovariance functions of a random function of two variables have been defined, the derivation of the various Fourier transform pairs that exist amongst the four filter autocorrelation functions can proceed.

The four filter autocorrelation functions are defined as follows:

$$R_h(\tau,\tau',t,t') \triangleq E\{h(\tau,t)h^*(\tau',t')\} \quad , \quad (2.3-8)$$

$$R_H(f,f',t,t') \triangleq E\{H(f,t)H^*(f',t')\} \quad , \quad (2.3-9)$$

$$R_S(\tau,\tau',\phi,\phi') \triangleq E\{S(\tau,\phi)S^*(\tau',\phi')\} \quad (2.3-10)$$

and

$$R_B(f, f', \phi, \phi') \triangleq E\{B(f, \phi)B^*(f', \phi')\} \quad (2.3-11)$$

With the proper interpretation, it can be shown, for example, that  $R_h$  and  $R_H$  form a two-dimensional Fourier transform pair, i.e.,

$$R_h(\tau, \tau', t, t') \xleftrightarrow[\tau, \tau']{} R_H(f, f', t, t') \quad (2.3-12)$$

In order to clarify the phrase "proper interpretation," let us take the two-dimensional forward Fourier transform of  $R_h$ , with respect to  $\tau$  and  $\tau'$ , using the standard sign convention, i.e.,

$$\int_{-\infty}^{\infty} \int_{-\infty}^{\infty} R_h(\tau, \tau', t, t') \exp[-j2\pi(f\tau + f'\tau')] d\tau d\tau' \quad (2.3-13)$$

Substituting Equation (2.3-8) into Equation (2.3-13), and interchanging the operations of integration and expectation yields:

$$E \left\{ \int_{-\infty}^{\infty} h(\tau, t) \exp(-j2\pi f\tau) d\tau \int_{-\infty}^{\infty} h^*(\tau', t') \exp(-j2\pi f'\tau') d\tau' \right\} \quad (2.3-14)$$

or

$$E\{H(f, t)H^*(-f', t')\} = R_H(f, -f', t, t') \quad (2.3-15)$$

Upon close inspection of the right-hand side of Equation (2.3-15), it can be seen that this is not the desired result as given by the right-hand side of Equation (2.3-12). However, if we define the forward Fourier transform of  $h(\tau', t')$  with respect to  $\tau'$  with a positive complex exponential term, i.e.,

$$F_{\tau}\{h(\tau', t')\} = \int_{-\infty}^{\infty} h(\tau', t') \exp(+j2\pi f' \tau') d\tau' = H(f', t'), \quad (2.3-16)$$

then,

$$H^*(f', t') = \int_{-\infty}^{\infty} h^*(\tau', t') \exp(-j2\pi f' \tau') d\tau' \quad (2.3-17)$$

which is identical to the second integral expression appearing in Equation (2.3-14). Therefore, Equation (2.3-14) reduces to:

$$E\{H(f, t) H^*(f', t')\} = R_H(f, f', t, t') \quad (2.3-18)$$

which is the desired result. Thus, if we use the convention that forward transforms with respect to  $\tau$  and  $t$  are defined with a negative complex exponential (inverse transforms are defined with a positive complex exponential), and forward transforms with respect to  $\tau'$  and  $t'$  are defined with a positive complex exponential (inverse transforms are defined with a negative complex exponential),<sup>8</sup> then the four system autocorrelation functions are related by the following Fourier transform pairs:

$$R_h(\tau, \tau', t, t') \xleftrightarrow[\tau, \tau']{} R_H(f, f', t, t') \quad , \quad (2.3-19)$$

where

$$R_H(f, f', t, t') = \int_{-\infty}^{\infty} \int_{-\infty}^{\infty} R_h(\tau, \tau', t, t') \cdot \exp[-j2\pi(f\tau - f'\tau')] d\tau d\tau' \quad (2.3-19a)$$

and

$$R_h(\tau, \tau', t, t') = \int_{-\infty}^{\infty} \int_{-\infty}^{\infty} R_H(f, f', t, t') \cdot \exp[+j2\pi(f\tau - f'\tau')] df df' ; \quad (2.3-19b)$$

$$R_H(f, f', t, t') \xleftrightarrow[t, t']{} R_B(f, f', \phi, \phi') \quad (2.3-20)$$

where

$$R_B(f, f', \phi, \phi') = \int_{-\infty}^{\infty} \int_{-\infty}^{\infty} R_H(f, f', t, t') \cdot \exp[-j2\pi(\phi t - \phi' t')] dt dt' \quad (2.3-20a)$$

and

$$R_H(f, f', t, t') = \int_{-\infty}^{\infty} \int_{-\infty}^{\infty} R_B(f, f', \phi, \phi') \cdot \exp[+j2\pi(\phi t - \phi' t')] d\phi d\phi' ; \quad (2.3-20b)$$

$$R_h(\tau, \tau', t, t') \xleftrightarrow[t, t']{} R_S(\tau, \tau', \phi, \phi') \quad (2.3-21)$$

where

$$R_S(\tau, \tau', \phi, \phi') = \int_{-\infty}^{\infty} \int_{-\infty}^{\infty} R_h(\tau, \tau', t, t') \cdot \exp[-j2\pi(\phi t - \phi' t')] dt dt' \quad (2.3-21a)$$

and

$$R_h(\tau, \tau', t, t') = \int_{-\infty}^{\infty} \int_{-\infty}^{\infty} R_S(\tau, \tau', \phi, \phi') \cdot \exp[+j2\pi(\phi t - \phi' t')] d\phi d\phi'; \quad (2.3-21b)$$

$$R_S(\tau, \tau', \phi, \phi') \xleftrightarrow[\tau, \tau']{} R_B(f, f', \phi, \phi') \quad , \quad (2.3-22)$$

where

$$R_B(f, f', \phi, \phi') = \int_{-\infty}^{\infty} \int_{-\infty}^{\infty} R_S(\tau, \tau', \phi, \phi') \cdot \exp[-j2\pi(f\tau - f'\tau')] d\tau d\tau' \quad (2.3-22a)$$

and

$$R_S(\tau, \tau', \phi, \phi') = \int_{-\infty}^{\infty} \int_{-\infty}^{\infty} R_B(f, f', \phi, \phi') \cdot \exp[+j2\pi(f\tau - f'\tau')] df df' \quad ; \quad (2.3-22b)$$

and finally,

$$R_h(\tau, \tau', t, t') \xleftrightarrow[\tau, \tau', t, t']{} R_B(f, f', \phi, \phi') \quad , \quad (2.3-23)$$

where

$$R_B(f, f', \phi, \phi') = \int_{-\infty}^{\infty} \int_{-\infty}^{\infty} \int_{-\infty}^{\infty} \int_{-\infty}^{\infty} R_h(\tau, \tau', t, t') \cdot \exp[-j2\pi(f\tau - f'\tau' + \phi t - \phi' t')] d\tau d\tau' dt dt' \quad (2.3-23a)$$

and

$$R_h(\tau, \tau', t, t') = \int_{-\infty}^{\infty} \int_{-\infty}^{\infty} \int_{-\infty}^{\infty} \int_{-\infty}^{\infty} R_B(f, f', \phi, \phi') \cdot \exp[+j2\pi(f\tau - f'\tau' + \phi t - \phi't')] df df' d\phi d\phi'.$$

(2.3-23b)

The interdependence which exists amongst these autocorrelation functions is illustrated in Figure 4. The forward Fourier transforms with respect to  $\tau$ ,  $\tau'$ ,  $t$ , and  $t'$  are denoted by the appearance of  $f$ ,  $f'$ ,  $\phi$ , and  $\phi'$ , respectively, beside the lines in Figure 4.

2.3.2 Uncorrelated spreading - the scattering function. As can be seen from Figure 4, the filter autocorrelation functions are, in general, dependent upon four variables. However, if it is assumed that the spreading function  $S(\tau, \phi)$  is uncorrelated with  $S(\tau', \phi')$  for all  $\tau \neq \tau'$  and  $\phi \neq \phi'$ , then the autocorrelation functions can be simplified.

The assumption of uncorrelated spreading is mathematically equivalent to stating that the autocovariance of  $S(\tau, \phi)$  and  $S(\tau', \phi')$  is zero for all  $\tau \neq \tau'$  and  $\phi \neq \phi'$ , i.e.,

$$C_S(\tau, \tau', \phi, \phi') = R_S(\tau, \tau', \phi, \phi') - \mu_S(\tau, \phi) \mu_S^*(\tau', \phi') = 0, \quad (2.3-24)$$

where  $\mu_S(\tau, \phi) = E\{S(\tau, \phi)\}$ . If it is assumed that  $\mu_S(\tau, \phi) = 0$ , then Equation (2.3-24) is equivalent to:

$$R_S(\tau, \tau', \phi, \phi') = R_S(\tau, \phi) \delta(\tau - \tau') \delta(\phi - \phi') \quad , \quad (2.3-25)$$



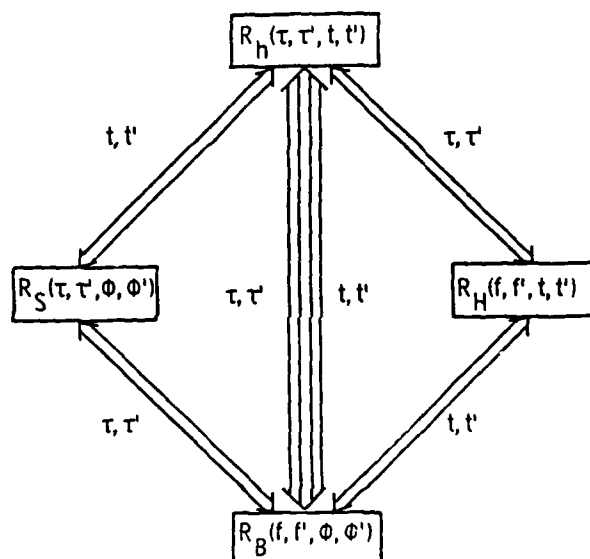


Figure 4. Interdependence amongst the four filter autocorrelation functions that characterize linear, time-varying, random channels.

where the function

$$R_S(\tau, \phi) = E\{|S(\tau, \phi)|^2\} \quad (2.3-26)$$

is called the scattering function and is equal to the variance of the spreading function.<sup>4-7</sup> The scattering function can be thought of as an average power density function which determines the average amount of spread that an input signal's power will undergo as a function of round-trip time delay  $\tau$  and frequency  $\phi$ . Note that  $R_S(\tau, \phi)$  is a real, non-negative function of  $\tau$  and  $\phi$ .

Equation (2.3-25) was the result of the assumption that  $\mu_S(\tau, \phi) = 0$ . However, even if  $S(\tau, \phi)$  is non-zero mean, it is an easy matter to do the analysis with a centered process  $S_C(\tau, \phi)$  obtained by subtracting from  $S(\tau, \phi)$  its mean value  $\mu_S(\tau, \phi)$ , i.e.,

$$S_C(\tau, \phi) = S(\tau, \phi) - \mu_S(\tau, \phi) \quad (2.3-27)$$

The random process  $S_C(\tau, \phi)$  has zero mean and its autocovariance is equal to:

$$C_{S_C}(\tau, \tau', \phi, \phi') = E\{S_C(\tau, \phi) S_C^*(\tau', \phi')\} \quad (2.3-28)$$

$$= C_S(\tau, \tau', \phi, \phi') \quad (2.3-29)$$

which is the autocovariance of  $S(\tau, \phi)$ .

Let us now examine the implications and the effect that the assumption of uncorrelated spreading will have on the other three system autocorrelation functions. As Figure 4 indicates,  $R_H(f, f', t, t')$  can be obtained by taking the inverse two-dimensional Fourier transform of  $R_S(\tau, \tau', \phi, \phi')$  with respect to  $\phi$  and  $\phi'$ , and then taking the

forward two-dimensional Fourier transform with respect to  $\tau$  and  $\tau'$ .

Doing so yields:

$$\begin{aligned}
 R_H(f, f', t, t') &= \int_{-\infty}^{\infty} \int_{-\infty}^{\infty} \int_{-\infty}^{\infty} R_S(\tau, \tau', \phi, \phi') \\
 &\quad \cdot \exp[+j2\pi(\phi t - \phi' t')] d\phi d\phi' \\
 &\quad \cdot \exp[-j2\pi(f\tau - f'\tau')] d\tau d\tau', \quad (2.3-30)
 \end{aligned}$$

where use has been made of Equations (2.3-19a) and (2.3-21b). Upon substituting Equation (2.3-25) into Equation (2.3-30), one obtains:

$$R_H(f, f', t, t') = R_H(\Delta f, \Delta t), \quad (2.3-31)$$

where

$$R_H(\Delta f, \Delta t) = \int_{-\infty}^{\infty} \int_{-\infty}^{\infty} R_S(\tau, \phi) \exp[-j2\pi(\Delta f\tau - \phi\Delta t)] d\tau d\phi, \quad (2.3-32)$$

where  $\Delta f = f - f'$  and  $\Delta t = t - t'$ . The expression  $R_H(\Delta f, \Delta t)$  is sometimes referred to as the time-frequency correlation function and it is generally a complex quantity.<sup>5,7</sup> It can be seen from Equation (2.3-31) that when uncorrelated spreading is assumed, the autocorrelation function  $R_H(f, f', t, t')$  becomes a function of time and frequency differences only. This implies that the random process  $H(f, t)$  is wide-sense stationary in both frequency and time. An additional requirement for  $H(f, t)$  to be wide-sense stationary in both frequency and time is that<sup>9</sup>

$$\mu_H(f, t) = E\{H(f, t)\} = \text{constant}. \quad (2.3-33)$$

Since the four filter functions are related by linear transformations (see Figure 3), if  $\mu_S(\tau, \phi) = 0$ , then  $\mu_h(\tau, t) = \mu_H(f, t) = \mu_B(f, \phi) = 0$ . Therefore, Equation (2.3-33) is satisfied since it was assumed that  $\mu_S(\tau, \phi) = 0$ , and hence,  $\mu_h(\tau, t) = 0$ . The condition of uncorrelated spreading (scattering) in round-trip time delay  $\tau$  is equivalent to a condition of wide-sense stationarity in frequency ( $\Delta f$ ).<sup>7</sup> The condition of uncorrelated spreading (scattering) in frequency  $\phi$  is equivalent to a condition of wide-sense stationarity in time ( $\Delta t$ ).<sup>7</sup> When uncorrelated spreading (scattering) in both  $\tau$  and  $\phi$  occur together, we have a wide-sense stationary uncorrelated scattering (WSSUS) channel.<sup>7,8,10</sup>

Next, consider the autocorrelation function  $R_h(\tau, \tau', t, t')$ . Upon substituting Equation (2.3-25) into Equation (2.3-21b), one obtains:

$$R_h(\tau, \tau', t, t') = R_h(\tau, \Delta t) \delta(\tau - \tau') \quad , \quad (2.3-34)$$

where

$$R_h(\tau, \Delta t) = \int_{-\infty}^{\infty} R_S(\tau, \phi) \exp(+j2\pi\phi\Delta t) d\phi \quad (2.3-35)$$

and  $\Delta t = t - t'$ . Equation (2.3-34) indicates that the random process  $h(\tau, t)$  is wide-sense stationary in time because of the  $\Delta t$  dependence and since  $\mu_h(\tau, t) = 0$ . Equation (2.3-34) also indicates that  $h(\tau, t)$  is uncorrelated for all values of  $\tau' \neq \tau$ .

And finally, upon substituting Equation (2.3-25) into Equation (2.3-22a), the autocorrelation function of the bi-frequency function reduces to:

$$R_B(f, f', \phi, \phi') = R_B(\Delta f, \phi) \delta(\phi - \phi') \quad , \quad (2.3-36)$$

where

$$R_B(\Delta f, \phi) = \int_{-\infty}^{\infty} R_S(\tau, \phi) \exp(-j2\pi\Delta f\tau) d\tau \quad (2.3-37)$$

and  $\Delta f = f - f'$ . Equation (2.3-36) indicates that the random process  $B(f, \phi)$  is wide-sense stationary in frequency because of the  $\Delta f$  dependence and since  $\mu_B(f, \phi) = 0$ . Equation (2.3-36) also indicates that  $B(f, \phi)$  is uncorrelated for all values of  $\phi' \neq \phi$ .

Let us now summarize the results obtained so far. Under the assumption of uncorrelated spreading, the four filter autocorrelation functions originally defined by Equations (2.3-8) through (2.3-11) reduce as follows:

$$R_H(\tau, \tau', t, t') = R_H(\tau, \Delta t) \delta(\tau - \tau') \quad , \quad (2.3-34)$$

$$R_H(f, f', t, t') = R_H(\Delta f, \Delta t) \quad , \quad (2.3-31)$$

$$R_S(\tau, \tau', \phi, \phi') = R_S(\tau, \phi) \delta(\tau - \tau') \delta(\phi - \phi') \quad (2.3-25)$$

and

$$R_B(f, f', \phi, \phi') = R_B(\Delta f, \phi) \delta(\phi - \phi') \quad , \quad (2.3-36)$$

where  $R_H(\Delta f, \Delta t)$  and  $R_S(\tau, \phi)$  are referred to as being the time-frequency correlation function and the scattering function, respectively, and  $\Delta f = f - f'$  and  $\Delta t = t - t'$ .

### 2.3.3 The scattering function and its Fourier transforms.

Since Equation (2.3-35) can be interpreted as being the inverse Fourier transform of the scattering function, then,

$$R_h(\tau, \Delta t) \xleftrightarrow{\Delta t} R_S(\tau, \phi) \quad , \quad (2.3-38)$$

where

$$R_S(\tau, \phi) = \int_{-\infty}^{\infty} R_h(\tau, \Delta t) \exp(-j2\pi\phi\Delta t) d\Delta t \quad (2.3-39)$$

and

$$R_h(\tau, \Delta t) = \int_{-\infty}^{\infty} R_S(\tau, \phi) \exp(+j2\pi\phi\Delta t) d\phi \quad . \quad (2.3-35)$$

Similarly, since Equation (2.3-37) can be interpreted as being the forward Fourier transform of the scattering function, then,

$$R_S(\tau, \phi) \xleftrightarrow{\tau} R_B(\Delta f, \phi) \quad , \quad (2.3-40)$$

where

$$R_B(\Delta f, \phi) = \int_{-\infty}^{\infty} R_S(\tau, \phi) \exp(-j2\pi\Delta f\tau) d\tau \quad (2.3-37)$$

and

$$R_S(\tau, \phi) = \int_{-\infty}^{\infty} R_B(\Delta f, \phi) \exp(+j2\pi\Delta f\tau) d\Delta f \quad . \quad (2.3-41)$$

Additional transform pairs can be obtained as follows. From Equations (2.3-32) and (2.3-35), we have:

$$R_h(\tau, \Delta t) \xleftrightarrow{\tau} R_H(\Delta f, \Delta t) \quad , \quad (2.3-42)$$

where

$$R_H(\Delta f, \Delta t) = \int_{-\infty}^{\infty} R_h(\tau, \Delta t) \exp(-j2\pi\Delta f\tau) d\tau \quad (2.3-43)$$

and

$$R_h(\tau, \Delta t) = \int_{-\infty}^{\infty} R_H(\Delta f, \Delta t) \exp(+j2\pi\Delta f\tau) d\Delta f \quad . \quad (2.3-44)$$

If Equation (2.3-39) is substituted into Equation (2.3-37), then one obtains the two-dimensional Fourier transform pair

$$R_h(\tau, \Delta t) \xleftrightarrow{\tau, \Delta t} R_B(\Delta f, \phi) \quad , \quad (2.3-45)$$

where

$$R_B(\Delta f, \phi) = \int_{-\infty}^{\infty} \int_{-\infty}^{\infty} R_h(\tau, \Delta t) \exp[-j2\pi(\Delta f\tau + \phi\Delta t)] d\tau d\Delta t \quad (2.3-46)$$

and

$$R_h(\tau, \Delta t) = \int_{-\infty}^{\infty} \int_{-\infty}^{\infty} R_B(\Delta f, \phi) \exp[+j2\pi(\Delta f\tau + \phi\Delta t)] d\Delta f d\phi \quad . \quad (2.3-47)$$

And, upon using Equation (2.3-43) in conjunction with Equation (2.3-46), one obtains:

$$R_H(\Delta f, \Delta t) \xleftrightarrow{\Delta t} R_B(\Delta f, \phi) \quad , \quad (2.3-48)$$

where

$$R_B(\Delta f, \phi) = \int_{-\infty}^{\infty} R_H(\Delta f, \Delta t) \exp(-j2\pi\phi\Delta t) d\Delta t \quad (2.3-49)$$

and

$$R_H(\Delta f, \Delta t) = \int_{-\infty}^{\infty} R_B(\Delta f, \phi) \exp(+j2\pi\phi\Delta t) d\phi \quad (2.3-50)$$

The various Fourier transform pairs are summarized in Figure 5. The forward transforms with respect to  $\tau$  and  $\Delta t$  are denoted by the appearance of  $\tau$  and  $\Delta t$ , respectively, beside the lines in Figure 5. The scattering function, or any of its three Fourier transforms, is a complete statistical description of a WSSUS channel at the second order.<sup>7</sup>

And finally, another very important two-dimensional Fourier transform relationship (not a transform pair) exists between the scattering function and the time-frequency correlation function besides Equation (2.3-32). It is obtained by substituting Equation (2.3-44) into Equation (2.3-39). Doing so yields:

$$R_S(\tau, \phi) = \int_{-\infty}^{\infty} \int_{-\infty}^{\infty} R_H(\Delta f, \Delta t) \exp[+j2\pi(\Delta f\tau - \phi\Delta t)] d\Delta f d\Delta t \quad (2.3-51)$$

The time-varying frequency response relationship of Equation (2.2-20) and the two-dimensional Fourier transform relationship of Equation (2.3-51) are the two fundamental results upon which the derivations of the volume reverberation, surface reverberation, and target scattering functions will be based.



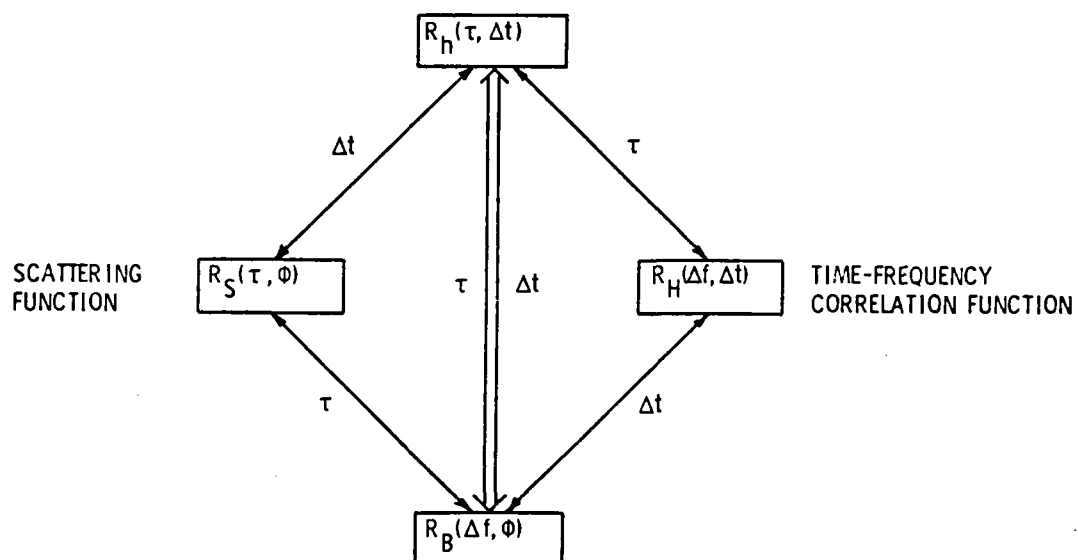


Figure 5. The scattering function and its Fourier transforms.

#### 2.3.4 Input-output relations - output power spectral density.

We will now proceed to derive an expression for the autocorrelation function of the output from a linear, time-varying, random channel. From Equation (2.2-26), we have that

$$y(t) = \int_{-\infty}^{\infty} \int x(t - \tau) \exp(+j2\pi\phi\tau) S(\tau, \phi) d\tau d\phi, \quad (2.3-52)$$

where  $x(t)$  is the deterministic input signal and  $S(\tau, \phi)$  is now the random spreading function of the filter. The output correlation function  $R_y(t, t')$  is defined as:

$$R_y(t, t') \triangleq E\{y(t)y^*(t')\}. \quad (2.3-53)$$

Substituting Equation (2.3-52) into Equation (2.3-53) and performing the indicated operations yields:

$$R_y(t, t') = \int_{-\infty}^{\infty} \int \int \int x(t - \tau) x^*(t' - \tau') \exp[+j2\pi(\phi\tau - \phi'\tau')] \\ \cdot R_S(\tau, \tau', \phi, \phi') d\tau d\phi d\tau' d\phi', \quad (2.3-54)$$

where  $R_S(\tau, \tau', \phi, \phi')$  is the autocorrelation function of the spreading function [see Equation (2.3-10)]. If we make the assumption that the filter exhibits uncorrelated spreading, then Equation (2.3-54) reduces to:

$$R_y(t, t') = \int_{-\infty}^{\infty} \int x(t - \tau) R_S(\tau, \phi) x^*(t' - \tau) \\ \cdot \exp(+j2\pi\phi\Delta t) d\tau d\phi, \quad (2.3-55)$$

where  $R_S(\tau, \phi)$  is the scattering function,  $\Delta t = t - t'$ , and use was made of Equation (2.3-25). Using Equation (2.3-55), an expression for the average output energy will be derived next.

The average instantaneous output power is given by:

$$R_y(t, t) = E\{|y(t)|^2\} \quad (2.3-56)$$

or, from Equation (2.3-55),

$$R_y(t, t) = \int_{-\infty}^{\infty} \int_{-\infty}^{\infty} |x(t - \tau)|^2 R_S(\tau, \phi) d\tau d\phi \quad (2.3-57)$$

The average output energy can be found by integrating both sides of Equation (2.3-57) with respect to  $t$ . If we define the energy of the output signal  $E_y$  as:

$$E_y \triangleq \int_{-\infty}^{\infty} |y(t)|^2 dt, \quad (2.3-58)$$

then the average output energy  $\bar{E}_y$  can be expressed as:

$$\bar{E}_y \triangleq E\{E_y\} = \int_{-\infty}^{\infty} E\{|y(t)|^2\} dt \quad (2.3-59)$$

or

$$\bar{E}_y = \int_{-\infty}^{\infty} R_y(t, t) dt \quad (2.3-60)$$

Substituting Equation (2.3-57) into Equation (2.3-60) yields:<sup>11,12</sup>

$$\bar{E}_y/E_x = \int_{-\infty}^{\infty} \int_{-\infty}^{\infty} R_S(\tau, \phi) d\tau d\phi, \quad (2.3-61)$$

where

$$E_x \triangleq \int_{-\infty}^{\infty} |x(t)|^2 dt \quad (2.3-62)$$

is the energy of the input signal. Equation (2.3-61) indicates that the ratio of output (received) average energy to input (transmitted) energy for a WSSUS channel can be obtained by integrating the scattering function of the channel with respect to both  $\tau$  and  $\phi$ . Also note that the average output energy is not a function of the input signal's shape.

Alternate expressions for  $R_y(t, t')$ , other than those given by Equations (2.3-54) and (2.3-55), can be obtained by representing the output as:

$$y(t) = \int_{-\infty}^{\infty} X(f)H(f, t)\exp(+j2\pi ft)df, \quad (2.3-63)$$

where  $X(f)$  is the Fourier transform of the deterministic input signal  $x(t)$ , and  $H(f, t)$  is now the random, time-varying frequency response of the filter. Substituting Equation (2.3-63) into Equation (2.3-53) and performing the indicated operations yields:

$$R_y(t, t') = \int_{-\infty}^{\infty} \int_{-\infty}^{\infty} X(f)X^*(f')R_H(f, f', t, t') \cdot \exp[+j2\pi(ft - f't')]dfdf' \quad (2.3-64)$$

If we make the assumption that the filter exhibits uncorrelated spreading, then Equation (2.3-64) reduces to:

$$R_y(t, t') = \int_{-\infty}^{\infty} \int_{-\infty}^{\infty} X(f) X^*(f') R_H(\Delta f, \Delta t) \cdot \exp[+j2\pi(ft - f't')] df df' , \quad (2.3-65)$$

where  $\Delta f = f - f'$  ,  $\Delta t = t - t'$  , and use was made of Equation (2.3-31). A relationship between the output and input power spectral densities can now be obtained from Equation (2.3-65).

If it is assumed that the input signal  $x(t)$  is a zero-mean, wide-sense stationary (WSS), random process which is uncorrelated with  $H(f, t)$  , then the output autocorrelation function given by Equation (2.3-65) becomes modified as follows:

$$R_y(t, t') = \int_{-\infty}^{\infty} \int_{-\infty}^{\infty} E\{X(f) X^*(f')\} R_H(\Delta f, \Delta t) \cdot \exp[+j2\pi(ft - f't')] df df' . \quad (2.3-65a)$$

Since  $x(t)$  was assumed to be WSS, then the following relationship:

$$E\{X(f) X^*(f')\} = S_x(f) \delta(f - f') \quad (2.3-66)$$

exists (e.g., see Zadeh<sup>13</sup>), and if Equation (2.3-66) is substituted into Equation (2.3-65a), one obtains:

$$R_y(\Delta t) = \int_{-\infty}^{\infty} S_x(f) R_H(0, \Delta t) \exp(+j2\pi f \Delta t) df , \quad (2.3-67)$$

where  $S_x(f)$  is the power spectral density of  $x(t)$  and is defined as the Fourier transform of the autocorrelation function  $R_x(\tau)$ . The output power spectral density  $S_y(f)$  can now be obtained by Fourier transforming both sides of Equation (2.3-67) with respect to  $\Delta t$ . Doing so yields:<sup>13,14</sup>

$$S_y(\eta) = \int_{-\infty}^{\infty} S_x(f) R_B(0, \eta - f) df, \quad (2.3-68)$$

where

$$R_B(0, \eta - f) = \int_{-\infty}^{\infty} R_H(0, \Delta t) [-j2\pi(\eta - f)\Delta t] d\Delta t. \quad (2.3-69)$$

Note that Equation (2.3-68) is in the form of a convolution integral just like Equation (2.2-41) for the deterministic case. The convolution process accounts for the frequency spreading of the input power spectral density.

### 2.3.5 Channel characterization via the scattering function.

An interesting consequence of Equation (2.3-61) is that the scattering function can be thought of as a two-dimensional density function.<sup>12</sup>

For example, if we define the constant  $K$  as:

$$K \triangleq \int_{-\infty}^{\infty} \int_{-\infty}^{\infty} R_S(\tau, \phi) d\tau d\phi, \quad (2.3-70)$$

then, Equation (2.3-61) can be rewritten as:

$$\int_{-\infty}^{\infty} \int_{-\infty}^{\infty} f_S(\tau, \phi) d\tau d\phi = 1, \quad (2.3-71)$$

where

$$f_S(\tau, \phi) = R_S(\tau, \phi)/K \quad (2.3-72)$$

is the normalized scattering function. The quantity  $f_S(\tau, \phi)$  has the properties of a density function since both the scattering function and the constant  $K$  are real, positive quantities, and  $f_S(\tau, \phi)$  integrates to one. As a result, a WSSUS channel can be characterized, at least to a certain extent, by calculating the first and second moments of both the round-trip time delay  $\tau$  and frequency spread  $\phi$ .<sup>12</sup> The mean round-trip time delay  $\mu_\tau$  can therefore be computed from:

$$\mu_\tau = \int_{-\infty}^{\infty} \tau f_S(\tau) d\tau, \quad (2.3-73)$$

where

$$f_S(\tau) = \int_{-\infty}^{\infty} f_S(\tau, \phi) d\phi \quad (2.3-74)$$

can be interpreted as being the marginal density function of the round-trip time delay variable  $\tau$ . An alternate expression for  $f_S(\tau)$  can be obtained by referring back to Equation (2.3-35) and setting  $\Delta t = 0$ . Doing so yields:

$$f_S(\tau) = R_h(\tau, 0)/K, \quad (2.3-75)$$

where

$$R_h(\tau, 0) = E\{|h(\tau, t)|^2\} = \int_{-\infty}^{\infty} R_S(\tau, \phi) d\phi \quad (2.3-76)$$

is referred to as the power impulse response and is the distribution of power as a function of  $\tau$  only.<sup>7,15</sup> Note that  $f_S(\tau)$  integrates to one. The mean-square time delay spread  $\sigma_\tau^2$  is given by:

$$\sigma_\tau^2 = \overline{(\tau^2)} - \mu_\tau^2, \quad (2.3-77)$$

where

$$\overline{(\tau^2)} = \int_{-\infty}^{\infty} \tau^2 f_S(\tau) d\tau. \quad (2.3-78)$$

Similarly, the mean value of the frequency spread  $\mu_\phi$  can be computed from:

$$\mu_\phi = \int_{-\infty}^{\infty} \phi f_S(\phi) d\phi, \quad (2.3-79)$$

where

$$f_S(\phi) = \int_{-\infty}^{\infty} f_S(\tau, \phi) d\tau \quad (2.3-80)$$

can be interpreted as being the marginal density function of the frequency spread variable  $\phi$ . An alternate expression for  $f_S(\phi)$  can also be obtained by referring back to Equation (2.3-37) and setting  $\Delta f = 0$ . Doing so yields:

$$f_S(\phi) = R_B(0, \phi)/K, \quad (2.3-81)$$

where

$$R_B(0, \phi) = E\{|B(f, \phi)|^2\} = \int_{-\infty}^{\infty} R_S(\tau, \phi) d\tau \quad (2.3-82)$$



is referred to as the echo power spectrum and is the distribution of power as a function of  $\phi$  only.<sup>7,15</sup> Note that  $f_S(\phi)$  integrates to one. The mean-square frequency spread  $\sigma_\phi^2$  is given by:

$$\sigma_\phi^2 = \overline{(\phi^2)} - \mu_\phi^2, \quad (2.3-83)$$

where

$$\overline{(\phi^2)} = \int_{-\infty}^{\infty} \phi^2 f_S(\phi) d\phi. \quad (2.3-84)$$

Scattering functions are frequently concentrated in a finite area of the  $\tau - \phi$  plane.<sup>12</sup> They occupy a certain band of frequencies along the  $\phi$  axis and/or a band of time delays along the  $\tau$  axis. If we refer to the band of frequencies as bandwidth  $B$  (in Hz) and the band of time delays as length  $L$  (in sec), then these two parameters provide an alternate way of describing the scattering function, and hence, the channel. For example, an underspread channel is defined as one whose  $BL$  product is less than one, i.e.,  $BL < 1$ ; and an overspread channel is defined as one whose  $BL$  product is greater than one, i.e.,  $BL > 1$ .<sup>5,12,15</sup>

In order to avoid frequency spreading, it is required that:

$$1/T \gg B, \quad (2.3-85)$$

where  $T$  is the duration of the transmit signal and  $1/T$  is a measure of its Doppler resolution.<sup>5,12</sup> Similarly, in order to avoid spreading in round-trip time delay (range), it is required that:

$$1/W \gg L, \quad (2.3-86)$$

where  $W$  is the bandwidth of the transmit signal and  $1/W$  is a measure of its range resolution.<sup>5,12</sup> If Equations (2.3-85) and (2.3-86) are multiplied together, then,

$$1/TW \gg BL \quad (2.3-87)$$

which is the requirement for avoiding both range and frequency spreading. Since, for any real bandpass transmit signal, the time-bandwidth product  $TW$  is equal to or greater than one,<sup>12,30</sup> i.e.,

$$TW \geq 1, \quad (2.3-88)$$

Equation (2.3-87) can only be satisfied for underspread channels.

Equation (2.3-88) is based upon the equivalent rectangular duration  $T$  (sec) and bandwidth  $W$ (Hz) of the transmit signal.<sup>30</sup> Although Equation (2.3-87) cannot be satisfied for overspread channels, one can choose a transmit signal such that either range or frequency spreading is avoided, but not both.

## CHAPTER III

### DETECTION IN THE PRESENCE OF REVERBERATION

#### 3.1 Introduction

The purpose of this chapter is threefold: (1) to specify the binary hypothesis testing problem to be considered in this dissertation, (2) to indicate the receiver structure which will be used to process the received signal, and (3) to introduce the important concept of the output signal-to-interference power ratio.

This chapter begins with a brief discussion of the complex envelope notation for bandpass signals since the hypothesis testing problem will be formulated in terms of the complex envelopes of the target, reverberation, and noise signals. The target and reverberation returns are modelled as the outputs from linear, time-varying, random filters which are assumed to be WSSUS communication channels.

The particular receiver structure used is a correlator followed by a magnitude squared operation. The magnitude squared output from the correlator is tested against a threshold which is determined from a probability of false alarm constraint in a Neyman-Pearson test.

Having specified both the binary hypothesis testing problem and the receiver, the signal-to-interference ratio (SIR) is derived for a doubly spread target and is shown to be dependent upon the target and reverberation scattering functions and the cross-ambiguity function of the transmit signal and the processing waveform, which is used in the correlator receiver. It is also demonstrated that the SIR for a slowly fluctuating point target can be obtained from the general SIR expression for a doubly spread target.

The final discussion in this chapter is devoted to the question of receiver optimality, i.e., when is our choice of receiver an optimum or sub-optimum receiver for detecting either a slowly fluctuating point target or a doubly spread target. The discussion on optimality introduces the performance measure  $\Delta$  which is shown to be equal to the SIR. The performance measure determines the probability of detection for a given probability of false alarm in the important case of Gaussian statistics. Maximizing  $\Delta$  is equivalent to maximizing the probability of detection and it is noted that this can be achieved by proper signal design.

### 3.2 A Binary Hypothesis Testing Problem

3.2.1 Complex envelope notation. Before discussing the underwater acoustic detection problem, the complex envelope notation for bandpass signals will be introduced and discussed briefly since it will be used extensively throughout the remainder of this dissertation.

Consider an arbitrary real bandpass signal  $g(t)$  whose amplitude spectrum  $|G(f)|$  is concentrated about  $f = +f_c$  and  $f = -f_c$  Hz. The complex envelope of  $g(t)$ , denoted by  $\tilde{g}(t)$ , is a complex signal whose amplitude spectrum  $|\tilde{G}(f)|$  is centered about  $f = 0$  Hz. The relationship between  $g(t)$  and  $\tilde{g}(t)$  is given by (e.g., see Whalen<sup>16</sup>):

$$g(t) = \text{Re} \{ \tilde{g}(t) \exp(+j2\pi f_c t) \} \quad , \quad (3.2-1)$$

where

$$\tilde{g}(t) = [g(t) + j\hat{g}(t)] \exp(-j2\pi f_c t) \quad , \quad (3.2-1a)$$

where  $\text{Re}$  means "take the real part" and  $\hat{g}(t)$  is the Hilbert transform of  $g(t)$ .

In Chapter II, no distinctions were made as to whether the input and output signals  $x(t)$  and  $y(t)$ , respectively, and the time-varying impulse response  $h(\tau, t)$  were real versus complex or lowpass versus bandpass. Since for most communication and detection problems (in particular, the detection problem to be discussed here)  $x(t)$ ,  $y(t)$ , and  $h(\tau, t)$  are bandpass waveforms, it is more convenient analytically to work with their respective complex envelopes. They are denoted by  $\tilde{x}(t)$ ,  $\tilde{y}(t)$ , and  $\tilde{h}(\tau, t)$  and are related to their real counterparts by:<sup>12,16</sup>

$$x(t) = \text{Re}\{\tilde{x}(t)\exp(+j2\pi f_c t)\} \quad , \quad (3.2-2)$$

$$y(t) = \text{Re}\{\tilde{y}(t)\exp(+j2\pi f_c t)\} \quad (3.2-3)$$

and

$$h(\tau, t) = \text{Re}\{2\tilde{h}(\tau, t)\exp(+j2\pi f_c \tau)\} \quad (3.2-4)$$

where (see Kailath<sup>3</sup>)

$$\tilde{h}(\tau, t) = [h(\tau, t) + j\hat{h}(\tau, t)]\exp(-j2\pi f_c \tau) \quad (3.2-4a)$$

and

$$\hat{h}(\tau, t) = \frac{1}{\pi} \int_{-\infty}^{\infty} \frac{h(\xi, t)}{\tau - \xi} d\xi \quad . \quad (3.2-4b)$$

We will now derive two different relationships between the input and output complex envelopes. The first relationship will be approximate while the second will be exact. Starting with Equation (2.2-25), i.e.,

$$y(t) = \int_{-\infty}^{\infty} x(t - \tau)h(\tau, t)d\tau \quad , \quad (2.2-25)$$

where it is assumed that  $x(t)$ ,  $y(t)$ , and  $h(\tau, t)$  are real signals, and using Equations (3.2-2) through (3.2-4) in conjunction with the identity

$$\operatorname{Re}\{Z\} \equiv (Z + Z^*)/2, \quad (3.2-5)$$

where  $Z$  is some arbitrary complex quantity, it can be shown that<sup>16</sup>

$$\begin{aligned} \tilde{y}(t) = & \int_{-\infty}^{\infty} \tilde{x}(t - \tau) \tilde{h}(\tau, t) d\tau \\ & + \int_{-\infty}^{\infty} \tilde{x}(t - \tau) \tilde{h}^*(\tau, t) \exp[-j2\pi(2f_c)\tau] d\tau. \end{aligned} \quad (3.2-6)$$

If it is assumed that both  $x(t)$  and  $h(\tau, t)$  are narrowband bandpass signals, then,  $\tilde{x}(t - \tau)$  and  $\tilde{h}(\tau, t)$  will be slowly varying functions of  $\tau$ . Therefore, the second integral appearing in Equation (3.2-6) will be approximately equal to zero, and as a result,<sup>12,16</sup>

$$\tilde{y}(t) \approx \int_{-\infty}^{\infty} \tilde{x}(t - \tau) \tilde{h}(\tau, t) d\tau \quad (3.2-7)$$

which is identical in form with Equation (2.2-25). Although Equation (3.2-7) is an approximate relationship based upon a narrowband assumption, this does not mean to imply that the concept of a complex envelope applies to narrowband bandpass signals only. Complex envelopes can be defined and used for wide-band bandpass signals, also.<sup>4</sup> In fact, the next relationship which will be derived is exact and does not involve a narrowband assumption.

Once again, assume that  $x(t)$ ,  $y(t)$ , and  $h(\tau, t)$  are real signals. Using Equations (3.2-2) and (3.2-5), the real input signal  $x(t)$  can be expressed as:

$$x(t) = [\tilde{x}(t) \exp(+j2\pi f_c t) + \tilde{x}^*(t) \exp(-j2\pi f_c t)]/2. \quad (3.2-8)$$

Taking the Fourier transform of both sides of Equation (3.2-8) yields:

$$X(f) = [\tilde{X}(f - f_c) + \tilde{X}^*(-f - f_c)]/2 \quad (3.2-9)$$

since

$$\tilde{x}(t)\exp(+j2\pi f_c t) \xleftrightarrow{t} \tilde{X}(f - f_c) \quad (3.2-10)$$

and

$$\tilde{x}^*(t) \xleftrightarrow{t} \tilde{X}^*(-f) \quad , \quad (3.2-11)$$

where

$$\tilde{x}(t) \xleftrightarrow{t} \tilde{X}(f) \quad . \quad (3.2-12)$$

Substituting Equation (3.2-9) into Equation (2.2-38), i.e.,

$$y(t) = \int_{-\infty}^{\infty} X(f)H(f,t)\exp(+j2\pi ft)df \quad (2.2-38)$$

yields

$$\begin{aligned} y(t) = & (1/2) \int_{-\infty}^{\infty} \tilde{X}(f)H(f + f_c, t) \\ & \cdot \exp(+j2\pi ft)df \exp(+j2\pi f_c t) \\ & + \left\{ (1/2) \int_{-\infty}^{\infty} \tilde{X}(f)H^*(-[f + f_c], t) \right. \\ & \left. \cdot \exp(+j2\pi ft)df \exp(+j2\pi f_c t) \right\}^* . \quad (3.2-13) \end{aligned}$$

Since

$$h(\tau, t) \xleftrightarrow{\tau} H(f, t) \quad , \quad (2.2-12)$$

where  $h(\tau, t)$  is a real function, then,

$$H^* (-(f + f_c), t) = H(f + f_c, t) \quad (3.2-14)$$

and upon substituting Equation (3.2-14) into Equation (3.2-13), we obtain:

$$y(t) = \text{Re} \{ \tilde{y}(t) \exp(+j2\pi f_c t) \} \quad , \quad (3.2-3)$$

where

$$\tilde{y}(t) = \int_{-\infty}^{\infty} \tilde{X}(f) H(f + f_c, t) \exp(+j2\pi f t) df \quad . \quad (3.2-15)$$

Equation (3.2-15) is the desired result which relates the output complex envelope  $\tilde{y}(t)$  to the spectrum of the input complex envelope  $\tilde{X}(f)$  (e.g., see Ishimaru<sup>10</sup>). Equation (3.2-15) is an exact relationship and no narrowband assumption was made.

An interesting interpretation of  $H(f, t)$  can be obtained from Equation (3.2-15). Assume that a sinusoidal signal is transmitted, i.e.,

$$x(t) = \cos(2\pi f_c t) = \text{Re} \{ 1 \exp(+j2\pi f_c t) \} \quad , \quad (3.2-16)$$

so that the complex envelope  $\tilde{x}(t) = 1$ . As a result, the spectrum  $\tilde{X}(f) = \delta(f)$ , and if this result is substituted into Equation (3.2-15), we obtain:

$$\tilde{y}(t) = H(f_c, t) \quad (3.2-17)$$

or

$$y(t) = \text{Re} \{ H(f_c, t) \exp(+j2\pi f_c t) \} \quad . \quad (3.2-18)$$



Thus, the time-varying frequency response  $H(f, t)$  is the complex envelope of the response of the channel to  $x(t) = \text{Re}\{\exp(+j2\pi ft)\}$ .<sup>1</sup>

If  $\tilde{y}(t)$  is a random process, then a more appropriate characterization of the output complex envelope is provided by the autocorrelation function

$$R_{\tilde{y}}(t, t') \triangleq E\{\tilde{y}(t)\tilde{y}^*(t')\} \quad (3.2-19)$$

Substituting Equation (3.2-15) into Equation (3.2-19) and performing the indicated operations yields:

$$R_{\tilde{y}}(t, t') = \int_{-\infty}^{\infty} \int_{-\infty}^{\infty} \tilde{X}(f)\tilde{X}^*(f')R_H(f + f_c, f' + f_c, t, t') \cdot \exp[+j2\pi(ft - f't')]dfdf' \quad (3.2-20)$$

where

$$R_H(f + f_c, f' + f_c, t, t') = E\{H(f + f_c, t)H^*(f' + f_c, t')\} \quad (3.2-21)$$

If the linear, time-varying, random filter is a WSSUS channel, then Equation (3.2-20) reduces to [see Equation (2.3-31)]:

$$R_{\tilde{y}}(t, t') = \int_{-\infty}^{\infty} \int_{-\infty}^{\infty} \tilde{X}(f)\tilde{X}^*(f')R_H(\Delta f, \Delta t) \cdot \exp[+j2\pi(ft - f't')]dfdf' \quad (3.2-22)$$

where  $\Delta f = f - f'$  and  $\Delta t = t - t'$ . Note that the form of Equations (3.2-22) and (2.3-65) are identical. And upon substituting Equation (2.3-32) into Equation (3.2-22), one obtains:

$$R_{\tilde{y}}(t, t') = \int_{-\infty}^{\infty} \int_{-\infty}^{\infty} \tilde{x}(t - \tau) R_S(\tau, \phi) \tilde{x}^*(t' - \tau) \cdot \exp(+j2\pi\phi\Delta t) d\tau d\phi, \quad (3.2-23)$$

where  $\Delta t = t - t'$ . Note that the form of Equations (3.2-23) and (2.3-55) are also identical. Using Equation (3.2-23) and following the development between Equations (2.3-55) and (2.3-62), it can also be shown that the average energy of the output complex envelope  $\overline{E}_{\tilde{y}}$  is given by [compare with Equation (2.3-61)]:

$$\overline{E}_{\tilde{y}} = E_{\tilde{x}} \int_{-\infty}^{\infty} \int_{-\infty}^{\infty} R_S(\tau, \phi) d\tau d\phi, \quad (3.2-24)$$

where

$$\overline{E}_{\tilde{y}} = \int_{-\infty}^{\infty} R_{\tilde{y}}(t, t) dt \quad (3.2-25)$$

and

$$E_{\tilde{x}} = \int_{-\infty}^{\infty} |\tilde{x}(t)|^2 dt. \quad (3.2-26)$$

And finally, the autocorrelation function of the real output  $R_y(t, t')$  can be obtained from  $R_{\tilde{y}}(t, t')$  by using the following approximate relationship:<sup>10,11</sup>

$$R_y(t, t') \approx (1/2) \operatorname{Re}\{R_{\tilde{y}}(t, t') \exp[+j2\pi f_c(t - t')]\}. \quad (3.2-27)$$

3.2.2 The signal-to-interference ratio for a doubly spread target. The detection problem to be considered in this dissertation is the following binary hypothesis testing problem:

$$H_1 : \tilde{r}(t) = \underset{\text{TRGT}}{\tilde{y}(t)} + \underset{\text{REV}}{\tilde{y}(t)} + \tilde{n}(t) \quad -\infty < t < \infty \quad (3.2-28)$$

$$H_0 : \tilde{r}(t) = \underset{\text{REV}}{\tilde{y}(t)} + \tilde{n}(t) \quad -\infty < t < \infty \quad (3.2-29)$$

where

$$\underset{\text{TRGT}}{\tilde{y}(t)} \approx \int_{-\infty}^{\infty} \tilde{x}(t - \tau) \tilde{h}(\tau, t) d\tau \quad (3.2-30)$$

or

$$\underset{\text{TRGT}}{\tilde{y}(t)} = \int_{-\infty}^{\infty} \tilde{X}(f) \underset{\text{TRGT}}{H(f + f_c, t)} \exp(+j2\pi ft) df \quad (3.2-30a)$$

and

$$\underset{\text{REV}}{\tilde{y}(t)} \approx \int_{-\infty}^{\infty} \tilde{x}(t - \tau) \tilde{h}(\tau, t) d\tau \quad (3.2-31)$$

or

$$\underset{\text{REV}}{\tilde{y}(t)} = \int_{-\infty}^{\infty} \tilde{X}(f) \underset{\text{REV}}{H(f + f_c, t)} \exp(+j2\pi ft) df \quad (3.2-31a)$$

Both the target and the reverberation are being modelled as linear, time-varying, random filters.<sup>12</sup> The approach of treating the ocean medium as a linear, time-varying, random communication channel is well-established (e.g., see References 4, 5, 7, 10, 12, 17, 18). This method has also been applied to problems in radar astronomy and communication channels in general.<sup>8,11,15</sup>

Hypothesis  $H_1$  states that the complex envelope of the received signal  $\tilde{r}(t)$  is equal to the sum of the target return  $\underset{\text{TRGT}}{\tilde{y}(t)}$ , the

reverberation return  $\tilde{y}_{\text{REV}}(t)$ , and noise  $\tilde{n}(t)$ . The noise is assumed to be zero mean, white, and uncorrelated with both the target and reverberation returns. It is also assumed that both  $\tilde{y}_{\text{TRGT}}(t)$  and  $\tilde{y}_{\text{REV}}(t)$  are zero mean and uncorrelated with one another. Hypothesis  $H_0$  states that  $\tilde{r}(t)$  is equal to the sum of the reverberation return and noise. The reverberation return, in general, is a composite of volume, surface, and bottom reverberation returns.

The particular receiver structure which will be used in this dissertation to process  $\tilde{r}(t)$  is illustrated in Figure 6. The function  $\tilde{g}(t)$  is to be referred to as the "processing waveform," as yet unspecified. The receiver performs the following test: choose hypothesis  $H_1$  if:

$$|\tilde{x}|^2 = \left| \int_{-\infty}^{\infty} \tilde{r}(t) \tilde{g}^*(t) dt \right|^2 > \gamma \quad (3.2-32)$$

and choose  $H_0$  otherwise. The threshold  $\gamma$  is chosen to satisfy the desired probability of false alarm constraint in a Neyman-Pearson test.

Any discussion concerning the optimality of the receiver illustrated in Figure 6, and hence, the test indicated by Equation (3.2-32), will be deferred until Section 3.3.

Let us now compute the output signal-to-interference power ratio (SIR) for the receiver shown in Figure 6. The SIR as used in this dissertation is defined as:

$$\text{SIR} \triangleq E \left\{ \left| \tilde{x}_{\tilde{y}_{\text{TRGT}}} \right|^2 \right\} / E \left\{ \left| \tilde{x}_{\tilde{v}} \right|^2 \right\}, \quad (3.2-33)$$

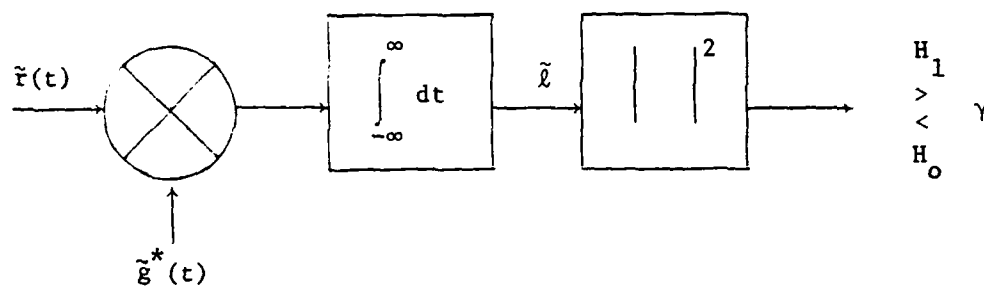


Figure 6. Receiver structure for processing  $\tilde{r}(t)$

where

$$\tilde{x}_{\tilde{y}_{\text{TRGT}}} = \int_{-\infty}^{\infty} \tilde{y}(t) \tilde{g}^*(t) dt, \quad (3.2-34)$$

$$\tilde{x}_{\tilde{v}} = \int_{-\infty}^{\infty} \tilde{v}(t) \tilde{g}^*(t) dt \quad (3.2-35)$$

and

$$\tilde{v}(t) = \tilde{y}_{\text{REV}}(t) + \tilde{n}(t). \quad (3.2-36)$$

Using Equations (3.2-34) through (3.2-36), it can be shown that:

$$E \left\{ \left| \tilde{x}_{\tilde{y}_{\text{TRGT}}} \right|^2 \right\} = \int_{-\infty}^{\infty} \int_{-\infty}^{\infty} \tilde{g}^*(t) R_{\tilde{y}_{\text{TRGT}}}(t, t') \tilde{g}(t') dt dt' \quad (3.2-37)$$

and

$$E \left\{ \left| \tilde{x}_{\tilde{v}} \right|^2 \right\} = \int_{-\infty}^{\infty} \int_{-\infty}^{\infty} \tilde{g}^*(t) R_{\tilde{v}}(t, t') \tilde{g}(t') dt dt' \quad (3.2-38)$$

where

$$R_{\tilde{v}}(t, t') = R_{\tilde{y}_{\text{REV}}}(t, t') + N_0 \delta(t - t') \quad (3.2-39)$$

where  $N_0$  is the spectral height of the complex white noise  $\tilde{n}(t)$ .

Substituting Equation (3.2-39) into Equation (3.2-38) yields:

$$E \left\{ \left| \tilde{x}_{\tilde{v}} \right|^2 \right\} = \int_{-\infty}^{\infty} \int_{-\infty}^{\infty} \tilde{g}^*(t) R_{\tilde{y}_{\text{REV}}}(t, t') \tilde{g}(t') dt dt' + N_0 \int_{-\infty}^{\infty} |\tilde{g}(t)|^2 dt \quad (3.2-40)$$

Now, if it is further assumed that the linear, time-varying, random filters which represent the target and the reverberation are WSSUS

communication channels, then the form of Equation (3.2-23) is applicable for the autocorrelation functions  $R_{\tilde{y}_{\text{TRGT}}}(t, t')$  and  $R_{\tilde{y}_{\text{REV}}}(t, t')$ . Therefore, with the use of Equation (3.2-23), Equations (3.2-37) and (3.2-40) can be rewritten as:

$$E \left\{ \left| \tilde{y}_{\text{TRGT}} \right|^2 \right\} = \int_{-\infty}^{\infty} \int_{-\infty}^{\infty} R_{S_{\text{TRGT}}}(\tau, \phi) \left| \chi_{\tilde{x}\tilde{g}}(\tau, \phi) \right|^2 d\tau d\phi \quad (3.2-41)$$

and

$$E \left\{ \left| \tilde{y}_{\tilde{v}} \right|^2 \right\} = \int_{-\infty}^{\infty} \int_{-\infty}^{\infty} R_{S_{\text{REV}}}(\tau, \phi) \left| \chi_{\tilde{x}\tilde{g}}(\tau, \phi) \right|^2 d\tau d\phi + N_o \int_{-\infty}^{\infty} |\tilde{g}(t)|^2 dt, \quad (3.2-42)$$

where

$$\chi_{\tilde{x}\tilde{g}}(\tau, \phi) = \int_{-\infty}^{\infty} \tilde{x}(t - \frac{\tau}{2}) \tilde{g}^*(t + \frac{\tau}{2}) \exp(+j2\pi\phi t) dt \quad (3.2-43)$$

is the cross-ambiguity function of the complex envelope of the transmit signal  $\tilde{x}(t)$ , and the complex envelope of the processing waveform  $\tilde{g}(t)$ . The expressions  $R_{S_{\text{TRGT}}}(\tau, \phi)$  and  $R_{S_{\text{REV}}}(\tau, \phi)$  are the target and reverberation scattering functions, respectively. Substituting Equations (3.2-41) and (3.2-42) into Equation (3.2-33) yields:

$$\text{SIR} = \frac{\int_{-\infty}^{\infty} \int_{-\infty}^{\infty} R_{S_{\text{TRGT}}}(\tau, \phi) \left| \chi_{\tilde{x}\tilde{g}}(\tau, \phi) \right|^2 d\tau d\phi}{\int_{-\infty}^{\infty} \int_{-\infty}^{\infty} R_{S_{\text{REV}}}(\tau, \phi) \left| \chi_{\tilde{x}\tilde{g}}(\tau, \phi) \right|^2 d\tau d\phi + N_o \int_{-\infty}^{\infty} |\tilde{g}(t)|^2 dt} \quad (3.2-44)$$

which is the output signal-to-interference power ratio for a doubly spread target. The term "doubly spread target" is used because of the appearance of the target scattering function  $R_{S_{TRGT}}(\tau, \phi)$  which implies that the target return  $\tilde{y}_{TRGT}(t)$  will exhibit a spread in both round-trip time delay  $\tau$  and frequency  $\phi$ . The SIR is almost always defined for a slowly fluctuating point target in the literature.<sup>19</sup> More will be said about the SIR for a slowly fluctuating point target in the next section. It is important to note that no Gaussian assumptions were made in the derivation of Equation (3.2-44).

The SIR expression for a doubly spread target as given by Equation (3.2-44) can also be obtained in a different way. This can be demonstrated by first defining the quantity  $\Delta$  as follows:

$$\Delta \triangleq \frac{E \left\{ |\tilde{x}|^2 \mid H_1 \right\} - E \left\{ |\tilde{x}|^2 \mid H_0 \right\}}{E \left\{ |\tilde{x}|^2 \mid H_0 \right\}}, \quad (3.2-45)$$

where under hypothesis  $H_1$ ,

$$\tilde{x} = \tilde{x}_{\tilde{y}_{TRGT}} + \tilde{x}_{\tilde{v}} \quad (3.2-46)$$

and under hypothesis  $H_0$ ,

$$\tilde{x} = \tilde{x}_{\tilde{v}}, \quad (3.2-47)$$

where  $\tilde{x}_{\tilde{y}_{TRGT}}$  and  $\tilde{x}_{\tilde{v}}$  are given by Equations (3.2-34) and (3.2-35),

respectively. Now, if we make the same assumptions as before, i.e., that  $\tilde{y}_{TRGT}(t)$ ,  $\tilde{y}_{REV}(t)$ , and  $\tilde{n}(t)$  are zero mean and uncorrelated with one another, and in addition, that  $\tilde{n}(t)$  is white, then, substituting



Equations (3.2-46) and (3.2-47) into Equation (3.2-45), and performing the indicated operations yields:

$$\Delta = E \left\{ \left| \tilde{x}_{\tilde{y}_{\text{TRGT}}} \right|^2 \right\} / E \left\{ \left| \tilde{x}_{\tilde{v}} \right|^2 \right\} = \text{SIR} \quad (3.2-48)$$

which is equal to the SIR definition given by Equation (3.2-33), and as a result,  $\Delta$  is also equal to Equation (3.2-44). Once again, note that no Gaussian assumptions were made in the derivation of Equation (3.2-48). More will be said about the definition of  $\Delta$ , as given by Equation (3.2-45), in Section 3.3.

The majority of the remaining analysis to appear in this dissertation will be centered around the SIR expression for a doubly spread target as given by Equation (3.2-44). However, for completeness, it will be demonstrated in the next section that the more common SIR expression for a slowly fluctuating point target can be obtained from the general SIR expression given by Equation (3.2-44). Besides, the point target problem is important in its own right.

3.2.3 The signal-to-interference ratio for a slowly fluctuating point target. The properties of a slowly fluctuating point target are as follows:<sup>12</sup> (1) It is the simplest model of a target. (2) It is assumed that the target characteristics, although random, are fixed (constant) during the time interval that it is being insonified by the transmit pulse. However, the target characteristics do change from time interval to time interval. Therefore, the transmit signal will acquire a random attenuation and a random phase shift. Since both the attenuation and phase shift are essentially constant over the time

interval of insonification, they can be modelled as random variables. And finally, (3) it is assumed that neither a range spread nor a Doppler spread is discernible in the target return.<sup>15</sup>

The target return from a slowly fluctuating point target is modelled as a time and frequency shifted replica of the transmit complex envelope, i.e.,

$$\tilde{y}_{\text{TRGT}}(t) = \tilde{b} \tilde{x}(t - \tau') \exp(+j2\pi\phi't) \quad , \quad (3.2-49)$$

where  $\tilde{b}$  is assumed to be a zero mean complex Gaussian random variable which accounts for random attenuation and random phase shift.<sup>12</sup> The magnitude of  $\tilde{b}$ ,  $|\tilde{b}|$ , is assumed to be Rayleigh distributed and the phase of  $\tilde{b}$  is assumed to be uniform. Thus, the magnitude and phase are statistically independent random variables. It is also assumed that the target is moving with a constant radial velocity.

The scattering function for a slowly fluctuating point target can be expressed as:<sup>15</sup>

$$R_{S_{\text{TRGT}}}(\tau, \phi) = E\{|\tilde{b}|^2\} \delta(\tau' - \tau) \delta(\phi' - \phi) \quad . \quad (3.2-50)$$

The quantity  $E\{|\tilde{b}|^2\}$  includes the array gains, propagation losses, and radar (sonar) cross-section of the target.<sup>12</sup>

The SIR for a slowly fluctuating point target can now be obtained by substituting Equation (3.2-50) into Equation (3.2-44). Doing so yields the desired result (e.g., see DeLong and Hofstetter<sup>19</sup>):

$$SIR = \frac{E\{|\tilde{\epsilon}|^2\} |\chi_{\tilde{x}\tilde{g}}(\tau', \phi')|^2}{\int_{-\infty}^{\infty} \int_{-\infty}^{\infty} R_{S_{REV}}(\tau, \phi) |\chi_{\tilde{x}\tilde{g}}(\tau, \phi)|^2 d\tau d\phi + N_o \int_{-\infty}^{\infty} |\tilde{g}(t)|^2 dt} \quad (3.2-51)$$

DeLong and Hofstetter<sup>19</sup> assumed that  $\tau' = \phi' = 0$  in their expression for the SIR for a point target. If these values for  $\tau'$  and  $\phi'$  are substituted into Equation (3.2-51), then,

$$\left( |\chi_{\tilde{x}\tilde{g}}(\tau', \phi')|^2 \right)_{\tau'=\phi'=0} = \left| \int_{-\infty}^{\infty} \tilde{x}(t) \tilde{g}^*(t) dt \right|^2 \quad (3.2-52)$$

which agrees with their result.

### 3.3 Optimum and Sub-Optimum Receivers

3.3.1 Optimum receivers for detecting a slowly fluctuating point target. In this section, we will discuss two cases when the receiver illustrated in Figure 6, and hence, the test given by Equation (3.2-32) is in fact optimal for detecting a slowly fluctuating point target. The first case is concerned with the detection of a point target return in the presence of white noise only. The second case is concerned with the detection of a point target return in the presence of both reverberation and white noise.

Consider the simple case when there is no reverberation present, i.e.,  $\tilde{y}(t) = 0$ . Assume that  $\tilde{n}(t)$  is Gaussian, zero mean, and white <sub>REV</sub> and that the target return is given by Equation (3.2-49). Recall that  $\tilde{y}(t)$  as specified by Equation (3.2-49) is also Gaussian and zero mean. <sub>TRGT</sub> Let us further assume that  $\tilde{y}(t)$  and  $\tilde{n}(t)$  are uncorrelated <sub>TRGT</sub> (statistically independent because of Gaussian statistics) and that

$\tau'$  and  $\phi'$  are known constants. If we process  $\tilde{r}(t)$  by a matched filter designed for the presence of white noise only and matched to

$$\tilde{s}(t) = \tilde{x}(t - \tau') \exp(+j2\pi\phi't) \quad , \quad (3.3-1)$$

then, the processing waveform  $\tilde{g}(t)$  is given by:

$$\tilde{g}(t) = \tilde{s}(t) = \tilde{x}(t - \tau') \exp(+j2\pi\phi't) \quad (3.3-2)$$

and the test indicated by Equation (3.2-32) is optimal. It is, in fact, the log-likelihood ratio test for detecting signals with random amplitude and phase, where  $|\tilde{x}|^2$  is the test statistic.<sup>12,16</sup> This case is also known as slow Rayleigh fading.<sup>16</sup>

Let us next compute the SIR for this receiver. If Equation (3.3-2) is substituted into Equation (3.2-43), then it can be shown that:

$$|\chi_{\tilde{x}\tilde{g}}(\tau', \phi')|^2 = E_{\tilde{x}}^2 \quad , \quad (3.3-3)$$

where

$$E_{\tilde{x}} = \int_{-\infty}^{\infty} |\tilde{x}(t)|^2 dt \quad (3.3-4)$$

is the energy of the complex envelope of the transmit signal. Also, note that:

$$\int_{-\infty}^{\infty} |\tilde{g}(t)|^2 dt = E_{\tilde{x}} \quad (3.3-5)$$

when  $\tilde{g}(t)$  is given by Equation (3.3-2). Since it was assumed that

$\tilde{y}(t) = 0$  , then  $R_{S, \text{REV}}(\tau, \phi) = 0$  , and if Equations (3.3-3) and (3.3-5) are

substituted into Equation (3.2-51), then the general expression for the SIR for a slowly fluctuating point target reduces to:

$$SIR = \frac{\bar{E}_{\tilde{y}_{TRGT}}}{N_o}, \quad (3.3-6)$$

where

$$\bar{E}_{\tilde{y}_{TRGT}} = E\{|\tilde{b}|^2\} E_{\tilde{x}} \quad (3.3-7)$$

is the average return energy from the point target. Equation (3.3-7) can easily be verified by substituting Equation (3.2-50) into Equation (3.2-24).

The error performance of this receiver is completely determined by Equation (3.3-6) since the probability of detection  $P_D$  for a given probability of false alarm  $P_F$  is given by:<sup>12,16</sup>

$$P_D = P_F^{1/(1+\Delta)}, \quad (3.3-8)$$

where

$$\Delta \equiv SIR = \frac{\bar{E}_{\tilde{y}_{TRGT}}}{N_o}. \quad (3.3-9)$$

It is obvious from Equation (3.3-8) that in order to increase the probability of detection for a given probability of false alarm, one must maximize  $\Delta$  (SIR), i.e., as  $\Delta \rightarrow \infty$ ,  $P_D \rightarrow 1$  for  $P_F$  constant. In this case, it can be seen from Equations (3.3-7) and (3.3-9) that  $\Delta$  (SIR) can be maximized by simply increasing the transmit energy  $E_{\tilde{x}}$ .

Recall that when  $\Delta$  was originally defined by Equation (3.2-45), it was not given any specific name, although it was shown to be equal

to the SIR as defined by Equation (3.2-33) when the same set of assumptions were used with both definitions. When  $\tilde{y}_{\text{TRGT}}(t)$ ,  $\tilde{y}_{\text{REV}}(t)$ , and  $\tilde{n}(t)$  are Gaussian, zero-mean, and uncorrelated (statistically independent) with one another, and  $\tilde{n}(t)$  is white; then  $\Delta$  as specified by Equations (3.2-45) through (3.2-47) is referred to as the performance measure of the receiver illustrated in Figure 6 by Van Trees<sup>12</sup> since the error performance of this receiver (whether it is optimal or not) is given by:

$$P_D = P_F^{1/(1+\Delta)} \quad (3.3-8)$$

Therefore, in the important case of Gaussian statistics, maximizing the SIR ( $\Delta$ ) is equivalent to maximizing the probability of detection for a given probability of false alarm in a Neyman-Pearson test.<sup>20</sup>

The second case to be considered in this section is the detection of a slowly fluctuating point target return in the presence of both reverberation and noise. Let us make the same assumptions that were made in the first case, and in addition, let us also assume that the reverberation return  $\tilde{y}_{\text{REV}}(t)$  is Gaussian, zero-mean, and uncorrelated (statistically independent) with both  $\tilde{y}_{\text{TRGT}}(t)$  and  $\tilde{n}(t)$ . Then, with the above assumptions, the test given by Equation (3.2-32) is optimal if the processing waveform  $\tilde{g}(t)$  satisfies the following integral equation:<sup>12</sup>

$$\int_{-\infty}^{\infty} R_{\tilde{y}_{\text{REV}}}(t, t') \tilde{g}(t') dt' + N_0 \tilde{g}(t) = \tilde{s}(t) \quad -\infty < t < \infty, \quad (3.3-10)$$

where

$$\tilde{s}(t) = \tilde{x}(t - \tau') \exp(+j2\pi\phi't) \quad (3.3-1)$$

and  $\tau'$  and  $\phi'$  are assumed to be known constants as before. The receiver specified by Equations (3.2-32) and (3.3-10) is the optimal, maximum likelihood receiver for detecting a slowly fluctuating point target return in the presence of colored Gaussian noise. The specification of  $\tilde{g}(t)$  as the solution of Equation (3.3-10) is equivalent to processing  $\tilde{r}(t)$  with a matched filter designed for colored noise and matched to  $\tilde{s}(t)$ .

Because of the assumption of Gaussian statistics, the error performance of this receiver is given by Equation (3.3-8), where the performance measure  $\Delta$  is equal to:

$$\Delta = \text{SIR} = \frac{E\{|\tilde{b}|^2\} |\chi_{\tilde{x}\tilde{g}}(\tau', \phi')|^2}{\int_{-\infty}^{\infty} \int_{-\infty}^{\infty} R_{S_{\text{REV}}}(\tau, \phi) |\chi_{\tilde{x}\tilde{g}}(\tau, \phi)|^2 d\tau d\phi + N_0 \int_{-\infty}^{\infty} |\tilde{g}(t)|^2 dt} \quad (3.2-51)$$

Note that in the presence of reverberation, the performance measure (SIR) given by Equation (3.2-51) is dependent upon the shape of  $\tilde{x}(t)$  via the cross-ambiguity function  $\chi_{\tilde{x}\tilde{g}}(\tau, \phi)$ . Since reverberation is caused by the scattering of the transmit signal, Equation (3.2-51) cannot be maximized by arbitrarily increasing the transmit energy. Increasing the transmit energy will increase both the target and reverberation returns. However,  $\Delta$  can be maximized by proper signal design via  $\chi_{\tilde{x}\tilde{g}}(\tau, \phi)$ .

3.3.2 Sub-optimum receiver for detecting a slowly fluctuating point target. In this section, we will consider the problem of detecting a slowly fluctuating point target return in the presence of both reverberation and noise by processing  $\tilde{r}(t)$  with  $\tilde{g}(t)$  as given by Equation (3.3-2). This is equivalent to using a matched filter which was designed for white noise only, to detect a point target return in colored noise.

If we make the usual assumptions regarding  $\tilde{y}_{\text{TRGT}}(t)$ ,  $\tilde{y}_{\text{REV}}(t)$ , and  $\tilde{n}(t)$  (including Gaussian statistics) as was done in the previous section, then it is clear that the test given by Equation (3.2-32) will not be optimal for our choice of  $\tilde{g}(t)$ ; namely,  $\tilde{g}(t)$  as given by Equation (3.3-2). However, because of the assumption of Gaussian statistics, the error performance of this sub-optimum receiver can be computed and is given by Equation (3.3-8), where an expression for  $\Delta$  which reflects our choice for  $\tilde{g}(t)$  will be obtained next.

If Equation (3.3-2) is substituted into Equation (3.2-43), then it can be shown that:

$$|\chi_{\tilde{x}\tilde{g}}(\tau, \phi)|^2 = |\chi_{\tilde{x}}(\tau' - \tau, \phi - \phi')|^2, \quad (3.3-11)$$

where

$$\chi_{\tilde{x}}(\tau, \phi) = \int_{-\infty}^{\infty} \tilde{x}(t) \tilde{x}^*(t - \tau) \exp(+j2\pi\phi t) dt \quad (3.3-12)$$

is the auto-ambiguity function of the transmit complex envelope  $\tilde{x}(t)$ . Substituting Equations (3.3-3), (3.3-5), and (3.3-11) into Equation (3.2-51) yields the desired result (e.g., see Van Trees<sup>12</sup>):



$$\Delta = \text{SIR} = \frac{E\{|\xi|^2\}}{\int_{-\infty}^{\infty} \int R_{S_{\text{REV}}}(\tau, \phi) |\psi_{\tilde{x}}(\tau' - \tau, \phi - \phi')|^2 d\tau d\phi + (N_o/E_{\tilde{x}})} \quad (3.3-13)$$

or

$$\Delta = \text{SIR} = \frac{E\{|\xi|^2\}}{R_{S_{\text{REV}}}(\tau, \phi) ** |\psi_{\tilde{x}}(\tau, -\phi)|^2 + (N_o/E_{\tilde{x}})}, \quad (3.3-14)$$

where the double asterisk means perform a two-dimensional convolution, and

$$\psi_{\tilde{x}}(\tau, \phi) = \chi_{\tilde{x}}(\tau, \phi) / E_{\tilde{x}} \quad (3.3-15)$$

is the normalized auto-ambiguity function such that  $|\psi_{\tilde{x}}(0, 0)| = 1$ .

Although  $\tilde{g}(t)$  as given by Equation (3.3-2) is not the optimal processing waveform to use in this case, it does have its advantages. As Van Trees<sup>12</sup> indicates, (1) it is simpler than the optimum  $\tilde{g}(t)$ , which is the solution of Equation (3.3-10), and (2) the autocorrelation function of the reverberation return  $R_{y_{\text{REV}}}(t, t')$  may not be known exactly a priori, so that the optimum solution for  $\tilde{g}(t)$  cannot be obtained anyway. Besides, since the performance measure  $\Delta$  of the sub-optimum receiver is known [see Equation (3.3-13)], it can be maximized by proper signal design. For example, suppose that  $\tilde{x}(t)$  was designed in such a way that the two-dimensional convolution integral appearing in Equation (3.3-13) was minimized. Then,  $\Delta$  would approach

Equation (3.3-9), which would be the maximum value that  $\Delta$  could attain in this case.

It is worth mentioning that, although  $R(t, t')$  may not be known exactly a priori, it can be learned in real time by using an appropriate adaptive signal processing scheme. Therefore, it is theoretically possible then to solve for the optimum  $\tilde{g}(t)$  in real time.

### 3.3.3 Sub-optimum receiver for detecting a doubly spread target.

The receiver illustrated in Figure 6 is not an optimal receiver for detecting a doubly spread target.<sup>12</sup> However, if the usual assumptions are made, i.e., that  $\tilde{y}_{\text{TRGT}}(t)$ ,  $\tilde{y}_{\text{REV}}(t)$ , and  $\tilde{n}(t)$  are Gaussian, zero-mean, and uncorrelated (statistically independent) with one another, and that  $\tilde{n}(t)$  is white, then, the error performance of this sub-optimum receiver in detecting a doubly spread target is known and is given by:

$$P_D = P_F^{1/(1+\Delta)}, \quad (3.3-8)$$

where

$$\Delta = \text{SIR} = \frac{\int_{-\infty}^{\infty} \int_{-\infty}^{\infty} R_{S_{\text{TRGT}}}(\tau, \phi) |\chi_{\tilde{xg}}(\tau, \phi)|^2 d\tau d\phi}{\int_{-\infty}^{\infty} \int_{-\infty}^{\infty} R_{S_{\text{REV}}}(\tau, \phi) |\chi_{\tilde{xg}}(\tau, \phi)|^2 d\tau d\phi + N_0 \int_{-\infty}^{\infty} |\tilde{g}(t)|^2 dt} \quad (3.2-44)$$

As was mentioned previously, the use of a sub-optimum receiver is not necessarily a hindrance since the performance measure, as given

by Equation (3.2-44), can be maximized by proper design of both  $\tilde{x}(t)$  and  $\tilde{g}(t)$ . And when  $\Delta$  is maximized, the probability of detection is maximized.

DeLong and Hofstetter<sup>19</sup> suggest that using the receiver illustrated in Figure 6 and designing  $\tilde{x}(t)$  and  $\tilde{g}(t)$  so that the SIR is maximized may well be a reasonable thing to do even in the case of non-Gaussian statistics. Of course, in the case of non-Gaussian statistics, the error performance of the receiver is no longer given by Equation (3.3-8).

It should be mentioned that Van Trees<sup>12</sup> gives a discussion on the optimum receiver to use for detecting a doubly spread target when  $\tilde{y}(t) = 0$ . In addition, a discussion on the detection of doubly spread radar astronomy targets is given by Price.<sup>21</sup>

From Equation (3.2-44), it can be seen that in order to maximize the SIR for a doubly spread target, one must be able to specify both the target and reverberation scattering functions. In general, the reverberation return is a composite of volume, surface, and bottom reverberation returns. However, only two kinds of reverberation will be considered in this dissertation; namely, volume and surface reverberation. In Chapter IV, both a volume reverberation and target scattering function will be derived, and in Chapter V, a surface reverberation scattering function will be derived.

## CHAPTER IV

### VOLUME REVERBERATION AND TARGET SCATTERING FUNCTIONS

#### 4.1 Introduction

Both the volume reverberation and target scattering functions are derived in this chapter.

Volume reverberation is modelled as the scattered acoustic pressure field from randomly distributed discrete point scatterers in deterministic plus random translational motion. The point scatterers are distributed in space according to an arbitrary volume density function with dimensions of number of scatterers per unit volume.

The autocorrelation function of the random, time-varying transfer function representing the volume reverberation communication channel is derived for a bistatic transmit/receive planar array geometry. A single scattering approximation is used and frequency dependent attenuation of sound pressure amplitude due to absorption is included. The scattered fields from different regions within the scattering volume are assumed to be uncorrelated. The volume reverberation scattering function is then obtained from the autocorrelation function via a two-dimensional Fourier transformation. The probability density function of random Doppler shift due to the random motion of the scatterers is also derived. In addition, an expression for the average received energy from volume reverberation is computed from the volume reverberation scattering function. Using several simplifying

assumptions, it is shown to reduce to the sonar equation for reverberation level.

The doubly spread target is modelled as a linear array of discrete highlights in deterministic translational motion. Recall that a doubly spread target is one whose return signal exhibits a spread in both round-trip time delay and Doppler. The target scattering function is obtained from the monostatic form of the volume reverberation scattering function by appropriately specifying the volume density function of the scatterers.

Computer simulation results for both volume reverberation and target scattering functions are presented as examples involving a monostatic transmit/receive array geometry. The volume reverberation scattering function predicts frequency spreading as a function of both beam tilt angle and random motion of the discrete point scatterers. Also predicted is a time spread and/or contraction as a function of Doppler shift. The target scattering function also predicts a spread in Doppler values and a time spread and/or contraction as a function of Doppler shift. Computer plots of the probability density function of the random Doppler shift are also presented for a monostatic geometry as a function of the standard deviation of the random motion of the scatterers.

#### 4.2 Volume Reverberation Scattering Function

In order to derive a mathematical expression for the volume reverberation scattering function  $R_{S,REV}(\tau, \phi)$ , the corresponding time-frequency correlation function  $R_{H,REV}(\Delta f, \Delta t)$  will be computed first. The scattering function will then be obtained from  $R_{H,REV}(\Delta f, \Delta t)$  via

the two-dimensional Fourier transform relationship given by Equation (2.3-51).

Volume reverberation is a result of the scattering of energy by the inherent inhomogeneities in the ocean medium (e.g., fish, bubbles, zooplankton, etc.) and its changing index of refraction.<sup>17,22</sup> In the analysis which follows, volume reverberation will be represented as the scattered field from a random distribution of discrete point scatterers which are distributed in space according to an arbitrary volume density function.<sup>10</sup> It is assumed that the particles are undergoing translational motion. A single scattering approximation is used throughout the analysis.

We begin by considering the physical situation depicted by Figure 7 and computing the scattered field at the receive array due to a single particle. Note that both the transmit and receive planar arrays are in a bistatic configuration and both are assumed not to be in motion. When transmission in the direction  $\hat{n}_T$  begins at  $t = 0$ , the range of the particle from the transmit array in the direction  $\hat{n}_T$  is equal to  $R_{o_T}$ . Similarly, the range of the particle from the receive array in the direction  $-\hat{n}_R$  at  $t = 0$  is equal to  $R_{o_R}$ . Both  $\hat{n}_T$  and  $\hat{n}_R$  are unit vectors. The particle's motion is described by the time-varying translational velocity vector  $\vec{V}(t)$ . Therefore, the range of the particle from the transmit array at any time  $t$ , in the direction  $\hat{n}_T$ , is given by:

$$R_T(t) = R_{o_T} + \int_0^t \vec{V}(t) \cdot \hat{n}_T dt \quad (4.2-1)$$

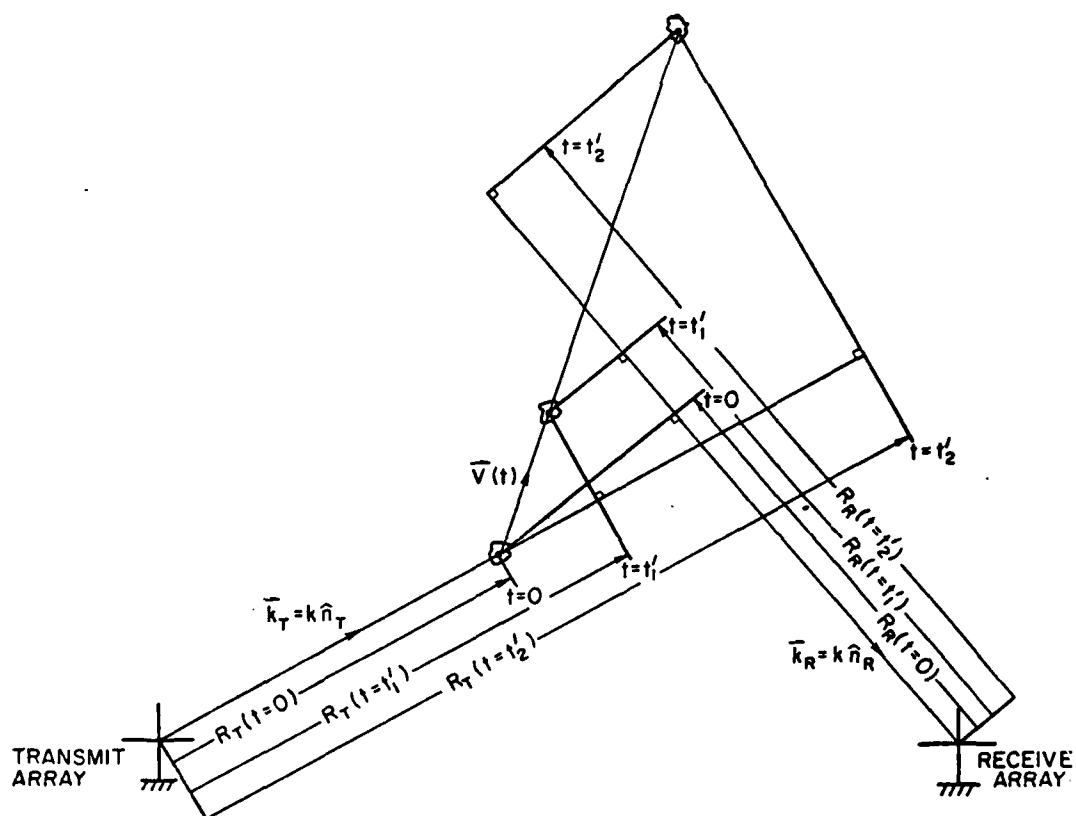


Figure 7. Geometry for calculation of scattered field from a single particle undergoing translational motion.

and, similarly, the range of the particle from the receive array at any time  $t$ , in the direction  $-\hat{n}_R$ , is:

$$R_R(t) = R_{O_R} + \int_0^t \vec{V}(t) \cdot (-\hat{n}_R) dt \quad (4.2-2)$$

Assume that a unit amplitude, time-harmonic signal is transmitted and that the moving particle is in the far-field region of both the transmit and receive arrays. At some time instant, say  $t = t'_1$ , the time-harmonic signal transmitted in the direction  $\hat{n}_T$  is incident upon the particle and some power is scattered towards the receive array in the direction  $\hat{n}_R$ . The scattered acoustic pressure field begins to appear at the output of the receive array at time  $t_1$ , where

$$t_1 = t'_1 + \frac{R_R(t'_1)}{c} \quad (4.2-3)$$

where  $c$  is the speed of sound (in m/sec) in the medium and is assumed to be constant. The output at time  $t_1$  is given by [see Equation (3.2-18)]:

$$y(t_1) = \text{Re} \{ H(f, t_1) \exp(+j2\pi f t_1) \} \quad (4.2-4)$$

where

$$H(f, t_1) = D_T(k_{x_T}, k_{y_T}) g(\hat{n}_R, \hat{n}_T, f) D_R(k_{x_R}, k_{y_R}) \cdot$$

$$\frac{\exp[-jkR_T(t'_1)]}{R_T(t'_1)} \exp[-\alpha_T(f)R_T(t'_1)] \cdot$$

$$\frac{\exp[-jkR_R(t'_1)]}{R_R(t'_1)} \exp[-\alpha_R(f)R_R(t'_1)] \quad (4.2-5)$$



when the transmit signal  $x(t) = \text{Re}\{\exp(+j2\pi ft)\}$  .

Equation (4.2-5) is the random, time-varying, transfer function of the communication channel corresponding to the physical situation of a single particle in translational motion for a bistatic transmit/receive array configuration. The term  $j = \sqrt{-1}$  and  $t'_1$  is the retarded time given by:

$$t'_1 = t_1 - \frac{R_R(t'_1)}{c} \quad (4.2-6)$$

The expressions  $D_T$  and  $D_R$  are the far-field directivity patterns of the transmit and receive arrays, respectively. The far-field directivity pattern of an acoustic planar array is given by the two-dimensional Fourier transform of the spatial distribution of normal driving velocity, say  $v(x,y)$  ; i.e.,

$$D(k_x, k_y) = \iint_R v(x,y) \exp[+j(k_x x + k_y y)] dx dy \quad (4.2-7)$$

when the baffle surrounding the active region  $R$  is assumed to be rigid.<sup>23</sup> The far-field radiated acoustic pressure field at a point  $(x,y,z)$  with corresponding spherical coordinates  $(r,\theta,\psi)$  is (see Morse and Ingard<sup>23</sup>):

$$p(x,y,z) \approx j\rho_0 f D(k_x, k_y) \exp(-jkr)/r ,$$

where  $r = (x^2 + y^2 + z^2)^{1/2}$ ,  $\rho_0$  is the ambient density of the medium, and the  $x$  and  $y$  components of the wave number  $k$  are given by:

$$k_x = k \sin\theta \cos\psi = ku \quad (4.2-8)$$

and

$$k_y = k \sin\theta \sin\psi = kv, \quad (4.2-9)$$

where

$$k = \frac{2\pi f}{c} = \frac{2\pi}{\lambda}. \quad (4.2-10)$$

The terms  $u = \sin\theta \cos\psi$  and  $v = \sin\theta \sin\psi$  are the direction cosines with respect to the positive  $x$  and  $y$  axes, respectively. Note that Equation (4.2-7) is also a valid expression for (1) the far-field directivity pattern of an electromagnetic planar array (antenna) when  $v(x,y)$  corresponds to a two-dimensional current distribution,<sup>24</sup> and (2) the Fraunhofer diffraction pattern of an aperture distribution  $v(x,y)$  in optics.<sup>25,26</sup> The expressions  $\alpha_T$  and  $\alpha_R$  are the frequency dependent amplitude attenuation coefficients due to sound absorption, with units of nepers/meter, along the transmit and receive paths, respectively.

The function  $g(\hat{n}_R, \hat{n}_T, f)$  is referred to as the scattering amplitude function.<sup>10</sup> It represents the random far-field amplitude of the scattered wave in the direction  $\hat{n}_R$  when the particle is illuminated (insonified) by a unit amplitude plane wave propagating in the direction  $\hat{n}_T$ . Thus, at large distances from the particle,<sup>10,23</sup>

$$g(\hat{n}_R, \hat{n}_T, f) = \frac{k^2}{4\pi} \int_{V_o} [\gamma_K(\vec{r}_o) p(\vec{r}_o) + j\gamma_\rho(\vec{r}_o) \frac{\hat{n}_R}{k} \cdot \nabla_o p(\vec{r}_o)] \cdot \exp(+jk\hat{n}_R \cdot \vec{r}_o) dV_o, \quad (4.2-11)$$

where  $\gamma_K(\vec{r}_o) = [K_e(\vec{r}_o) - K_o]/K_o$  and  $\gamma_\rho(\vec{r}_o) = [\rho_e(\vec{r}_o) - \rho_o]/\rho_e(\vec{r}_o)$ . The particle occupies a volume  $V_o$ , where  $K_e$  and  $\rho_e$  are the

compressibility and density, respectively, inside the particle, and  $K_o$  and  $\rho_o$  are the compressibility and density of the surrounding medium. The term  $p(\vec{r}_o)$  is the actual pressure field within  $V_o$ . Depending upon the physical situation, Equation (4.2-11) can be simplified by using the Rayleigh, Born, or WKB approximation.<sup>10</sup>

In order to simplify Equation (4.2-5), assume that the velocity of the particle is constant during the time it is insonified, i.e.,  $\vec{V}(t) = \vec{V}$  and that

$$R_{o_T} \gg \int_0^{t'_1} \vec{V}(t) \cdot \hat{n}_T dt \quad (4.2-12)$$

and

$$R_{o_R} \gg \int_0^{t'_1} \vec{V}(t) \cdot (-\hat{n}_R) dt \quad (4.2-13)$$

Also assume that  $\alpha_T(f) = \alpha_R(f) = \alpha(f)$ . Therefore, upon using these assumptions [Equations (4.2-12) and (4.2-13) are only used in simplifying the denominator], Equation (4.2-5) reduces to:

$$H(f, t_1) = F(f) \frac{\exp \{-jk_{EFF}[R_{o_T} + R_{o_R} + (\hat{n}_T - \hat{n}_R) \cdot \vec{V}t'_1]\}}{R_{o_T} R_{o_R}}, \quad (4.2-14)$$

where

$$t'_1 = \left[ t_1 - \frac{R_{o_R}}{c} \right] / \left[ 1 - \frac{\vec{V} \cdot \hat{n}_R}{c} \right], \quad (4.2-15)$$

$$F(f) \triangleq D_T(k_{x_T}, k_{y_T}) g(\hat{n}_R, \hat{n}_T, f) D_R(k_{x_R}, k_{y_R}) \quad (4.2-16)$$

and  $k_{\text{EFF}}$  is the complex effective wave number defined by:

$$k_{\text{EFF}} \triangleq k - j\alpha(f) = \frac{2\pi f}{c} - j\alpha(f) \quad (4.2-17)$$

Next, consider the problem of calculating  $H(f,t)$  when several moving particles occupy an elemental volume  $dV$ . The problem is illustrated in Figure 8 where it has been assumed that only three particles occupy  $dV$  for example purposes. Assuming that the transmission and scattering processes are linear, the principle of superposition is used to express the complex envelope of the output field (reverberation return) as:

$$H_{\text{REV}}(f, t_1) = H_1(f, t_1) + H_2(f, t_1) + H_3(f, t_1) \quad (4.2-18)$$

where  $H_1$ ,  $H_2$ , and  $H_3$  represent the complex envelopes of the individual output fields due to the scattering of the transmit signal  $x(t) = \text{Re}\{\exp(+j2\pi ft)\}$  from each of the three moving particles.

Using Equation (4.2-18), the autocorrelation function

$$R_{H_{\text{REV}}}(f_1, f_2, t_1, t_2) = E\{H_{\text{REV}}(f_1, t_1)H_{\text{REV}}^*(f_2, t_2)\} \quad (4.2-19)$$

is equal to:

$$\begin{aligned} R_{H_{\text{REV}}}(f_1, f_2, t_1, t_2) &= E\{H_1(f_1, t_1)H_1^*(f_2, t_2)\} + \\ &\quad E\{H_2(f_1, t_1)H_2^*(f_2, t_2)\} + \\ &\quad E\{H_3(f_1, t_1)H_3^*(f_2, t_2)\} \end{aligned} \quad (4.2-20)$$

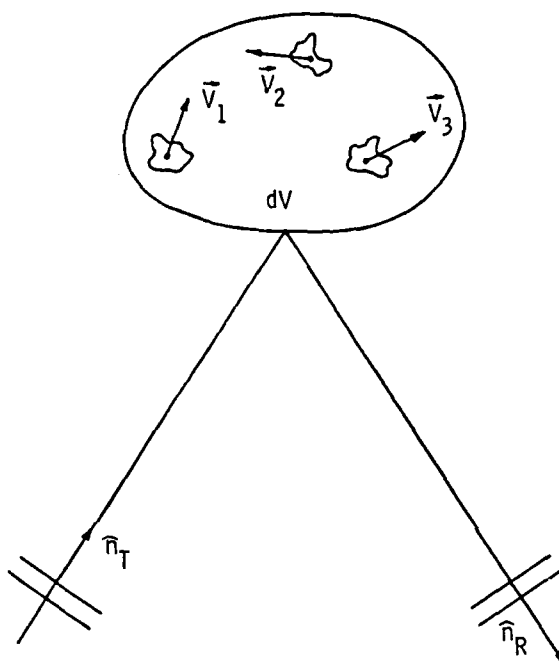


Figure 8. Scatter in the direction  $\hat{n}_R$  from several moving particles occupying an elemental volume  $dV$  when insonified in the direction  $\hat{n}_T$ .

AD-A105 593 PENNSYLVANIA STATE UNIV UNIVERSITY PARK APPLIED RESE--ETC F/G 20/1  
A SCATTERING FUNCTION APPROACH TO UNDERWATER ACOUSTIC DETECTION--ETC(U)  
OCT 81 L J ZIOMEK. N00024-79-C-6043  
UNCLASSIFIED ARL/PSU/TM-81-14 NL

AD-A105 593 PENNSYLVANIA STATE UNIV UNIVERSITY PARK APPLIED RESE--ETC F/G 20/1  
A SCATTERING FUNCTION APPROACH TO UNDERWATER ACOUSTIC DETECTION--ETC(U)  
OCT 81 L J ZIOMEK. N00024-79-C-6043  
UNCLASSIFIED ARL/PSU/TM-81-14 NL

AD-A105 593 PENNSYLVANIA STATE UNIV UNIVERSITY PARK APPLIED RESE--ETC F/G 20/1  
A SCATTERING FUNCTION APPROACH TO UNDERWATER ACOUSTIC DETECTION--ETC(U)  
OCT 81 L J ZIOMEK. N00024-79-C-6043  
UNCLASSIFIED ARL/PSU/TH-81-14 NL

AD-A105 593 PENNSYLVANIA STATE UNIV UNIVERSITY PARK APPLIED RESE--ETC F/G 20/1  
A SCATTERING FUNCTION APPROACH TO UNDERWATER ACOUSTIC DETECTION--ETC(U)  
OCT 81 L J ZIOMEK. N00024-79-C-6043  
UNCLASSIFIED ARL/PSU/TM-81-14 NL

AD-A105 593 PENNSYLVANIA STATE UNIV UNIVERSITY PARK APPLIED RESE--ETC F/G 20/1  
A SCATTERING FUNCTION APPROACH TO UNDERWATER ACOUSTIC DETECTION--ETC(U)  
OCT 81 L J ZIOMEK. N00024-79-C-6043  
UNCLASSIFIED ARL/PSU/TM-81-14 NL

AD-A105 593 PENNSYLVANIA STATE UNIV UNIVERSITY PARK APPLIED RESE--ETC F/G 20/1  
A SCATTERING FUNCTION APPROACH TO UNDERWATER ACOUSTIC DETECTION--ETC(U)  
OCT 81 L J ZIOMEK. N00024-79-C-6043  
UNCLASSIFIED ARL/PSU/TM-81-14 NL

AD-A105 593 PENNSYLVANIA STATE UNIV UNIVERSITY PARK APPLIED RESE--ETC F/G 20/1  
A SCATTERING FUNCTION APPROACH TO UNDERWATER ACOUSTIC DETECTION--ETC(U)  
OCT 81 L J ZIOMEK. N00024-79-C-6043  
UNCLASSIFIED ARL/PSU/TM-81-14 NL

AD-A105 593 PENNSYLVANIA STATE UNIV UNIVERSITY PARK APPLIED RESE--ETC F/G 20/1  
A SCATTERING FUNCTION APPROACH TO UNDERWATER ACOUSTIC DETECTION--ETC(U)  
OCT 81 L J ZIOMEK. N00024-79-C-6043  
UNCLASSIFIED ARL/PSU/TM-81-14 NL

or

$$R_{H_{REV}}(f_1, f_2, t_1, t_2) = R_{H_1}(f_1, f_2, t_1, t_2) + R_{H_2}(f_1, f_2, t_1, t_2) + R_{H_3}(f_1, f_2, t_1, t_2) \quad , \quad (4.2-21)$$

where it has been assumed that

$$E\{H_i(f_1, t_1)H_j^*(f_2, t_2)\} = R_{H_i}(f_1, f_2, t_1, t_2)\delta_{ij} \quad ; \quad i, j = 1, 2, 3 \quad , \quad (4.2-22)$$

where

$$\delta_{ij} = \begin{cases} 1, & i = j \\ 0, & i \neq j \end{cases} \quad (4.2-23)$$

is the Kronecker delta. Equation (4.2-22) indicates that the scattered fields from different individual particles occupying the elemental volume  $dV$  are assumed to be uncorrelated.<sup>10</sup>

In general, each term on the right-hand side of Equation (4.2-21) will not be equal to one another since each particle can have (1) a different scattering amplitude function  $g_i(\hat{n}_R, \hat{n}_T, f)$  for  $i = 1, 2, 3$ ; (2) a different constant translational velocity vector  $\vec{V}_i$  for  $i = 1, 2, 3$ ; and (3) different initial ranges  $(R_{o_T})_i$  and  $(R_{o_R})_i$  for  $i = 1, 2, 3$  which together with the different velocity vectors yields different values for the retarded times  $t'_1$  and  $t'_2$  [see Equations (4.2-14) through (4.2-17)]. However, if it is assumed that the three properties described above are identical for all particles occupying  $dV$ , then Equation (4.2-21) can be rewritten as:

$$R_{H_{REV}}(f_1, f_2, t_1, t_2) = R_H(f_1, f_2, t_1, t_2) \rho_V dV, \quad (4.2-24)$$

where  $\rho_V$  is the volume density function of the point scatterers (number of scatterers per unit volume) and  $R_{H_1} = R_{H_2} = R_{H_3} = R_H$ . Next, integrate the right-hand side of Equation (4.2-24) over the scattering volume which is common to both the transmit and receive arrays, i.e.,

$$\begin{aligned} R_{H_{REV}}(f_1, f_2, t_1, t_2) &= \int_V R_H(f_1, f_2, t_1, t_2) \rho_V dV \\ &= \int_V E\{H(f_1, t_1) H^*(f_2, t_2)\} \rho_V dV. \end{aligned} \quad (4.2-25)$$

Upon substituting Equation (4.2-14) into Equation (4.2-25) and performing the indicated operations, it can be shown that:

$$\begin{aligned} R_{H_{REV}}(f_1, f_2, t_1, t_2) &= \int_V E\{F(f_1) F^*(f_2)\} \cdot \\ &\quad E\{\exp(-j[(\hat{n}_T - \hat{n}_R) \cdot \vec{V}][k_{EFF_1} t_1' - k_{EFF_2}^* t_2'])]\} \cdot \\ &\quad \exp\{-[\alpha(f_1) + \alpha(f_2)][R_{o_T} + R_{o_R}]\} \cdot \\ &\quad \exp\{-j2\pi \frac{(R_{o_T} + R_{o_R})}{c} (f_1 - f_2)\} \cdot \\ &\quad \frac{\rho_V}{R_{o_T}^2 R_{o_R}^2} dV, \end{aligned} \quad (4.2-26)$$

where  $V$  is the scattering volume common to both arrays and



$$E\{F(f_1)F^*(f_2)\} = D_T(k_{1u_T}, k_{1v_T})D_T^*(k_{2u_T}, k_{2v_T}) \cdot$$

$$E\{g(\hat{n}_R, \hat{n}_T, f_1)g^*(\hat{n}_R, \hat{n}_T, f_2)\} \cdot$$

$$D_R(k_{1u_R}, k_{1v_R})D_R^*(k_{2u_R}, k_{2v_R}) , \quad (4.2-27)$$

$$k_i = \frac{2\pi f_i}{c} ; \quad i = 1, 2 , \quad (4.2-28)$$

$$k_{EFF_1} = k_1 - j\alpha(f_1) \quad (4.2-29)$$

and

$$k_{EFF_2}^* = k_2 + j\alpha(f_2) \quad (4.2-30)$$

The derivation of Equation (4.2-26) was based upon the assumption that the scattered fields from different spatial locations within  $V$  are uncorrelated. For simplicity, all particles within the common scattering volume  $V$  are assumed to have the same scattering amplitude function  $g(\hat{n}_R, \hat{n}_T, f)$  and velocity vector  $\vec{V}$ . Otherwise, they would have to be shown as functions of position. Note, however,  $g(\hat{n}_R, \hat{n}_T, f)$  is still a function of geometry because of its dependence upon  $\hat{n}_T$  and  $\hat{n}_R$ .

Next, replace  $f_1$  and  $f_2$  with  $f + f_c$  and  $f' + f_c$ , respectively, where  $f_c$  is the center or carrier frequency of the bandpass transmit signal. Upon substituting Equation (4.2-15) for  $t_1'$  and an analogous expression for  $t_2'$  into Equation (4.2-26) and expanding, the following general expression for the autocorrelation function is obtained:

$$\begin{aligned}
R_{H_{REV}}(f+f_c, f'+f_c, t_1, t_2) &= \int_V E\{F(f+f_c)F^*(f'+f_c)\} \cdot \\
&E \left\{ \exp \left\{ -j2\pi[(f+f_c)t_1 - (f'+f_c)t_2] \left[ \frac{(\hat{n}_T - \hat{n}_R) \cdot \vec{V}}{c - \vec{V} \cdot \hat{n}_R} \right] \right\} \right. \\
&\exp \left\{ +j2\pi(f-f') \left[ \frac{(\hat{n}_T - \hat{n}_R) \cdot \vec{V}}{c - \vec{V} \cdot \hat{n}_R} \frac{R_{OR}}{c} \right] \right\} \cdot \\
&\exp \left\{ - \left[ \alpha(f+f_c) \left( t_1 - \frac{R_{OT}}{c} \right) + \alpha(f'+f_c) \left( t_2 - \frac{R_{OR}}{c} \right) \right] \right. \\
&\left. \left[ \frac{(\hat{n}_T - \hat{n}_R) \cdot \vec{V}}{1 - \frac{\vec{V} \cdot \hat{n}_R}{c}} \right] \right\} \cdot \\
&\exp \left\{ - \left[ \alpha(f+f_c) + \alpha(f'+f_c) \right] (R_{OT} + R_{OR}) \right\} \cdot \\
&\exp \left\{ - j2\pi \frac{(R_{OT} + R_{OR})}{c} (f-f') \right\} \frac{\rho_V}{R_{OT}^2 R_{OR}^2} dV \cdot
\end{aligned}
\tag{4.2-31}$$

Ishimaru<sup>10</sup> refers to the autocorrelation function of the random, time-varying transfer function  $R_H(f, f', t, t') = E\{H(f, t)H^*(f', t')\}$  as the two-frequency correlation function or the two-frequency mutual coherence function. The expression  $R_H(f, f', t, t')$  is equal to the correlation which exists between the complex envelopes of the output fields  $H(f, t)$  and  $H(f', t')$  at two different times ( $t$  and  $t'$ ) due to the application of time-harmonic input fields at two different frequencies ( $f$  and  $f'$ ). If two time-harmonic waves are transmitted

at the same frequency  $f$  and the resulting output fields are observed at two different times  $t$  and  $t'$ , the correlation between the output fields decreases as the time difference  $\Delta t = t - t'$  increases.<sup>10</sup> The value of the time difference  $\Delta t$  at which the correlation function  $R_H(f, f, t, t') = E\{H(f, t)H^*(f, t')\}$  is approximately equal to zero or decreases to a specified level is called the coherence time.<sup>10</sup> It is a measure of the correlation which exists between the output fields at two different times at the same frequency. The reciprocal of the coherence time is equal to the frequency spectrum broadening a wave will undergo as it propagates in a random, time-varying medium.<sup>10</sup>

Similarly, if two time-harmonic waves are transmitted at two different frequencies  $f$  and  $f'$  and the resulting output fields are observed at the same time  $t$ , the correlation between the two output fields decreases as the frequency difference  $\Delta f = f - f'$  increases.<sup>10</sup> The value of the frequency difference  $\Delta f$  at which the correlation function  $R_H(f, f', t, t) = E\{H(f, t)H^*(f', t)\}$  is approximately equal to zero or decreases to a specified level is called the coherence bandwidth.<sup>10</sup> It is a measure of the correlation which exists between the output fields at two different frequencies at the same time. The reciprocal of the coherence bandwidth is equal to the time delay broadening a wave will undergo as it propagates in a random, time-varying medium.<sup>10</sup>

Therefore, both the coherence time and the coherence bandwidth, and hence, the spectrum broadening and time broadening associated with our model of volume reverberation can be computed from Equation (4.2-31).

Since Equation (4.2-31) is not a function of  $\Delta f = f - f'$  and  $\Delta t = t_1 - t_2$ , the volume reverberation scattering function cannot be obtained from it via Fourier transformation. However, if Equation (4.2-31) is substituted into Equation (3.2-20), a mathematical expression for  $R_y(t_1, t_2)$  can be obtained in terms of the pertinent system functions and geometry of the physical situation. Let us now investigate whether or not it is possible to reduce Equation (4.2-31) to a function of  $\Delta f$  and  $\Delta t$ .

As of yet, no distinction has been made between narrowband versus broadband bandpass transmit signals. However, it will be shown in the subsequent analysis that in order for the two-frequency correlation function to be wide-sense stationary in frequency, a narrowband transmit signal must be used. The condition of wide-sense stationarity in frequency does not hold for broadband transmission.<sup>7</sup> Therefore, assume that the transmit signal is indeed narrowband. Referring back to Equation (3.2-20) for a moment, one notices that the frequency variables  $f$  and  $f'$  are associated with the low pass spectrum of the complex envelope of the transmit signal. Therefore, as a consequence of the narrowband assumption, it is reasonable to assume that  $|f| \ll f_c$  and  $|f'| \ll f_c$  so that

$$E\{F(f + f_c)F^*(f' + f_c)\} \approx E\{|F(f_c)|^2\}, \quad (4.2-32)$$

$$\alpha(f + f_c) \approx \alpha(f_c) \quad (4.2-33)$$

and

$$\alpha(f' + f_c) \approx \alpha(f_c). \quad (4.2-34)$$

Substituting Equations (4.2-32) through (4.2-34) into Equation (4.2-31) yields:

$$R_{H_{REV}}(\Delta f, t_1, t_2) = \int_V E\{|F(f_c)|^2\} E\left\{\exp\left\{-j2\pi f_c(t_1 - t_2) \left[\frac{(\hat{n}_T - \hat{n}_R) \cdot \vec{V}}{c - \vec{V} \cdot \hat{n}_R}\right]\right\}\right\} \cdot$$

$$\exp\left\{+j2\pi \Delta f \left[\frac{(\hat{n}_T - \hat{n}_R) \cdot \vec{V}}{(c - \vec{V} \cdot \hat{n}_R)}\right] \frac{R_{OR}}{c}\right\} \cdot$$

$$\exp\left\{-\alpha(f_c) \left[(t_1 + t_2) - \frac{2R_{OR}}{c}\right] \left[\frac{(\hat{n}_T - \hat{n}_R) \cdot \vec{V}}{1 - (\vec{V} \cdot \hat{n}_R/c)}\right]\right\} \cdot$$

$$\exp\left\{-2\alpha(f_c) [R_{OT} + R_{OR}]\right\} \exp\left\{-j2\pi \frac{(R_{OT} + R_{OR})}{c} \Delta f\right\} \frac{\rho_V}{R_{OT}^2 R_{OR}^2} dV, \quad (4.2-35)$$

where  $\Delta f = f - f'$ . The two-frequency correlation function is still not a function of  $\Delta t = t_1 - t_2$  due to the presence of the term  $t_1 + t_2$  appearing in the third exponential factor, involving attenuation due to sound absorption.

Some additional observations are appropriate at this point in order to facilitate simplifying Equation (4.2-35). First of which is the fact that in our analysis problem, it will certainly be true that:

$$\frac{|\vec{V}|}{c} \ll 1 \quad (4.2-36)$$

Now, with regard to the significance of the third exponential factor appearing in the integrand of Equation (4.2-35) to attenuation, consider

the following order of magnitude argument. The time instants  $t_1$  and  $t_2$  correspond to the times at which signal returns are monitored at the receive array and are approximately equal to:

$$t_1 \approx \frac{R_{oT} + R_{oR}}{c} \quad (4.2-37)$$

and

$$t_2 \approx \frac{R_{oT} + R_{oR}}{c} + \delta t, \quad (4.2-38)$$

where  $\delta t$  is some relatively small time increment since it is assumed that  $t_2 > t_1$ . Therefore, using Equations (4.2-36) through (4.2-38), it can be shown that

$$\begin{aligned} & \exp \left\{ -\alpha(f_c) \left[ t_1 + t_2 - \frac{2R_{oR}}{c} \right] \left[ \frac{(\hat{n}_T - \hat{n}_R) \cdot \vec{V}}{\vec{V} \cdot \hat{n}_R} \right] \right\} \\ & \approx \exp \left\{ -\alpha(f_c) [2R_{oT} + c\delta t] (\hat{n}_T - \hat{n}_R) \cdot \frac{\vec{V}}{c} \right\} \end{aligned} \quad (4.2-39)$$

which is negligible compared to the attenuation due to

$$\exp \left\{ -\alpha(f_c) [2R_{oT} + 2R_{oR}] \right\}$$

and can therefore be ignored. Making use of these observations and assuming that  $\vec{V}$  can be expressed as the sum of a deterministic and random component, Equation (4.2-35) finally reduces to the desired result:

$$\begin{aligned}
R_{H,REV}(\Delta f, \Delta t) &= \int_V E \left\{ |F(f_c)|^2 \right\} \exp \left\{ -j2\pi \left[ \Delta t - \frac{\Delta f}{f_c} \frac{R_{oR}}{c} \right] \phi_{DET} \right\} \cdot \\
&\quad E \left\{ \exp \left\{ -j2\pi \left[ \Delta t - \frac{\Delta f}{f_c} \frac{R_{oR}}{c} \right] \phi_{RND} \right\} \right\} \cdot \\
&\quad \exp \left\{ -2\alpha(f_c) \left[ R_{oT} + R_{oR} \right] \right\} \cdot \\
&\quad \exp \left\{ -j2\pi \frac{\left( R_{oT} + R_{oR} \right)}{c} \Delta f \right\} \frac{\rho_V}{R_{oT}^2 R_{oR}^2} dV, \\
&\hspace{15em} (4.2-40)
\end{aligned}$$

where  $\phi_{DET}$  is the deterministic Doppler shift defined as:

$$\phi_{DET} \triangleq \frac{f_c (\hat{n}_T - \hat{n}_R) \cdot \vec{U}}{c}, \quad (4.2-41)$$

$\vec{U}$  being the deterministic component of the velocity vector  $\vec{V}$ , and  $\phi_{RND}$  is the random Doppler shift defined as:

$$\phi_{RND} \triangleq \frac{f_c (\hat{n}_T - \hat{n}_R) \cdot \vec{V}_f}{c} \quad (4.2-42)$$

$\vec{V}_f$  being the fluctuating or random component of  $\vec{V}$ . Note that the Doppler shifts  $\phi_{DET}$  and  $\phi_{RND}$  are functions of angle due to the presence of the inner product. For example, in the spherical coordinate system,  $\phi_{DET}$  is a function of the spherical angles  $(\theta, \psi)$ . And since the directivity functions  $D_T$  and  $D_R$  are also functions of  $(\theta, \psi)$ ,

different deterministic Doppler shifts are weighted differently by the beam patterns. Thus, a frequency spread will result because of the finite extent of the beamwidths of both the transmit and receive beam patterns. Now, if Equation (4.2-40) is substituted into Equation (2.3-51), one obtains the volume reverberation scattering function:

$$R_{S_{REV}}(\tau, \phi) = \int_V E\{|F(f_c)|^2\} p_{\phi_{RND}}(\phi + \phi_{DET}) \delta[\tau - \tau(\phi)] \cdot \exp\left\{-2\alpha(f_c) [R_{oT} + R_{oR}]\right\} \frac{\rho_V}{R_{oT}^2 R_{oR}^2} dV \quad (4.2-43)$$

which is a function of the time delay  $\tau$  (in sec) and the Doppler spread  $\phi$  (in Hz), where

$$\tau(\phi) \triangleq \tau_o + [(\phi R_{oR}) / (f_c c)] \quad , \quad (4.2-44)$$

$$\tau_o \triangleq (R_{oT} + R_{oR}) / c \quad (4.2-45)$$

and

$$E\{|F(f_c)|^2\} = |D_T(ku_T, kv_T)|^2 E\{|g(\hat{n}_R, \hat{n}_T, f_c)|^2\} \cdot |D_R(ku_R, kv_R)|^2 \quad , \quad (4.2-46)$$

where  $k = 2\pi f_c / c$  and  $p_{\phi_{RND}}(\cdot)$  is the probability density function of the random Doppler shift which is given by:

$$p_{\phi_{RND}}(\phi) = \left( \frac{c}{|\hat{n}_T - \hat{n}_R| f_c \sigma} \right)^3 \frac{\sqrt{2}}{\pi \sqrt{\pi}} \cdot \int_{|\phi|}^{\infty} \frac{x^2}{\sqrt{x^2 - \phi^2}} \exp\left\{-\frac{1}{2} \left( \frac{c}{|\hat{n}_T - \hat{n}_R| f_c \sigma} \right)^2 x^2\right\} dx; \quad |\phi| < x < \infty \quad (4.2-47)$$



where  $\sigma$  is the standard deviation of  $|\vec{V}_f|$ . Note that  $\tau(\phi)$  as defined by Equation (4.2-44) is not the round-trip time delay (see Appendix A and References 27-29). However, it is shown in Appendix A that the round-trip time delay can be obtained from  $\tau(\phi)$  by dividing it by the dimensionless scale factor  $[1 + (\phi/f_c)]$ . That is, the round-trip time delay is given by  $\tau(\phi)/[1 + (\phi/f_c)]$ .

The derivation of the probability density function of the random variable

$$\phi_{\text{RND}} \triangleq \frac{f_c (\hat{n}_T - \hat{n}_R) \cdot \vec{V}_f}{c} = \frac{f_c |\hat{n}_T - \hat{n}_R| |\vec{V}_f| \cos \xi}{c} \quad (4.2-48)$$

can be found in Appendix B and was based upon the assumptions that  $|\vec{V}_f|$  was Maxwell distributed, the angle  $\xi$  was uniformly distributed, and that the random variables  $|\vec{V}_f|$  and  $\cos \xi$  are statistically independent (use was made of References 30-32 in the derivation of the density function). The function  $E\{|g(\hat{n}_R, \hat{n}_T, f_c)|^2\} = \sigma_d(\hat{n}_R, \hat{n}_T, f_c)$  is referred to as the average differential scattering cross section of one of the point scatterers and has units of area.<sup>10,33,34</sup> The average bistatic radar cross section is equal to

$$4\pi E\{|g(\hat{n}_R, \hat{n}_T, f_c)|^2\} = 4\pi \sigma_d(\hat{n}_R, \hat{n}_T, f_c) \quad .$$

The volume reverberation scattering function given by Equation (4.2-43) predicts that the input signal's power will undergo both a frequency spread--via the transmit and receive beam patterns and the probability density function  $p_{\phi_{\text{RND}}}$ --and a time spread or contraction--via the scale factor  $1 + \phi/f_c$ . For a monostatic transmit/receive array geometry, let

$$R_{OT} = R_{OR} = r ,$$

$$u_T = u_R = u ,$$

$$v_T = v_R = v$$

(4.2-49)

and

$$\hat{n}_R = -\hat{n}_T ,$$

where  $u$  and  $v$  are the direction cosines with respect to the positive  $x$  and  $y$  axes, respectively.

In the case of a monostatic geometry, the average backscatter radar cross section of one of the point scatterers is equal to

$$4\pi E\{|g(-\hat{n}_T, \hat{n}_T, f_c)|^2\} = 4\pi\sigma_d(-\hat{n}_T, \hat{n}_T, f_c) .$$

The target strength of an individual point scatterer is given by:<sup>34</sup>

$$10 \log_{10} [\sigma_d(-\hat{n}_T, \hat{n}_T, f_c)/A_1] \text{dB re } A_1 , \quad (4.2-50)$$

where  $A_1 = 1 \text{ m}^2$  and  $\text{re}$  means "relative to." Thus, the target strength or volume reverberation backscattering strength is a decibel measure of the differential backscattering cross section.<sup>33,34</sup> The volume reverberation backscattering strength is dependent upon the type and density of scatterers per unit volume.<sup>33,34</sup> For example, the backscattering strength per unit volume is given by:<sup>34</sup>

$$10 \log_{10} [\rho_V \sigma_d(-\hat{n}_T, \hat{n}_T, f_c) R_1] \text{dB re } R_1 , \quad (4.2-51)$$

where  $\rho_V$  is the volume density of the scatterers and  $R_1$  is the reference distance, usually chosen to be 1 m.

As an example, the average received energy (in dB) from volume reverberation will be computed from the expression [see Equation (2.3-61)]

$$\bar{E}_y = E_x \int_{-\infty}^{\infty} \int R_{S_{REV}}(\tau, \phi) d\tau d\phi, \quad (4.2-52)$$

where  $\bar{E}_y$  is the average received energy,  $E_x$  is the transmit energy, and  $R_{S_{REV}}(\tau, \phi)$  is the volume reverberation scattering function given by Equation (4.2-43). For simplicity, assume a monostatic transmit/receive array geometry and no motion, i.e.,  $\phi_{DET} = \phi_{RND} = 0$  and as a result,  $p_{\phi_{RND}}(\phi + \phi_{DET}) = p_{\phi_{RND}}(\phi) \equiv \delta(\phi)$ . With these assumptions, Equation (4.2-43) becomes:

$$R_{S_{REV}}(\tau, \phi) = \int_V E\{|F(f_c)|^2\} \delta(\phi) \delta\left[\tau - \left(\frac{2r}{c} + \frac{\phi}{f_c} \frac{r}{c}\right)\right] \cdot \exp\{-4\alpha(f_c)r\} (\rho_V/r^4) dV \quad (4.2-53)$$

or

$$R_{S_{REV}}(\tau, \phi) = R_{S_{REV}}(\tau) \delta(\phi), \quad (4.2-54)$$

where

$$R_{S_{REV}}(\tau) = \int_V E\{|F(f_c)|^2\} \delta[\tau - (2r/c)] \exp\{-4\alpha(f_c)r\} (\rho_V/r^4) dV \quad (4.2-55)$$

and from Equations (4.2-46) and (4.2-49):

$$E\{|F(f_c)|^2\} = |D_T(ku, kv)|^2 \sigma_d(-\hat{n}_T, \hat{n}_T, f_c) |D_R(ku, kv)|^2. \quad (4.2-56)$$

Now, if Equation (4.2-54) is substituted into Equation (4.2-52), one obtains:

$$\bar{E}_y = E_x \int_{-\infty}^{\infty} R_{S_{REV}}(\tau) d\tau \quad (4.2-57)$$

and substituting Equation (4.2-55) into Equation (4.2-57) yields:

$$\bar{E}_y = E_x \int_V E\{|F(f_c)|^2\} \left[ \int_{-\infty}^{\infty} \delta[\tau - (2r/c)] d\tau \right] \exp\{-4\alpha(f_c)r\} (\rho_V/r^4) dV \quad (4.2-58)$$

or

$$\bar{E}_y = E_x \int_V E\{|F(f_c)|^2\} \exp\{-4\alpha(f_c)r\} (\rho_V/r^4) dV. \quad (4.2-59)$$

Next, assume a spherical coordinate system so that  $dV = r^2 \sin\theta dr d\theta d\psi$  and that  $\rho_V$  is not a function of position. In addition, assume that  $\sigma_d(-\hat{n}_T, \hat{n}_T, f_c)$  does not depend upon  $\hat{n}_T$ , i.e., assume that  $\sigma_d(-\hat{n}_T, \hat{n}_T, f_c)$  is omnidirectional and is equal to a constant. Therefore, with these assumptions, Equation (4.2-59) can be expressed as:

$$\bar{E}_y = E_x (\rho_V \sigma_d) \int_{r-(\Delta r/2)}^{r+(\Delta r/2)} (\exp\{-4\alpha(f_c)r\}/r^4) r^2 dr \cdot \int_{\theta=0}^{\pi/2} \int_{\psi=0}^{2\pi} |D_T(ku, kv)|^2 |D_R(ku, kv)|^2 \sin\theta d\theta d\psi \quad (4.2-60)$$

where  $u = \sin\theta \cos\psi$  and  $v = \sin\theta \sin\psi$ . If it is further assumed that the range interval  $\Delta r$  is negligible compared to  $r$ , then the integrand of the range integral is approximately constant so that:

$$\int_{r-(\Delta r/2)}^{r+(\Delta r/2)} (\exp\{-4\alpha(f_c)r\}/r^4)r^2 dr \approx [\exp\{-4\alpha(f_c)r\}r^{-4}](r^2\Delta r) \quad (4.2-61)$$

and as a result, Equation (4.2-60) simplifies to:

$$\bar{E}_y = E_x(\rho_V\sigma_d) [\exp\{-4\alpha(f_c)r\}r^{-4}](r^2\Delta r\psi) \quad , \quad (4.2-62)$$

where

$$\psi = \int_{\theta=0}^{\pi/2} \int_{\psi=0}^{2\pi} |D_T|^2 |D_R|^2 \sin\theta d\theta d\psi \quad . \quad (4.2-63)$$

Therefore, the average received energy from volume reverberation in decibels is:

$$\begin{aligned} 10 \log_{10} \bar{E}_y &= 10 \log_{10} E_x + 10 \log_{10}(\rho_V\sigma_d) - 40 \log_{10} r + \\ &\quad 10 \log_{10}[\exp\{-4\alpha(f_c)r\}] + 10 \log_{10}(r^2\Delta r\psi) \quad . \end{aligned} \quad (4.2-64)$$

Equation (4.2-64) is the sonar equation for volume reverberation level (e.g., see Urick<sup>33</sup>) since (1)  $10 \log_{10} E_x$  is the source level, (2)  $10 \log_{10}(\rho_V\sigma_d)$  is the volume reverberation backscattering strength per unit volume, (3)  $-40 \log_{10} r$  is the two-way transmission loss due to spherical spreading, (4)  $10 \log_{10}[\exp\{-4\alpha(f_c)r\}]$  is the two-way transmission loss due to sound absorption, and (5) the expression  $r^2\Delta r\psi$  corresponds to what Urick<sup>33</sup> calls the "reverberating volume."

And finally, for the sole purpose of comparison, an alternate expression for the volume reverberation scattering function as is found

in Moose<sup>17</sup> will be presented. As Moose<sup>17</sup> indicates, several researchers (e.g., see References 22, 35, 36) have modelled the reverberation return as:

$$\tilde{y}_{\text{REV}}(t) = \sum_{i=1}^{N(t)} a_i \tilde{x}(t - \tau_i) \exp\{+j2\pi\phi_i t\} \quad , \quad (4.2-65)$$

where  $N(t)$  is a Poisson random variable which governs the number of reflections from the discrete point scatterers that contribute to the sum at time  $t$ . The  $a_i$  are random coefficients which include all such factors as transducer patterns, propagation loss, and the cross sections of the scatterers. If the  $a_i$  are zero-mean statistically independent random variables, then Moose<sup>17</sup> shows that the autocorrelation function  $R_{\tilde{y}_{\text{REV}}}(t, t')$  of Equation (4.2-65) is of the same form as Equation (3.2-23) and that the scattering function is given by

$$R_{S_{\text{REV}}}(\tau, \phi) = E\{|a(\tau, \phi)|^2\} \rho(\tau, \phi) \quad , \quad (4.2-66)$$

where  $E\{|a(\tau, \phi)|^2\} \sim E\{|a_i|^2\}$  for scatterers with ranges and Doppler shifts near  $(\tau, \phi)$  and  $\rho(\tau, \phi)$  is the Poisson parameter which describes the density of scatterers near  $(\tau, \phi)$ , i.e.,

$$P(N; \tau, \phi) = \frac{[\rho(\tau, \phi) \Delta\tau \Delta\phi]^N}{N!} \exp\{-[\rho(\tau, \phi) \Delta\tau \Delta\phi]\} \quad (4.2-67)$$

is the probability of exactly  $N$  scatterers that have Doppler shifts between  $\phi$  and  $\phi + \Delta\phi$  and time delays between  $\tau$  and  $\tau + \Delta\tau$ . The product  $\rho(\tau, \phi) \Delta\tau \Delta\phi$  is the expected number of scatterers in the area  $\Delta\tau \Delta\phi$ .

The differences between the volume reverberation scattering functions given by Equations (4.2-43) and (4.2-66) are obvious.

#### 4.3 Target Scattering Function

The target scattering function for a doubly spread target will be derived in this section. The doubly spread target is modelled as a linear array of discrete highlights in deterministic translational motion. Each highlight is represented by its own average differential backscattering cross section. The scattered acoustic pressure fields from the individual highlights are assumed to be uncorrelated with one another.

In order to derive the scattering function for a simple line target composed of discrete point scatterers, start with the monostatic form of the volume reverberation scattering function given by Equation (4.2-43) in the spherical coordinate system, i.e.,

$$R_{S,TRGT}(\tau, \phi) = \int_{\theta} \int_{\psi} \left[ \frac{2 + \phi/f_c}{c\tau} \right]^2 \exp \left\{ -4\alpha(f_c) \left( \frac{c\tau}{2 + \phi/f_c} \right) \right\} \cdot \\ \rho_V \left( \frac{c\tau}{2 + \phi/f_c}, \theta, \psi \right) E\{|F(f_c)|^2\} \cdot \\ \delta(\phi + \phi_{DET}) d\psi \sin\theta d\theta ;$$

$$\frac{R_U}{c} (2 + \phi/f_c) \geq \tau \geq \frac{R_L}{c} (2 + \phi/f_c) , \quad (4.3-1)$$

where  $R_L$  and  $R_U$  are the lower and upper limits of integration, respectively, with respect to range (in meters), and where

$p_{\phi_{\text{RND}}}(\phi + \phi_{\text{DET}}) \equiv \delta(\phi + \phi_{\text{DET}})$  since it is assumed that the target, and hence, the scatterers, have only deterministic translational motion.

The problem now is to mathematically represent the volume density function  $\rho_V$  of the scatterers.

Toward this end, refer to Figure 9 where the line target is represented by the vector  $\vec{r}_{AB}$ . The length of the target is  $|\vec{r}_{AB}| = L$  meters and it has a velocity vector  $\vec{U} = |\vec{U}|\hat{n}_{AB}$ , where  $\hat{n}_{AB}$  is a unit vector in the direction of  $\vec{r}_{AB}$ . Thus, all the highlights will also have the same velocity vector  $\vec{U}$ . Both the transmit and receive arrays lie in the xy plane. The relative orientation of the target with respect to the arrays is specified by the position vectors  $\vec{r}_A$  and  $\vec{r}_B$  to the endpoints A and B of the target, respectively. Note that  $\vec{r}_{AB} = \vec{r}_B - \vec{r}_A$ . The vector  $\vec{r} = \vec{r}_A + d\hat{n}_{AB}$  is the position vector to any discrete highlight along the target. Any particular highlight is designated by its distance  $d$  (in meters) from endpoint A.

The term  $c\tau/(2 + \phi/f_c)$  appearing in the argument of  $\rho_V$  is the range to a highlight. The range, however, can also be specified in terms of its corresponding time delay  $\tau$ . Therefore, the volume density function can be expressed as:

$$\rho_V(\tau, \theta, \psi) = \sum_{n=1}^N \delta(\tau - \tau_n) \delta(\theta - \theta_n) \delta(\psi - \psi_n), \quad (4.3-2)$$

where

$$\tau_n = \frac{r_n}{c} [2 + \phi/f_c] \quad (4.3-3)$$

and the spherical coordinates  $(r_n, \theta_n, \psi_n)$  of the  $n^{\text{th}}$  highlight are given by:



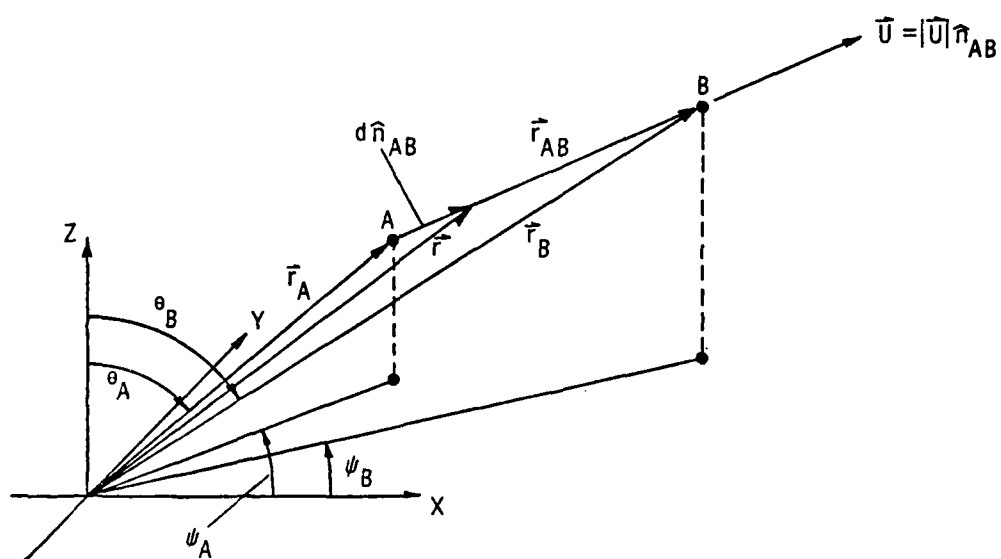


Figure 9. Orientation of line target with respect to the transmit and receive arrays.

$$r_n = |\vec{r}_n| = \left\{ \left\{ [1 - (d_n/L)] |\vec{r}_A| u_A + (d_n/L) |\vec{r}_B| u_B \right\}^2 + \right. \\ \left. \left\{ [1 - (d_n/L)] |\vec{r}_A| v_A + (d_n/L) |\vec{r}_B| v_B \right\}^2 + \right. \\ \left. \left\{ [1 - (d_n/L)] |\vec{r}_A| w_A + (d_n/L) |\vec{r}_B| w_B \right\}^2 \right\}^{1/2}, \quad (4.3-4)$$

$$\theta_n = \cos^{-1} \left\{ (1/r_n) \left\{ [1 - (d_n/L)] |\vec{r}_A| w_A + (d_n/L) |\vec{r}_B| w_B \right\} \right\} \quad (4.3-5)$$

and

$$\psi_n = \cos^{-1} \left\{ [1/(r_n \sin \theta_n)] \left\{ [1 - (d_n/L)] |\vec{r}_A| u_A + \right. \right. \\ \left. \left. (d_n/L) |\vec{r}_B| u_B \right\} \right\}, \quad (4.3-6)$$

where

$$\begin{aligned} u_A &= \sin \theta_A \cos \psi_A & u_B &= \sin \theta_B \cos \psi_B \\ v_A &= \sin \theta_A \sin \psi_A & v_B &= \sin \theta_B \sin \psi_B \\ w_A &= \cos \theta_A & w_B &= \cos \theta_B \end{aligned} \quad (4.3-7)$$

where  $u_A$  and  $u_B$ ,  $v_A$  and  $v_B$ , and  $w_A$  and  $w_B$  are the direction cosines of the endpoints A and B of the line target with respect to the positive x, y, and z axes, respectively, and N is the total number of highlights. The parameter  $d_n$  is the distance (in m) of the  $n^{\text{th}}$  highlight from endpoint A. Substituting Equation (4.3-2) into Equation (4.3-1) yields the target scattering function:

$$R_{S_{TRGT}}(\tau, \phi) = \sum_{n=1}^N [(2 - \phi_{DET_n}/f_c)/(c\tau_n)]^2 \cdot \exp\{-4\alpha(f_c)[(c\tau_n)/(2 - \phi_{DET_n}/f_c)]\} \cdot E\{|F_n(f_c)|^2\} \sin\theta_n \delta(\tau - \tau_n) \delta(\phi + \phi_{DET_n}) ,$$

(4.3-8)

where

$$\tau_n = (r_n/c)(2 - \phi_{DET_n}/f_c) ,$$

(4.3-9)

$$E\{|F_n(f_c)|^2\} = |D_T(ku_n, kv_n)|^2 E\{|g_n(-\hat{n}_T, \hat{n}_T, f_c)|^2\} \cdot |D_R(ku_n, kv_n)|^2$$

(4.3-10)

and from Equation (4.2-41):

$$\phi_{DET_n} = (2f_c/c)(|\vec{U}|/L) \{u_n[|\vec{r}_B|u_B - |\vec{r}_A|u_A] + v_n[|\vec{r}_B|v_B - |\vec{r}_A|v_A] + w_n[|\vec{r}_B|w_B - |\vec{r}_A|w_A]\} ,$$

(4.3-11)

where

$$u_n = \sin\theta_n \cos\psi_n ,$$

$$v_n = \sin\theta_n \sin\psi_n$$

(4.3-12)

and

$$w_n = \cos\theta_n$$

are the direction cosines of the  $n^{\text{th}}$  highlight with respect to the positive  $x$  ,  $y$  , and  $z$  axes, respectively.

The average monostatic (backscatter) radar cross section of the  $n^{\text{th}}$  highlight is given by  $4\pi E\{|g_n(-\hat{n}_T, \hat{n}_T, f_c)|^2\} = 4\pi\sigma_{d_n}(-\hat{n}_T, \hat{n}_T, f_c)$ , where  $\sigma_{d_n}(-\hat{n}_T, \hat{n}_T, f_c)$  is the average differential backscattering cross section of the  $n^{\text{th}}$  highlight. Therefore, the target strength of the  $n^{\text{th}}$  highlight is<sup>34</sup> [see Equation (4.2-50)]:

$$10 \log_{10} [\sigma_{d_n}(-\hat{n}_T, \hat{n}_T, f_c)/A_1] \text{ dB re } A_1, \quad (4.3-13)$$

where  $A_1 = 1 \text{ m}^2$ .

Since the target is being modelled as a linear array of  $N$  highlights (sources) radiating in random phase, the average differential backscattering cross section of the target is given by:<sup>34</sup>

$$\sigma_d(-\hat{n}_T, \hat{n}_T, f_c) \approx \sum_{i=1}^N \sigma_{d_i}(-\hat{n}_T, \hat{n}_T, f_c). \quad (4.3-14)$$

Another way of stating this result is that Equation (4.3-14) is a valid expression for  $\sigma_d(-\hat{n}_T, \hat{n}_T, f_c)$  when the  $N$  scattered fields are uncorrelated, and as a result, intensities add. When the  $N$  sources are radiating in phase (i.e., the  $N$  scattered fields are correlated):

$$\sigma_d(-\hat{n}_T, \hat{n}_T, f_c) \approx \left[ \sum_{i=1}^N [\sigma_{d_i}(-\hat{n}_T, \hat{n}_T, f_c)]^{1/2} \right]^2 \quad (4.3-15)$$

since amplitudes add.<sup>34</sup> The corresponding target strength can be obtained by computing

$$10 \log_{10} [\sigma_d(-\hat{n}_T, \hat{n}_T, f_c) / A_1] \text{ dB re } A_1, \quad (4.3-16)$$

where  $A_1 = 1 \text{ m}^2$ . In our case, Equation (4.3-14) is the applicable expression.

#### 4.4 Example Problem Calculations

4.4.1 Volume reverberation scattering function. A computer solution of the volume reverberation scattering function will be presented for an example problem involving a monostatic transmit/receive array geometry.

The monostatic form of the volume reverberation scattering function in spherical coordinates is obtained from Equation (4.2-43):

$$R_{S_{REV}}(\tau, \phi) = \left( \frac{2 + \phi/f_c}{c\tau} \right)^2 \exp \left\{ -4\alpha(f_c) \left( \frac{c\tau}{2 + \phi/f_c} \right) \right\} .$$

$$\int_{\theta=0}^{\pi/2} \int_{\psi=0}^{2\pi} \rho_V \left( \frac{c\tau}{2 + \phi/f_c}, \theta, \psi \right) E\{|F(f_c)|^2\} .$$

$$p_{\phi_{RND}}(\phi + \phi_{DET}) d\psi \sin\theta d\theta ; \quad (4.4-1)$$

$$\frac{R_U}{c} (2 + \phi/f_c) \geq \tau \geq \frac{R_L}{c} (2 + \phi/f_c) ,$$

where  $R_L$  and  $R_U$  are the lower and upper limits of integration with respect to range, respectively. It is assumed that the array lies in the  $xy$  plane. Thus, the positive  $z$  axis is normal to the face of the array. In this example problem, both the transmit and receive directivity functions are identical, i.e.,  $D_T = D_R = D$ . As a result,

$$E\{|F(f_c)|^2\} = |D(ku, kv)|^4 E\{|g(-\hat{n}_T, \hat{n}_T, f_c)|^2\}, \quad (4.4-2)$$

where the directivity function actually used was:

$$D(ku, kv) = \frac{\sum_{n=1}^5 Q_n \cos \left[ \frac{(2n-1)\pi d}{\lambda} (u - u_0) \right]}{\sum_{n=1}^5 Q_n} \frac{\sin \left[ \frac{10\pi d}{\lambda} v \right]}{10 \sin \left[ \frac{\pi d}{\lambda} v \right]} \quad (4.4-3)$$

Equation (4.4-3) corresponds to a  $(10 \times 10)$  planar array composed of 10-element, amplitude shaded, linear arrays parallel to the  $x$  axis and 10-element, uniformly shaded, linear arrays parallel to the  $y$  axis where  $Q_1 = 1.0$ ,  $Q_2 = 0.8389$ ,  $Q_3 = 0.5801$ ,  $Q_4 = 0.3153$ ,  $Q_5 = 0.1251$ , and  $d/\lambda = 0.4$ . The parameter  $d$  is the uniform spacing (in m) between elements and  $\lambda$  is the wavelength (in m) corresponding to the frequency  $f_c$  (in Hz). This particular choice of amplitude shading coefficients ensures 40 dB down sidelobe levels in the  $xz$  plane for  $y = 0$ . The phase shift  $u_0 = \sin\theta_0 \cos\psi_0$  is used for beam tilting in the  $xz$  plane.

We will assume that the array is in motion in the positive  $z$  direction and that the relative, deterministic velocity of the discrete point scatterers with respect to the array is  $\vec{U} = -20.0 \hat{z}$  m/sec so that

$$\phi_{DET} = - \frac{40.0 f_c}{c} \cos\theta \text{ Hz} \quad (4.4-4)$$

Before we can evaluate Equation (4.4-1), we must evaluate  $p_{\phi_{RND}}(\phi + \phi_{DET})$ . Values for the probability density function of the random Doppler shift  $p_{\phi_{RND}}(\cdot)$  as given by Equation (4.2-47) were

calculated via numerical integration. Figures 10a and 10b are plots of  $p_{\phi_{\text{RND}}}(\cdot)$  for  $\sigma = 0.1$  m/sec and  $\sigma = 1.0$  m/sec, respectively, for a monostatic transmit/receive array geometry. Recall that  $\sigma$  is the standard deviation of  $|\vec{V}_f|$ .

Finally, for simplicity, also assume that the scatterers are uniformly distributed in space, i.e.,  $\rho_V = \text{constant}$ ; and that the average differential backscattering cross section of an individual point scatterer is omnidirectional, i.e.,  $E\{|g(-\hat{n}_T, \hat{n}_T, f_c)|^2\}$  does not depend upon  $\hat{n}_T$  and is therefore equal to a constant  $\sigma_d$ .

Let us first consider the case of relative, deterministic motion only. Using the aforementioned assumptions and replacing  $p_{\phi_{\text{RND}}}(\phi + \phi_{\text{DET}})$  by  $\delta(\phi + \phi_{\text{DET}})$ , Equation (4.4-1) reduces to:

$$R_{S_{\text{REV}}}(\tau, \phi) = K \int_{\psi=0}^{2\pi} |D(ku, kv)|^4 d\psi \sin\theta, \quad (4.4-5)$$

where  $\theta$  is such that:

$$\frac{40.0 f_c}{c} \cos\theta = \phi \text{ Hz}; \quad \frac{\pi}{2} \geq \theta \geq 0 \quad (4.4-6)$$

and

$$\frac{R_U}{c} (2 + \phi/f_c) \geq \tau \geq \frac{R_L}{c} (2 + \phi/f_c) \quad (4.4-7)$$

and where

$$K = \rho_V \left( \frac{2 + \phi/f_c}{c\tau} \right)^2 \exp \left\{ -4\alpha(f_c) \left( \frac{c\tau}{2 + \phi/f_c} \right) \right\} \sigma_d. \quad (4.4-8)$$

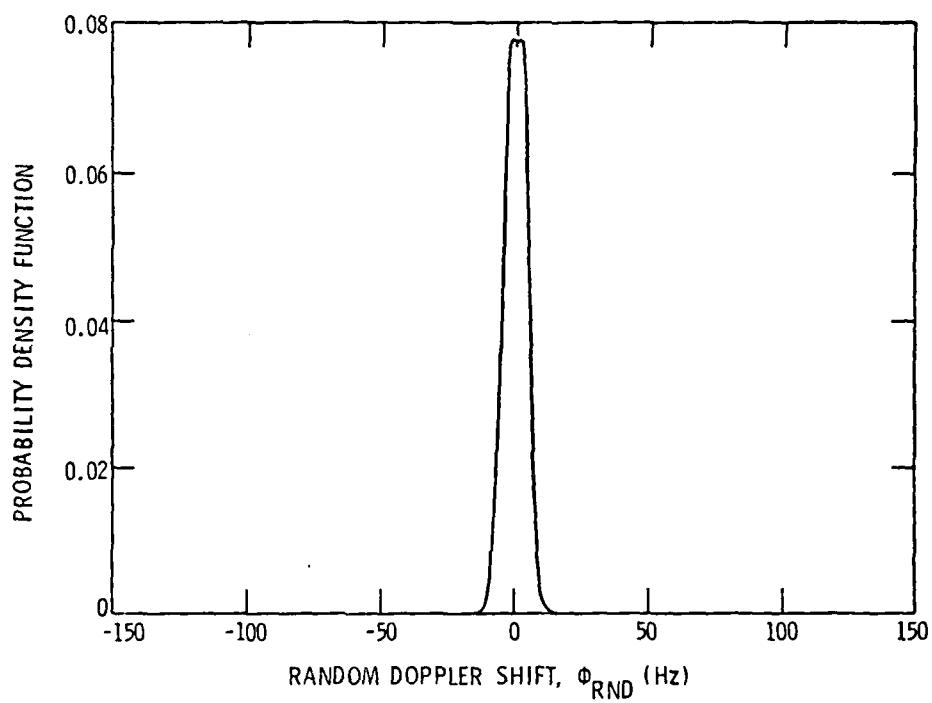


Figure 10a. Probability density function of the random Doppler shift for a monostatic transmit/receive array geometry,  $\sigma = 0.1$  m/sec .



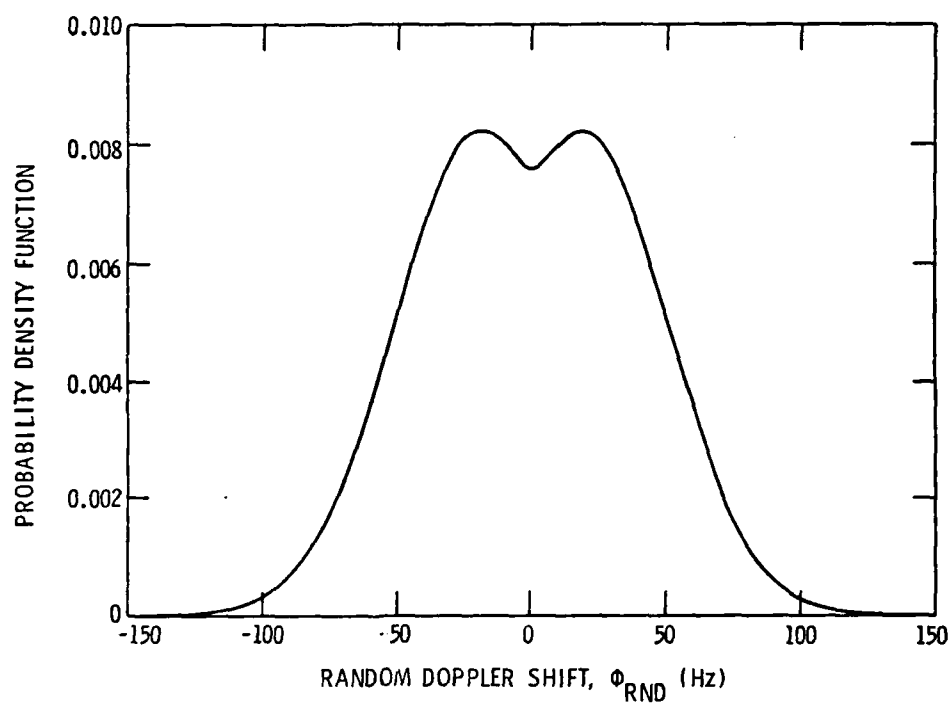


Figure 10b. Probability density function of the random Doppler shift for a monostatic transmit/receive array geometry,  $\sigma = 1.0$  m/sec .

Figures 11, 12, and 13 are normalized Doppler profiles (range constant) of Equation (4.4-5) for beam tilts of  $\theta_0 = 0^\circ$ ,  $\psi_0 = 0^\circ$ ;  $\theta_0 = 30^\circ$ ,  $\psi_0 = 0^\circ$ ; and  $\theta_0 = 45^\circ$ ,  $\psi_0 = 0^\circ$ , respectively. The values of  $c = 1500$  m/sec,  $\alpha(f_c) = 4.9 \times 10^{-4}$  nepers/m, and  $f_c = 25$  kHz were used in connection with Figures 11-13. Note the increase in frequency spread, measured at the 3 dB down level, as the beam tilt angle  $\theta_0$  is increased. Also observe from Figure 11 that the scattering function peaks at  $\phi = 664$  Hz, which corresponds to  $\theta = 5^\circ$ , rather than peaking at  $\phi = 667$  Hz, which corresponds to  $\theta = \theta_0 = 0^\circ$ . Mathematically, this is due to the  $\sin\theta$  dependence of the scattering function. Physically speaking, however,  $\theta = 0^\circ$  implies that the elemental scattering volume  $dV$  is zero; and hence, there is no scattered power. These plots demonstrate the effect of tilting a given beam pattern on frequency spread. Figure 15, however, demonstrates the additional effect of random motion of the scatterers on frequency spread.

Figure 14 corresponds to relative, deterministic motion only [see Equation (4.4-5)] with  $\theta_0 = 45^\circ$ ,  $\psi_0 = 0^\circ$ ,  $f_c = 25$  kHz,  $\alpha(f_c) = 4.7 \times 10^{-4}$  nepers/m, and  $c = 1505$  m/sec. If we now allow the discrete point scatterers to have random motion, Equation (4.4-1) reduces to:

$$R_{S_{REV}}(\tau, \phi) = K \int_{\psi=0}^{2\pi} \int_{\theta=0}^{\pi/2} |D(ku, kv)|^4 \cdot$$

$$P_{\phi_{RND}}\left(\phi - \frac{40.0 f_c}{c} \cos\theta\right) \sin\theta d\theta d\psi, (4.4-9)$$

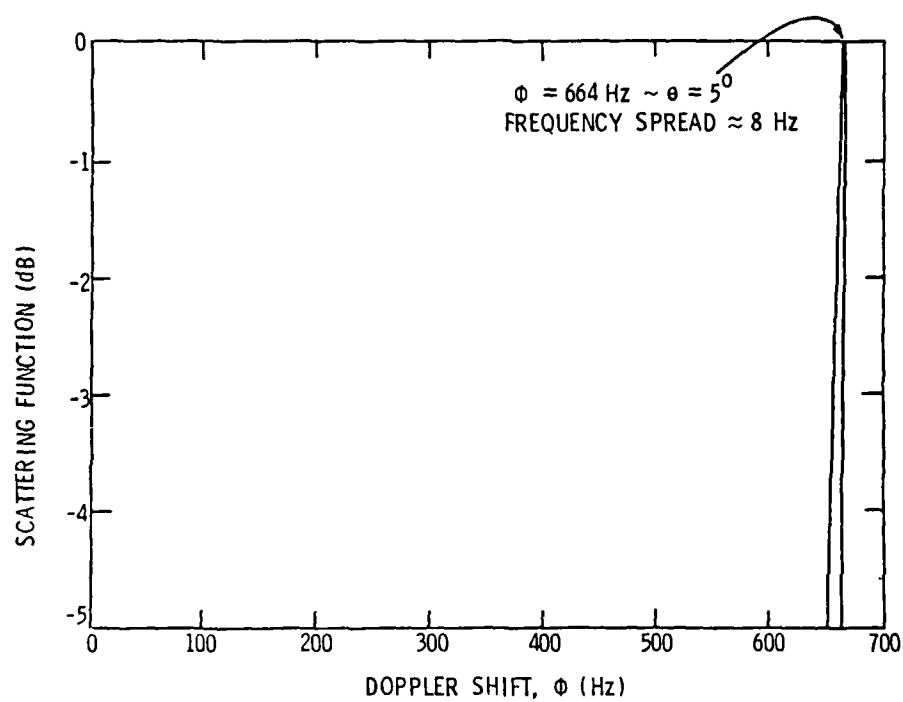


Figure 11. Normalized Doppler profile of volume reverberation scattering function,  $\theta_o = 0^\circ$ ,  $\psi_o = 0^\circ$ .

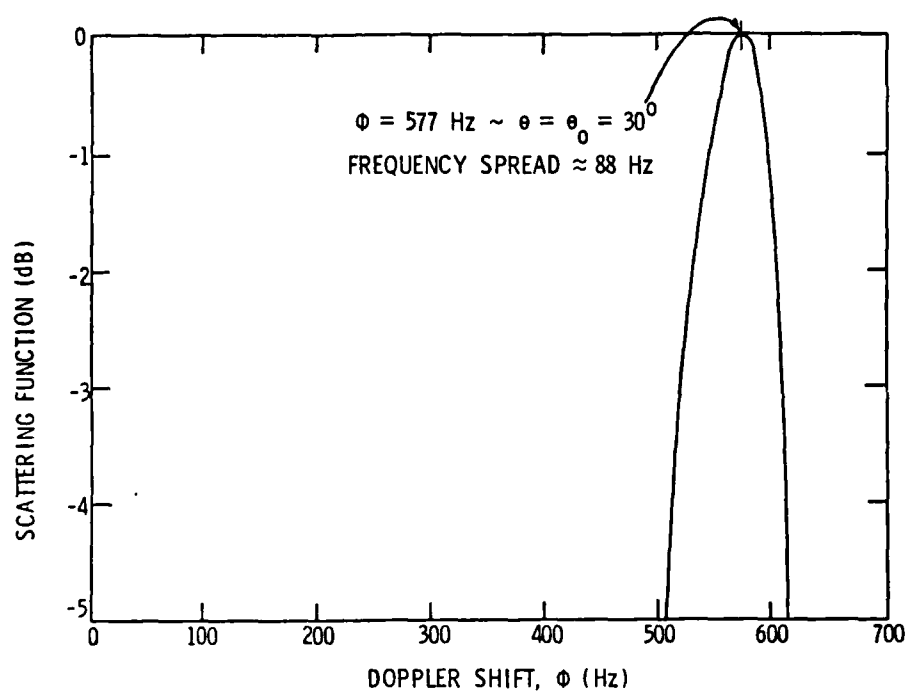


Figure 12. Normalized Doppler profile of volume reverberation scattering function,  $\theta_0 = 30^\circ$ ,  $\psi_0 = 0^\circ$ .

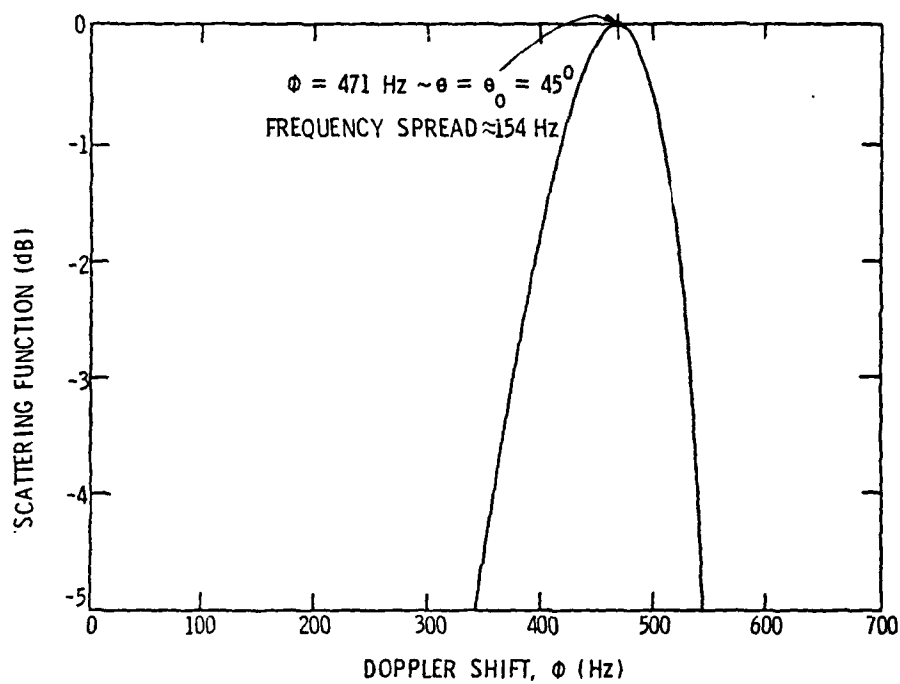


Figure 13. Normalized Doppler profile of volume reverberation scattering function,  $\theta_0 = 45^\circ$ ,  $\psi_0 = 0^\circ$ .

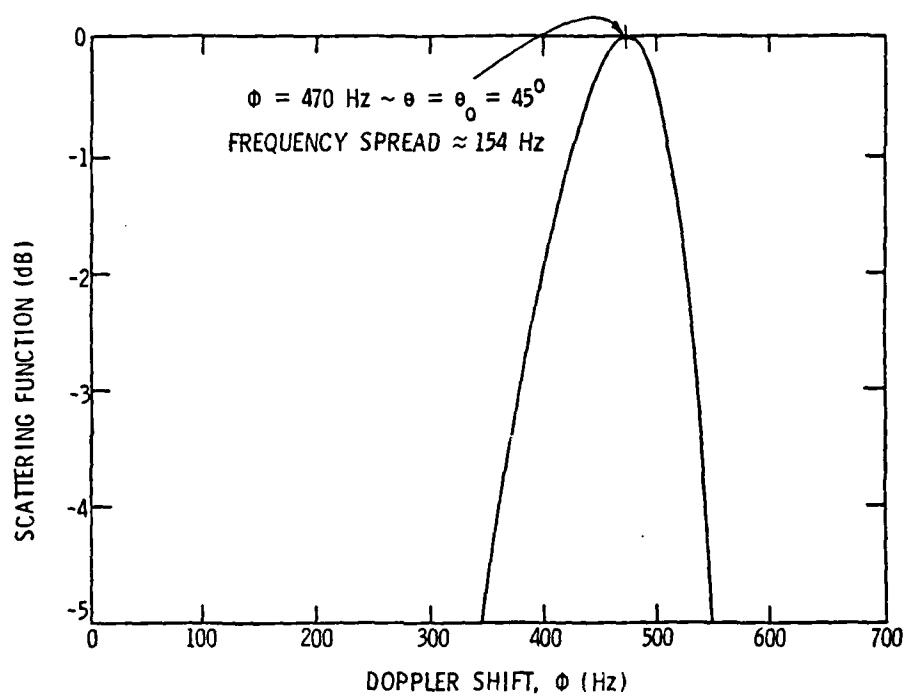


Figure 14a. Normalized Doppler profile of volume reverberation scattering function. Relative deterministic motion only ( $\theta_0 = 45^\circ$ ,  $\psi_0 = 0^\circ$ ).

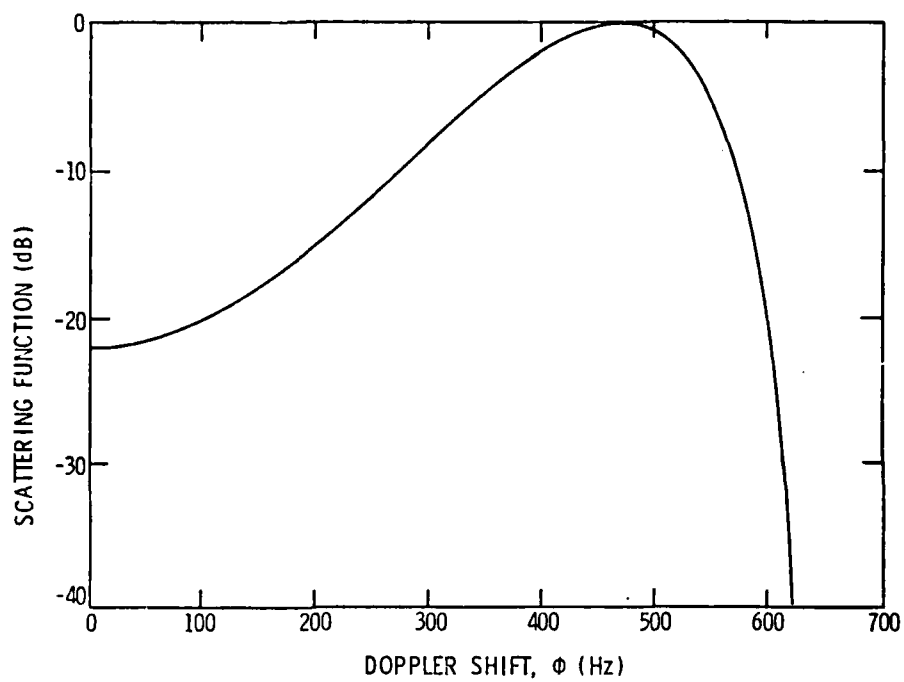


Figure 14b. Normalized Doppler profile of volume reverberation scattering function. Relative deterministic motion only ( $\theta_o = 45^\circ$ ,  $\psi_o = 0^\circ$ ).

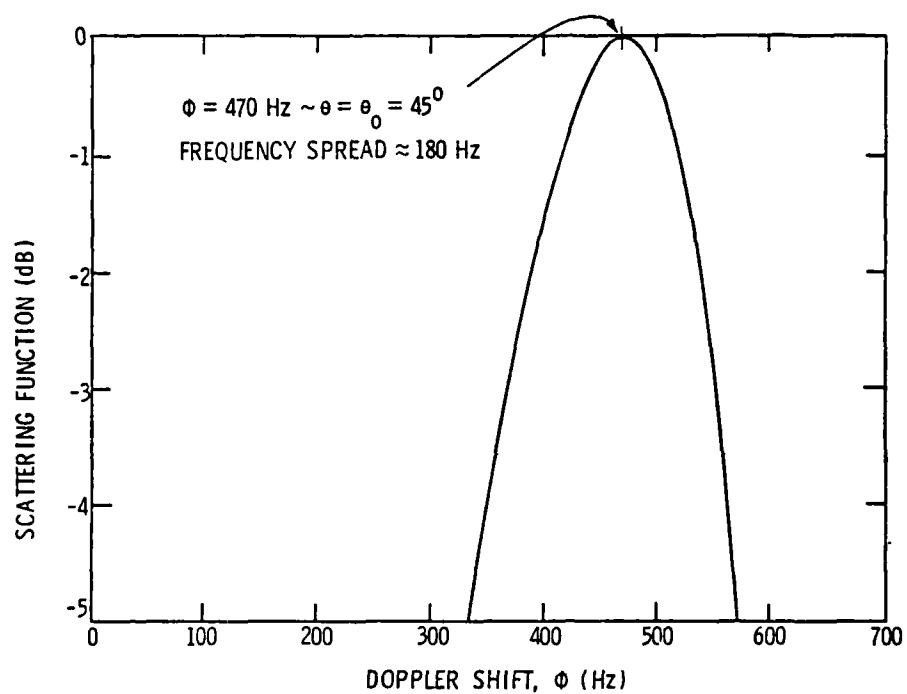


Figure 15a. Normalized Doppler profile of volume reverberation scattering function. Relative deterministic plus random motion ( $\theta_0 = 45^\circ$ ,  $\psi_0 = 0^\circ$ ).



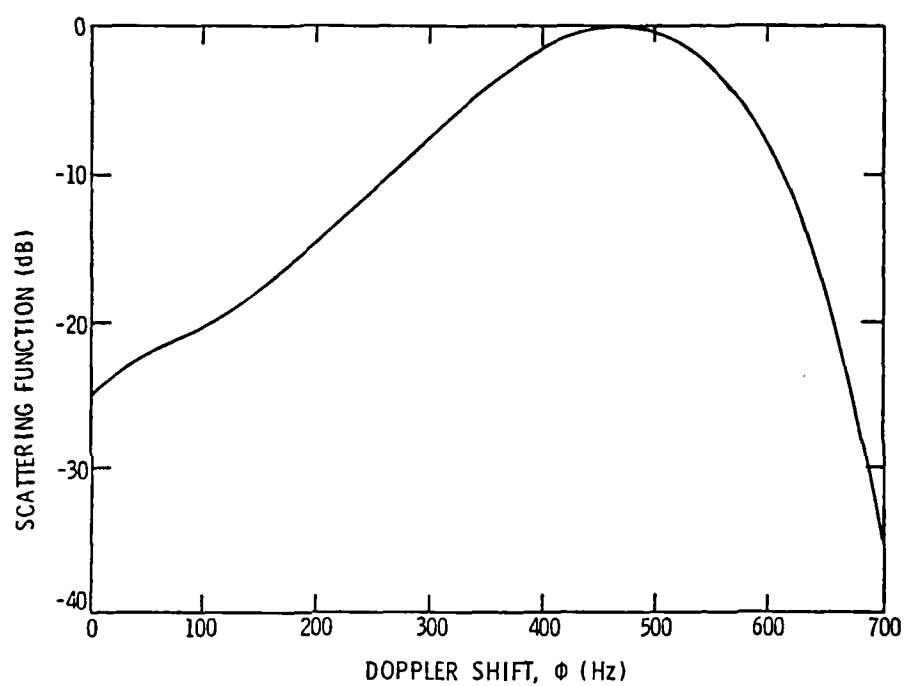


Figure 15b. Normalized Doppler profile of volume reverberation scattering function. Relative deterministic plus random motion ( $\theta_o = 45^\circ$ ,  $\psi_o = 0^\circ$ ).

where  $K$  is given by Equation (4.4-8), the directivity function  $D$  by Equation (4.4-3), and  $p_{\phi}^{RND}(\cdot)$  by Equation (4.2-47) with  $\sigma = 1.0$  m/sec (see Figure 10b). Figure 15 is a normalized Doppler profile of Equation (4.4-9). The values of the parameters used for Figure 15 are identical with those used for Figure 14. By comparing Figures 14 and 15, it is seen that an additional frequency spread of 26 Hz is introduced by the random motion of the scatterers for  $\sigma = 1.0$  m/sec. This represents an increase of approximately 17%.

**4.4.2 Target scattering function.** The target scattering function given by Equation (4.3-8) is calculated for an example problem using the monostatic transmit/receive array geometry depicted in Figure 9. In this example, the array is not in motion. The magnitude of the deterministic velocity of the target is  $|\vec{U}| = 20.0$  m/sec. The location of the endpoints  $A$  and  $B$  of the target with respect to the array is specified by the following constants:  $|\vec{r}_A| = 500$  m,  $\theta_A = \theta_B = 5.739^\circ$ ,  $\psi_A = 180^\circ$ , and  $\psi_B = 0^\circ$ . With this information,  $|\vec{r}_B|$  can be calculated. The length of the target is  $L = 100$  m and the number of highlights being considered is 10. The first highlight is located 5 m from point  $A$  and the spacing between the remaining highlights thereafter is 10 m. The values  $\theta_o = 45^\circ$ ,  $\psi_o = 0^\circ$ ,  $c = 1500.342$  m/sec,  $\alpha(f_c) = 4.9 \times 10^{-4}$  nepers/m, and  $f_c = 25$  kHz are used. It is assumed that  $D_T = D_R = D$ , where the directivity function  $D$  is given by Equation (4.4-3). It is also assumed that  $E\{|g_n(-\hat{n}_T, \hat{n}_T, f_c)|^2\}$  is equal to a constant value which is the same for all  $N$  highlights.

Values for the normalized target scattering function, as a function of  $\tau$  and  $\phi$ , are presented in Table I. Upon inspecting Table I, it can be seen that highlights 1 through 5 have positive Doppler shifts which indicate that these five highlights are approaching the array which is in agreement with the geometry of the problem. Also note that highlights 6 through 10 have negative Doppler shifts which indicate that these five highlights are receding from the array which is also physically correct. Highlights 5 and 6 have Doppler shifts which are almost equal to zero since the position vectors  $\vec{r}_5$  and  $\vec{r}_6$  for these two highlights are nearly perpendicular to the array. Note that the magnitude of the scattering function is larger for highlights 6 through 10 as compared to highlights 1 through 5. And, in fact, the scattering function has its maximum value at highlight 8. This is also in agreement with the geometry of the problem since the beam pattern was tilted in the general direction of highlights 6 through 10.

The time delay parameter  $\tau_n$  given by Equation (4.3-9) does not correspond to round-trip time delay, and hence, the values for  $\tau_n$  appearing in Table I do not correspond to round-trip time delays. However, as was discussed previously in Section 4.2 with regard to the volume reverberation scattering function, the round-trip time delay can be computed from  $\tau_n$  by dividing it by  $[1 - (\phi_{\text{DET}_n}/f_c)]$ , i.e., the round-trip time delay corresponding to the  $n^{\text{th}}$  highlight is given by  $\tau_n/[1 - (\phi_{\text{DET}_n}/f_c)]$ .

Table II presents values for the range  $r_n$ , the simple round-trip time delay  $2r_n/c$ , and the actual round-trip time delay  $\tau_n/[1 - (\phi_{\text{DET}_n}/f_c)]$ , for the ten highlights. The simple round-trip

TABLE 1

## NORMALIZED TARGET SCATTERING FUNCTION

Highlight	$\tau = \tau_n$	$\phi = -\phi_{\text{DET}_n}$	$R_{S_{\text{TRGT}}}(\tau, \phi)$
<u>n</u>	<u>(sec)</u>	<u>(Hz)</u>	<u>(dB)</u>
1	0.666680	59.851	-0.376507E 02
2	0.665438	46.579	-0.243289E 02
3	0.664461	33.255	-0.107524E 02
4	0.663752	19.888	-0.592028E 01
5	0.663310	6.481	-0.686279E 01
6	0.663137	- 6.858	-0.511047E 01
7	0.663231	-20.276	-0.328704E 00
8	0.663592	-33.638	-0.000000E 00
9	0.664220	-46.960	-0.294615E 01
10	0.665115	-60.229	-0.109380E 02

---

TABLE 2

## ROUND-TRIP TIME DELAY CALCULATIONS

Highlight	$r_n$	$2r_n/c$	$\tau_n/[1 - (\phi_{\text{DET}_n}/f_c)]$
<u>n</u>	<u>(m)</u>	<u>(sec)</u>	<u>(sec)</u>
1	499.526	0.6658828	0.6650877
2	498.728	0.664819	0.6642005
3	498.128	0.6640192	0.6635783
4	497.730	0.6634887	0.6632244
5	497.531	0.6632234	0.6631381
6	497.534	0.6632274	0.6633189
7	497.738	0.6634993	0.6637693
8	498.143	0.6640392	0.664486
9	498.747	0.6648444	0.66547
10	499.552	0.6659175	0.6667211

time delay does not depend upon Doppler shift while the actual round-trip time delay does. The range values  $r_n$  were computed from Equation (4.3-4). Upon inspecting Table II, it can be seen that the actual round-trip time delays for highlights 1 through 5 are smaller than the corresponding simple round-trip time delays since these five highlights have positive Doppler shifts and are therefore approaching the array. Similarly, the actual round-trip time delays for highlights 6 through 10 are larger than the corresponding simple round-trip time delays since these five highlights have negative Doppler shifts and are therefore receding from the array.

## CHAPTER V

### SURFACE REVERBERATION SCATTERING FUNCTION

#### 5.1 Introduction

The underwater acoustic propagation path between transmit and receive planar arrays via the surface of the ocean is treated as a linear, time-varying, random WSSUS (wide-sense stationary uncorrelated spreading) communication channel. The random, time-varying, surface reverberation transfer function is derived for a bistatic geometry using a generalized Kirchhoff approach. The result for the bistatic configuration can then be easily reduced to either the specular or backscatter geometries.

The generalized Kirchhoff approach uses a Fresnel corrected Kirchhoff integral, no small slope approximation, and the Rayleigh hypothesis that the scattered acoustic pressure field can be represented as a sum of plane waves travelling in many different directions. The transfer function obtained in this chapter is shown to be greater in magnitude than those transfer functions previously derived by the classical Kirchhoff approach, especially for the specular and backscatter geometries.

The randomly rough, time-varying surface is assumed to be a zero mean, wide-sense stationary, Gaussian process. Two second order functions are derived from the transfer function. They are the two-frequency correlation function and the surface reverberation scattering function. These second order functions are shown to be dependent upon

the directional wave number spectrum of the ocean surface. The scattering function analysis predicts both a spread in round-trip time delay and in frequency.

## 5.2 Surface Reverberation Transfer Function

5.2.1 Background discussion. The bistatic underwater propagation path from transmit array to receive array via the ocean surface is assumed to be a linear, time-varying, random communication channel. If one transmits a time-harmonic signal of the form  $\exp(+j2\pi ft)$ , then the acoustic pressure field at the receive array due to scatter from the ocean surface can be obtained from Green's Theorem.<sup>37</sup>

Consider Figure 16 which depicts the transmit array  $T$ , the receive array  $R$ , and the ocean medium as being enclosed by the closed surface  $S' = S + S''$ , where  $S$  is the ocean surface, and  $S''$  is an arbitrary contour to be specified later. Assuming a time-harmonic input signal of the form  $\exp(+j2\pi ft)$ , the spatial factor for the acoustic pressure field at the receive array is obtained from Green's Theorem as<sup>23</sup>

$$p(\vec{r}_R) = \int_{V'} \rho(\vec{r}') G(\vec{r}_R | \vec{r}') dV' + \oint_{S'} [G(\vec{r}_R | \vec{r}') \frac{\partial}{\partial n'} p(\vec{r}') - p(\vec{r}') \frac{\partial}{\partial n'} G(\vec{r}_R | \vec{r}')] dS', \quad (5.2-1)$$

where  $V'$  is the volume enclosed by  $S'$ ,  $\rho(\vec{r}')$  is the source distribution,  $G(\vec{r}_R | \vec{r}')$  is the Green's function for the bounded medium,  $p(\vec{r}')$  is the total acoustic pressure field at each point on the closed surface  $S'$ , and  $\partial/\partial n'$  signifies a partial derivative in the outward normal direction (away from the enclosed volume) evaluated at each point



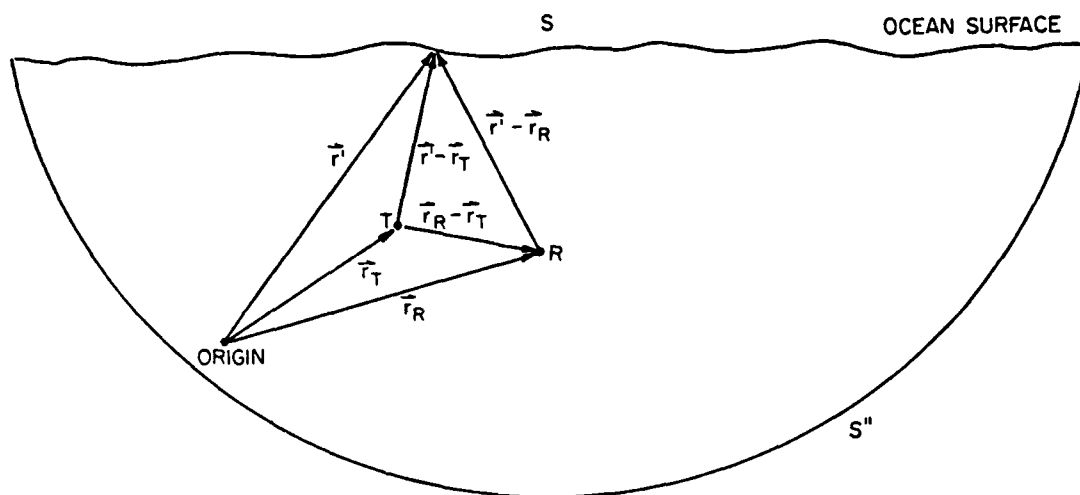


Figure 16. Transmit array T , receive array R , and ocean medium being enclosed by the closed surface  $S' = S + S''$ .

on  $S'$ . Equation (5.2-1) is valid if the receive array's location, denoted by the position vector  $\vec{r}_R$ , is either on or inside the closed surface  $S'$ , and Equation (5.2-1) is invalid if  $\vec{r}_R$  is outside  $S'$ . It can be seen from Equation (5.2-1) that the total field at the receive array is equal to the sum of the field due to the elementary sources and the field due to scatter from the boundary. As an example, assume that the source is a point source, i.e.,  $\rho(\vec{r}') = \delta(\vec{r}' - \vec{r}_T)$ . As a result, the volume integral in Equation (5.2-1) reduces to:

$$\int_{V'} \rho(\vec{r}') G(\vec{r}_R | \vec{r}') dV' = \int_{V'} \delta(\vec{r}' - \vec{r}_T) G(\vec{r}_R | \vec{r}') dV' \quad (5.2-2)$$

or

$$\int_{V'} \rho(\vec{r}') G(\vec{r}_R | \vec{r}') dV' = G(\vec{r}_R | \vec{r}_T) \quad , \quad (5.2-3)$$

where  $G(\vec{r}_R | \vec{r}_T)$  represents the direct acoustic pressure field from transmit array to receive array.

The direct acoustic pressure field from transmit array to receive array is of no concern in this chapter. The important quantity of interest is the acoustic pressure field due to scatter from the boundary. Therefore, from Equation (5.2-1), the expression for the acoustic pressure field at the receive array due to scatter from the boundary  $S'$  is given by:

$$p_S(\vec{r}_R) = \oint_{S'} \left[ G(\vec{r}_R | \vec{r}') \frac{\partial}{\partial n'} p(\vec{r}') - p(\vec{r}') \frac{\partial}{\partial n'} G(\vec{r}_R | \vec{r}') \right] dS' \quad (5.2-4)$$

If we follow the Kirchhoff approximation and let  $G(\vec{r}_R|\vec{r}')$  be equal to the free-space Green's function,<sup>26</sup> i.e.,

$$G(\vec{r}_R|\vec{r}') = \frac{\exp(-jk|\vec{r}' - \vec{r}_R|)}{|\vec{r}' - \vec{r}_R|}, \quad (5.2-5)$$

where  $k = 2\pi f/c$  is the wave number, and then substitute Equation (5.2-5) into Equation (5.2-4), we obtain:

$$p_S(\vec{r}_R) = \oint_{S'} \left[ \frac{\exp(-jkR_R)}{R_R} \frac{\partial}{\partial n'} p(\vec{r}') - p(\vec{r}') \frac{\partial}{\partial n'} \frac{\exp(-jkR_R)}{R_R} \right] dS' \quad (5.2-6)$$

which is the integral theorem of Helmholtz and Kirchhoff,<sup>26</sup> where

$$R_R = |\vec{R}_R| \triangleq |\vec{r}' - \vec{r}_R| \quad (5.2-7)$$

Equation (5.2-6) can be further simplified by choosing the contour  $S''$  to be an infinite hemisphere centered about the receive array's location (it is assumed that the ocean bottom is infinitely far away). Therefore, since  $S' = S + S''$ ,

$$\oint_{S'} = \int_S + \int_{S''} = \int_S \quad (5.2-8)$$

since

$$\int_{S''} = 0 \quad (5.2-9)$$

by Sommerfeld's radiation condition.<sup>26,37</sup>

As a result of Equation (5.2-8), Equation (5.2-6) reduces to:

$$p_S(\vec{r}_R) = \int_S \left[ \frac{\exp(-jkR_R)}{R_R} \frac{\partial}{\partial n} p(\vec{r}) - p(\vec{r}) \frac{\partial}{\partial n} \frac{\exp(-jkR_R)}{R_R} \right] dS, \quad (5.2-10)$$

where  $p(\vec{r})$  is the total field at each point on the ocean surface  $S$ ,  $\partial/\partial n$  signifies a partial derivative in the outward normal direction (away from the ocean medium) evaluated at each point on  $S$ , and

$$R_R = |\vec{r} - \vec{r}_R|, \quad (5.2-11)$$

where the prime symbol " ' " has been removed from the position vector  $\vec{r}'$  (see Figure 16).

Before proceeding further with the discussion, let us refer to Figure 17 which describes the geometry of the problem to be considered in this chapter. Note that the transmit and receive arrays occupy the  $X_T Y_T$  and  $X_R Y_R$  planes, respectively. The  $Z_T$  and  $Z_R$  axes are perpendicular to the  $X_T Y_T$  and  $X_R Y_R$  planes, respectively. The reference coordinate system is  $XYZ$ . If the ocean surface was perfectly smooth, it would occupy the  $XY$  plane. Any vertical deviation of the ocean surface from the  $XY$  plane is represented by  $Z = \xi(x, y, t)$ . The random process  $\xi(x, y, t)$  describes the randomly rough, time-varying, ocean surface. It is assumed to have a zero mean, i.e.,  $E\{\xi(x, y, t)\} = 0$ . Note that  $\xi(x, y, t)$  is a function of both

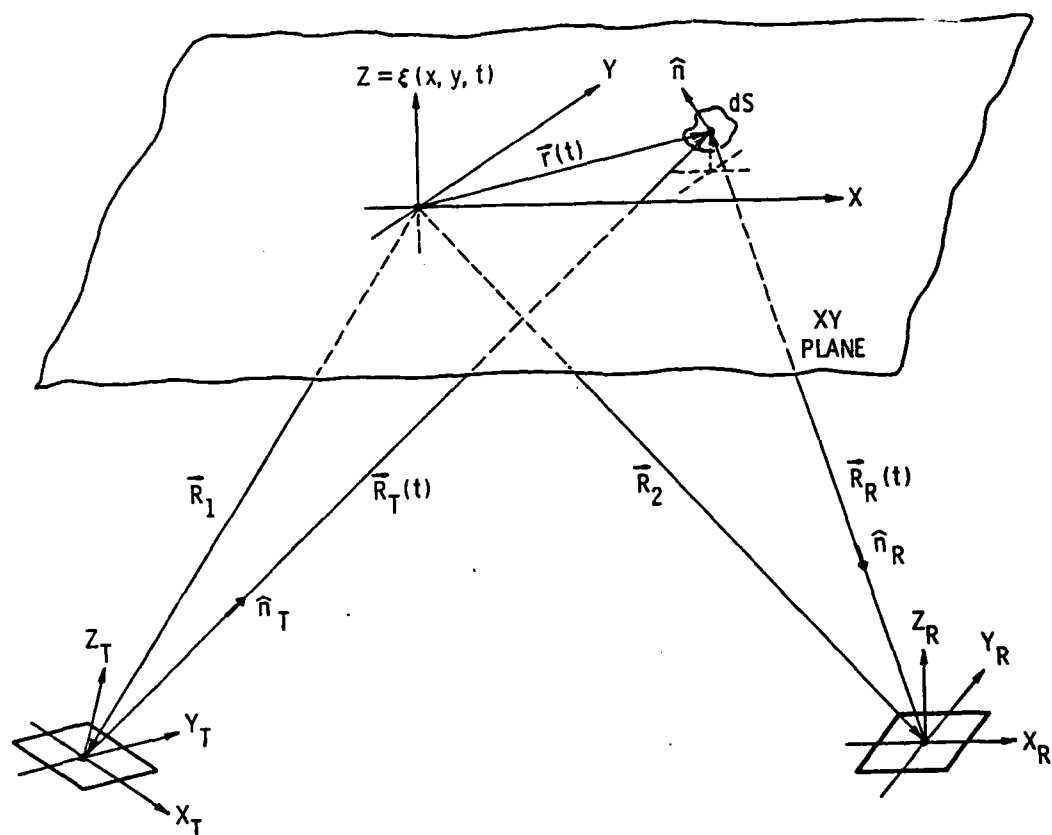


Figure 17. Bistatic geometry for surface-scatter communication channel.

position and time. The time-varying position vector  $\vec{r}(t)$  locates the infinitesimal surface area element  $dS$ . The unit vector  $\hat{n}$  is normal to  $dS$  and is pointing in the conventional outward direction away from the ocean. The position vectors  $\vec{R}_1$  and  $\vec{R}_2$  are chosen to be colinear with the axes of the main lobes of the transmit and receive directivity patterns, respectively. The time-varying position vector  $\vec{R}_T(t)$  gives the range of  $dS$  from the transmit array, at any time  $t$ , in the direction  $\hat{n}_T$ . Similarly, the vector  $\vec{R}_R(t)$  gives the range of  $dS$  from the receive array, at any time  $t$ , in the direction  $(-\hat{n}_R)$ . Both  $\hat{n}_T$  and  $\hat{n}_R$  are unit vectors. Based upon the geometry of Figure 17, Equation (5.2-11) becomes:

$$R_R \rightarrow R_R(t) = |\vec{R}_R(t)| \triangleq |\vec{r}(t) - \vec{R}_2|, \quad (5.2-12)$$

where  $\vec{r}_R \equiv \vec{R}_2$ .

Equation (5.2-10) and the geometry of Figure 17 have been the basic starting points for many researchers who worked on various aspects of the problem of acoustic scattering from the ocean surface.

Eckart<sup>38</sup> started with Equation (5.2-10); however, he defined  $p(\vec{r})$  as the scattered acoustic pressure field on the ocean surface and not as the total (incident plus scattered) field. Approximating the ocean surface as an ideal pressure release boundary and assuming that it was locally plane compared to the wavelength of the incident radiation, Eckart<sup>38</sup> reduced Equation (5.2-10) to:

$$p_S(\vec{r}_R) = \int_S \frac{\partial}{\partial n} \left[ p_I(\vec{r}) \frac{\exp(-jkR_R)}{R_R} \right] dS, \quad (5.2-13)$$

where  $p_I(\vec{r})$  is the known incident radiation given by:

$$p_I(\vec{r}) = D_T(k, \vec{r}) \frac{\exp(-jkR_T)}{R_T} \quad (5.2-14)$$

and, from Figure 17,

$$R_T \rightarrow R_T(t) = |\vec{R}_T(t)| \stackrel{\Delta}{=} |\vec{r}(t) - \vec{R}_1| \quad , \quad (5.2-15)$$

where  $\vec{r}_T$  in Figure 16 is equivalent to  $\vec{R}_1$  in Figure 17. The directivity function of the transmit array projected onto the ocean surface is represented by  $D_T(k, \vec{r})$ . Although Eckart<sup>38</sup> did not consider time-varying position vectors, he did make two important additional assumptions. The first is referred to as the small slope approximation since he replaced the normal partial derivative with  $\partial/\partial Z$  and  $dS$  with  $dx dy$ . Doing so and using Equation (5.2-14), Equation (5.2-13) becomes:

$$p_S(\vec{r}_R) = \iint D_T(k, x, y) \frac{\partial}{\partial Z} \left[ \frac{\exp\{-jk(R_T + R_R)\}}{R_T R_R} \right] dx dy \quad , \quad (5.2-16)$$

where  $D_T(k, x, y)$  is the projection of the directivity function of the transmit array onto the XY plane. The second assumption Eckart<sup>38</sup> made was that the directivity function of the transmit array was highly directional (very narrow beamwidth). Thus, Eckart<sup>38</sup> limited himself to a Fraunhofer approximation when he expanded the ranges  $R_T$  and  $R_R$  appearing in the complex exponential in terms of  $r$ ,  $R_1$ , and  $R_2$ . Eckart<sup>38</sup> based his subsequent analysis on Equation (5.2-16).

Following the basic approach of Eckart,<sup>38</sup> Gulin<sup>39</sup> also started his analysis of acoustic scattering from a sinusoidal surface with Equation (5.2-16). Although Gulin<sup>39</sup> did not include a transmit beam pattern, he used a Fresnel approximation to expand the ranges  $R_T$  and  $R_R$  in the complex exponential rather than a Fraunhofer approximation.

As was previously mentioned, Eckart<sup>38</sup> justified using a Fraunhofer approximation on the assumption that the beam pattern of the transmit array was sufficiently directional. However, Melton and Horton,<sup>40</sup> and Horton and Melton,<sup>41</sup> stimulated by Gulin's<sup>39</sup> work, disagreed with Eckart's<sup>38</sup> justification for the use of the Fraunhofer approximation. They noted that the beamwidths of practical acoustic sources are large enough to make one question the validity of using a Fraunhofer approximation, especially since the area of insonification of the ocean surface increases as the distance from the source to the surface increases. Thus, the beamwidth of the directivity pattern plus the geometry of the physical situation must both be taken into account when deciding upon the Fraunhofer versus Fresnel approximation.<sup>40</sup> In fact, Horton and Melton<sup>41</sup> showed that for their particular experimental arrangement, the Fresnel approximation was superior to the Fraunhofer approximation for the calculation of scattered intensity. The question of the Fraunhofer versus Fresnel approximation will be discussed further in Section 5.2.2.

Several authors have approached the problem of surface scatter by viewing the ocean surface as a linear, time-varying, random filter as will be done in this chapter (see References 14, 37, and 42-45).



Following Gulin,<sup>39</sup> the authors of References 14 and 43-45 also used Equation (5.2-16) in conjunction with the Fresnel approximation as their starting point with the notable exception that a Gaussian functional form for the projected transmit beam pattern was used throughout their analysis.

Horton and Melton<sup>41</sup> suggested that the approximation that most critically limited their theoretical analysis was the small slope approximation, i.e., using the partial derivative with respect to  $Z$  to approximate the normal partial derivative  $\partial/\partial n$ . Several investigators have used the Kirchhoff approach to describe scatter from a randomly rough surface without making the small slope approximation.<sup>42, 46-48</sup> They started their analysis with Equation (5.2-10) and defined  $p(\vec{r})$  as the total acoustic pressure on the ocean surface, i.e., incident plus scattered. And by taking into account the normal partial derivative, a slope correction factor was obtained.<sup>46</sup> However, they used a Fraunhofer approximation and no transmit directivity function was included.

Tolstoy and Clay<sup>49</sup> also began with Equation (5.2-10) but they defined  $p(\vec{r})$  as scattered acoustic pressure only and used a Fraunhofer approximation after Eckart.<sup>38</sup> However, unlike Eckart,<sup>38</sup> they did not make a small slope approximation and they did include a Gaussian functional form for the projected transmit beam pattern. Clay and Medwin,<sup>34</sup> on the other hand, followed Gulin's<sup>39</sup> initial approach with the exception that they also included a Gaussian functional form for the projected transmit beam pattern. And finally, the results of the analysis reported in References 14, 40, 41, and 43-45 pertain only to

a specular orientation between the transmit and receive arrays, whereas the results reported in References 34, 42, and 46-49 pertain to a general bistatic geometry and are not limited to a specular geometry.

As one can see, many different combinations of assumptions have been made by the investigators mentioned above although each began with Green's theorem and the Kirchhoff integral. However, the following important but overlooked assumption is common to all: the fact that the position vectors  $\vec{R}_1$  and  $\vec{R}_T$  are not parallel, and that the vectors  $\vec{R}_2$  and  $\vec{R}_R$  are also not parallel, is ignored.<sup>49</sup> The assumption that these pairs of vectors are parallel is very much dependent upon a sufficiently narrow beamwidth.<sup>42</sup> Therefore, the following pattern emerges: if the beamwidth of the transmit directivity function is relatively narrow so that a Fraunhofer approximation is sufficient, then the "parallel assumption" is reasonable. But if the beamwidth is relatively broad, a Fresnel approximation must be used and the "parallel assumption" is no longer valid. Although References 14, 40, 41, and 43-45 used a Fresnel approximation in order to handle the relatively broad beamwidths of practical acoustic sources, they still assumed that the "parallel assumption" was valid.

The derivation of the random, time-varying, transfer function of surface reverberation in this chapter is also based upon the form of Equation (5.2-10), where  $p(\vec{r})$  is defined as the total acoustic pressure field on  $S$ . Both a transmit and receive directivity function are included. Receive directivity functions have either been

ignored in the past or stipulated as omnidirectional.<sup>43</sup> No specific functional forms for the beam patterns are assumed, but rather, they are kept as general frequency dependent expressions. Also included is the frequency dependent attenuation of sound pressure amplitude due to sound absorption. The small slope approximation is not made. A Fresnel approximation is used, and the results for the transfer function pertain to a general bistatic configuration which can then be easily reduced to either a specular or a monostatic (backscatter) orientation.

A generalized Kirchhoff approach is used since the vectors  $\vec{R}_1$  and  $\vec{R}_T$  are not assumed to be parallel, and vectors  $\vec{R}_2$  and  $\vec{R}_R$  are also not assumed to be parallel. By not assuming  $\vec{R}_R$  is parallel to  $\vec{R}_2$ , we are following a Rayleigh approach only in the sense that the total scattered field at the receive array is represented as the superposition of plane waves travelling in different directions (sum of all wave modes).<sup>46</sup> When one assumes  $\vec{R}_R$  is parallel to  $\vec{R}_2$ , this is consistent with the classical Kirchhoff approach of representing the scattered field as a superposition of plane waves travelling in only one particular direction (an individual wave mode), i.e., in the direction of  $\vec{R}_2$ .<sup>46</sup>

5.2.2 Analysis. From Equation (5.2-10), one can express the scattered acoustic pressure field at the receive array at time  $t = t_1$  as:

$$p_S(\vec{R}_2, t_1) = \int_S \left[ G[\vec{R}_2 | \vec{r}(t'_1)] \frac{\partial}{\partial n} p[\vec{r}(t'_1)] - p[\vec{r}(t'_1)] \frac{\partial}{\partial n} G[\vec{R}_2 | \vec{r}(t'_1)] \right] dS, \quad (5.2-17)$$

where the total acoustic pressure on the ocean surface at  $\vec{r}(t'_1)$  is defined as:

$$p[\vec{r}(t'_1)] \triangleq p_I[\vec{r}(t'_1)] + p_S[\vec{r}(t'_1)], \quad (5.2-18)$$

$G(\cdot | \cdot)$  is the free-space Green's function to be specified later, and

$$t'_1 = t_1 - \frac{R_R(t'_1)}{c} \quad (5.2-19)$$

is the retarded time<sup>37</sup> where  $R_R(\cdot)$  is defined by Equation (5.2-12) and  $c$  is the speed of sound in the ocean. The expressions  $p_I(\cdot)$  and  $p_S(\cdot)$  refer to the incident and scattered acoustic pressure fields, respectively. The Kirchhoff approximation will now be used to obtain an expression for  $p[\vec{r}(t'_1)]$  as defined by Equation (5.2-18).

In the Kirchhoff approximation, it is assumed that the ocean surface is locally plane, i.e., the radius of curvature at all points on the surface is assumed to be much greater than a wavelength.<sup>46,48</sup> The field on the surface is approximated by the field which would exist if the surface were replaced by an infinite plane, tangent to the surface at the point of insonification. Since the ocean surface is assumed to be in the far-field of the transmit array, Equation (5.2-18) can be approximated by:

$$p[\vec{r}(t_1')] \approx p_I[\vec{r}(t_1')] + C_{REF}[\vec{r}(t_1')] p_I[\vec{r}(t_1')] \quad , \quad (5.2-20)$$

where  $C_{REF}[\vec{r}(t_1')]$  is the plane wave pressure amplitude reflection coefficient evaluated at the point  $\vec{r}(t_1')$  on the surface. Multiple scattering effects at the surface have been ignored and it has been assumed that there is no shadow problem. The fundamental assumption in the Kirchhoff approximation which limits the validity of the solution is the extent to which the reflection coefficient  $C_{REF}(\cdot)$ , which is applicable to an infinite plane wave at an infinite plane boundary, can be used at every point of a rough surface.<sup>34,46</sup> The boundary condition represented by Equation (5.2-20) will be a very good approximation for locally flat surfaces composed of irregularities with small curvature, i.e., large radii of curvature compared to a wavelength.<sup>46</sup> In the case of a perfectly smooth surface when  $Z = \xi(x,y,t) = 0$ , Equation (5.2-20) is exact.

The roughness of a surface depends on three parameters:<sup>46</sup>

(1) the height  $h$  of the surface irregularities with respect to the XY plane; (2) the angle of incidence  $\theta_1$  measured from the Z axis; and (3) the wavelength  $\lambda$  of the incident field. For randomly rough surfaces, the parameter  $h$  should be replaced by  $\sigma$ , the standard deviation of the height variation of the rough surface.<sup>48</sup> According to the Rayleigh criterion, a random surface is considered smooth if<sup>46,48</sup>

$$\frac{\sigma}{\lambda} < \frac{1}{8 \cos \theta_1} \quad . \quad (5.2-21)$$

Therefore, from Equation (5.2-21), it can be seen that a surface approaches being smooth as either  $\sigma/\lambda \rightarrow 0$  or  $\theta_1 \rightarrow \pi/2$ .

A simple criterion for the radius of curvature restriction can be obtained if one assumes that the roughness of the surface can be represented by a two-dimensional spatial Fourier series. For example, consider height variations along the  $x$  direction only and let

$$Z = \sigma \sin \left( \frac{2\pi}{\Lambda_{\text{MIN}}} x \right), \quad (5.2-22)$$

where  $\Lambda_{\text{MIN}}$  is the minimum surface wavelength (see Figure 18) of the various surface height components along the  $x$  direction. The radius of curvature  $\rho$  of Equation (5.2-22) evaluated at  $x = \frac{\Lambda_{\text{MIN}}}{4}$  is:

$$\rho = \frac{\Lambda_{\text{MIN}}^2}{4\pi^2\sigma}. \quad (5.2-23)$$

Therefore, the Kirchhoff restriction requiring that the radius of curvature be large compared to a wavelength yields the criterion

$$\lambda \ll \frac{\Lambda_{\text{MIN}}^2}{4\pi^2\sigma} \quad (5.2-24)$$

for the boundary represented by Equation (5.2-22). Note that Equation (5.2-24) is a high frequency condition. That is, the higher the transmit frequency, the smaller the wavelength  $\lambda$  and the better the inequality given by Equation (5.2-24) will be observed.

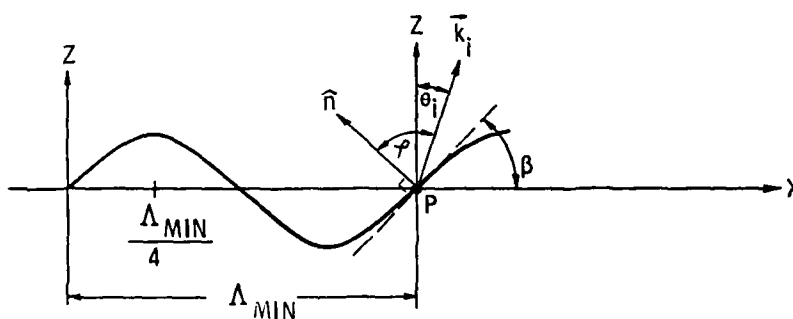


Figure 18. Geometry for example calculation of the radius of curvature criterion and the shadow prevention criterion in the incident direction. By definition, the angles  $\varphi$ ,  $\theta_i$ , and  $\beta$  are all positive.

A simple criterion for the prevention of shadows in the transmit direction can also be obtained for the surface represented by Equation (5.2-22). From Figure 18, we have that

$$\theta_1 + \beta = \gamma, \quad (5.2-25)$$

where  $\theta_1$  is the angle of incidence,  $\beta$  is the angle between the positive  $x$  axis and the dashed line which is tangent to the curve at the point of inflection  $P$ , where  $x = \lambda_{\text{MIN}}$ , and  $\gamma$  is the angle between the unit vector  $\hat{n}$  normal to the surface at  $P$  and the incident propagation vector  $\vec{k}_1$ . In order to prevent shadows,  $\gamma$  must be less than  $\pi/2$ , and since

$$\tan\beta = \left. \frac{dz}{dx} \right|_{x=\lambda_{\text{MIN}}}, \quad (5.2-26)$$

we obtain, from Equation (5.2-25), the criterion

$$\cot\theta_1 > \frac{2\pi\sigma}{\lambda_{\text{MIN}}} \quad (5.2-27)$$

for the prevention of shadows in the transmit direction. Fortuin<sup>37</sup> indicates that, according to Kinsman,<sup>50</sup> the slopes of sea surface waves cannot exceed the value of  $2/7$ . Therefore, this implies that the angle  $\beta$  in Figure 18 is less than  $16^\circ$ ; i.e.,  $\beta < \tan^{-1}(2/7) \approx 16^\circ$ .

The major problem before us is the evaluation of Equation (5.2-17). In order to evaluate Equation (5.2-17), functional forms for  $p(\cdot)$  and  $G(\cdot|\cdot)$  must be specified. Therefore, let

$$p_I[\vec{r}(t'_1)] = D_T[k, \vec{r}(t'_1)] \frac{\exp[-jk_{\text{EFF}} R_T(t'_1)]}{R_T(t'_1)} \quad (5.2-28)$$



and

$$G[\vec{R}_2 | \vec{r}(t'_1)] = D_R[k, \vec{r}(t'_1)] \frac{\exp[-jk_{\text{EFF}} R_R(t'_1)]}{R_R(t'_1)}, \quad (5.2-29)$$

where  $D_T[k, \vec{r}(t'_1)]$  and  $D_R[k, \vec{r}(t'_1)]$  are the transmit and receive directivity functions, respectively, projected onto the surface;

$k_{\text{EFF}}$  is the complex, effective wave number defined as:

$$k_{\text{EFF}} \triangleq k - j\alpha(f), \quad (5.2-30)$$

where  $\alpha(f)$  is the frequency dependent pressure amplitude attenuation coefficient (in nepers/m) due to sound absorption, and from Figure 17:

$$R_T(t'_1) = |\vec{r}(t'_1) - \vec{R}_1| \quad (5.2-31)$$

and

$$R_R(t'_1) = |\vec{r}(t'_1) - \vec{R}_2| \quad (5.2-32)$$

Having specified  $p(\cdot)$  and  $G(\cdot | \cdot)$ , it is now possible to obtain expressions for the normal partial derivatives of  $p(\cdot)$  and  $G(\cdot | \cdot)$ . It can be shown that the normal partial derivative of  $p(\cdot)$  as given by Equation (5.2-20) is:

$$\frac{\partial}{\partial n} p[\vec{r}(t'_1)] \approx -(\hat{n} \cdot \hat{n}_T)[1 - C_{\text{REF}}]jk_{\text{EFF}}p_I[\vec{r}(t'_1)], \quad (5.2-33)$$

where it has been assumed that  $C[\vec{r}(t'_1)] = C_{\text{REF}}$  (a constant),

$|k_{\text{EFF}} R_T(t'_1)| \gg 1$ , and

$$\frac{|\hat{n} \cdot \nabla D_T[k, \vec{r}(t'_1)]|}{|(\hat{n} \cdot \hat{n}_T)k_{\text{EFF}}D_T[k, \vec{r}(t'_1)]|} \ll 1 \quad (5.2-34)$$

Equation (5.2-33) is derived in Appendix C where use has been made of References 26, 46, 51, and 52.

Since for the ocean-air interface the difference in the characteristic impedances of the two media is so large, the reflection coefficient is effectively no longer a function of the local angle of incidence or of position on the ocean surface for that matter. Hence, the assumption that the reflection coefficient is a constant is very reasonable; in fact,  $C_{REF} \approx -1$ . With  $C_{REF} = -1$ , Equation (5.2-20) is equal to zero and Equation (5.2-33) is a maximum which are correct results for a pressure release boundary like the ocean surface. The assumption that  $|k_{EFF} R_T(t'_1)| \gg 1$  is commonly referred to as the far-field assumption and indicates that the transmit array is many wavelengths away from the ocean surface. Equation (5.2-34) stipulates that the ratio of the magnitude of the gradient of the projected transmit directivity function to the projected directivity function itself must be small compared to the reciprocal of the wavelength. The inequality given by Equation (5.2-34) will be observed best over the projected beamwidth of the directivity function. In addition, Equation (5.2-34) is a high frequency condition similar to the radius of curvature criterion because of the appearance of  $k_{EFF}$  in the denominator. As the frequency of the transmit signal increases,  $k_{EFF}$  also increases, and as a result, the left-hand side of Equation (5.2-34) decreases and the inequality is better observed. Although high frequencies make directivity patterns more directional (i.e., the beamwidth decreases as the frequency increases<sup>24</sup>), the gradient of the projected transmit directivity function over its beamwidth will still remain small since it was assumed that the ocean surface was in the

far-field of the transmit array. For example, consider an arbitrary directivity pattern  $D(ku, kv)$ , where  $k = 2\pi/\lambda$ ,  $u = \sin\theta\cos\psi$ , and  $v = \sin\theta\sin\psi$ . The gradient of  $D(ku, kv)$  in spherical coordinates is given by:

$$\begin{aligned} \nabla D(ku, kv) = & (1/r) \frac{\partial}{\partial \theta} D(ku, kv) \hat{a}_\theta + \\ & (1/[r\sin\theta]) \frac{\partial}{\partial \psi} D(ku, kv) \hat{a}_\psi \end{aligned} \quad (5.2-35)$$

since the directivity function is not a function of range  $r$ . Therefore, it can be seen from Equation (5.2-35) that  $|\nabla D(ku, kv)|$  decreases as the range  $r$  from the array increases. As a consequence of the requirement imposed by Equation (5.2-34), the expression for  $\frac{\partial}{\partial n} p[\vec{r}(t'_1)]$  as given by Equation (5.2-33) will be a good approximation for that region of the ocean surface which is insonified by the beam-width of the transmit directivity function. Equation (5.2-34) is analogous to the condition (see Tolstoy<sup>53</sup>)

$$\frac{\nabla^2 D(ku, kv)}{k^2 D(ku, kv)} \ll 1 \quad (5.2-36)$$

which must be satisfied if  $p = D(ku, kv)\exp(-jkr)/r$  is to be an approximate solution to the Helmholtz wave equation  $(\nabla^2 + k^2)p = 0$ .

And finally, note that the dot product  $(\hat{n} \cdot \hat{n}_T)$  in the denominator of Equation (5.2-34) is a possible source of trouble, i.e., it may equal zero at some point  $\vec{r}(t'_1)$  on the ocean surface. However, refer to Figure 18 and to the cone defined by the  $Z$  axis and dashed line which is tangent to the curve at point  $P$ . All rays with their respective directions of propagation  $\vec{k}_1$ , and hence, angles of incidence  $\theta_1$  delimited by this cone satisfy the shadow prevention

criterion of Equation (5.2-27). Now assume that the transmit array is positioned in such a way that the various directions of propagation defined by the beamwidth of its directivity function coincide with those within the cone. Then, the expression  $(\hat{n} \cdot \hat{n}_T)$  will never equal zero, and Equation (5.2-34) will always be finite for at least those rays emanating from within the beamwidth (note that  $\vec{k}_i = k\hat{n}_T$ ).

Similarly, upon taking the normal partial derivation of  $G(\cdot|\cdot)$  as given by Equation (5.2-29), one obtains:

$$\frac{\partial}{\partial n} G[\vec{R}_2 | \vec{r}(t'_1)] \approx + (\hat{n} \cdot \hat{n}_R) jk_{\text{EFF}} G[\vec{R}_2 | \vec{r}(t'_1)] , \quad (5.2-37)$$

where it has been assumed that  $|k_{\text{EFF}} R_R(t'_1)| \gg 1$  and that

$$\frac{|\hat{n} \cdot \nabla D_R[k, \vec{r}(t'_1)]|}{|(\hat{n} \cdot \hat{n}_R) k_{\text{EFF}} D_R[k, \vec{r}(t'_1)]|} \ll 1 , \quad (5.2-38)$$

where

$$\nabla \left( \frac{\exp[-jk_{\text{EFF}} R_R(t'_1)]}{R_R(t'_1)} \right) = \frac{\partial}{\partial R_R(t'_1)} \left( \frac{\exp[-jk_{\text{EFF}} R_R(t'_1)]}{R_R(t'_1)} \right) \cdot (-\hat{n}_R) , \quad (5.2-39)$$

since  $R_R(t'_1) = |\vec{R}_R(t'_1)|$  is a distance measured in the direction  $(-\hat{n}_R)$  (see Figure 17 and refer to References 26, 46, or 52). Note the term  $(\hat{n} \cdot \hat{n}_R)$  in the denominator of Equation (5.2-38). Refer to Figure 19 and to the cone defined by the Z axis and the dashed line which is tangent to the curve at point P. All rays with their respective directions of propagation  $\vec{k}_S$ , and hence, angles of scatter  $\theta_S$  delimited by this cone satisfy the criterion

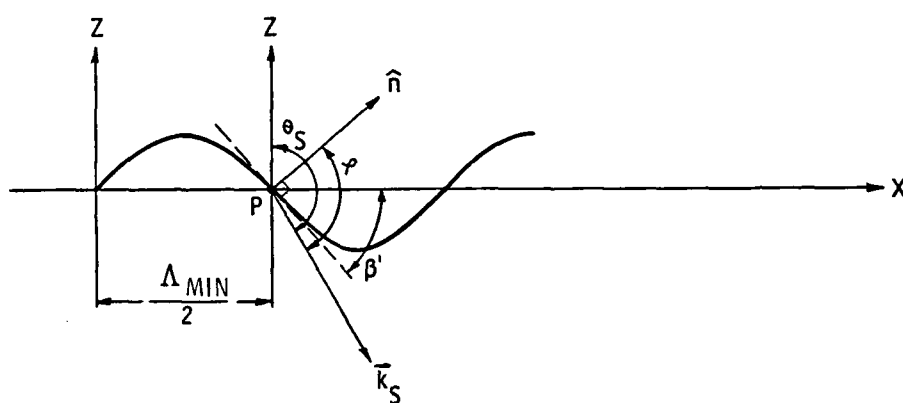


Figure 19. Geometry for example calculation of the shadow prevention criterion in the scatter direction. By definition, the angles  $\gamma$  and  $\theta_S$  are positive, while the angle  $\beta'$  is negative.

$$-\cot\theta_S > \frac{2\pi\sigma}{\lambda_{\text{MIN}}} \quad (5.2-40)$$

which, if obeyed, prevents the shadowing of the scattered radiation. With the exception of the minus sign, Equation (5.2-40) is analogous to Equation (5.2-27). The minus sign is required since  $\theta_S > \pi/2$ , and as a result,  $\cot\theta_S < 0$ . Also note from Figure 19 that the point of inflection P at  $x = \lambda_{\text{MIN}}/2$  was used and in order to prevent shadowing in the scatter direction,  $\varphi > \pi/2$ . Now, assume that the receive array is also positioned in such a way that the various directions of propagation defined by the beamwidth of its directivity function coincide with those within the cone. Then, the expression  $(\hat{n} \cdot \hat{n}_R)$  will never equal zero, and Equation (5.2-38) will always be finite for at least those rays entering within the beamwidth (note that  $\vec{k}_S = k\hat{n}_R$ ).

Upon substituting Equations (5.2-20), (5.2-33), (5.2-37), (5.2-28), and (5.2-29) into Equation (5.2-17), and dropping the multiplicative term  $jk_{\text{EFF}}$  from in front of the integral, one obtains the random, time-varying transfer function

$$H_{\text{REV}}(f, t_1) = \int_S D_T[k, \vec{r}(t_1')] D_R[k, \vec{r}(t_1')] \cdot \frac{\exp\{-jk_{\text{EFF}}[R_T(t_1') + R_R(t_1')]\}}{R_T(t_1') R_R(t_1')} \cdot [\hat{n} \cdot (\hat{n}_T - \hat{n}_R) C_{\text{REF}} - \hat{n} \cdot (\hat{n}_T + \hat{n}_R)] dS \quad (5.2-41)$$

of the linear, time-varying, random communication channel consisting of the ocean surface and a bistatic transmit/receive array geometry as illustrated in Figure 17. The subscript "REV" denotes surface reverberation. Note that  $p_S(\vec{R}_2, t_1) \sim H_{REV}(f, t_1)$  since a time-harmonic input signal of frequency  $f$  (Hz) was transmitted<sup>37</sup> [see Equations (3.2-16) - (3.2-18)]. The unit vectors  $\hat{n}$ ,  $\hat{n}_T$ , and  $\hat{n}_R$  are all functions of position along the ocean surface. In addition,  $\hat{n}$  is also a function of the retarded time  $t'_1$ . The integration in Equation (5.2-41) is meant to be performed over that region of the surface which corresponds to the intersection of the projected beam-widths of both the transmit and receive directivity functions. It is interesting to note that when one defines  $p[\vec{r}(t'_1)]$  in Equation (5.2-17) as being equal to incident plus scattered acoustic pressure [see Equation (5.2-18)], one obtains both of the terms  $(\hat{n}_T - \hat{n}_R)C_{REF}$  and  $(\hat{n}_T + \hat{n}_R)$  in Equation (5.2-41) [e.g., see Beckmann and Spizzichino<sup>46</sup> or Ishimaru<sup>48</sup>]. However, if one defines  $p[\vec{r}(t'_1)]$  in Equation (5.2-17) as being equal to scattered acoustic pressure only, then one obtains only the term  $(\hat{n}_T - \hat{n}_R)C_{REF}$  in Equation (5.2-41) [e.g., see Tolstoy and Clay<sup>49</sup>].

Let us now consider the ranges  $R_T(t'_1)$  and  $R_R(t'_1)$  which appear in the denominator of Equation (5.2-41). From Equations (5.2-31) and (5.2-32), we obtain the following approximations:

$$R_T(t'_1) = |\vec{r}(t'_1) - \vec{R}_1| \approx R_1 \quad (5.2-42)$$

and

$$R_R(t'_1) = |\vec{r}(t'_1) - \vec{R}_2| \approx R_2, \quad (5.2-43)$$

where  $R_1 = |\vec{R}_1|$  and  $R_2 = |\vec{R}_2|$ , and where it has been assumed that  $|\vec{r}(t'_1)/\vec{R}_1| < 1$  and  $|\vec{r}(t'_1)/\vec{R}_2| < 1$ . While Equations (5.2-42) and (5.2-43) are suitable approximations for amplitude attenuation due to spherical spreading, they are not appropriate for the phase information represented by the complex exponential appearing in the integrand of Equation (5.2-41). Therefore, for the phase information, both  $R_T(t'_1)$  and  $R_R(t'_1)$  will be expressed in terms of a binomial expansion.

Starting with Equation (5.2-31),  $R_T(t'_1)$  can be rewritten as follows:

$$R_T(t'_1) = |\vec{r}(t'_1) - \vec{R}_1| = \sqrt{[\vec{r}(t'_1) - \vec{R}_1] \cdot [\vec{r}(t'_1) - \vec{R}_1]}$$

(5.2-44)

or

$$R_T(t'_1) = R_1 \sqrt{1 + b_T}, \quad (5.2-45)$$

where

$$b_T = \left\{ \frac{r(t'_1)}{R_1} \right\}^2 - 2 \frac{\hat{r}_1 \cdot \vec{r}(t'_1)}{R_1}, \quad (5.2-46)$$

$$\vec{r}(t'_1) = x \hat{x} + y \hat{y} + \xi(x, y, t'_1) \hat{z}, \quad (5.2-47)$$

$$r^2(t'_1) = |\vec{r}(t'_1)|^2 = x^2 + y^2 + \xi^2(x, y, t'_1) \quad (5.2-48)$$

and

$$\hat{r}_1 = \sin\theta_1 \cos\psi_1 \hat{x} + \sin\theta_1 \sin\psi_1 \hat{y} + \cos\theta_1 \hat{z} \quad (5.2-49)$$

is the unit vector of  $\vec{R}_1$  (see Figure 20). Note that the azimuth angles  $\psi_1$  and  $\psi_2$  are measured in a counterclockwise direction from the positive X axis. In order to use a binomial expansion on



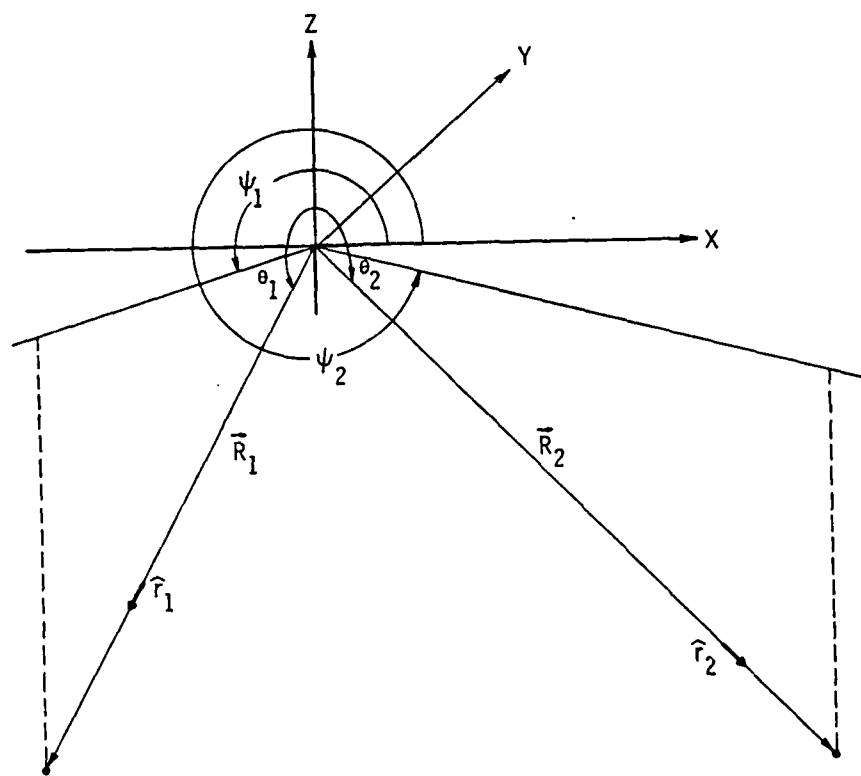


Figure 20. Spherical angles  $\theta_1$ ,  $\psi_1$  and  $\theta_2$ ,  $\psi_2$  of the unit vectors  $\hat{r}_1$  and  $\hat{r}_2$ , respectively.

Equation (5.2-45), two questions must be answered. First, is the inequality  $|b_T| < 1$  satisfied, and second, if the inequality is indeed observed, how many terms in the expansion should be used?

Some insight into the answers to these two questions can be obtained by referring to Figure 21. The position vector  $\vec{r}(t'_1)$  is shown lying in the XY plane. Since the ocean surface will eventually be projected onto the XY plane later in the analysis, this situation is representative of our problem. The angle  $\epsilon$  is the beamwidth of the directivity pattern, and  $\gamma$  is the grazing angle. From Figure 21 and the Law of Sines,

$$\frac{r(t'_1)}{R_1} = \frac{\sin(\epsilon/2)}{\sin(\gamma - \frac{\epsilon}{2})} \quad (5.2-50)$$

Substituting Equation (5.2-50) into Equation (5.2-46), and taking the absolute value of both sides of the resulting equation yields:

$$|b_T| = \left| \frac{\sin(\epsilon/2)}{\sin(\gamma - \frac{\epsilon}{2})} \left[ \frac{\sin(\epsilon/2)}{\sin(\gamma - \frac{\epsilon}{2})} - 2\cos(\pi - \gamma) \right] \right|, \quad (5.2-51)$$

where  $(\pi - \gamma)$  is the angle between  $\hat{r}_1$  and  $\vec{r}(t'_1)$ .

Table 3 lists values of  $|b_T|$  computed from Equation (5.2-51) for several different values of beamwidth  $\epsilon$  and grazing angle  $\gamma$ . One can see two trends from the data of Table 3. The inequality  $|b_T| < 1$  is observed best for narrow beamwidths and for grazing angles approaching  $90^\circ$ . However, with the exception of  $\gamma = 90^\circ$ , the values of  $|b_T|$  are not, in general significantly less than 1. In fact, for

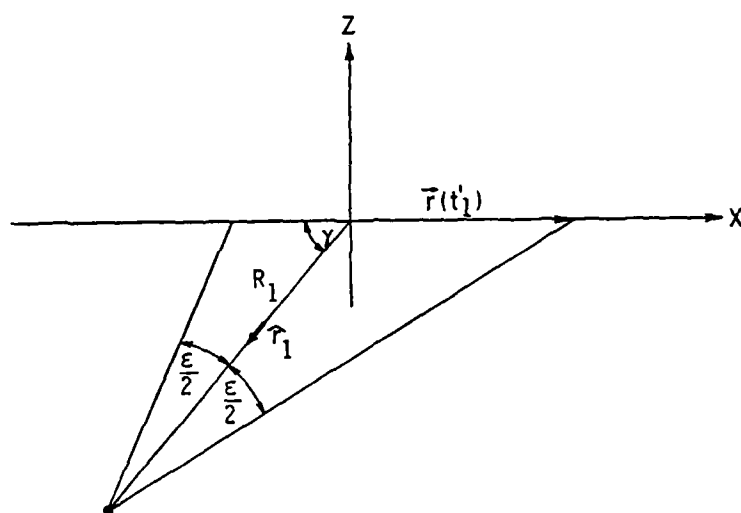


Figure 21. Geometry for the calculation of the binomial expansion criterion. The angle  $\epsilon$  is the beamwidth of the directivity pattern and  $\gamma$  is the grazing angle.

TABLE 3

VALUES OF THE BINOMIAL EXPANSION FACTOR  $|b_T|$   
 FOR DIFFERENT COMBINATIONS OF BEAMWIDTH  $\epsilon$   
 AND GRAZING ANGLE  $\gamma$

<u><math>\epsilon</math> (deg)</u>	<u><math>\gamma</math> (deg)</u>	<u><math> b_T </math></u>
10	30	0.4
10	45	0.209
10	60	0.117
10	90	0.008
20	30	1.137
20	45	0.52
20	60	0.279
20	90	0.031
30	30	2.732
30	45	1.001
30	60	0.5
30	90	0.072

---

$\epsilon = 20^\circ$  and  $\gamma = 30^\circ$ ,  $\epsilon = 30^\circ$  and  $\gamma = 30^\circ$ , and  $\epsilon = 30^\circ$  and  $\gamma = 45^\circ$ ,  $|b_T| > 1.0$ , and as a result, a binomial expansion is not valid for these combinations of parameters. Therefore, Equation (5.2-45) will be expanded to include second order terms (Fresnel approximation) as opposed to only first order terms (Fraunhofer approximation).

Assuming that  $|b_T| < 1$ , Equation (5.2-45) can be expressed as

$$R_T(t'_1) \approx R_1 \left[ 1 + \frac{b_T}{2} - \frac{b_T^2}{8} \right], \quad (5.2-52)$$

and upon substituting Equations (5.2-46) through (5.2-49) into Equation (5.2-52), one obtains:

$$\begin{aligned} R_T(t'_1) \approx & R_1 + \frac{(1 - \sin^2 \theta_1 \cos^2 \psi_1)}{2R_1} x^2 + \\ & \frac{(1 - \sin^2 \theta_1 \sin^2 \psi_1)}{2R_1} y^2 + \\ & \frac{\sin^2 \theta_1}{2R_1} \xi^2(x, y, t'_1) - \\ & \left\{ x \sin \theta_1 \cos \psi_1 \left[ 1 + \frac{y}{R_1} \sin \theta_1 \sin \psi_1 + \right. \right. \\ & \left. \left. \frac{\xi(x, y, t'_1)}{R_1} \cos \theta_1 \right] + y \sin \theta_1 \sin \psi_1 \cdot \right. \\ & \left. \left[ 1 + \frac{\xi(x, y, t'_1)}{R_1} \cos \theta_1 \right] + \xi(x, y, t'_1) \cos \theta_1 \right\}, \end{aligned} \quad (5.2-53)$$

where individual and cross product terms involving  $x$ ,  $y$ , and  $\xi(x, y, t'_1)$  raised to powers higher than 2 were not included in the expansion. Equation (5.2-53) can be simplified considerably if one orients the XYZ coordinate system in such a way that  $\vec{R}_1$  lies in the XZ plane, i.e., let  $\psi_1 = \pi$ . With  $\psi_1 = \pi$ , Equation (5.2-53) reduces to:

$$\begin{aligned}
 R_T(t'_1) \approx & R_1 + \frac{\cos^2 \theta_1}{2R_1} x^2 + \frac{1}{2R_1} y^2 + \frac{\sin^2 \theta_1}{2R_1} \xi^2(x, y, t'_1) \\
 & - \left\{ -x \sin \theta_1 \left[ 1 + \frac{\xi(x, y, t'_1)}{R_1} \cos \theta_1 \right] + \right. \\
 & \left. \xi(x, y, t'_1) \cos \theta_1 \right\} , \quad (5.2-54)
 \end{aligned}$$

where the cross product terms involving  $xy$  and  $y\xi(x, y, t'_1)$  have cancelled out. Assuming that

$$\frac{\sin^2 \theta_1}{2R_1} \sigma^2 \ll 1 , \quad (5.2-55)$$

where  $\sigma^2 = E\{\xi^2(x, y, t'_1)\}$  is the variance of the zero-mean, random process,  $\xi(x, y, t'_1)$ , and

$$\left| \frac{\cos \theta_1}{R_1} \sigma \right| \ll 1 , \quad (5.2-56)$$

then Equation (5.2-54) further reduces to:

$$R_T(t'_1) \approx R_1 - \hat{r}_1 \cdot \vec{r}(t'_1) + \frac{\cos^2 \theta_1}{2R_1} x^2 + \frac{1}{2R_1} y^2, \quad (5.2-57)$$

where

$$\hat{r}_1 \cdot \vec{r}(t'_1) = -x \sin \theta_1 + \xi(x, y, t'_1) \cos \theta_1 \quad (5.2-58)$$

and  $\psi_1 = \pi$ .

Similarly,  $R_R(t'_1)$  can be expanded as:

$$R_R(t'_1) \approx R_2 \left[ 1 + \frac{b_R}{2} - \frac{b_R^2}{8} \right]; \quad |b_R| < 1, \quad (5.2-59)$$

where

$$b_R = \left( \frac{r(t'_1)}{R_2} \right)^2 - 2 \frac{\hat{r}_2 \cdot \vec{r}(t'_1)}{R_2} \quad (5.2-60)$$

and

$$\hat{r}_2 = \sin \theta_2 \cos \psi_2 \hat{x} + \sin \theta_2 \sin \psi_2 \hat{y} + \cos \theta_2 \hat{z} \quad (5.2-61)$$

is the unit vector of  $\vec{R}_2$ . Substituting Equations (5.2-60), (5.2-61), (5.2-47), and (5.2-48) into Equation (5.2-59) yields:

$$\begin{aligned} R_R(t'_1) \approx R_2 + \frac{(1 - \sin^2 \theta_2 \cos^2 \psi_2)}{2R_2} x^2 + \\ \frac{(1 - \sin^2 \theta_2 \sin^2 \psi_2)}{2R_2} y^2 + \frac{\sin^2 \theta_2}{2R_2} \xi^2(x, y, t'_1) - \\ \left\{ x \sin \theta_2 \cos \psi_2 \left[ 1 + \frac{y}{R_2} \sin \theta_2 \sin \psi_2 + \right. \right. \end{aligned}$$

$$\frac{\xi(x,y,t'_1)}{R_2} \cos\theta_2 \Big] + y \sin\theta_2 \sin\psi_2 \cdot$$

$$\left[ 1 + \frac{\xi(x,y,t'_1)}{R_2} \cos\theta_2 \right] + \xi(x,y,t'_1) \cos\theta_2 \Big\} , \quad (5.2-62)$$

where, as before, individual and cross product terms involving  $x$ ,  $y$ , and  $\xi(x,y,t'_1)$  raised to powers higher than 2 were not included in the expansion. Assuming that

$$\frac{\sin^2\theta_2}{2R_2} \sigma^2 \ll 1 , \quad (5.2-63)$$

$$\left| \frac{\cos\theta_2}{R_2} \sigma \right| \ll 1 \quad (5.2-64)$$

and, in addition, that

$$\frac{y}{R_2} \sin\theta_2 \sin\psi_2 \ll 1 , \quad (5.2-65)$$

Equation (5.2-62) reduces to:

$$R_R(t'_1) \approx R_2 - \hat{r}_2 \cdot \vec{r}(t'_1) + \frac{(1 - \sin^2\theta_2 \cos^2\psi_2)}{2R_2} x^2 +$$

$$\frac{(1 - \sin^2\theta_2 \sin^2\psi_2)}{2R_2} y^2 , \quad (5.2-66)$$

where

$$\hat{r}_2 \cdot \vec{r}(t'_1) = x \sin\theta_2 \cos\psi_2 + y \sin\theta_2 \sin\psi_2 + \xi(x,y,t'_1) \cos\theta_2 . \quad (5.2-67)$$



Note that since  $\psi_1 = \pi$ , if one chooses  $\psi_2 = 2\pi$  for a specular geometry or  $\psi_2 = \pi$  for a backscatter geometry, then the left-hand side of Equation (5.2-65) equals zero (see Figure 20).

Upon substituting Equations (5.2-42), (5.2-43), (5.2-57), (5.2-58), (5.2-66), and (5.2-67) into Equation (5.2-41), the following expression for the transfer function of ocean surface reverberation is obtained:

$$\begin{aligned}
 H_{REV}(f, t_1) = & \frac{\exp(-jk_{EFF}[R_1 + R_2])}{R_1 R_2} \int_S D_T[k, \vec{r}(t_1')] D_R[k, \vec{r}(t_1')] \cdot \\
 & \exp\{-jk_{EFF}[\ell x + my + n\xi(x, y, t_1')]\} \cdot \\
 & \exp\{-jk_{EFF}[(\ell_f/2)x^2 + (m_f/2)y^2]\} \cdot \\
 & [\hat{n} \cdot (\hat{n}_T - \hat{n}_R) C_{REF} - \hat{n} \cdot (\hat{n}_T + \hat{n}_R)] dS, \\
 & (5.2-68)
 \end{aligned}$$

where

$$\ell = \sin\theta_1 - \sin\theta_2 \cos\psi_2, \quad (5.2-69)$$

$$m = -\sin\theta_2 \sin\psi_2, \quad (5.2-70)$$

$$n = -(\cos\theta_1 + \cos\theta_2), \quad (5.2-71)$$

$$\ell_f = \frac{\cos^2\theta_1}{R_1} + \frac{(1 - \sin^2\theta_2 \cos^2\psi_2)}{R_2}, \quad (5.2-72)$$

and

$$m_f = \frac{1}{R_1} + \frac{(1 - \sin^2\theta_2 \sin^2\psi_2)}{R_2}, \quad (5.2-73)$$

where the subscript  $f$  denotes "Fresnel approximation term." If a Fraunhofer approximation happens to be sufficient for a particular problem, one can simply let the Fresnel coefficients  $\ell_f$  and  $m_f$  equal zero.

Our efforts will now be devoted to simplifying the term

$$I \triangleq [\hat{n} \cdot (\hat{n}_T - \hat{n}_R) C_{REF} - \hat{n} \cdot (\hat{n}_T + \hat{n}_R)] dS \quad (5.2-74)$$

which appears in the integrand of Equation (5.2-68).

The difficulty with Equation (5.2-74) is trying to specify  $\hat{n}$ ,  $\hat{n}_T$ , and  $\hat{n}_R$  which are functions of position along the randomly rough, time-varying, ocean surface  $S$ . This problem can be avoided by projecting  $S$  onto the  $XY$  plane as follows.

Let vectors  $\vec{a}(x,y)$  and  $\vec{b}(x,y)$  be defined as:

$$\begin{aligned} \vec{a}(x,y) &\triangleq \hat{n}_T(x,y) - \hat{n}_R(x,y) = a_x(x,y)\hat{x} + \\ &\quad a_y(x,y)\hat{y} + a_z(x,y)\hat{z} \end{aligned} \quad (5.2-75)$$

and

$$\begin{aligned} \vec{b}(x,y) &\triangleq \hat{n}_T(x,y) + \hat{n}_R(x,y) = b_x(x,y)\hat{x} + \\ &\quad b_y(x,y)\hat{y} + b_z(x,y)\hat{z} \end{aligned} \quad (5.2-76)$$

and also express the unit vector  $\hat{n}(x,y,t'_1)$  in rectangular components, i.e.,

$$\hat{n}(x,y,t'_1) = n_x(x,y,t'_1)\hat{x} + n_y(x,y,t'_1)\hat{y} + n_z(x,y,t'_1)\hat{z} \quad (5.2-77)$$

Since an infinitesimal surface area element  $dS$  is related to its projection onto the  $XY$  plane  $dxdy$  by<sup>48,49,51</sup>

$$dS = \frac{dxdy}{n_z}, \quad (5.2-78)$$

and since

$$\frac{n_x}{n_z} = - \frac{\partial}{\partial x} \xi(x, y, t'_1) \quad (5.2-79)$$

and

$$\frac{n_y}{n_z} = - \frac{\partial}{\partial y} \xi(x, y, t'_1), \quad (5.2-80)$$

then, substituting Equations (5.2-75) through (5.2-80) into Equation (5.2-74) yields:

$$\begin{aligned} I(x, y, t'_1) = & \left\{ \left[ -a_x \frac{\partial}{\partial x} \xi(x, y, t'_1) - \right. \right. \\ & \left. \left. a_y \frac{\partial}{\partial y} \xi(x, y, t'_1) + a_z \right] C_{REF} - \right. \\ & \left[ -b_x \frac{\partial}{\partial x} \xi(x, y, t'_1) - \right. \\ & \left. \left. b_y \frac{\partial}{\partial y} \xi(x, y, t'_1) + b_z \right] \right\} dxdy \quad (5.2-81) \end{aligned}$$

or

$$\begin{aligned} I(x, y, t'_1) = & \left\{ -\nabla_{xy} \xi(x, y, t'_1) \cdot [C_{REF} \vec{a} - \vec{b}] + \right. \\ & \left. [C_{REF} a_z - b_z] \right\} dxdy, \quad (5.2-82) \end{aligned}$$

where  $\nabla_{xy}$  is the two-dimensional gradient defined as:

$$\nabla_{xy} \triangleq \frac{\partial}{\partial x} \hat{x} + \frac{\partial}{\partial y} \hat{y} \quad (5.2-83)$$

Substituting Equation (5.2-81) into Equation (5.2-68) yields:

$$\begin{aligned} H_{REV}(f, t_1) = & \frac{\exp(-jk_{EFF}[R_1 + R_2])}{R_1 R_2} \int_x \int_y D_T(k, x, y) D_R(k, x, y) \cdot \\ & \exp\{-jk_{EFF}[\ell x + my + n\xi(x, y, t'_1)]\} \cdot \\ & \exp\{-jk_{EFF}[(\ell_f/2)x^2 + (m_f/2)y^2]\} \cdot \\ & \left\{ \left[ -a_x \frac{\partial}{\partial x} \xi(x, y, t'_1) - \right. \right. \\ & \quad \left. \left. a_y \frac{\partial}{\partial y} \xi(x, y, t'_1) + a_z \right] C_{REF} - \right. \\ & \quad \left[ -b_x \frac{\partial}{\partial x} \xi(x, y, t'_1) - \right. \\ & \quad \left. \left. b_y \frac{\partial}{\partial y} \xi(x, y, t'_1) + b_z \right] \right\} dx dy, \quad (5.2-84) \end{aligned}$$

where  $D_T(k, x, y)$  and  $D_R(k, x, y)$  are the transmit and receive directivity functions, respectively, projected onto the XY plane. Recall that the coefficients  $a_x$ ,  $a_y$ ,  $a_z$ ,  $b_x$ ,  $b_y$ , and  $b_z$  are also functions of  $x$  and  $y$ .

Let us consider the physical significance of Equation (5.2-82) for a moment. This equation indicates that the integration along the

ocean surface itself  $dS$  has been replaced by an integration in the  $XY$  plane  $dx dy$ . However, the price we pay is the need to evaluate the gradient of the random process  $\xi(x, y, t'_1)$ . This problem can be avoided by performing an integration by parts to be discussed later, but for now, the presence of the gradient yields some important information.

For a perfectly smooth ocean surface (i.e., an infinite plane boundary),  $\xi(x, y, t'_1) = 0$ , and hence,  $\nabla_{xy} \xi(x, y, t'_1) = 0$ . Therefore, Equation (5.2-82) reduces to:

$$I(x, y, t'_1) = [C_{REF} a_z(x, y) - b_z(x, y)] dx dy \quad (5.2-85)$$

for a perfectly smooth ocean surface. Thus, the term  $[C_{REF} a_z - b_z]$  represents the specular contribution to the total scattered acoustic pressure field, while the term  $\nabla_{xy} \xi(x, y, t'_1)$  represents the contribution due to surface roughness.

The next objective, as mentioned previously, is to eliminate the partial derivatives of  $\xi(x, y, t'_1)$  by performing an integration by parts.<sup>46,48,49</sup> For example, consider the following double integral from Equation (5.2-84):

$$\begin{aligned} & \int_y \exp(-jk_{EFF} my) \exp(-jk_{EFF} \frac{m_f}{2} y^2) \int_x D_T(k, x, y) D_R(k, x, y) \cdot \\ & \exp(-jk_{EFF} lx) \exp(-jk_{EFF} \frac{l_f}{2} x^2) a_x C_{REF} \cdot \\ & \exp[-jk_{EFF} n \xi(x, y, t'_1)] \frac{\partial}{\partial x} \xi(x, y, t'_1) dx dy . \end{aligned} \quad (5.2-86)$$

Although the minus sign appearing before  $a_x$  in Equation (5.2-84) is not included in Equation (5.2-86), it will be accounted for later in the analysis. Perform an integration by parts with respect to the  $x$  integration by letting

$$u = D_T(k, x, y) D_R(k, x, y) \exp(-jk_{\text{EFF}} l x) \exp(-jk_{\text{EFF}} \frac{l_f}{2} x^2) a_x C_{\text{REF}} \quad (5.2-87)$$

and

$$dv = \exp[-jk_{\text{EFF}} n \xi(x, y, t'_1)] \frac{\partial}{\partial x} \xi(x, y, t'_1) dx. \quad (5.2-88)$$

Next, perform the following total differentiation:

$$\begin{aligned} \frac{d}{dx} \exp[-jk_{\text{EFF}} n \xi(x, y, t'_1)] &= \frac{\partial}{\partial x} \exp[-jk_{\text{EFF}} n \xi(x, y, t'_1)] + \\ &\quad \frac{\partial}{\partial t'_1} \left\{ \exp[-jk_{\text{EFF}} n \xi(x, y, t'_1)] \right\} \frac{dt'_1}{dx} \end{aligned} \quad (5.2-89)$$

or

$$\begin{aligned} \frac{d}{dx} \exp[-jk_{\text{EFF}} n \xi(x, y, t'_1)] &= -jk_{\text{EFF}} n \exp[-jk_{\text{EFF}} n \xi(x, y, t'_1)] \cdot \\ &\quad \left[ \frac{\partial}{\partial x} \xi(x, y, t'_1) + \frac{\partial}{\partial t'_1} \xi(x, y, t'_1) \frac{dt'_1}{dx} \right], \end{aligned} \quad (5.2-90)$$

where, from Equations (5.2-19), (5.2-66), and (5.2-67), it can be shown that:

$$\begin{aligned}
\frac{dt'_1}{dx} \left[ 1 - \frac{\cos\theta_2}{c} \frac{\partial}{\partial t'_1} \xi(x,y,t'_1) \right] &= \left( \frac{1}{c} \right) \left[ \sin\theta_2 \cos\psi_2 - \right. \\
&\quad \left. \frac{(1 - \sin^2\theta_2 \cos^2\psi_2)}{R_2} x \right] + \\
&\quad \left( \frac{\cos\theta_2}{c} \right) \frac{\partial}{\partial x} \xi(x,y,t'_1) \quad . \quad (5.2-91)
\end{aligned}$$

Since the magnitudes of both  $(\cos\theta_2/c)$  and the first term on the right-hand side of Equation (5.2-91) is  $\ll 1$ , and if it is further assumed that  $\xi(x,y,t'_1)$  is a slowly varying function of time during the interval of insonification of the ocean surface, i.e.,

$$\frac{\partial}{\partial t'_1} \xi(x,y,t'_1) \approx 0 \quad , \quad (5.2-92)$$

then, Equation (5.2-91) reduces to:

$$\frac{dt'_1}{dx} \approx \left( \frac{\cos\theta_2}{c} \right) \frac{\partial}{\partial x} \xi(x,y,t'_1) \quad . \quad (5.2-93)$$

Note that the magnitude of the partial derivative of  $\xi(x,y,t'_1)$  in the  $x$  direction may be large. Substituting Equation (5.2-93) into Equation (5.2-90) yields:

$$\begin{aligned}
\frac{d}{dx} \exp[-jk_{\text{EFF}} n \xi(x,y,t'_1)] &\approx \\
&-jk_{\text{EFF}} n \exp[-jk_{\text{EFF}} n \xi(x,y,t'_1)] \left[ \frac{\partial}{\partial x} \xi(x,y,t'_1) \right] \quad . \\
\left[ 1 + \left( \frac{\cos\theta_2}{c} \right) \frac{\partial}{\partial t'_1} \xi(x,y,t'_1) \right] &\quad (5.2-94)
\end{aligned}$$

and upon using Equation (5.2-92), one obtains:

$$\frac{d[\exp\{-jk_{EFF}n\xi(x,y,t'_1)\}]}{(-jk_{EFF}n)} \approx \exp[-jk_{EFF}n\xi(x,y,t'_1)] \cdot$$

$$\frac{\partial}{\partial x} \xi(x,y,t'_1) dx = dv.$$

(5.2-95)

Therefore, from Equation (5.2-95),

$$v \approx - \frac{\exp[-jk_{EFF}n\xi(x,y,t'_1)]}{jk_{EFF}n} \quad (5.2-96)$$

The last piece of information needed for the integration by parts is  $du/dx$ . From Equation (5.2-87),

$$\begin{aligned} du = & C_{REF} \exp(-jk_{EFF}\ell x) \exp(-jk_{EFF} \frac{\ell_f}{2} x^2) \cdot \\ & \left\{ -jk_{EFF} a_x D_T(k,x,y) D_R(k,x,y) [\ell + \ell_f x] + \right. \\ & a_x D_T(k,x,y) \frac{\partial}{\partial x} D_R(k,x,y) + a_x D_R(k,x,y) \frac{\partial}{\partial x} D_T(k,x,y) + \\ & \left. D_T(k,x,y) D_R(k,x,y) \frac{\partial}{\partial x} a_x \right\} dx \quad (5.2-97) \end{aligned}$$

With the use of Equations (5.2-87), (5.2-88), (5.2-96), and (5.2-97), the integration with respect to  $x$  in Equation (5.2-86) can be expressed as:

$$\int_{x_L}^{x_U} dx = - \frac{C_{REF}}{jk_{EFF}n} [J_1 + J_2] \quad , \quad (5.2-98)$$



where

$$J_1 \triangleq a_x D_T(k, x, y) D_R(k, x, y) \exp\{-jk_{\text{EFF}}[\ell x + n\xi(x, y, t'_1)]\} \cdot \exp(-jk_{\text{EFF}} \frac{\ell_f}{2} x^2) \Big|_{x=x_L}^{x_U} \quad (5.2-99)$$

and

$$J_2 \triangleq \int_{x_L}^{x_U} \exp\{-jk_{\text{EFF}}[\ell x + n\xi(x, y, t'_1)]\} \exp(-jk_{\text{EFF}} \frac{\ell_f}{2} x^2) \cdot \left\{ \begin{aligned} &jk_{\text{EFF}} a_x D_T(k, x, y) D_R(k, x, y) [\ell + \ell_f x] - \\ &a_x D_T(k, x, y) \frac{\partial}{\partial x} D_R(k, x, y) - \\ &a_x D_R(k, x, y) \frac{\partial}{\partial x} D_T(k, x, y) - \\ &D_T(k, x, y) D_R(k, x, y) \frac{\partial}{\partial x} a_x \end{aligned} \right\} dx \quad , \quad (5.2-100)$$

where the lower and upper  $x$  limits  $x_L$  and  $x_U$  define the extent along the  $X$  axis of the common region of overlap between the transmit and receive projected beamwidths.

The  $J_1$  term is referred to as the edge effect<sup>46</sup> and its magnitude can be approximated by the absolute value of the difference between the products of the two beam patterns evaluated at the upper and lower  $x$  limits, i.e.,

$$|J_1| \approx |D_T(k, x_U, y) D_R(k, x_U, y) - D_T(k, x_L, y) D_R(k, x_L, y)| \quad (5.2-101)$$

since the complex exponentials are phase terms of unit magnitude.

The  $J_2$  term defined by Equation (5.2-100) can be simplified by deciding which terms appearing inside the braces,  $\{ \}$ , are dominant. Note that the first term inside the braces is the only expression which includes the parameter  $k_{EFF}$  whose magnitude  $|k_{EFF}| \gg 1$  for high frequencies. Since it has been previously assumed that the magnitudes of the gradients of the beam patterns are small over their respective projected beamwidths [see Equations (5.2-34), (5.2-35), and (5.2-38)], then the second and third terms within the braces of Equation (5.2-100) are negligible compared to the first term. Assuming also that the fourth term within the braces is negligible compared to the first, Equation (5.2-100) can therefore be approximated as:

$$J_2 \approx jk_{EFF} \int_{x_L}^{x_U} \exp\{-jk_{EFF}[\ell x + n\xi(x,y,t_1')]\} \cdot \exp(-jk_{EFF} \frac{\ell_f}{2} x^2) \cdot \left\{ a_x D_T(k,x,y) D_R(k,x,y) [\ell + \ell_f x] \right\} dx. \quad (5.2-102)$$

It can be seen from Equation (5.2-102) that the magnitude of  $J_2$  depends upon  $k_{EFF}$  and the integral of the product  $D_T(k,x,y) \cdot D_R(k,x,y)$  over the entire range of the  $x$  limits. By comparing  $J_2$  [as given by Equation (5.2-102)] with  $J_1$  [as given by Equation (5.2-99)], it is clear that  $J_2$  is the dominant expression. As a result, Equation (5.2-98) becomes:

$$\int_{x_L}^{x_U} dx \approx - \left( \frac{C_{REF}}{jk_{EFF}^n} \right) J_2, \quad (5.2-103)$$

where  $J_2$  is given by Equation (5.2-102). Substituting Equations (5.2-103) and (5.2-102) into Equation (5.2-86), and multiplying the result by  $(-1)$  to account for  $(-a_x)$ , yields:

$$\left( \frac{C_{REF}}{n} \right) \iint_{x,y} D_T(k,x,y) D_R(k,x,y) \cdot \exp\{-jk_{EFF}[\ell x + my + n\xi(x,y,t'_1)]\} \cdot \exp\{-jk_{EFF}[(\ell_f/2)x^2 + (m_f/2)y^2]\} a_x[\ell + \ell_f x] dx dy \quad (5.2-104)$$

which is an approximation to the first surface integral of  $H(f,t_1)_{REV}$  as given by Equation (5.2-84). The remaining surface integrals of Equation (5.2-84) involving the  $a_y$ ,  $b_x$ , and  $b_y$  terms can also be approximated by analogous expressions by following the procedure just outlined. By doing so, the following general expression for the random, time-varying, transfer function of ocean surface reverberation is obtained:

$$H_{REV}(f,t_1) = \frac{\exp(-jk_{EFF}[R_1 + R_2])}{R_1 R_2} \cdot \iint_{x,y} D_T(k,x,y) D_R(k,x,y) K(x,y) \cdot \exp\{-jk_{EFF}[\ell x + my + n\xi(x,y,t'_1)]\} \cdot \exp\{-jk_{EFF}[(\ell_f/2)x^2 + (m_f/2)y^2]\} dx dy, \quad (5.2-105)$$

where

$$K(x,y) \triangleq K_1(x,y) - K_2(x,y) + K_3(x,y) - K_4(x,y) , \quad (5.2-106)$$

$$K_1(x,y) \triangleq [a_x(x,y)(l/n) + a_y(x,y)(m/n) + a_z(x,y)]C_{REF} , \quad (5.2-107)$$

$$K_2(x,y) \triangleq [b_x(x,y)(l/n) + b_y(x,y)(m/n) + b_z(x,y)] , \quad (5.2-108)$$

$$K_3(x,y) \triangleq [a_x(x,y)(l_f/n)x + a_y(x,y)(m_f/n)y]C_{REF} \quad (5.2-109)$$

and

$$K_4(x,y) \triangleq [b_x(x,y)(l_f/n)x + b_y(x,y)(m_f/n)y] . \quad (5.2-110)$$

The functional dependence of  $D_T$  ,  $D_R$  , and the "a" and "b" terms on the  $(x,y)$  coordinates are given in Appendix D where use was made of Butkov.<sup>54</sup>

By making the appropriate combination of assumptions, Equation (5.2-105) will simplify to the forms of previously published results for the acoustic pressure field scattered from the ocean surface [i.e.,  $H(f,t_1)_{REV}$ ] obtained by using a Kirchhoff approach. For example, assume that a Fraunhofer approximation is sufficient so that  $l_f = m_f = 0$  . In addition, make the following assumptions which are associated with the classical Kirchhoff approach (e.g., see References 42 and 49):

$$\hat{n}_T(x,y) \approx -\hat{r}_1 \quad (5.2-111)$$

and

$$\hat{n}_R(x,y) \approx \hat{r}_2 ,$$

where  $\hat{r}_1$  and  $\hat{r}_2$  are given by Equations (5.2-49) and (5.2-61), respectively. Upon substituting Equation (5.2-111) into Equation (5.2-75), it can be shown that

$$\begin{aligned} a_x(x,y) &= l, \\ a_y(x,y) &= m \end{aligned} \quad (5.2-112)$$

and

$$a_z(x,y) = n,$$

where  $l$ ,  $m$ , and  $n$  are given by Equations (5.2-69) through (5.2-71), respectively. Similarly, substituting Equation (5.2-111) into Equation (5.2-76) yields:

$$\begin{aligned} b_x(x,y) &= \sin\theta_1 + \sin\theta_2 \cos\psi_2, \\ b_y(x,y) &= \sin\theta_2 \sin\psi_2 \end{aligned} \quad (5.2-113)$$

and

$$b_z(x,y) = -\cos\theta_1 + \cos\theta_2.$$

If Equations (5.2-112) and (5.2-113) are substituted into Equations (5.2-107) and (5.2-108), respectively, one obtains:

$$K_1(x,y) = F(\theta_1, \theta_2, \psi_2) C_{REF} \quad (5.2-114)$$

and

$$K_2(x,y) = 0, \quad (5.2-115)$$

where

$$F(\theta_1, \theta_2, \psi_2) \triangleq - \frac{2(1 - \sin\theta_1 \sin\theta_2 \cos\psi_2 + \cos\theta_1 \cos\theta_2)}{(\cos\theta_1 + \cos\theta_2)} \quad (5.2-116)$$

Using the results of Equations (5.2-114) and (5.2-115), and noting that  $K_3(x,y) = K_4(x,y) = 0$  when  $\ell_f = m_f = 0$ , Equation (5.2-105) reduces to:

$$H(f, t_1)_{REV} = \frac{\exp(-jk_{EFF}[R_1 + R_2])}{R_1 R_2} \cdot$$

$$F(\theta_1, \theta_2, \psi_2) C_{REF} \int \int_{x y} D_T(k, x, y) D_R(k, x, y) \cdot$$

$$\exp\{-jk_{EFF}[\ell x + m y + n \xi(x, y, t_1')]\} dx dy$$

(5.2-117)

which is in the same form as the Kirchhoff solutions presented in References 42, 48, and 49.

It is interesting to note that when the approximations given by Equation (5.2-111) are made, the term  $K_2(x,y) = 0$ . The presence of the  $K_2(x,y)$  term in Equation (5.2-106) is due to the form of Equation (5.2-18), i.e., the acoustic pressure field on the ocean surface was set equal to incident plus scattered acoustic pressure. Tolstoy and Clay<sup>49</sup> also used the approximations given by Equation (5.2-111), but they defined the acoustic pressure field on the ocean surface as equal to scattered acoustic pressure only. Therefore, when a Fraunhofer approximation is used in conjunction with Equation (5.2-111), it does not matter whether the right-hand side of Equation (5.2-18) equals incident plus scattered or scattered pressure only--the final results are identical. This will not be true for the Fresnel approximation as is demonstrated next.

Another simplified version of Equation (5.2-105), which appears frequently in the literature, can be obtained by using a Fresnel approximation in conjunction with Equation (5.2-111) for a specular orientation between the transmit and receive arrays. For a specular geometry,  $\theta_1 = \theta_2$  and  $\psi_2 = 2\pi$  since  $\psi_1 = \pi$ .

As a result of using the assumptions given by Equation (5.2-111), the  $a_x$ ,  $a_y$ , and  $a_z$  terms are given by Equation (5.2-112); and for a specular geometry, they reduce to:

$$a_x(x,y) = a_y(x,y) = 0$$

and

(5.2-118)

$$a_z(x,y) = -2 \cos\theta_1,$$

and the  $b_x$ ,  $b_y$ , and  $b_z$  coefficients given by Equation (5.2-113) become:

$$b_x(x,y) = 2 \sin\theta_1$$

and

(5.2-119)

$$b_y(x,y) = b_z(x,y) = 0.$$

Also, for a specular geometry,

$$l_f = \cos^2\theta_1 \frac{(R_1 + R_2)}{R_1 R_2} \quad (5.2-120)$$

and

$$m_f = \frac{(R_1 + R_2)}{R_1 R_2} \quad (5.2-121)$$

Substituting Equations (5.2-118) through (5.2-121) into Equations (5.2-107) through (5.2-110) yields:

$$\begin{aligned}
H_{REV}(f, t_1) = & \frac{\exp(-jk_{EFF}[R_1 + R_2])}{R_1 R_2} \int \int_{x y} D_T(k, x, y) D_R(k, x, y) \cdot \\
& \exp\{+jk_{EFF}\xi(x, y, t'_1)2\cos\theta_1\} \cdot \\
& \exp\{-jk_{EFF}[(R_1 + R_2)/(2R_1 R_2)][x^2 \cos^2\theta_1 + y^2]\} \cdot \\
& \left\{ -2C_{REF}\cos\theta_1 + x \sin\theta_1 \cos\theta_1 \frac{(R_1 + R_2)}{(R_1 R_2)} \right\} dx dy .
\end{aligned}$$

(5.2-122)

With the exception of the second term within the braces, Equation (5.2-122) is in the same form as the Kirchhoff solution presented in McDonald,<sup>43</sup> for example. The additional term or "information" appearing in Equation (5.2-122) is due to the fact that Equation (5.2-105) was not based on the "small slope approximation" while the solution presented in McDonald,<sup>43</sup> for example, was. In addition, Equation (5.2-105) was based upon setting the acoustic pressure field on the ocean surface equal to incident plus scattered acoustic pressure and this gives rise to the "b" terms as was discussed earlier. However, the transfer function presented in McDonald<sup>43</sup> was based upon setting the acoustic pressure field on the ocean surface equal to scattered acoustic pressure only.

Besides a specular geometry, it is clear that the assumptions most responsible for simplifying Equation (5.2-105) are those given by Equation (5.2-111). The next obvious question then is what does the transfer function given by Equation (5.2-105) look like when the assumptions given by Equation (5.2-111) are not made, i.e., when the "a" and "b" terms are indeed functions of  $x$  and  $y$  [refer to



Appendix D, Equations (D17) and (D18)]. In particular, let us compare  $H_{REV 1}(f, t_1)$ , as specified by Equations (5.2-105), (D17), and (D18), for both a specular and backscatter orientation to previously published results for the transfer function which were based upon the classical Kirchhoff assumptions represented by Equation (5.2-111).

For a specular orientation,  $\theta_1 = \theta_2 = \theta$ ,  $\psi_2 = 2\pi$  since  $\psi_1 = \pi$ , and  $\alpha_R = 0$  (see Figure D-2). Also, assume for simplicity that both the transmit and receive beam patterns are untilted so that  $\beta_T = \beta_R = \beta$ , where  $\beta = \pi - \theta$ . Therefore, Equation (D17) reduces to:

$$\begin{aligned} a_x(x, y) &= x \left[ \frac{R_T(x, y) + R_R(x, y)}{R_T(x, y)R_R(x, y)} \right] + \\ &\quad \sin\theta \left[ \frac{R_1}{R_T(x, y)} - \frac{R_2}{R_R(x, y)} \right], \\ a_y(x, y) &= y \left[ \frac{R_T(x, y) + R_R(x, y)}{R_T(x, y)R_R(x, y)} \right] \end{aligned} \quad (5.2-123)$$

and

$$a_z(x, y) = -\cos\theta \left[ \frac{R_1}{R_T(x, y)} + \frac{R_2}{R_R(x, y)} \right]$$

for a specular orientation, and Equation (D18) reduces to:

$$\begin{aligned} b_x(x, y) &= -x \left[ \frac{R_T(x, y) - R_R(x, y)}{R_T(x, y)R_R(x, y)} \right] + \\ &\quad \sin\theta \left[ \frac{R_1}{R_T(x, y)} + \frac{R_2}{R_R(x, y)} \right], \\ b_y(x, y) &= -y \left[ \frac{R_T(x, y) - R_R(x, y)}{R_T(x, y)R_R(x, y)} \right] \end{aligned} \quad (5.2-124)$$

and

$$b_z(x,y) = -\cos\theta \left[ \frac{R_1}{R_T(x,y)} - \frac{R_2}{R_R(x,y)} \right] .$$

Equations (5.2-123) and (5.2-124) were obtained by choosing the positive sign (+) for  $w_T(x,y)$  in Equation (D4) and the negative sign (-) for  $w_R(x,y)$  in Equation (D12). From Equations (5.2-69) through (5.2-71), we also obtain:

$$\begin{aligned} l &= m = 0 \\ n &= -2 \cos\theta \end{aligned} \tag{5.2-125}$$

and  $l_f$  and  $m_f$  are given by Equations (5.2-120) and (5.2-121), respectively for a specular geometry.

For comparison purposes, one need only compute the quantity  $K(x,y)$  as defined by Equation (5.2-106) since the remaining terms in Equation (5.2-105) are identical in form to previously published results. Upon substituting Equations (5.2-120), (5.2-121), and (5.2-123) through (5.2-125) into Equations (5.2-107) through (5.2-110) and letting  $C_{REF} = -1$ , Equation (5.2-106) becomes:

$$\begin{aligned} K(x,y) &= 2 \cos\theta \frac{R_1}{R_T(x,y)} + \left[ x^2 \cos\theta + y^2 \left( \frac{1}{\cos\theta} \right) \right] \cdot \\ &\quad \left[ \frac{(R_1 + R_2)}{R_1 R_2 R_T(x,y)} \right] + x \sin\theta \cos\theta \frac{(R_1 + R_2)}{R_T(x,y) R_2} \end{aligned} \tag{5.2-126}$$

for a specular orientation. The transfer function appearing in McDonald,<sup>43</sup> for example, contains only one integrand term for a

specular orientation; namely,  $2 \sin\psi$  which is equal to  $-2 \cos\theta$  since  $\psi = \theta - \frac{\pi}{2}$  in our notation. Therefore, the term  $2 \sin\psi$  in McDonald<sup>43</sup> is analogous to the first term in Equation (5.2-126). It is also instructive to compare Equation (5.2-126) with the expression within the braces of the integrand in Equation (5.2-122). Recall that Equation (5.2-122) was obtained from Equation (5.2-105) by using the classical Kirchhoff assumptions given by Equation (5.2-111). The first and second terms within the braces in Equation (5.2-122) are analogous to the first and third terms, respectively, of Equation (5.2-126).

One can therefore see that Equation (5.2-126) contains additional important information represented by the middle expression involving  $x^2$  and  $y^2$ . Note that for shallow grazing angles, i.e., as  $\theta \rightarrow \pi/2$  (see Figure 20),  $\cos\theta \rightarrow 0$  and  $1/\cos\theta \rightarrow \infty$ . Thus,  $H(f, t_1)_{\text{REV } 1}$ , as given by Equations (5.2-105) and (5.2-126), will be greater in magnitude for a specular orientation than the other previously derived transfer functions obtained from the classical Kirchhoff approach. This is encouraging since Horton and Melton<sup>41</sup> reported that the Kirchhoff approach, in conjunction with the Fresnel and small slope approximations, began to fail for a specular geometry at a Rayleigh parameter larger than 2, and predicted values for the scattering coefficient that were systematically smaller than the experimental values. The Rayleigh parameter is equal to  $2k\sigma\sin\psi$  for a specular geometry where  $\psi$  is the grazing angle.<sup>40,41,44</sup>

For a monostatic (backscatter) geometry,  $\theta_1 = \theta_2 = \theta$ ,  $\psi_1 = \psi_2 = \pi$ ,  $R_1 = R_2 = R$ ,  $R_T(x, y) = R_R(x, y) = R(x, y)$ , and  $\hat{n}_T(x, y) = -\hat{n}_R(x, y)$ . As before, it will be assumed that both the

transmit and receive beam patterns are untilted so that  $\beta_T = \beta_R = \beta$ , where  $\beta = \pi - \theta$ . It can be shown that

$$K(x,y) = 2 \frac{R}{\cos\theta R(x,y)} + 2x \frac{\sin\theta \cos\theta}{R(x,y)} + 2x \frac{\tan\theta}{R(x,y)} + \left[ \frac{2}{R(x,y)R} \right] \left[ x^2 \cos\theta + y^2 \frac{1}{\cos\theta} \right] \quad (5.2-127)$$

for the backscatter case. The transfer function derived in Clay and Medwin<sup>34</sup> contains only one integrand term for the backscatter case; namely,  $2/\cos\theta_1$  which is equal to  $-2/\cos\theta$  since  $\theta_1 = \pi - \theta$  in our notation. Therefore, the term  $2/\cos\theta_1$  in Clay and Medwin<sup>34</sup> is analogous to the first term in Equation (5.2-127). One can also compute the "a" and "b" terms according to Equations (5.2-112) and (5.2-113), respectively, for the backscatter geometry as was done for the specular geometry. Using Equations (5.2-112), (5.2-113), (5.2-69) through (5.2-73), and (5.2-107) through (5.2-110), Equation (5.2-106) becomes:

$$\frac{2}{\cos\theta} + 2x \frac{\sin\theta \cos\theta}{R} \quad (5.2-128)$$

which is analogous to the first and second terms of Equation (5.2-127).

As was apparent with Equation (5.2-126) for the specular geometry is also true with Equation (5.2-127) for the backscatter geometry. That is, Equation (5.2-127) contains additional important information represented by the last expression involving  $x^2$  and  $y^2$ . Therefore,  $H(f, t_1)_{REV}$ , as given by Equations (5.2-105) and (5.2-127), will be greater in magnitude for a backscatter orientation than the

other previously derived transfer functions obtained from the classical Kirchhoff approach. For example, see Parkins<sup>47</sup> who indicates that his predicted backscattering strengths were much lower than experimental values for very rough surfaces, especially at small grazing angles. Parkins<sup>47</sup> expression for scattered acoustic pressure was based upon the Kirchhoff approach in conjunction with the Fraunhofer approximation; however, he did not make the small slope approximation.

Another important point worth mentioning again is that the transmit and receive beam patterns can be projected exactly onto the XY plane (see Appendix D). In previously published works (e.g., see References 14, 43, 44, and 55), a Gaussian form for the projected transmit beam pattern was commonly assumed for mathematical convenience. However, as was pointed out in Zornig and McDonald,<sup>55</sup> the fact that the actual projected transmit and receive beam patterns are not likely to be Gaussian when doing experimental work leads to a major source of error when comparing theoretical predictions with experimental results.

### 5.3 Second Order Functions

5.3.1 Two-frequency correlation function. Since the transfer function given by Equation (5.2-105) is random, a more appropriate expression to work with is the two-frequency correlation function defined as:

$$R_H(f_1, f_2, t_1, t_2) \triangleq E\{H(f_1, t_1)H^*(f_2, t_2)\} \quad , \quad (5.3-1)$$

where  $E\{\cdot\}$  is the expectation operator and the asterisk denotes complex conjugation. By defining the expression  $Z(k, x, y)$  as:

$$Z(k, x, y) \triangleq D_T(k, x, y)K(x, y)D_R(k, x, y) \quad , \quad (5.3-2)$$

where  $K(x,y)$  is given by Equation (5.2-106), Equation (5.2-105) can be rewritten as:

$$\begin{aligned}
 H_{REV}(f, t_1) &= \frac{\exp(-jk_{EFF}[R_1 + R_2])}{R_1 R_2} \int_x \int_y Z(k, x, y) \cdot \\
 &\quad \exp\{-jk_{EFF}[\ell x + my + n\xi(x, y, t_1')]\} \cdot \\
 &\quad \exp\left\{-jk_{EFF}\left[\left(\frac{\ell_f}{2}\right)x^2 + \left(\frac{m_f}{2}\right)y^2\right]\right\} dx dy .
 \end{aligned}
 \tag{5.3-3}$$

With the use of Equation (5.3-3), and by replacing  $f_1$  with  $(f + f_c)$  and  $f_2$  with  $(f' + f_c)$ , Equation (5.3-1) becomes:

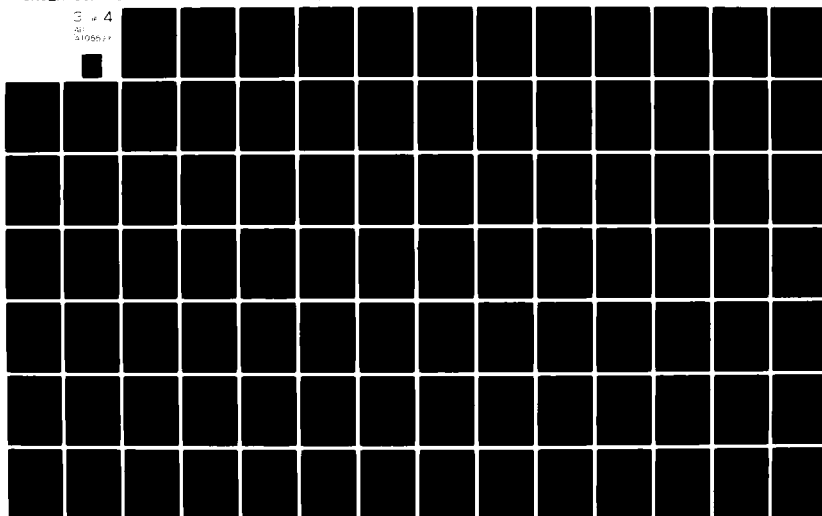
$$\begin{aligned}
 R_{H,REV}(f + f_c, f' + f_c, t_1, t_2) &= \frac{\exp\left\{-j[k_{EFF1} - k_{EFF2}^*][R_1 + R_2]\right\}}{(R_1 R_2)^2} \cdot \\
 &\quad \int_{x_1} \int_{y_1} \int_{x_2} \int_{y_2} Z\left(\frac{2\pi[f + f_c]}{c}, x_1, y_1\right) \cdot \\
 &\quad Z^*\left(\frac{2\pi[f' + f_c]}{c}, x_2, y_2\right) \cdot \\
 &\quad \exp\left[-j\ell\left[k_{EFF1}x_1 - k_{EFF2}^*x_2\right]\right] \cdot \\
 &\quad \exp\left[-jm\left[k_{EFF1}y_1 - k_{EFF2}^*y_2\right]\right] \phi(v_1, v_2)_{\xi_1, \xi_2} \cdot \\
 &\quad \exp\left[-j\left(\frac{\ell_f}{2}\right)\left[k_{EFF1}x_1^2 - k_{EFF2}^*x_2^2\right]\right] \cdot \\
 &\quad \exp\left[-j\left(\frac{m_f}{2}\right)\left[k_{EFF1}y_1^2 - k_{EFF2}^*y_2^2\right]\right] \cdot \\
 &\quad dx_2 dy_2 dx_1 dy_1 ,
 \end{aligned}
 \tag{5.3-4}$$

AD-A105 593

PENNSYLVANIA STATE UNIV UNIVERSITY PARK APPLIED RESE--ETC F/6 20/1  
A SCATTERING FUNCTION APPROACH TO UNDERWATER ACOUSTIC DETECTION--ETC(U)  
OCT 81 L J ZIOMEK N00024-79-C-6043  
ARL/PSU/TM-81-144 NL

UNCLASSIFIED

3 of 4  
201  
31055077



where  $f_c$  is the center or carrier frequency of the bandpass transmitted signal,  $f$  and  $f'$  correspond to frequency deviations from  $f_c$  [see Equation (3.2-20)], and the characteristic function  $\phi(v_1, v_2)$  is given by:

$$\phi(v_1, v_2) = E\{\exp(j[v_1 \xi(x_1, y_1, t_1') + v_2 \xi(x_2, y_2, t_2')])\} \quad (5.3-5)$$

where

$$v_1 = -nk_{EFF_1} \quad (5.3-6)$$

$$v_2 = +nk_{EFF_2}^* \quad (5.3-7)$$

$$k_{EFF_1} = \frac{2\pi(f + f_c)}{c} - j\alpha(f + f_c) \quad (5.3-8)$$

and

$$k_{EFF_2}^* = \frac{2\pi(f' + f_c)}{c} + j\alpha(f' + f_c) \quad (5.3-9)$$

Equation (5.3-4) is the general expression for the two-frequency correlation function of the ocean surface-scatter communication channel. As was discussed in Chapter IV,  $R_{H_{REV}}(f + f_c, f' + f_c, t_1, t_2)$  contains information concerning the amount of correlation which exists between the acoustic pressure fields  $H(f + f_c, t)$  and  $H(f' + f_c, t)$  at the two different frequencies  $f + f_c$  and  $f' + f_c$  for  $t_1 = t_2 = t$ , or the amount of correlation between  $H(f + f_c, t_1)$  and  $H(f + f_c, t_2)$  at the two different times  $t_1$  and  $t_2$  for  $f = f'$ . Both the coherence time and the coherence bandwidth, and hence, the frequency spectrum and time delay broadening associated with surface reverberation can be computed from Equation (5.3-4).



If Equation (5.3-4) can be reduced to a function of  $\Delta f = f - f'$  and  $\Delta t = t_1 - t_2$ ; i.e., if  $H(f, t)_{\text{REV}}$  can be shown to be wide-sense stationary in both frequency and time, then the surface reverberation scattering function can be obtained from  $R_{H, \text{REV}}(\Delta f, \Delta t)$  via a two-dimensional Fourier transformation [see Equation (2.3-51)].

5.3.2 Surface reverberation scattering function. Equation (5.3-4) can be simplified by making the following assumptions. Let us first assume that the bandpass transmit signal is narrowband so that  $|f_c| \gg |f|$  and  $|f_c| \gg |f'|$ . As a result,

$$Z \left[ \frac{2\pi[f + f_c]}{c}, x_1, y_1 \right] \approx Z(k, x_1, y_1) \quad , \quad (5.3-10)$$

$$Z^* \left[ \frac{2\pi[f' + f_c]}{c}, x_2, y_2 \right] \approx Z^*(k, x_2, y_2) \quad , \quad (5.3-11)$$

$$\alpha(f + f_c) \approx \alpha(f_c) \quad , \quad (5.3-12)$$

$$\alpha(f' + f_c) \approx \alpha(f_c) \quad (5.3-13)$$

and

$$k_{\text{EFF}1} k_{\text{EFF}2}^* \approx k^2 \quad , \quad (5.3-14)$$

where  $k = 2\pi f_c / c$ .

By substituting Equations (5.3-8), (5.3-9), and Equations (5.3-10) through (5.3-13) into Equation (5.3-4), and letting  $x_1 = x_2 + \Delta x$  and  $y_1 = y_2 + \Delta y$ , one obtains:

$$R_{H_{REV}}(f+f_c, f'+f_c, t_1, t_2) = \frac{\exp(-j \frac{2\pi\Delta f}{c} [R_1+R_2])}{(R_1 R_2)^2} \cdot$$

$$\exp\{-2\alpha(f_c)[R_1 + R_2]\} \cdot$$

$$\int_{-\infty}^{\infty} \int J(k, \Delta x, \Delta y) \exp \left\{ -jk \left[ \ell \Delta x + m \Delta y + \left( \frac{\ell f}{2} \right) (\Delta x)^2 + \left( \frac{m f}{2} \right) (\Delta y)^2 \right] \right\} \cdot$$

$$\exp \left\{ -\alpha(f_c) \left[ \ell \Delta x + m \Delta y + \left( \frac{\ell f}{2} \right) (\Delta x)^2 + \left( \frac{m f}{2} \right) (\Delta y)^2 \right] \right\} d\Delta x d\Delta y \quad , \quad (5.3-15)$$

where

$$J(k, \Delta x, \Delta y) = \int_x \int_y Z(k, x+\Delta x, y+\Delta y) Z^*(k, x, y) \phi(\nu_1, \nu_2)_{\xi_1, \xi_2} \cdot$$

$$\exp \left\{ -j \frac{2\pi\Delta f}{c} \left[ \ell x + m y + \left( \frac{\ell f}{2} \right) x^2 + \left( \frac{m f}{2} \right) y^2 \right] \right\} \cdot$$

$$\exp \left\{ -2\alpha(f_c) \left[ \ell x + m y + \left( \frac{\ell f}{2} \right) x^2 + \left( \frac{\ell f}{2} \right) x \Delta x + \left( \frac{m f}{2} \right) y^2 + \left( \frac{m f}{2} \right) y \Delta y \right] \right\} \cdot$$

$$\exp \left\{ -j \frac{2\pi}{c} (f+f_c) \left[ \left( \frac{\ell f}{2} \right) 2x \Delta x + \left( \frac{m f}{2} \right) 2y \Delta y \right] \right\} dx dy \quad (5.3-16)$$

and  $\Delta f = f - f'$  .

Now, let us turn our attention to the characteristic function appearing in Equation (5.3-16); namely,  $\Phi_{\xi_1, \xi_2}(v_1, v_2)$  as given by Equation (5.3-5). Since the attenuation due to the random deviations of  $\xi(x, y, t)$  from the XY plane is negligible in comparison with the other terms contributing to attenuation, one can set  $\alpha(f_c) = 0$  in Equation (5.3-5). If it is also assumed that  $\xi(x, y, t)$  is Gaussian, zero-mean, and wide-sense stationary, then it can be shown<sup>44</sup> that Equation (5.3-5) becomes:

$$\begin{aligned} \Phi_{\xi_1, \xi_2}(\Delta x, \Delta y, \Delta t') &= \exp \left\{ - \left( \frac{2\pi[f + f_c]}{c} \sigma_{\xi}^n \right)^2 \right. \\ &\quad \left. \left( 1 - \frac{R_{\xi}(\Delta x, \Delta y, \Delta t')}{\sigma_{\xi}^2} \right) \left( 1 - \frac{\Delta f}{f + f_c} \right) \right\} \cdot \\ &\quad \exp \left\{ - \frac{1}{2} \left( \frac{2\pi[f + f_c]}{c} \sigma_{\xi}^n \right)^2 \left( \frac{\Delta f}{f + f_c} \right)^2 \right\}, \end{aligned} \quad (5.3-17)$$

where

$$R_{\xi}(\Delta x, \Delta y, \Delta t') = E[\xi(x + \Delta x, y + \Delta y, t'_1)\xi(x, y, t'_2)] \quad (5.3-18)$$

and

$$E[\xi^2(x, y, t)] = \sigma_{\xi}^2, \quad (5.3-19)$$

where  $\sigma_{\xi}^2$  is a constant, and  $\Delta t' = t'_1 - t'_2$ . Using the narrowband assumption, i.e.,  $f + f_c \approx f_c$  and  $f + f_c \gg \Delta f$ , Equation (5.3-17) reduces to:

$$\begin{aligned} \Phi_{\xi_1, \xi_2}(\Delta x, \Delta y, \Delta t') &= \exp \left\{ - (k\sigma_{\xi n})^2 \left[ 1 - \frac{R_{\xi}(\Delta x, \Delta y, \Delta t')}{\sigma_{\xi}^2} \right] \right\} \cdot \\ &\exp \left\{ - \frac{1}{2} (k\sigma_{\xi n})^2 \left[ \frac{\Delta f}{f_c} \right]^2 \right\} . \quad (5.3-20) \end{aligned}$$

If Equation (5.3-18) can be shown to be a function of  $\Delta t$ , then Equation (5.3-15) becomes a function of  $\Delta f$  and  $\Delta t$  which is our desired result. Indeed, in Appendix E, it is shown that  $R_{\xi}(\Delta x, \Delta y, \Delta t') \equiv R_{\xi}(\Delta x, \Delta y, \Delta t)$ , where  $R_{\xi}(\Delta x, \Delta y, \Delta t)$  is given by Equation (E10), i.e.,

$$\begin{aligned} R_{\xi}(\Delta x, \Delta y, \Delta t) &= (1/4) \int_{-\infty}^{\infty} \int_{-\infty}^{\infty} W(p, q) \exp[+j\omega(p, q)\Delta t] \cdot \\ &\exp \left\{ -j \left[ p - \omega(p, q) \frac{\sin\theta_2 \cos\psi_2}{c} \right] \Delta x \right\} \cdot \\ &\exp \left\{ -j \left[ q - \omega(p, q) \frac{\sin\theta_2 \sin\psi_2}{c} \right] \Delta y \right\} dpdq , \quad (E10) \end{aligned}$$

where  $W(p, q)$  is the directional wave number spectrum of the ocean surface and the corresponding angular frequency (in rad/sec) is given by:

$$\omega(p, q) = \pm \left[ g(p^2 + q^2)^{1/2} \right]^{1/2} , \quad (E11)$$

where  $g$  is the acceleration due to gravity.<sup>48</sup> The directional wave number spectrum and corresponding angular frequency are discussed further in Appendix E. Therefore, Equation (5.3-20) can be written as:

$$\begin{aligned} \Phi_{\xi_1, \xi_2}(\Delta x, \Delta y, \Delta t') &\equiv \Phi_{\xi_1, \xi_2}(\Delta x, \Delta y, \Delta t) = \\ &\exp \left\{ - (k\sigma_{\xi} n)^2 \left[ 1 - \frac{R_{\xi}(\Delta x, \Delta y, \Delta t)}{\sigma_{\xi}^2} \right] \right\} \cdot \\ &\exp \left\{ - \frac{1}{2} (k\sigma_{\xi} n)^2 \left[ \frac{\Delta f}{f_c} \right]^2 \right\}, \quad (5.3-21) \end{aligned}$$

where  $R_{\xi}(\Delta x, \Delta y, \Delta t)$  is given by Equation (E10). Thus, the characteristic function originally given by Equation (5.3-5) has been reduced to the expression given by Equation (5.3-21).

With the use of Equation (5.3-21), and assuming that  $f + f_c \approx f_c$  in the last complex exponential term in Equation (5.3-16), the two-frequency correlation function given by Equation (5.3-15) can be written as a function of  $\Delta f$  and  $\Delta t$ , i.e.,

$$\begin{aligned} R_{H, REV}(\Delta f, \Delta t) &= \frac{\exp[-2\alpha(f_c)(R_1 + R_2)]}{(R_1 R_2)^2} \int_{-\infty}^{\infty} \int J(k, \Delta x, \Delta y, \Delta f) \cdot \\ &\exp \left\{ - (k\sigma_{\xi} n)^2 \left[ 1 - \frac{R_{\xi}(\Delta x, \Delta y, \Delta t)}{\sigma_{\xi}^2} \right] \right\} \cdot \\ &\exp \left\{ - jk \left[ l\Delta x + m\Delta y + \left( \frac{l_f}{2} \right) (\Delta x)^2 + \right. \right. \\ &\quad \left. \left. \left( \frac{m_f}{2} \right) (\Delta y)^2 \right] \right\} \cdot \\ &\exp \left\{ -\alpha(f_c) \left[ l\Delta x + m\Delta y + \left( \frac{l_f}{2} \right) (\Delta x)^2 + \right. \right. \\ &\quad \left. \left. \left( \frac{m_f}{2} \right) (\Delta y)^2 \right] \right\} d\Delta x d\Delta y, \quad (5.3-22) \end{aligned}$$

where

$$\begin{aligned}
 J(k, \Delta x, \Delta y, \Delta f) = & \int_x \int_y Z(k, x + \Delta x, y + \Delta y) Z^*(k, x, y) \cdot \\
 & \exp \left\{ -\frac{1}{2} (k \sigma_{\xi n})^2 \left( \frac{\Delta f}{f_c} \right)^2 \right\} \cdot \\
 & \exp \left\{ -j \frac{2\pi \Delta f}{c} \left[ l x + m y + \left( \frac{l_f}{2} \right) x^2 + \right. \right. \\
 & \quad \left. \left. \left( \frac{m_f}{2} \right) y^2 + (R_1 + R_2) \right] \right\} \cdot \\
 & \exp \left\{ -2\alpha(f_c) \left[ l x + m y + \left( \frac{l_f}{2} \right) x^2 + \right. \right. \\
 & \quad \left. \left. \left( \frac{l_f}{2} \right) x \Delta x + \left( \frac{m_f}{2} \right) y^2 + \left( \frac{m_f}{2} \right) y \Delta y \right] \right\} \cdot \\
 & \exp \left\{ -jk \left[ \left( \frac{l_f}{2} \right) 2x \Delta x + \right. \right. \\
 & \quad \left. \left. \left( \frac{m_f}{2} \right) 2y \Delta y \right] \right\} dx dy . \quad (5.3-23)
 \end{aligned}$$

The scattering function can be obtained from  $R_{H_{REV}}(\Delta f, \Delta t)$  by substituting Equation (5.3-22) into Equation (2.3-51). Doing so yields:

$$\begin{aligned}
R_{S_{REV}}(\tau, \phi) &= \frac{\exp[-2\alpha(f_c)(R_1 + R_2)]}{(R_1 R_2)^2} \cdot \\
&\int_{-\infty}^{\infty} \int_{-\infty}^{\infty} J(k, \Delta x, \Delta y, \tau) \Gamma(\Delta x, \Delta y, \phi) \cdot \\
&\exp \left\{ -jk[\ell \Delta x + m \Delta y] \right\} \cdot \\
&\exp \left\{ -jk \left[ \left[ \frac{\ell_f}{2} \right] (\Delta x)^2 + \left[ \frac{m_f}{2} \right] (\Delta y)^2 \right] \right\} \cdot \\
&\exp \left\{ -\alpha(f_c)[\ell \Delta x + m \Delta y] \right\} \cdot \\
&\exp \left\{ -\alpha(f_c) \left[ \left[ \frac{\ell_f}{2} \right] (\Delta x)^2 + \right. \right. \\
&\left. \left. \left[ \frac{m_f}{2} \right] (\Delta y)^2 \right] \right\} d\Delta x d\Delta y, \quad (5.3-24)
\end{aligned}$$

where  $k = 2\pi f_c / c$ ,

$$\begin{aligned}
J(k, \Delta x, \Delta y, \tau) &= |b| \int_{-\infty}^{\infty} \int_{-\infty}^{\infty} Z(k, x + \Delta x, y + \Delta y) Z^*(k, x, y) \cdot \\
&\exp\{-\pi b^2[\tau - \tau_o(x, y)]^2\} \cdot \\
&\exp \left\{ -jk \left[ \left[ \frac{\ell_f}{2} \right] 2x\Delta x + \right. \right. \\
&\left. \left[ \frac{m_f}{2} \right] 2y\Delta y \right] \right\} \exp \left\{ -2\alpha(f_c) \cdot \right. \\
&\left. \left[ \ell x + my + \left[ \frac{\ell_f}{2} \right] x^2 + \left[ \frac{\ell_f}{2} \right] x\Delta x + \right. \right. \\
&\left. \left. \left[ \frac{m_f}{2} \right] y^2 + \left[ \frac{m_f}{2} \right] y\Delta y \right] \right\} dx dy, \quad (5.3-25)
\end{aligned}$$

$$\tau_o(x,y) = \left( \frac{1}{c} \right) \left[ lx + my + \left( \frac{l_f}{2} \right) x^2 + \left( \frac{m_f}{2} \right) y^2 + (R_1 + R_2) \right], \quad (5.3-26)$$

$$b = c / (n\sigma_\xi \sqrt{2\pi}) \quad (5.3-27)$$

and

$$\Gamma(\Delta x, \Delta y, \phi) = \int_{-\infty}^{\infty} \exp \left\{ - (k\sigma_\xi n)^2 \left[ 1 - \frac{R_\xi(\Delta x, \Delta y, \Delta t)}{\sigma_\xi^2} \right] \right\} \cdot \exp(-j2\pi\phi\Delta t) d\Delta t. \quad (5.3-28)$$

Equation (5.3-24) is the scattering function of ocean surface reverberation. It determines how the input signal's power will be spread in round-trip time delay  $\tau$  (sec), and frequency  $\phi$  (Hz) after being scattered from the ocean surface.

The spread in round-trip time delay is due to the presence of the Gaussian function in  $\tau$  appearing in the integrand of Equation (5.3-25) and to the variety of possible propagation paths which exist between the transmit and receive arrays as specified by Equation (5.3-26). These paths are associated with different portions of the insonified area of the surface. The most obvious propagation path is, of course,  $(R_1 + R_2)$ .

And from Equation (5.3-28), it can be seen that the frequency spread is due to the time variations or motion of the ocean surface itself as characterized by  $R_\xi(\Delta x, \Delta y, \Delta t)$ .



McDonald and Tuteur,<sup>44</sup> and Tuteur, McDonald, and Tung<sup>45</sup> also derived expressions for the ocean surface reverberation scattering function. Their scattering functions were based upon a Fresnel corrected Kirchhoff integral and a small slope approximation and pertain only to a specular geometry. In addition, they did not include a receive directivity function and they assumed a Gaussian functional form for the projected transmit beam pattern. And furthermore, they assumed very specific models for the ocean surface rather than relating their scattering functions to the general form of the directional wave number spectrum.

In contrast, the surface reverberation scattering function given by Equation (5.3-24) is applicable to a general bistatic geometry. As a result, expressions for both the specular and backscatter geometries can easily be obtained from it. Equation (5.3-24) is a result of a generalized Kirchhoff approach which includes a Fresnel corrected Kirchhoff integral, no small slope approximation, and the Rayleigh hypothesis that the scattered acoustic pressure field can be represented as a sum of plane waves travelling in many different directions. In addition, the transmit and receive directivity functions are general, frequency dependent expressions. The necessary transformation equations which will project both the transmit and receive directivity functions exactly onto the  $xy$  plane are provided in Appendix D. And finally, the scattering function given by Equation (5.3-24) is dependent upon the general form of the directional wave number spectrum. Hence, the models of the ocean surface used by McDonald and Tuteur,<sup>44</sup> and Tuteur, McDonald, and Tung<sup>45</sup> are automatically included as special cases.

## CHAPTER VI

### MAXIMIZATION OF THE SIGNAL-TO-INTERFERENCE

#### RATIO FOR A DOUBLY SPREAD TARGET:

#### PROBLEMS IN NONLINEAR PROGRAMMING

### 6.1 Introduction

The main purpose of this chapter is to consider the problem of maximizing the signal-to-interference ratio (SIR) for a doubly spread target via signal design. Recall that the SIR for a doubly spread target is given by [see Equation (3.2-44)]:

$$\text{SIR} = \frac{\int_{-\infty}^{\infty} \int_{-\infty}^{\infty} R_{S_{\text{TRGT}}}(\tau, \phi) \left| \frac{\chi(\tau, \phi)}{\tilde{x}\tilde{g}} \right|^2 d\tau d\phi}{\int_{-\infty}^{\infty} \int_{-\infty}^{\infty} R_{S_{\text{REV}}}(\tau, \phi) \left| \frac{\chi(\tau, \phi)}{\tilde{x}\tilde{g}} \right|^2 d\tau d\phi + N_o E_{\tilde{g}}}, \quad (6.1-1)$$

where

$$\frac{\chi(\tau, \phi)}{\tilde{x}\tilde{g}} = \int_{-\infty}^{\infty} \tilde{x}(t - \frac{\tau}{2}) \tilde{g}^*(t + \frac{\tau}{2}) \exp(+j2\pi\phi t) dt \quad (6.1-2)$$

is the cross-ambiguity function of the complex envelope of the transmit signal  $\tilde{x}(t)$ , and the complex envelope of the processing waveform  $\tilde{g}(t)$ ;

$$E_{\tilde{g}} = \int_{-\infty}^{\infty} |\tilde{g}(t)|^2 dt \quad (6.1-3)$$

is the energy of the processing waveform;  $N_0$  is the spectral height of the complex white noise  $\tilde{n}(t)$ , and  $R_{S_{TRGT}}(\tau, \phi)$  and  $R_{S_{REV}}(\tau, \phi)$  are the target and reverberation scattering functions, respectively. Target and volume reverberation scattering functions were both derived in Chapter IV and a surface reverberation scattering function was derived in Chapter V. If volume reverberation is the dominant source of interference, then one would use the volume reverberation scattering function in Equation (6.1-1). Similarly, if surface reverberation is dominant, then one would use the surface reverberation scattering function. However, in the analysis which follows, the mathematical expressions for the scattering functions will not be substituted into Equation (6.1-1) for reasons of simplicity and generality.

In contrast, the SIR for a slowly fluctuating point target is given by [see Equation (3.2-51)]:

$$SIR = \frac{E\{|\tilde{b}|^2\} \left| \chi_{\tilde{xg}}(\tau', \phi') \right|^2}{\int_{-\infty}^{\infty} \int R_{S_{REV}}(\tau, \phi) \left| \chi_{\tilde{xg}}(\tau, \phi) \right|^2 d\tau d\phi + N_0 E_{\tilde{g}}}, \quad (6.1-4)$$

where  $\tilde{b}$  is a zero mean complex Gaussian random variable which accounts for random attenuation and random phase shift. The magnitude of  $\tilde{b}$  is assumed to be Rayleigh distributed and the phase of  $\tilde{b}$  is assumed to be uniform. As a result, the magnitude and phase are statistically independent random variables. The quantity  $E\{|\tilde{b}|^2\}$  includes the array gains, propagation losses, and scattering cross-section of the

target. The details of the derivations of both Equations (6.1-1) and (6.1-4) are discussed in Section 3.2.2.

The SIR optimization problem has been approached in a variety of ways. The discussion which follows on the next several pages is a brief survey of the relevant literature on this subject matter. Stutt and Spafford<sup>56</sup> considered the point target problem and assumed that the transmit signal  $\tilde{x}(t)$  was arbitrary but given (fixed). They concerned themselves with maximizing the SIR [as given by Equation (6.1-4)] with respect to the processing waveform  $\tilde{g}(t)$  subject to constraints on the output signal power  $\left| \chi(\tau', \phi') \right|_{\tilde{x}\tilde{g}}^2$  and output noise power  $E_{\tilde{g}}$ . Rummler<sup>57</sup> also considered the point target problem and not only assumed that the transmit signal was fixed, but that its form was fixed as well. Specifically, the transmit signal was assumed to be a uniformly spaced train of rectangular pulses with no phase or amplitude weighting. The optimum processing waveform was approximated by one which was matched to the shape of the transmit pulse train, but with complex weighted subpulses. Consideration was given to the problem of determining the optimum, complex weighting vector for the processing waveform; i.e., the weighting vector which maximized the SIR. Rummler<sup>57</sup> assumed in his analysis that the joint probability density function for the clutter (the analog of the reverberation scattering function) was a separable function and that the clutter was uniformly distributed in both range and Doppler. These assumptions are not true in general and limit the usefulness of his analytical results.

Unlike Stutt and Spafford,<sup>56</sup> and Rummler,<sup>57</sup> DeLong and Hofstetter<sup>19</sup> considered the joint optimization problem of finding the

optimum transmit-processing waveform pair that would maximize the SIR for a point target subject to energy constraints on both  $\tilde{x}(t)$  and  $\tilde{g}(t)$ . They restricted both the transmit and processing waveforms to be uniformly spaced, phase and amplitude weighted pulse trains of identically shaped subpulses. However, the shape of the subpulse was arbitrary. For example, it was not restricted to be rectangular as was done by Rummler.<sup>57</sup> Like Rummler,<sup>57</sup> DeLong and Hofstetter<sup>19</sup> approximated the optimum processing waveform by one which was matched to the shape of the transmit pulse train. In addition, unlike Rummler,<sup>57</sup> the clutter density function (reverberation scattering function) was kept as an arbitrary, general function of round-trip time delay and Doppler shift. DeLong and Hofstetter<sup>19</sup> presented an iterative algorithm for finding the optimum, transmit-processing, complex weighting vector pair which maximizes the SIR for a point target subject to energy constraints on both  $\tilde{x}(t)$  and  $\tilde{g}(t)$ . It appears that their iteration technique was the first systematic procedure for the design of clutter-resistant radar waveforms.

DeLong and Hofstetter<sup>58</sup> extended their analytical results obtained in DeLong and Hofstetter<sup>19</sup> by presenting an iterative signal design algorithm for the joint optimization problem for the case where the energy constraints were replaced by a dynamic-range constraint, i.e., the ratio of maximum to minimum transmit signal amplitude was limited. By introducing maximum and minimum constraints on the amplitudes of the transmit subpulses, signal energy was also limited and thus, the energy constraints were no longer necessary. DeLong and

Hofstetter<sup>58</sup> formulated the original point target SIR optimization problem into an equivalent nonlinear programming problem.

Rummler<sup>59</sup> also generalized his earlier work somewhat (see Rummler<sup>57</sup>) by allowing the subpulses of both the transmit and processing pulse trains to be complex weighted. However, the pulse trains were once again composed of uniformly spaced rectangular subpulses. Similarly, the clutter density function was once again assumed to be separable, but this time, it was represented by a summation of elementary clutter density functions; specifically, uniform distributions of varying amplitudes in range and Doppler. Rummler<sup>59</sup> also described an iterative technique for finding the optimum, transmit-processing, complex weighting vector pair which maximizes the SIR for a point target. The iterative technique of Rummler<sup>59</sup> is identical with that of DeLong and Hofstetter.<sup>19</sup> However, the analysis and equations of DeLong and Hofstetter<sup>19</sup> are more general. Spafford<sup>20</sup> also considered the joint optimization problem for a point target.

Thompson and Titlebaum<sup>60</sup> approached the problem of maximizing the SIR for a point target by assuming that the transmit signal was given and then optimizing with respect to the processing waveform, subject to constraints on peak and average power. However, the transmit and processing waveforms were not restricted to be pulse trains. Furthermore, the clutter was modelled as a finite number of point-clutter elements. As a result, the clutter density function contained Dirac delta functions in both range and Doppler. The SIR expression for a point target was ultimately represented by a finite number of state variables and use was then made of the Pontryagin Maximum Principle.

And finally, in a more recent paper devoted to the problem of maximizing the SIR for a slowly fluctuating point target, Sibul and Titlebaum<sup>61</sup> demonstrated that in the case of Gaussian interference, the joint optimization of transmit and processing waveforms reduces to the optimization of the transmit signal only. The maximum-likelihood receiver for detecting a slowly fluctuating point target return in colored Gaussian interference is determined by the transmit signal, the reverberation scattering function, and the level of the white noise power spectral density. Only the design of the transmit signal is required. As noted by Sibul and Titlebaum,<sup>61</sup> this simplifying observation has not been explicitly pointed out in the literature.

All of the research work discussed so far has dealt with a slowly fluctuating point target. Efforts to treat more complicated target models in the context of the SIR optimization problem were made by Kooij<sup>62</sup> and Moose.<sup>17</sup> They modelled the target as a linear, time-invariant, deterministic filter. The target could then be considered as a singly spread target rather than as a point target. The time-invariant assumption implies no relative target motion, and hence, no target Doppler. Therefore, the target spread is in round-trip time delay values only.

Kooij<sup>62</sup> derived both the optimum transmit signal frequency spectrum and the corresponding optimum processing filter transfer function that would maximize the ratio of target echo power to background power, subject to an energy constraint on the transmit signal. The background was defined as the sum of reverberation and colored noise. Kooij<sup>62</sup> also modelled the reverberation as a linear,

time-invariant, random filter. Once again, because of the time-invariant assumption, no relative motion was allowed, and hence, no reverberation Doppler. Kooij<sup>62</sup> did not restrict the transmit and processing waveforms to be pulse trains.

Moose<sup>17</sup> attacked the problem of maximizing the detection index for a known signal (i.e., the ratio of target echo power to background power) by using the optimum receiver and then optimizing with respect to the transmit signal. The background was defined as the sum of reverberation and white noise. The reverberation was represented by a reverberation scattering function which was assumed to be a function of Doppler shift only. Moose<sup>17</sup> restricted the transmit signal to be a periodic waveform composed of  $N$  harmonics. As a result, this signal had a finite Fourier series representation. The problem then became one of maximizing the detection index with respect to the magnitudes of the Fourier coefficients, subject to an energy constraint on the transmit signal. Moose<sup>17</sup> formulated the original optimization problem into an equivalent nonlinear programming problem, as was done by DeLong and Hofstetter,<sup>58</sup> and used Rosen's gradient projection method<sup>63,64</sup> to investigate the solution.

As mentioned earlier, the main problem considered in this chapter is the maximization of the SIR for a doubly spread target as given by Equation (6.1-1). In our analysis, both the transmit and processing waveforms will be limited to pulse trains. However, each subpulse of the transmit pulse train is allowed to be arbitrary in shape and can occupy the entire interpulse spacing interval if desired. This represents a generalization of previously published approaches. For



example, although DeLong and Hofstetter<sup>19,58</sup> allowed the shape of the subpulse to be arbitrary, the shape of each subpulse was identical; and Rummler<sup>57,59</sup> restricted the duration of each subpulse to be less than one-half of the interpulse spacing. In this chapter, each subpulse of both the transmit and processing waveforms is allowed to be complex weighted. The reasons behind limiting  $\tilde{x}(t)$  and  $\tilde{g}(t)$  to pulse trains are as follows.

In order to avoid unrealistic solutions when maximizing the SIR with respect to both  $\tilde{x}(t)$  and  $\tilde{g}(t)$ , for example, constraints must be specifically imposed upon  $\tilde{x}(t)$ . For example, these may include bandwidth and duration constraints which serve the purpose of restricting the range and Doppler resolution of the admissible transmit signal. Otherwise, the optimal solution for  $\tilde{x}(t)$  may require an infinite bandwidth or infinite duration or both. Moreover, as DeLong and Hofstetter<sup>19</sup> point out:

. . . even if it is possible to find the optimum  $\tilde{x}(t)$  and  $\tilde{g}(t)$  subject to a given set of constraints, it is not obvious that they will yield a 'practical' solution to the optimization problem. The optimum  $\tilde{x}(t)$  may not be of the type that can be transmitted . . . and the optimum  $\tilde{g}(t)$  may be so complicated as to present insurmountable realization problems.

Rummler<sup>57</sup> also notes that although it is known that the impulse response of the optimum receiver for detecting a point target return immersed in noise plus clutter may be obtained as the solution of an integral equation, the most serious objection to its use is that it is difficult to realize. In addition, since for a given transmit signal the form of the frequency response of the optimum filter is dependent upon the probability density function of the clutter (reverberation scattering

function), each new clutter situation requires the synthesis of a new receiver with a specially designed frequency response.<sup>57</sup> "This design problem becomes especially severe for large time-bandwidth signals such as chirped pulses."<sup>57</sup> However, when the transmit signal and processing waveforms are pulse trains, the realization difficulties are minimized.<sup>19,20,57</sup> When the transmit signal is a pulse train, the optimum processing waveform may be approximated by one which is matched to the shape of the transmit pulse train, but with complex weighted subpulses. In general, this complex weighted receiver will not perform quite as well as the true optimum filter, but it is to be preferred since it may be realized in a straightforward manner.<sup>19,57</sup> However, it should be mentioned here that with the current technology, the optimum receiver can be calculated adaptively in real time.

Pulse trains have other desirable properties. They possess simultaneously both high range and Doppler resolution.<sup>20,57,65</sup> Constraints on the energy, bandwidth, and duration can be achieved by suitably altering the parameters of the pulse train. Thus, if one chooses, the constraints can be built into the transmit pulse train while leaving its complex weights to be determined via the optimization process. In addition, any arbitrary signal of a particular duration and bandwidth can be approximated by a pulse train.<sup>19</sup> And finally, restricting  $\tilde{x}(t)$  and  $\tilde{g}(t)$  to be complex weighted pulse trains allows the integral expression of the SIR to be transformed into an equivalent vector-matrix form. Thus, the original problem of finding the optimum time functions  $\tilde{x}(t)$  and  $\tilde{g}(t)$ , for example, is transformed into a

parameter optimization problem of finding the optimum transmit-processing complex weighting vector pair.

The basic approach taken by DeLong and Hofstetter<sup>19,58</sup> will be followed in this chapter. Their method of transforming the integral expression of the SIR for a slowly fluctuating point target into an equivalent vector-matrix expression will be discussed, generalized, and extended to doubly spread targets in Section 6.2. The fact that each subpulse of the transmit pulse train is allowed to be arbitrary in shape makes the approach described in Section 6.2 analogous to the Rayleigh-Ritz technique.<sup>66</sup>

Although the point target problem is not of primary concern in this chapter, it is an important and interesting problem in its own right and is included for completeness. In Section 6.3, two different optimization problems concerning the maximization of the SIR for a slowly fluctuating point target are discussed. The first problem is to find the optimum, unit-energy, complex processing weighting vector that will maximize the SIR when the complex transmit weighting vector and the parameters of the subpulses are given. The second problem is to find the optimum, transmit-processing, complex weighting vector pair that will maximize the SIR when the parameters of the subpulses are given and when the maximization is subject to unit-energy constraints on both  $\tilde{x}(t)$  and  $\tilde{g}(t)$ . The iterative technique due to DeLong and Hofstetter<sup>19</sup> for solving this joint optimization problem will be discussed.

Section 6.4 addresses the main purpose of this chapter. Three different optimization problems concerning the maximization of the SIR for a doubly spread target are discussed. The first problem is to find

the optimum complex processing weighting vector that will maximize the SIR when the complex transmit weighting vector and the parameters of the subpulses are given and when the maximization is subject to a unit-energy constraint on the processing weighting vector and a constraint on the desired amount of reverberation to be removed by the processing weighting vector. The second problem is to find the optimum, transmit-processing, complex weighting vector pair that will maximize the SIR when the parameters of the subpulses are given and when the maximization is subject to a dynamic range constraint on the transmit weighting vector, a unit-energy constraint on the processing weighting vector, and a constraint on the desired amount of reverberation to be removed by the processing weighting vector.

And finally, the third problem is to maximize the SIR for a doubly spread target with respect to the parameters of the subpulses. For this particular optimization problem, it is assumed that both the transmit and processing weighting vectors are equal and given and that the maximization is subject to a constraint on the desired amount of reverberation to be removed by the processing waveforms and constraints on the subpulse parameters themselves.

The approach taken in Section 6.4 is to formulate the optimization problems into equivalent nonlinear programming problems defined on a real space. As a result, one need not develop algorithms to solve these problems, but rather, one can simply use standard computer programs which are available for solving nonlinear programming problems (e.g., see Kuester and Mize<sup>67</sup>). Note that all three optimization problems in Section 6.4 are originally defined on a complex space.

## 6.2 Mathematical Preliminaries - Problem Formulation

Following DeLong and Hofstetter,<sup>19</sup> the first step will be to normalize the expression for the SIR as given by Equation (6.1-1). Toward this end, let

$$\tilde{u}(t) \triangleq \frac{\tilde{x}(t)}{\sqrt{E_{\tilde{x}}}} \quad (6.2-1)$$

and

$$\tilde{w}(t) \triangleq \frac{\tilde{g}(t)}{\sqrt{E_{\tilde{g}}}} \quad , \quad (6.2-2)$$

where the energy of the transmit signal is given by:

$$E_{\tilde{x}} = \int_{-\infty}^{\infty} |\tilde{x}(t)|^2 dt \quad (6.2-3)$$

and the energy of the processing waveform  $E_{\tilde{g}}$  is given by Equation (6.1-3). Equations (6.2-1) and (6.2-2) define the normalized transmit and processing waveforms, respectively, such that:

$$\int_{-\infty}^{\infty} |\tilde{u}(t)|^2 dt = \int_{-\infty}^{\infty} |\tilde{w}(t)|^2 dt = 1 \quad . \quad (6.2-4)$$

Also, let:

$$\sigma_{\text{TRGT}} \triangleq \int_{-\infty}^{\infty} \int_{-\infty}^{\infty} R_{S_{\text{TRGT}}}(\tau, \phi) d\tau d\phi \quad , \quad (6.2-5)$$

$$\sigma_{\text{REV}} \triangleq \int_{-\infty}^{\infty} \int_{-\infty}^{\infty} R_{S_{\text{REV}}}(\tau, \phi) d\tau d\phi \quad , \quad (6.2-6)$$

$$\sigma_{\text{TRGT}}(\tau, \phi) \triangleq R_{S_{\text{TRGT}}}(\tau, \phi) / \sigma_{\text{TRGT}} \quad (6.2-7)$$

and

$$\sigma_{\text{REV}}(\tau, \phi) \triangleq R_{\text{S}_{\text{REV}}}(\tau, \phi) / \sigma_{\text{REV}} \quad (6.2-8)$$

Equations (6.2-5) and (6.2-6) define the total scattering cross-sections of the target and reverberation, respectively, and Equations (6.2-7) and (6.2-8) define the normalized target and reverberation scattering functions, respectively, such that:

$$\int_{-\infty}^{\infty} \int_{-\infty}^{\infty} \sigma_{\text{TRGT}}(\tau, \phi) d\tau d\phi = \int_{-\infty}^{\infty} \int_{-\infty}^{\infty} \sigma_{\text{REV}}(\tau, \phi) d\tau d\phi = 1 \quad (6.2-9)$$

Since scattering functions are real, non-negative functions of round-trip time delay  $\tau$  and Doppler shift  $\phi$ , the normalized functions  $\sigma_{\text{TRGT}}(\tau, \phi)$  and  $\sigma_{\text{REV}}(\tau, \phi)$  can be thought of as density functions.

Substituting Equations (6.2-1) and (6.2-2) into Equation (6.1-2) yields:

$$\chi_{\tilde{x}\tilde{g}}(\tau, \phi) = \sqrt{E_{\tilde{x}} E_{\tilde{g}}} \chi_{\tilde{u}\tilde{w}}(\tau, \phi) \quad (6.2-10)$$

and if Equations (6.2-7), (6.2-8), and (6.2-10) are substituted into Equation (6.1-1), one obtains:

$$\frac{\rho}{\rho_0} \triangleq \frac{\int_{-\infty}^{\infty} \int_{-\infty}^{\infty} \sigma_{\text{TRGT}}(\tau, \phi) |\chi_{\tilde{u}\tilde{w}}(\tau, \phi)|^2 d\tau d\phi}{\rho_0 \lambda \int_{-\infty}^{\infty} \int_{-\infty}^{\infty} \sigma_{\text{REV}}(\tau, \phi) |\chi_{\tilde{u}\tilde{w}}(\tau, \phi)|^2 d\tau d\phi + 1} \quad (6.2-11)$$

where  $\rho$  is the normalized SIR for a doubly spread target,

$$\rho_o \triangleq \frac{\sigma_{\text{TRGT}} E_{\text{x}}}{N_o} \quad (6.2-12)$$

and

$$\lambda \triangleq \sigma_{\text{REV}} / \sigma_{\text{TRGT}} \quad (6.2-13)$$

The numerator of Equation (6.2-12) is nothing more than the total average energy returned by the target [see Equation (3.2-24)].

Therefore, the expression  $\rho_o$  is the signal-to-noise ratio (SNR), and  $\lambda$  is the ratio of total reverberation scattering cross-section to total target scattering cross-section.<sup>19</sup> Generally speaking, the optimization problem is to find that pair (or pairs) of unit-energy waveforms  $\tilde{u}(t)$  and  $\tilde{w}(t)$  that will maximize the normalized SIR  $\rho$ , as given by Equation (6.2-11) for constant  $\rho_o$  and  $\lambda$ .

The normalized complex envelope of the transmit signal  $\tilde{u}(t)$  is restricted to be a pulse train consisting of uniformly spaced, complex weighted subpulses; i.e.,

$$\tilde{u}(t) = \sum_{n=0}^{N-1} \tilde{u}_n \tilde{p}_n(t - nT_p) \quad , \quad (6.2-14)$$

where  $\tilde{u}_n$  is an arbitrary complex weight applied to the  $n^{\text{th}}$  subpulse  $\tilde{p}_n(\cdot)$ ;  $T_p$  is the interpulse spacing, and  $N$  is the total number of subpulses in the pulse train. The duration of each subpulse  $\tau < T_p$  is identical for all subpulses and the total duration of  $\tilde{u}(t)$  is  $T_d = NT_p$ . Note that each subpulse is allowed to be arbitrary in

shape, except for the time duration constraint  $T < T_p$ . For example, if each subpulse is a linear frequency modulated (LFM) pulse, then:

$$\tilde{p}_n(t) = \frac{1}{\sqrt{T}} \exp(+jb_n t^2) \exp(+j2\pi f_n t) ;$$

$$n = 0, 1, \dots, N-1; \quad 0 \leq t \leq T, \quad (6.2-15)$$

where  $(b_n T)/\pi$  is the swept bandwidth (in Hz) and  $f_n$  is the frequency deviation from the carrier (in Hz) of the  $n^{\text{th}}$  subpulse. The quantity  $1/\sqrt{T}$  is a normalization factor such that:

$$\int_{-\infty}^{\infty} |\tilde{p}_n(t)|^2 dt = 1; \quad n = 0, 1, \dots, N-1. \quad (6.2-16)$$

The normalized complex envelope of the processing waveform  $\tilde{w}(t)$  is chosen to be a time ( $\tau'$ ) and frequency ( $\phi'$ ) shifted version of  $\tilde{u}(t)$ , i.e.,

$$\tilde{w}(t) = \tilde{u}(t - \tau') \exp(+j2\pi\phi't), \quad (6.2-17)$$

or substituting Equation (6.2-14) into Equation (6.2-17),

$$\tilde{w}(t) = \sum_{n=0}^{N-1} \tilde{w}_n \tilde{p}_n(t - [\tau' + nT_p]) \exp(+j2\pi\phi't), \quad (6.2-18)$$

where  $\tilde{w}_n$  is an arbitrary complex weight applied to the  $n^{\text{th}}$  subpulse.<sup>19</sup> When  $\tilde{u}_n \neq \tilde{w}_n$  for  $n = 0, 1, \dots, N-1$ , this is referred to as the "mismatched filter" case. However, when  $\tilde{u}_n = \tilde{w}_n$  for  $n = 0, 1, \dots, N-1$ , this is referred to as the "matched filter" case. The parameters  $\tau'$  and  $\phi'$  are assumed to be known constants.



For the case of a doubly spread target, the parameters  $\tau'$  and  $\phi'$  can be chosen as the mean round-trip time delay and the mean Doppler shift [see Equations (2.3-73) and (2.3-79)].

Since one of the optimization problems to be discussed in this chapter is the joint optimization of  $\rho$  with respect to the unknown time functions  $\tilde{u}(t)$  and  $\tilde{w}(t)$ , the form of Equations (6.2-14) and (6.2-18) are significant. They can be thought of as trial functions, i.e., linear combinations of a finite number of different, preselected functions. The preselected functions for  $\tilde{u}(t)$  are the  $N$  subpulses  $\tilde{p}_n(t - nT_p)$ , and for  $\tilde{w}(t)$ , they are  $\tilde{p}_n(t - [\tau' + nT_p])\exp(+j2\pi\phi't)$ . When Equations (6.2-14) and (6.2-18) are substituted into Equation (6.2-11), the joint optimization of  $\rho$  will be with respect to the unknown complex constant coefficients  $\tilde{u}_n$  and  $\tilde{w}_n$  for  $n = 0, 1, \dots, N - 1$ , and no longer with respect to the time functions  $\tilde{u}(t)$  and  $\tilde{w}(t)$ . This is exactly analogous to the Rayleigh-Ritz technique for finding the extremum of a functional which involves quadratic terms of the unknown time function.<sup>66</sup> With the use of Equations (6.2-14) and (6.2-18), the integral expression for  $\rho$  can be transformed into an equivalent vector-matrix expression. But before this procedure is begun, let us examine the constraints that must be placed upon  $\tilde{u}_n$  and  $\tilde{w}_n$  for  $n = 0, 1, \dots, N - 1$  due to the form of Equations (6.2-14) and (6.2-18).

If one computes the energy of  $\tilde{u}(t)$  and  $\tilde{w}(t)$  using Equations (6.2-14) and (6.2-18), respectively, it can be shown that:

$$\int_{-\infty}^{\infty} |\tilde{u}(t)|^2 dt = \sum_{n=0}^{N-1} |\tilde{u}_n|^2 = \underline{\tilde{u}}^\dagger \underline{\tilde{u}} = |\underline{\tilde{u}}|^2 \quad (6.2-19)$$

and

$$\int_{-\infty}^{\infty} |\tilde{w}(t)|^2 dt = \sum_{n=0}^{N-1} |\tilde{w}_n|^2 = \underline{\tilde{w}}^\dagger \underline{\tilde{w}} = |\underline{\tilde{w}}|^2, \quad (6.2-20)$$

where

$$\underline{\tilde{u}} \triangleq [\tilde{u}_0 \ \tilde{u}_1 \ \dots \ \tilde{u}_{N-1}]^T \quad (6.2-21)$$

is the  $(N \times 1)$  complex transmit weighting vector, and

$$\underline{\tilde{w}} \triangleq [\tilde{w}_0 \ \tilde{w}_1 \ \dots \ \tilde{w}_{N-1}]^T \quad (6.2-22)$$

is the  $(N \times 1)$  complex processing weighting vector. The dagger "+" denotes complex conjugate transpose and the superscript "T" denotes transpose. In deriving Equations (6.2-19) and (6.2-20), use was made of the orthonormal properties of  $\tilde{p}_n(t - nT_p)$ , i.e.,

$$\int_{-\infty}^{\infty} \tilde{p}_m(t - mT_p) \tilde{p}_n^*(t - nT_p) dt = \begin{cases} 0 & ; m \neq n \\ 1 & ; m = n \end{cases}, \quad (6.2-23)$$

where it has been assumed that each  $\tilde{p}_n(\cdot)$  is normalized [see Equation (6.2-16)]. In order to satisfy the unit-energy requirements of  $\tilde{u}(t)$  and  $\tilde{w}(t)$ , the vectors  $\underline{\tilde{u}}$  and  $\underline{\tilde{w}}$  must also be constrained to have unit-energy, i.e.,

$$|\underline{\tilde{u}}|^2 = |\underline{\tilde{w}}|^2 = 1 \quad (6.2-24)$$

We are now in a position to transform the integral expression for  $\rho$  into an equivalent vector-matrix expression. Consider the magnitude squared cross-ambiguity function

$$\left| \chi_{\tilde{u}\tilde{w}}(\tau, \phi) \right|^2 = \left| \int_{-\infty}^{\infty} \tilde{u}(t - \frac{\tau}{2}) \tilde{w}^*(t + \frac{\tau}{2}) \exp(+j2\pi\phi t) dt \right|^2. \quad (6.2-25)$$

Substituting Equations (6.2-14) and (6.2-18) into Equation (6.2-25) yields:

$$\left| \chi_{\tilde{u}\tilde{w}}(\tau, \phi) \right|^2 = \left| \sum_{m=0}^{N-1} \sum_{n=0}^{N-1} \tilde{u}_m \tilde{w}_n^* \exp(+j\pi[\phi - \phi']) \cdot \right. \\ \left. [m+n]T_p \right) \chi_{\tilde{p}_m \tilde{p}_n} [2\varepsilon(\tau), \phi - \phi'] \right|^2, \quad (6.2-26)$$

where

$$\varepsilon_{mn}(\tau) \triangleq [\tau - \tau' + (m - n)T_p] / 2. \quad (6.2-27)$$

Equation (6.2-26) can also be written as:

$$\left| \chi_{\tilde{u}\tilde{w}}(\tau, \phi) \right|^2 = \left| \tilde{\underline{w}}^{\dagger} \underline{H}(\tau, \phi) \tilde{\underline{u}} \right|^2, \quad (6.2-28)$$

where element  $(mn)$  of the  $(N \times N)$  matrix  $\underline{H}(\tau, \phi)$  is defined as:

$$\tilde{h}_{mn}(\tau, \phi) \triangleq \exp(+j\pi[\phi - \phi'] [m + n] T_p) \chi_{\tilde{p}_m \tilde{p}_n} (2\epsilon(\tau), \phi - \phi') ;$$

$$m, n = 0, 1, \dots, N - 1 \quad . \quad (6.2-29)$$

Using Equation (6.2-28), one can write

$$\int_{-\infty}^{\infty} \int_{\text{TRGT}} \sigma(\tau, \phi) |\chi_{\tilde{u}\tilde{w}}(\tau, \phi)|^2 d\tau d\phi = \tilde{w}^+ \underline{C}_T(\tilde{u}) \tilde{w} \quad (6.2-30)$$

and

$$\int_{-\infty}^{\infty} \int_{\text{REV}} \sigma(\tau, \phi) |\chi_{\tilde{u}\tilde{w}}(\tau, \phi)|^2 d\tau d\phi = \tilde{w}^+ \underline{C}_R(\tilde{u}) \tilde{w} \quad , \quad (6.2-31)$$

where

$$\underline{C}_T(\tilde{u}) \triangleq \int_{-\infty}^{\infty} \int_{\text{TRGT}} \sigma(\tau, \phi) \underline{H}(\tau, \phi) \tilde{u} [\underline{H}(\tau, \phi) \tilde{u}]^+ d\tau d\phi \quad (6.2-32)$$

is the  $(N \times N)$  Hermitian "target matrix," and

$$\underline{C}_R(\tilde{u}) \triangleq \int_{-\infty}^{\infty} \int_{\text{REV}} \sigma(\tau, \phi) \underline{H}(\tau, \phi) \tilde{u} [\underline{H}(\tau, \phi) \tilde{u}]^+ d\tau d\phi \quad (6.2-33)$$

is the  $(N \times N)$  Hermitian "reverberation matrix." Upon substituting Equations (6.2-30) and (6.2-31) into Equation (6.2-11), one obtains:

$$\frac{\rho}{\rho_0} = \frac{\tilde{w}^+ \underline{C}_T(\tilde{u}) \tilde{w}}{\tilde{w}^+ [\underline{I} + \rho_0 \lambda \underline{C}_R(\tilde{u})] \tilde{w}} \quad , \quad (6.2-34)$$

where  $\underline{I}$  is the  $(N \times N)$  identity matrix. Equation (6.2-34) is the

desired vector-matrix expression of the normalized SIR  $\rho$  for a doubly spread target.

The normalized version of the SIR  $\rho$  for a slowly fluctuating point target is:

$$\frac{\rho}{\rho_0} = \frac{|\chi_{\tilde{u}\tilde{w}}(\tau', \phi')|^2}{\rho_0 \lambda \int_{-\infty}^{\infty} \int_{-\infty}^{\infty} \sigma(\tau, \phi) |\chi_{\tilde{u}\tilde{w}}(\tau, \phi)|^2 d\tau d\phi + 1}, \quad (6.2-35)$$

where  $\rho_0$  and  $\lambda$  are given by Equations (6.2-12) and (6.2-13), respectively, with

$$\sigma_{\text{TRGT}} = E\{|\xi|^2\}. \quad (6.2-36)$$

If one evaluates Equation (6.2-26) at  $\tau = \tau'$  and  $\phi = \phi'$ , one obtains:

$$|\chi_{\tilde{u}\tilde{w}}(\tau', \phi')|^2 = \left| \sum_{m=0}^{N-1} \sum_{n=0}^{N-1} \tilde{u}_m \tilde{w}_n^* \chi_{\tilde{p}_m \tilde{p}_n}([m-n]T_p, 0) \right|^2. \quad (6.2-37)$$

Since

$$\chi_{\tilde{p}_m \tilde{p}_n}([m-n]T_p, 0) = \begin{cases} 1, & m = n \\ 0, & m \neq n \end{cases}, \quad (6.2-38)$$

then

$$|\chi_{\tilde{u}\tilde{w}}(\tau', \phi')|^2 = \left| \sum_{n=0}^{N-1} \tilde{u}_n \tilde{w}_n^* \right|^2 = |\tilde{\underline{w}}^+ \tilde{\underline{u}}|^2. \quad (6.2-39)$$

Upon substituting Equations (6.2-31) and (6.2-39) into Equation (6.2-35), one obtains:

$$\frac{\rho}{\rho_o} = \frac{|\tilde{\mathbf{w}}^+ \tilde{\mathbf{u}}|^2}{\tilde{\mathbf{w}}^+ [\mathbf{I} + \rho_o \lambda \mathbf{C}_R(\tilde{\mathbf{u}})] \tilde{\mathbf{w}}} \quad (6.2-40)$$

which is the desired vector-matrix expression of the normalized SIR  $\rho$  for a slowly fluctuating point target.

### 6.3 Maximization of the SIR for a Slowly Fluctuating Point Target

6.3.1 The optimum processing waveform for a given transmit signal. In this section, we will consider the problem of finding the optimum unit-energy processing weighting vector  $\tilde{\mathbf{w}}_{\text{OPT}}$  that will maximize the SIR when the unit-energy transmit weighting vector  $\tilde{\mathbf{u}}$  and the parameters of the subpulses are given.

Since  $\tilde{\mathbf{u}}$  and  $\tilde{p}_n(\cdot)$  for  $n = 0, 1, \dots, N-1$  are assumed to be given, the elements of the reverberation matrix  $\mathbf{C}_R(\tilde{\mathbf{u}})$  are known complex constants. Also, since  $\mathbf{C}_R(\tilde{\mathbf{u}})$  is positive semi-definite Hermitian in general, and the identity matrix  $\mathbf{I}$  is positive definite Hermitian, the  $(N \times N)$  matrix  $[\mathbf{I} + \rho_o \lambda \mathbf{C}_R(\tilde{\mathbf{u}})]$  is positive definite Hermitian since the sum of two Hermitian matrices is also Hermitian<sup>68</sup> and the sum of a positive semi-definite matrix and a positive definite matrix is a positive definite matrix.<sup>69</sup> Therefore, since  $[\mathbf{I} + \rho_o \lambda \mathbf{C}_R(\tilde{\mathbf{u}})]$  is positive definite Hermitian, there then exists a unique  $(N \times N)$  positive definite Hermitian matrix  $\mathbf{S}$  such that:

$$\mathbf{I} + \rho_o \lambda \mathbf{C}_R(\tilde{\mathbf{u}}) = \mathbf{S} \mathbf{S}^H, \quad (6.3-1)$$

where  $\underline{S}$  is called the square root<sup>70</sup> of  $[\underline{I} + \rho_0 \lambda \underline{C}_R(\underline{u})]$ . Using Equation (6.3-1), Equation (6.2-40) can be rewritten as:

$$\frac{\rho}{\rho_0} = \frac{|\underline{\tilde{w}}^+ \underline{S} \underline{S}^{-1} \underline{\tilde{u}}|^2}{\underline{\tilde{w}}^+ \underline{S} \underline{S} \underline{\tilde{w}}} \quad (6.3-2)$$

which can be bounded from above by applying the Cauchy inequality to the numerator.

The numerator of Equation (6.3-2) can be rewritten as:

$$|\underline{\tilde{w}}^+ \underline{S} \underline{S}^{-1} \underline{\tilde{u}}|^2 = |\underline{\tilde{x}} \underline{\tilde{y}}|^2, \quad (6.3-3)$$

where the  $(1 \times N)$  complex vector  $\underline{\tilde{x}}$  is:

$$\underline{\tilde{x}} \triangleq \underline{\tilde{w}}^+ \underline{S} \quad (6.3-4)$$

and the  $(N \times 1)$  complex vector  $\underline{\tilde{y}}$  is:

$$\underline{\tilde{y}} \triangleq \underline{S}^{-1} \underline{\tilde{u}}. \quad (6.3-5)$$

The scalar product

$$\underline{\tilde{x}} \underline{\tilde{y}} = \sum_{i=1}^N \tilde{x}_i \tilde{y}_i \quad (6.3-6)$$

so that

$$|\underline{\tilde{x}} \underline{\tilde{y}}|^2 \leq \sum_{i=1}^N |\tilde{x}_i|^2 \sum_{i=1}^N |\tilde{y}_i|^2 \quad (6.3-7)$$

by application of Cauchy's inequality.<sup>9</sup> Since  $\underline{\tilde{x}}$  is a  $(1 \times N)$  vector, then:

$$\underline{\tilde{x}} \underline{\tilde{x}}^+ = |\underline{\tilde{x}}|^2 = \sum_{i=1}^N |\tilde{x}_i|^2 \quad (6.3-8)$$

and since  $\tilde{\underline{y}}$  is a  $(N \times 1)$  vector, then:

$$\tilde{\underline{y}}^\dagger \tilde{\underline{y}} = |\tilde{\underline{y}}|^2 = \sum_{i=1}^N |\tilde{y}_i|^2 \quad (6.3-9)$$

Substituting Equations (6.3-7) through (6.3-9) into Equation (6.3-3) yields:

$$|\tilde{\underline{w}}^\dagger \underline{\underline{S}} \underline{\underline{S}}^{-1} \tilde{\underline{u}}|^2 \leq \tilde{\underline{w}}^\dagger \underline{\underline{S}} \underline{\underline{S}} \tilde{\underline{w}} \tilde{\underline{u}}^\dagger (\underline{\underline{S}} \underline{\underline{S}})^{-1} \tilde{\underline{u}} \quad (6.3-10)$$

since  $\underline{\underline{S}} = \underline{\underline{S}}^\dagger$ ,  $(\underline{\underline{S}}^{-1})^\dagger = (\underline{\underline{S}}^\dagger)^{-1}$ , and  $(\underline{\underline{S}}^{-1} \underline{\underline{S}}^{-1}) = (\underline{\underline{S}} \underline{\underline{S}})^{-1}$ . And upon substituting Equation (6.3-10) into Equation (6.3-2), one obtains the desired result:

$$\frac{\rho}{\rho_0} \leq \tilde{\underline{u}}^\dagger [\underline{\underline{I}} + \rho_0 \lambda \underline{\underline{C}}_R(\tilde{\underline{u}})]^{-1} \tilde{\underline{u}} \quad (6.3-11)$$

The inequality in Equation (6.3-11) becomes an equality only when

$$\tilde{\underline{x}} = \tilde{k} \tilde{\underline{y}}^\dagger \quad (6.3-12)$$

or equivalently:

$$\tilde{\underline{w}} = \tilde{k} [\underline{\underline{I}} + \rho_0 \lambda \underline{\underline{C}}_R(\tilde{\underline{u}})]^{-1} \tilde{\underline{u}} \quad (6.3-13)$$

where  $\tilde{k}$  is an arbitrary complex constant. Since  $\tilde{k}$  is arbitrary, it can be chosen in such a way that the unit-energy requirement of Equation (6.2-24) is met. It can be shown that the value of  $\tilde{k}$  which satisfies  $|\tilde{\underline{w}}|^2 = 1$  is given by:

$$k^2 = \frac{1}{\tilde{\underline{u}}^\dagger [\underline{\underline{I}} + \rho_0 \lambda \underline{\underline{C}}_R(\tilde{\underline{u}})]^{-2} \tilde{\underline{u}}} \quad (6.3-14)$$



where  $\tilde{k} = k$  is a real constant since the denominator of Equation (6.3-14) is a quadratic positive definite Hermitian form, and hence, a real non-zero positive scalar quantity.

Therefore, when  $\tilde{\mathbf{u}}$  and  $\tilde{p}_n(\cdot)$  for  $n = 0, 1, \dots, N - 1$  are given, the optimum processing weighting vector is:

$$\tilde{\mathbf{w}}_{\text{OPT}} = k[\mathbf{I} + \rho_o \lambda \mathbf{C}_R(\tilde{\mathbf{u}})]^{-1} \tilde{\mathbf{u}}, \quad (6.3-15)$$

where  $k$  is given by Equation (6.3-14). When  $\tilde{\mathbf{w}}_{\text{OPT}}$  is used, the normalized SIR  $\rho$  for a slowly fluctuating point target is maximized and this maximum value is:

$$\left(\frac{\rho}{\rho_o}\right)_{\text{MAX}} = \tilde{\mathbf{u}}^\dagger [\mathbf{I} + \rho_o \lambda \mathbf{C}_R(\tilde{\mathbf{u}})]^{-1} \tilde{\mathbf{u}}. \quad (6.3-16)$$

**6.3.2 The optimum transmit-processing waveform pair - an iterative technique.** In order to develop an iterative technique for finding the optimum pair  $(\tilde{\mathbf{u}}_{\text{OPT}}, \tilde{\mathbf{w}}_{\text{OPT}})$ , one must maximize Equation (6.3-16) over the set of all unit-energy vectors  $\tilde{\mathbf{u}}$ . In this section, an iterative algorithm will be described that yields a sequence of increasingly better transmit weighting vectors, along with the corresponding processing weighting vectors.<sup>19,59</sup> This sequence of transmit-processing, complex weighting vector pairs has the property that  $\rho_{n+1} \geq \rho_n$ .<sup>19,59</sup>

The basis for the iterative procedure is the following symmetry property of the cross-ambiguity function:

$$|\chi_{\tilde{\mathbf{u}}\tilde{\mathbf{w}}}(\tau, \phi)|^2 = |\chi_{\tilde{\mathbf{w}}'\tilde{\mathbf{u}}'}(\tau, \phi)|^2, \quad (6.3-17)$$

where

$$\tilde{u}'(t) = \tilde{u}(-t) \quad (6.3-18)$$

and

$$\tilde{w}'(t) = \tilde{w}(-t) \quad (6.3-19)$$

By referring to Equations (6.2-11) and (6.2-35), it can be seen that the SIR obtained from a transmit signal  $\tilde{u}(t)$  and processing waveform  $\tilde{w}(t)$  is the same as would be obtained from a transmit signal  $\tilde{w}'(t)$  and processing waveform  $\tilde{u}'(t)$ . For the case when the transmit and processing waveforms are pulse trains, this invariance principle is equivalent to the statement that the SIR, as given by Equations (6.2-34) or (6.2-40) is invariant under the transformation

$$\underline{\tilde{u}} \rightarrow \underline{\tilde{w}'} \quad \text{and} \quad \underline{\tilde{w}} \rightarrow \underline{\tilde{u}'},$$

where

$$\underline{\tilde{u}'} = \underline{I'} \underline{\tilde{u}} \quad (6.3-20)$$

$$\underline{\tilde{w}'} = \underline{I'} \underline{\tilde{w}} \quad (6.3-21)$$

and

$$\underline{I'} = \begin{bmatrix} 0 & 0 & 0 & \cdot & \cdot & \cdot & 1 \\ 0 & \cdot & \cdot & \cdot & 0 & 1 & 0 \\ \cdot & & & & \cdot & & \\ \cdot & & \cdot & & & & \cdot \\ \cdot & \cdot & & & & & \cdot \\ 0 & 1 & & & & & \cdot \\ 1 & 0 & \cdot & \cdot & \cdot & \cdot & 0 \end{bmatrix} \quad (6.3-22)$$

Note that the prime symbol " ' " does not indicate transpose. Also note that premultiplication of a matrix by  $\underline{I'}$  reverses the order of the rows of that matrix and post-multiplication reverses the order of the columns.<sup>19</sup>

The iterative technique due to DeLong and Hofstetter<sup>19</sup> which finds the optimum pair  $(\tilde{\underline{u}}_{\text{OPT}}, \tilde{\underline{w}}_{\text{OPT}})$  that maximizes  $\rho$  for a point target when  $\tilde{p}_n(\cdot)$ ;  $n = 0, 1, \dots, N - 1$  is given and the maximization is subject to unit-energy constraints on both  $\tilde{\underline{u}}_{\text{OPT}}$  and  $\tilde{\underline{w}}_{\text{OPT}}$ , is discussed next.

Start with an arbitrary, unit-energy, transmit weighting vector  $\tilde{\underline{u}}_1$  and compute its corresponding optimum processing weighting vector from Equations (6.3-14) and (6.3-15), i.e.,

$$\tilde{\underline{w}}_{\text{OPT}_1} = k_1 [\underline{I} + \rho_o \lambda \underline{C}_R(\tilde{\underline{u}}_1)]^{-1} \tilde{\underline{u}}_1, \quad (6.3-23)$$

where

$$k_1 = \frac{1}{(\tilde{\underline{u}}_1^\dagger [\underline{I} + \rho_o \lambda \underline{C}_R(\tilde{\underline{u}}_1)]^{-2} \tilde{\underline{u}}_1)^{1/2}}. \quad (6.3-24)$$

The pair  $(\tilde{\underline{u}}_1, \tilde{\underline{w}}_{\text{OPT}_1})$  results in  $\rho_1$  as given by [see Equation (6.3-16)]:

$$\rho_1 = \rho_o \tilde{\underline{u}}_1^\dagger [\underline{I} + \rho_o \lambda \underline{C}_R(\tilde{\underline{u}}_1)]^{-1} \tilde{\underline{u}}_1. \quad (6.3-25)$$

By the invariance property described previously, the pair  $(\tilde{\underline{w}}'_{\text{OPT}_1}, \tilde{\underline{u}}'_1)$  yields the same SIR  $\rho_1$  as given by Equation (6.3-25). However,  $\tilde{\underline{u}}'_1$  is not necessarily the optimum processing weighting vector to use with the transmit weighting vector  $\tilde{\underline{w}}'_{\text{OPT}_1}$ . Therefore, the optimum processing weighting vector corresponding to  $\tilde{\underline{w}}'_{\text{OPT}_1}$  must yield a SIR no smaller than  $\rho_1$ . Let

$$\tilde{\underline{u}}_2 = \tilde{\underline{w}}'_{\text{OPT}_1}. \quad (6.3-26)$$

which can be rewritten as [see Equation (6.3-21)]:

$$\tilde{\underline{u}}_2 = \underline{I}' \tilde{\underline{w}}_{\text{OPT}_1} \quad (6.3-27)$$

Substituting Equations (6.3-23) and (6.3-24) into Equation (6.3-27) yields:

$$\tilde{\underline{u}}_2 = \frac{\underline{I}' [\underline{I} + \rho_o \lambda \underline{C}_R(\tilde{\underline{u}}_1)]^{-1} \tilde{\underline{u}}_1}{\{\tilde{\underline{u}}_1^+ [\underline{I} + \rho_o \lambda \underline{C}_R(\tilde{\underline{u}}_1)]^{-2} \tilde{\underline{u}}_1\}^{1/2}} \quad (6.3-28)$$

The optimum processing weighting vector corresponding to  $\tilde{\underline{u}}_2$  is [see Equations (6.3-14) and (6.3-15)]:

$$\tilde{\underline{w}}_{\text{OPT}_2} = \frac{[\underline{I} + \rho_o \lambda \underline{C}_R(\tilde{\underline{u}}_2)]^{-1} \tilde{\underline{u}}_2}{\{\tilde{\underline{u}}_2^+ [\underline{I} + \rho_o \lambda \underline{C}_R(\tilde{\underline{u}}_2)]^{-2} \tilde{\underline{u}}_2\}^{1/2}} \quad (6.3-29)$$

and from Equation (6.3-16):

$$\rho_2 = \rho_o \tilde{\underline{u}}_2^+ [\underline{I} + \rho_o \lambda \underline{C}_R(\tilde{\underline{u}}_2)]^{-1} \tilde{\underline{u}}_2 \geq \rho_1 \quad (6.3-30)$$

Therefore the second iteration would yield the pair  $(\tilde{\underline{u}}_2, \tilde{\underline{w}}_{\text{OPT}_2})$  as given by Equations (6.3-28) and (6.3-29), respectively, and this particular pair would yield the SIR  $\rho_2$  as given by Equation (6.3-30).

Equation (6.3-28) can be generalized so that

$$\tilde{\underline{u}}_{n+1} = T(\tilde{\underline{u}}_n) ; \quad n = 1, 2, 3, \dots \quad (6.3-31)$$

where  $T(\cdot)$  is the nonlinear transformation defined by:

$$T(\tilde{\underline{u}}_n) \triangleq \frac{\underline{I}' [\underline{I} + \rho_o \lambda C_R(\tilde{\underline{u}}_n)]^{-1} \tilde{\underline{u}}_n}{\{\tilde{\underline{u}}_n^+ [\underline{I} + \rho_o \lambda C_R(\tilde{\underline{u}}_n)]^{-2} \tilde{\underline{u}}_n\}^{1/2}} \quad (6.3-32)$$

and  $\tilde{\underline{u}}_1$  is an arbitrary, unit-energy transmit weighting vector used to initiate the iterative algorithm of Equation (6.3-31). The optimum processing weighting vector corresponding to  $\tilde{\underline{u}}_{n+1}$  is:

$$\tilde{\underline{w}}_{\text{OPT } n+1} = \frac{[\underline{I} + \rho_o \lambda C_R(\tilde{\underline{u}}_{n+1})]^{-1} \tilde{\underline{u}}_{n+1}}{\{\tilde{\underline{u}}_{n+1}^+ [\underline{I} + \rho_o \lambda C_R(\tilde{\underline{u}}_{n+1})]^{-2} \tilde{\underline{u}}_{n+1}\}^{1/2}} ; \quad (6.3-33)$$

$$n = 0, 1, 2, \dots$$

The pair  $(\tilde{\underline{u}}_{n+1}, \tilde{\underline{w}}_{\text{OPT } n+1})$  results in a SIR given by:

$$\rho_{n+1} = \rho_o \tilde{\underline{u}}_{n+1}^+ [\underline{I} + \rho_o \lambda C_R(\tilde{\underline{u}}_{n+1})]^{-1} \tilde{\underline{u}}_{n+1} ; \quad (6.3-34)$$

$$n = 0, 1, 2, \dots$$

where  $\rho_{n+1} \geq \rho_n$ .

The sequence  $\rho_{n+1}$  given by Equation (6.3-34) is monotonic and so must converge.<sup>19</sup> Therefore, in order to find the optimum pair  $(\tilde{\underline{u}}_{\text{OPT}}, \tilde{\underline{w}}_{\text{OPT}})$ , the iterative algorithm given by Equations (6.3-31) through (6.3-33) should be continued until there is no further change in  $\rho$  as given by Equation (6.3-34).

However, this particular algorithm does have its shortcomings. Although the sequence of  $\rho_n$ 's will ultimately converge, the limiting value is a relative maximum at least, but not necessarily the global maximum.<sup>19,59</sup> In addition, the procedure does not provide a unique optimum solution.<sup>59</sup> The pair of complex weighting vectors  $(\tilde{u}_{OPT}, \tilde{w}_{OPT})$  to which the procedure converges is strongly dependent upon the initial choice of the transmit weighting vector used to start the iteration scheme.<sup>59</sup> And the maximum value of  $\rho$  to which the algorithm converges is also dependent upon the initial choice of  $\tilde{u}$ .<sup>59</sup> As with any iterative algorithm, the initial choice required to start the iteration should always be an intelligent choice based upon a priori information (if available) rather than an arbitrary one.

DeLong and Hofstetter<sup>58</sup> also point out another drawback of this iterative technique. Based upon computational experience with their own algorithm, they found that pulse trains optimized under a unit-energy constraint tend to have large amplitude variations. Since it is undesirable to have the amplitude vary widely from subpulse to subpulse, it is desirable to control the amount of amplitude taper permitted in the signal design. Therefore, DeLong and Hofstetter<sup>58</sup> suggested replacing the energy constraints with a dynamic range constraint. A dynamic range constraint limits the maximum and minimum values allowed for the subpulse amplitudes in the transmit weighting vector. And since a dynamic range constraint also limits signal energy, energy constraints are no longer necessary. Since their iterative technique<sup>19</sup> was not suited for handling a dynamic range

constraint, DeLong and Hofstetter<sup>58</sup> formulated their new optimization problem into an equivalent nonlinear programming problem.

The nonlinear programming problem which they considered was the maximization of Equation (6.3-16) with respect to  $\underline{\tilde{u}}$ , subject to the constraints

$$A_{\text{MIN}} \leq |\tilde{u}_i| \leq A_{\text{MAX}}; \quad i = 0, 1, \dots, N - 1, \quad (6.3-35)$$

where both  $A_{\text{MIN}}$  and  $A_{\text{MAX}}$  are positive, real constants. In this problem, the waveforms  $\tilde{u}(t)$  and  $\tilde{w}(t)$  are identically equal to  $\tilde{x}(t)$  and  $\tilde{g}(t)$ , respectively, and hence, are not unit energy. Thus, the parameter  $\rho_0$  is equal to  $E\{|\tilde{b}|^2\}/N_0$ .

The approach taken by DeLong and Hofstetter<sup>58</sup> was to construct an iteration scheme that, if convergent, would converge to a vector  $\underline{\tilde{u}}$  satisfying the Kuhn-Tucker conditions. The Kuhn-Tucker conditions are necessary conditions which an optimal solution must satisfy.<sup>58</sup>

DeLong and Hofstetter<sup>58</sup> mention that it is not known whether their algorithm will always converge. Also, even if the sequence of values of  $\rho$  converges to a relative maximum, they state that it is theoretically possible that the sequence of transmit weighting vectors might not converge.

Luenberger<sup>71</sup> notes that there are two basic approaches for handling complex optimization problems by numerical techniques: (1) formulate the necessary conditions describing the optimal solution and solve these equations numerically (usually by some iterative scheme), or (2) bypass the formulation of the necessary conditions

and implement a direct iterative search for the optimum. Obviously, DeLong and Hofstetter<sup>58</sup> took the first approach and ran into some theoretical difficulties.

Luenberger<sup>71</sup> states that the second approach appears to be the most effective since progress during the iterations can be measured by monitoring the corresponding values of the objective functional. Therefore, instead of using the algorithm proposed by DeLong and Hofstetter,<sup>58</sup> one should implement a direct iterative search for the optimum  $\tilde{u}$  that will maximize Equation (6.3-16).

A direct iterative search for the optimum solution is also recommended to handle the more complicated optimization problems to be discussed in Section 6.4.

#### 6.4 Maximization of the SIR for a Doubly Spread Target

6.4.1 The optimum processing waveform for a given transmit signal. As with the point target optimization problem discussed in Section 6.3, we will first consider the problem of finding  $\tilde{w}_{OPT}$  for  $\tilde{u}$  and  $\tilde{p}_n(\cdot)$ ;  $n = 0, 1, \dots, N - 1$  given. In Sections 6.4.1 and 6.4.2,  $\tilde{u}(t)$  and  $\tilde{w}(t)$  are no longer considered to be the unit-energy, normalized versions of  $\tilde{x}(t)$  and  $\tilde{g}(t)$ , respectively, but rather  $\tilde{u}(t) \equiv \tilde{x}(t)$  and  $\tilde{w}(t) \equiv \tilde{g}(t)$ . As a result, the energy of  $\tilde{u}(t)$  and  $\tilde{w}(t)$  are given by Equations (6.2-19) and (6.2-20), respectively. Also, the parameter  $\rho_o$  appearing in Equation (6.2-34) is now equal to:

$$\rho_o = \frac{\sigma_{TRGT}}{N_o} \quad (6.4-1)$$



The optimization problem to be considered in this section is the maximization of

$$\frac{\rho}{\rho_0} = \frac{\tilde{\mathbf{w}}^{\dagger} \underline{\mathbf{C}}_T(\tilde{\mathbf{u}}) \tilde{\mathbf{w}}}{\tilde{\mathbf{w}}^{\dagger} [\underline{\mathbf{I}} + \rho_0 \lambda \underline{\mathbf{C}}_R(\tilde{\mathbf{u}})] \tilde{\mathbf{w}}} \quad (6.2-34)$$

with respect to  $\tilde{\mathbf{w}}$  for  $\tilde{\mathbf{u}}$  and  $\tilde{p}_n(\cdot)$ ;  $n = 0, 1, \dots, N-1$  given. The quadratic form in the numerator of Equation (6.2-34) precludes the direct application of the Cauchy inequality as was done in the point target case. Therefore, in order to find the optimum  $\tilde{\mathbf{w}}$  to use with a given  $\tilde{\mathbf{u}}$  which satisfies, for example, a dynamic range constraint

$$A_{\text{MIN}} \leq |\tilde{u}_i| \leq A_{\text{MAX}}; \quad i = 0, 1, \dots, N-1, \quad (6.4-2)$$

and with  $\tilde{p}_n(\cdot)$ ;  $n = 0, 1, \dots, N-1$  also given, one must maximize the quadratic

$$\tilde{\mathbf{w}}^{\dagger} \underline{\mathbf{C}}_T(\tilde{\mathbf{u}}) \tilde{\mathbf{w}}, \quad (6.4-3)$$

or equivalently, minimize the quadratic<sup>69</sup>

$$-\tilde{\mathbf{w}}^{\dagger} \underline{\mathbf{C}}_T(\tilde{\mathbf{u}}) \tilde{\mathbf{w}} \quad (6.4-4)$$

with respect to  $\tilde{\mathbf{w}}$ , subject to the following nonlinear constraints:

$$|\tilde{\mathbf{w}}|^2 = \sum_{i=0}^{N-1} |\tilde{w}_i|^2 = 1 \quad (6.4-5)$$

and

$$\tilde{\mathbf{w}}^{\dagger} \underline{\mathbf{C}}_R(\tilde{\mathbf{u}}) \tilde{\mathbf{w}} \leq K \leq 0, \quad (6.4-6)$$

where  $K$  is a real, positive constant since  $\underline{C}_R(\tilde{u})$  is positive semi-definite. Since  $\tilde{u}$  and  $\tilde{p}_n(\cdot)$ ;  $n = 0, 1, \dots, N - 1$  are given,  $\underline{C}_T(\tilde{u})$  and  $\underline{C}_R(\tilde{u})$  are known, constant matrices [see Equations (6.2-32) and (6.2-33), respectively]. The choice of a unit-energy constraint, as given by Equation (6.4-5), was arbitrary since a scaling of the processing waveform leaves the SIR unchanged.<sup>19</sup> The real, positive constant  $K$  in Equation (6.4-6) represents the level to which the reverberation has been reduced by the processing waveform for  $\tilde{u}$  and  $\tilde{p}_n(\cdot)$ ;  $n = 0, 1, \dots, N - 1$  given. For example,  $K = 0$  means that the processing waveform has completely removed all the reverberation.<sup>19</sup> It should be noted that it is not necessary to reduce the reverberation to zero, even if such a reduction were possible.<sup>56</sup> A final reverberation level comparable with the noise, if achievable, would usually be all that was required.<sup>56</sup>

Equations (6.4-4) through (6.4-6) represent a problem in nonlinear programming involving the  $(N \times 1)$  complex vectors  $\tilde{u}$  and  $\tilde{w}$  and the  $(N \times N)$  complex matrices  $\underline{C}_T(\tilde{u})$  and  $\underline{C}_R(\tilde{u})$ . The minimization of the quadratic given by Equation (6.4-4) was chosen since most of the standard computer programs available for handling nonlinear programming problems are written in terms of minimizing the nonlinear objective function. The main purpose of this section is to formulate the above nonlinear programming problem, which is defined on a complex  $N$ -space, into an equivalent nonlinear programming problem defined on a real  $2N$ -space.

The  $(N \times 1)$  complex vectors  $\tilde{u}$  and  $\tilde{w}$  can be represented by  $(2N \times 1)$  real vectors by treating the real and imaginary parts

of both  $\underline{\tilde{u}}$  and  $\underline{\tilde{w}}$  as independent variables.<sup>58</sup> For example, let the complex weighting vector  $\underline{\tilde{w}}$  be given by:

$$\underline{\tilde{w}} = \underline{a} + j\underline{b} \quad (6.4-7)$$

or

$$\begin{bmatrix} \tilde{w}_0 \\ \tilde{w}_1 \\ . \\ . \\ . \\ \tilde{w}_{N-1} \end{bmatrix} = \begin{bmatrix} a_0 \\ a_1 \\ . \\ . \\ . \\ a_{N-1} \end{bmatrix} + j \begin{bmatrix} b_0 \\ b_1 \\ . \\ . \\ . \\ b_{N-1} \end{bmatrix} \quad (6.4-8)$$

so that

$$\underline{\tilde{w}}^* = \underline{a} - j\underline{b} \quad , \quad (6.4-9)$$

where  $\underline{a}$  and  $\underline{b}$  are real  $(N \times 1)$  vectors. From Equation (6.4-7), one can see immediately that the constraint given by Equation (6.4-5) in terms of the complex unknowns  $\tilde{w}_i$  can be rewritten as:

$$|\underline{\tilde{w}}|^2 \equiv a_0^2 + a_1^2 + \dots + a_{N-1}^2 + b_0^2 + b_1^2 + \dots + b_{N-1}^2 = 1 \quad (6.4-10)$$

in terms of the real unknowns  $a_i$  and  $b_i$ ;  $i = 0, 1, \dots, N-1$ .

Let us now attempt to express the constraint given by Equation (6.4-6) in terms of the real unknowns  $a_i$  and  $b_i$ , also.

First note that the quadratic form  $\underline{\tilde{w}}^+ \underline{C}_R(\underline{\tilde{u}}) \underline{\tilde{w}}$  can be expressed as:<sup>68</sup>

$$\tilde{\mathbf{w}}^{\dagger} \underline{\mathbf{C}}_{\mathbf{R}}(\tilde{\mathbf{u}}) \tilde{\mathbf{w}} = \sum_{\ell=1}^N \sum_{m=1}^N \tilde{r}_{\ell m} \tilde{\mathbf{w}}_{\ell-1}^* \tilde{\mathbf{w}}_{m-1}, \quad (6.4-11)$$

where  $\tilde{r}_{\ell m}$  is element  $(\ell m)$  of the  $(N \times N)$  Hermitian matrix  $\underline{\mathbf{C}}_{\mathbf{R}}(\tilde{\mathbf{u}})$ . Making use of the fact that the reverberation matrix is Hermitian, i.e.,  $\tilde{r}_{ij} = \tilde{r}_{ji}^*$ , the expansion of Equation (6.4-11) becomes:

$$\begin{aligned} \tilde{\mathbf{w}}^{\dagger} \underline{\mathbf{C}}_{\mathbf{R}}(\tilde{\mathbf{u}}) \tilde{\mathbf{w}} = & r_{11} |\tilde{\mathbf{w}}_0|^2 + r_{22} |\tilde{\mathbf{w}}_1|^2 + \dots + r_{NN} |\tilde{\mathbf{w}}_{N-1}|^2 + \\ & 2\text{Re} \left\{ \tilde{r}_{12} \tilde{\mathbf{w}}_0^* \tilde{\mathbf{w}}_1 + \tilde{r}_{13} \tilde{\mathbf{w}}_0^* \tilde{\mathbf{w}}_2 + \dots + \tilde{r}_{1N} \tilde{\mathbf{w}}_0^* \tilde{\mathbf{w}}_{N-1} + \right. \\ & \tilde{r}_{23} \tilde{\mathbf{w}}_1^* \tilde{\mathbf{w}}_2 + \tilde{r}_{24} \tilde{\mathbf{w}}_1^* \tilde{\mathbf{w}}_3 + \dots + \tilde{r}_{2N} \tilde{\mathbf{w}}_1^* \tilde{\mathbf{w}}_{N-1} + \dots + \\ & \tilde{r}_{(N-2)(N-1)} \tilde{\mathbf{w}}_{N-3}^* \tilde{\mathbf{w}}_{N-2} + \tilde{r}_{(N-2)N} \tilde{\mathbf{w}}_{N-3}^* \tilde{\mathbf{w}}_{N-1} + \\ & \left. \tilde{r}_{(N-1)N} \tilde{\mathbf{w}}_{N-2}^* \tilde{\mathbf{w}}_{N-1} \right\}, \quad (6.4-12) \end{aligned}$$

where  $r_{11}, r_{22}, \dots, r_{NN}$  are real constants. Also, note that the expression

$$\begin{aligned} \tilde{r}_{(\ell-1)(m+2)} \tilde{\mathbf{w}}_{\ell-2}^* \tilde{\mathbf{w}}_{m+1} ; \quad \ell = 2, 3, \dots, N \\ m = 0, 1, \dots, N-2 \end{aligned} \quad (6.4-13)$$

will match any cross term appearing in Equation (6.4-12) so long as the difference between  $\ell$  and  $m$  is not greater than positive 2, i.e.,

$$-\infty < \ell - m \leq +2. \quad (6.4-14)$$

Now let

$$\tilde{r}_{\ell m} = x_{\ell m} + jy_{\ell m}, \quad (6.4-15)$$

where  $x_{\ell m}$  and  $y_{\ell m}$  are real, known constants since  $\underline{C}_R(\underline{\tilde{u}})$  is a known, constant matrix. Recalling that

$$\tilde{w}_i = a_i + jb_i \quad (6.4-16)$$

and upon substituting Equations (6.4-15) and (6.4-16) into Equation (6.4-13) and then taking the real part, Equation (6.4-12) can be expressed as:

$$\begin{aligned} \tilde{w}^\dagger \underline{C}_R(\underline{\tilde{u}}) \tilde{w} &\equiv \sum_{k=1}^N x_{kk} (a_{k-1}^2 + b_{k-1}^2) + \\ &2 \sum_{\ell=2}^N \sum_{m=0}^{N-2} \left\{ [a_{\ell-2} a_{m+1} + b_{\ell-2} b_{m+1}] x_{(\ell-1)(m+2)} + \right. \\ &\quad \left. -\infty < \ell - m < +2 \right. \\ &\quad \left. [a_{m+1} b_{\ell-2} - a_{\ell-2} b_{m+1}] y_{(\ell-1)(m+2)} \right\} \leq K \leq 0 \end{aligned} \quad (6.4-17)$$

since  $r_{11}, r_{22}, \dots, r_{NN}$  are real constants, and hence, from Equation (6.4-15),  $r_{11} = x_{11}$ ,  $r_{22} = x_{22}$ ,  $\dots$ ,  $r_{NN} = x_{NN}$ . Equation (6.4-17) expresses the original nonlinear constraint as given by Equation (6.4-6) in terms of the real unknowns  $a_i$  and  $b_i$ .

Similarly, if one denotes element  $(\ell m)$  of the  $(N \times N)$  Hermitian matrix  $\underline{C}_T(\underline{\tilde{u}})$  as:

$$\tilde{t}_{\ell m} = \alpha_{\ell m} + j\beta_{\ell m}, \quad (6.4-18)$$

where both  $\alpha_{\ell m}$  and  $\beta_{\ell m}$  are real, known constants, then the nonlinear objective function given by Equation (6.4-4) can be expressed as:

$$\begin{aligned}
-\tilde{\mathbf{w}}^{\dagger} \mathbf{C}_T(\tilde{\mathbf{u}}) \tilde{\mathbf{w}} &\equiv - \sum_{k=1}^N \alpha_{kk} [a_{k-1}^2 + b_{k-1}^2] - \\
&2 \sum_{\ell=2}^N \sum_{m=0}^{N-2} \left\{ [a_{\ell-2} a_{m+1} + b_{\ell-2} b_{m+1}] \cdot \right. \\
&\quad \left. -\infty < \ell - m < +2 \right. \\
&\quad \left. \alpha_{(\ell-1)(m+2)} + [a_{m+1} b_{\ell-2} - a_{\ell-2} b_{m+1}] \cdot \right. \\
&\quad \left. \beta_{(\ell-1)(m+2)} \right\} . \quad (6.4-19)
\end{aligned}$$

The task of formulating the original nonlinear programming problem which was defined on a complex  $N$ -space into an equivalent problem defined on a real  $2N$ -space has been accomplished. For a given complex transmit weighting vector which satisfies Equation (6.4-2), and with the parameters of the subpulses also given, the equivalent problem is to minimize the nonlinear objective function given by Equation (6.4-19) with respect to the real unknowns  $a_i$  and  $b_i$ ;  $i = 0, 1, \dots, N-1$  subject to the nonlinear constraints given by Equations (6.4-10) and (6.4-17). Once the optimum pair  $(\underline{a}_{\text{OPT}}, \underline{b}_{\text{OPT}})$  is found, the corresponding optimum complex processing weighting vector can be computed from

$$\tilde{\mathbf{w}}_{\text{OPT}} = \underline{a}_{\text{OPT}} + j \underline{b}_{\text{OPT}} \quad (6.4-20)$$

One of the most common nonlinear programming techniques for handling constraints is to use the method of steepest descent in conjunction with the gradient projection method.<sup>66,71</sup> The gradient projection method is due to Rosen.<sup>63,64</sup>

6.4.2 The optimum transmit-processing waveform pair. Using the results of Section 6.4.1, a joint optimization nonlinear programming problem will be formulated in this section, the solution of which will yield the optimum pair  $(\underline{\tilde{u}}_{\text{OPT}}, \underline{\tilde{w}}_{\text{OPT}})$  that maximizes the SIR  $\rho$  for a doubly spread target subject to a dynamic range constraint on the transmit weighting vector and the amount of reverberation to be removed. Once again it is assumed that the parameters of the subpulses are given.

Consider the following  $(N \times N)$  positive semi-definite Hermitian matrix

$$\underline{C}(\underline{\tilde{u}}) = \int_{-\infty}^{\infty} \int \sigma(\tau, \phi) \underline{H}(\tau, \phi) \underline{\tilde{u}} [\underline{H}(\tau, \phi) \underline{\tilde{u}}]^{\dagger} d\tau d\phi, \quad (6.4-21)$$

where the subscripts "T" and "R" have been removed for now. If one expresses the  $(N \times N)$  matrix  $\underline{H}(\tau, \phi)$  as:

$$\underline{H}(\tau, \phi) = \begin{bmatrix} \tilde{h}_{00} & \tilde{h}_{01} & \cdot & \cdot & \cdot & \tilde{h}_{0(N-1)} \\ \tilde{h}_{10} & \tilde{h}_{11} & \cdot & \cdot & \cdot & \tilde{h}_{1(N-1)} \\ \cdot & \cdot & \cdot & \cdot & \cdot & \cdot \\ \cdot & \cdot & \cdot & \cdot & \cdot & \cdot \\ \cdot & \cdot & \cdot & \cdot & \cdot & \cdot \\ \tilde{h}_{(N-1)0} & \tilde{h}_{(N-1)1} & \cdot & \cdot & \cdot & \tilde{h}_{(N-1)(N-1)} \end{bmatrix}, \quad (6.4-22)$$

where  $\tilde{h}_{mn} \equiv \tilde{h}_{mn}(\tau, \phi)$ , then it can be shown that element  $(ij)$  of the  $(N \times N)$  matrix  $\underline{H}(\tau, \phi) \underline{\tilde{u}} [\underline{H}(\tau, \phi) \underline{\tilde{u}}]^{\dagger}$  is:

$$\left( \sum_{\ell=0}^{N-1} \tilde{u}_{\ell} \tilde{h}_{i\ell} \right) \cdot \left( \sum_{m=0}^{N-1} \tilde{u}_m^* \tilde{h}_{jm}^* \right); \quad (6.4-23)$$

$$i, j = 0, 1, \dots, N-1$$

and as a result, element  $(ij)$  of  $\underline{C}(\underline{\tilde{u}})$  is given by:

$$[\underline{C}(\underline{\tilde{u}})]_{ij} = \sum_{\ell=0}^{N-1} \sum_{m=0}^{N-1} \tilde{u}_{\ell} \tilde{u}_m^* \int_{-\infty}^{\infty} \int \sigma(\tau, \phi) \tilde{h}_{(i-1)\ell} \tilde{h}_{(j-1)m}^* d\tau d\phi;$$

$$i, j = 1, 2, \dots, N, \quad (6.4-24)$$

where  $\tilde{h}_{mn}(\tau, \phi)$  is defined by Equation (6.2-29) and

$$\chi_{\tilde{p}_m \tilde{p}_n}^{[2\varepsilon(\tau), \phi - \phi']} = \int_{-\infty}^{\infty} \tilde{p}_m[t - \varepsilon(\tau)] \tilde{p}_n^*[t + \varepsilon(\tau)] \cdot$$

$$\exp(+j2\pi[\phi - \phi']t) dt, \quad (6.4-25)$$

where  $\varepsilon(\tau)$  is defined by Equation (6.2-27). Since

$$\tilde{t}_{ij} = [\underline{C}_T(\underline{\tilde{u}})]_{ij} \quad (6.4-26)$$

and

$$\tilde{r}_{ij} = [\underline{C}_R(\underline{\tilde{u}})]_{ij}, \quad (6.4-27)$$

Equation (6.4-24) can be used to write

$$\tilde{t}_{ij} = \sum_{\ell=0}^{N-1} \sum_{m=0}^{N-1} \tilde{u}_{\ell} \tilde{u}_m^* \tilde{T}_{i,j,\ell,m}; \quad (6.4-28)$$

$$i, j = 1, 2, \dots, N$$



and

$$\tilde{r}_{ij} = \sum_{\ell=0}^{N-1} \sum_{m=0}^{N-1} \tilde{u}_{\ell} \tilde{u}_m^* \tilde{R}_{i,j,\ell,m} ; i, j = 1, 2, \dots, N , \quad (6.4-29)$$

where

$$\tilde{T}_{i,j,\ell,m} \triangleq \int_{-\infty}^{\infty} \int \sigma(\tau, \phi) \tilde{h}_{(i-1)\ell} \tilde{h}_{(j-1)m}^* d\tau d\phi \quad (6.4-30)$$

and

$$\tilde{R}_{i,j,\ell,m} \triangleq \int_{-\infty}^{\infty} \int \sigma(\tau, \phi) \tilde{h}_{(i-1)\ell} \tilde{h}_{(j-1)m}^* d\tau d\phi \quad (6.4-31)$$

The expressions  $\tilde{T}_{i,j,\ell,m}$  and  $\tilde{R}_{i,j,\ell,m}$  are known, complex constants since the subpulses  $\tilde{p}_n(\cdot)$  ;  $n = 0, 1, \dots, N-1$  are given.

Next, represent the complex elements of the transmit weighting vector as:

$$\tilde{u}_i = \mu_i + j\eta_i ; i = 0, 1, \dots, N-1 , \quad (6.4-32)$$

where both  $\mu_i$  and  $\eta_i$  are real, unknown constants. Upon substituting Equation (6.4-32) into Equations (6.4-28) and (6.4-29), one obtains:

$$\begin{aligned} \tilde{r}_{ij} = & \sum_{\ell=0}^{N-1} \sum_{m=0}^{N-1} \{ (\mu_{\ell}\mu_m + \eta_{\ell}\eta_m) \operatorname{Re}(\tilde{T}_{i,j,\ell,m}) - \\ & (\mu_m\eta_{\ell} - \mu_{\ell}\eta_m) \operatorname{Im}(\tilde{T}_{i,j,\ell,m}) + \\ & j[(\mu_{\ell}\mu_m + \eta_{\ell}\eta_m) \operatorname{Im}(\tilde{T}_{i,j,\ell,m}) + \end{aligned}$$

$$(\mu_m \eta_\ell - \mu_\ell \eta_m) \operatorname{Re}(\tilde{T}_{i,j,\ell,m}) \}}; \quad (6.4-33)$$

$$i, j = 1, 2, \dots, N$$

and

$$\begin{aligned} \tilde{r}_{ij} = & \sum_{\ell=0}^{N-1} \sum_{m=0}^{N-1} \{ (\mu_\ell \mu_m + \eta_\ell \eta_m) \operatorname{Re}(\tilde{R}_{i,j,\ell,m}) - \\ & (\mu_m \eta_\ell - \mu_\ell \eta_m) \operatorname{Im}(\tilde{R}_{i,j,\ell,m}) + \\ & j [ (\mu_\ell \mu_m + \eta_\ell \eta_m) \operatorname{Im}(\tilde{R}_{i,j,\ell,m}) + \\ & (\mu_m \eta_\ell - \mu_\ell \eta_m) \operatorname{Re}(\tilde{R}_{i,j,\ell,m}) ] \}; \quad (6.4-34) \end{aligned}$$

$$i, j = 1, 2, \dots, N$$

Equations (6.4-33) and (6.4-34) express the complex unknown elements of the target and reverberation matrices, respectively, in terms of the real unknowns  $\mu_i$  and  $\eta_i$ . Note that the  $j$  term multiplying the square brackets in both Equations (6.4-33) and (6.4-34) is equal to  $\sqrt{-1}$ , and hence, is not an index. All the information required to formulate the joint optimization nonlinear programming problem in terms of real unknowns is now available.

The nonlinear programming problem can be stated as follows:

minimize the nonlinear objective function given by Equation (6.4-19)

with respect to the real unknowns  $\mu_i$ ,  $\eta_i$ ,  $a_i$ , and  $b_i$ ;

$i = 0, 1, \dots, N-1$ , where  $\alpha_{ij} = \operatorname{Re}(\tilde{r}_{ij})$  and  $\beta_{ij} = \operatorname{Im}(\tilde{r}_{ij})$  can be obtained from Equation (6.4-33). The minimization is subject to

the following nonlinear constraints: (1) Equation (6.4-17), where  $x_{ij} = \text{Re}(\tilde{r}_{ij})$  and  $y_{ij} = \text{Im}(\tilde{r}_{ij})$  can be obtained from Equation (6.4-34); (2) the dynamic range constraint

$$A_{\text{MIN}} \leq |\tilde{u}_i| \leq A_{\text{MAX}} ; i = 0, 1, \dots, N-1 \quad (6.4-2)$$

or equivalently,

$$A_{\text{MIN}} \leq (\mu_i^2 + \eta_i^2)^{1/2} \leq A_{\text{MAX}} ; i = 0, 1, \dots, N-1, \quad (6.4-35)$$

and (3) the unit-energy constraint

$$a_0^2 + a_1^2 + \dots + a_{N-1}^2 + b_0^2 + b_1^2 + \dots + b_{N-1}^2 = 1 \quad (6.4-10)$$

Once the optimum vectors  $\underline{a}_{\text{OPT}}$ ,  $\underline{b}_{\text{OPT}}$ ,  $\underline{\mu}_{\text{OPT}}$ , and  $\underline{\eta}_{\text{OPT}}$  are found, the corresponding optimum transmit and processing complex weighting vectors can be computed from:

$$\underline{\tilde{u}}_{\text{OPT}} = \underline{\mu}_{\text{OPT}} + j\underline{\eta}_{\text{OPT}} \quad (6.4-36)$$

and

$$\underline{\tilde{w}}_{\text{OPT}} = \underline{a}_{\text{OPT}} + j\underline{b}_{\text{OPT}} \quad (6.4-37)$$

The optimization problem to be considered in Section 6.4.3 is totally different from those discussed in Sections 6.4.1 and 6.4.2. In Section 6.4.3, the transmit and processing weighting vectors are assumed to be equal and given. The maximization of the SIR will be with respect to the parameters of the subpulses.

6.4.3 Maximization of the SIR for a doubly spread target with respect to the subpulse parameters. Consider the "matched filter" version of Equation (6.2-34). That is, if one lets  $\tilde{w} = \tilde{u}$ , Equation (6.2-34) becomes:

$$\frac{\rho}{\rho_0} = \frac{\tilde{u}^+ \underline{C}_T(\tilde{u}) \tilde{u}}{\tilde{u}^+ [\underline{I} + \rho_0 \lambda \underline{C}_R(\tilde{u})] \tilde{u}}, \quad (6.4-38)$$

where it is assumed that  $\tilde{u}$  is given. In this section, the waveform  $\tilde{u}(t)$  is once again the normalized version of  $\tilde{x}(t)$ . Hence,  $|\tilde{u}|^2 = 1$  and  $\rho_0$  is given by Equation (6.2-12). The optimization problem is to maximize Equation (6.4-38). More specifically, minimize the nonlinear objective function

$$- \tilde{u}^+ \underline{C}_T(\tilde{u}) \tilde{u} \quad (6.4-39)$$

with respect to the subpulse parameters, subject to the nonlinear constraint

$$\tilde{u}^+ \underline{C}_R(\tilde{u}) \tilde{u} \leq K \leq 0 \quad (6.4-40)$$

and suitable constraints on the subpulse parameters. Note that although  $\tilde{u}$  is given, the target and reverberation matrices are unknown, constant matrices. They are both functions of the subpulse parameters for this optimization problem. The complex scalars  $\tilde{h}_{mn}$ ;  $m, n = 0, 1, \dots, N-1$  are not only functions of  $\tau$  and  $\phi$  but they are also functions of the parameters of the subpulses  $\tilde{p}_m(\cdot)$  and  $\tilde{p}_n(\cdot)$  via the cross-ambiguity function  $\chi(\cdot, \cdot)$ .

$\tilde{p}_m \tilde{p}_n$

Let the  $n^{\text{th}}$  subpulse  $\tilde{p}_n(t)$  be given by the general expression

$$\tilde{p}_n(t) = \frac{1}{\sqrt{T}} \exp[+j\Psi_n(t)] ; 0 \leq t \leq T < T_p, \quad (6.4-41)$$

where  $\Psi_n(t)$  is the instantaneous phase function. Note that  $\tilde{p}_n(t)$  satisfies the orthonormality condition given by Equation (6.2-23).

Upon substituting Equation (6.4-41) into Equation (6.4-25), and then substituting this result back into Equation (6.2-29), one obtains:

$$c_{mn} = \text{Re}\{\tilde{h}_{mn}\} = \frac{1}{T} \int_{-\infty}^{\infty} \cos\{\Psi_m[t - \varepsilon(\tau)] - \Psi_n[t + \varepsilon(\tau)] + \pi(\phi - \phi')[2t + (m+n)T_p]\} dt \quad (6.4-42)$$

and

$$d_{mn} = \text{Im}\{\tilde{h}_{mn}\} = \frac{1}{T} \int_{-\infty}^{\infty} \sin\{\Psi_m[t - \varepsilon(\tau)] - \Psi_n[t + \varepsilon(\tau)] + \pi(\phi - \phi')[2t + (m+n)T_p]\} dt, \quad (6.4-43)$$

where

$$\tilde{h}_{mn} = c_{mn} + jd_{mn} ; m, n = 0, 1, \dots, N-1. \quad (6.4-44)$$

Using Equation (6.4-44), the expression  $\tilde{h}_{(i-1)\ell} \tilde{h}_{(j-1)m}^*$  appearing in both Equations (6.4-30) and (6.4-31) can be rewritten as:

$$\begin{aligned} \tilde{h}_{(i-1)\ell} \tilde{h}_{(j-1)m}^* &= c_{(i-1)\ell} c_{(j-1)m} + d_{(i-1)\ell} d_{(j-1)m} + \\ &\quad j[c_{(j-1)m} d_{(i-1)\ell} - c_{(i-1)\ell} d_{(j-1)m}] \end{aligned} \quad (6.4-45)$$

Note that the  $j$  term multiplying the square brackets in Equation (6.4-45) is equal to  $\sqrt{-1}$ , and hence, is not an index. Keep in mind that since  $\tilde{h}_{mn}$  is a function of  $\tau$ ,  $\phi$ , and the subpulse parameters, then both  $c_{mn}$  and  $d_{mn}$  are also functions of these same variables. For example, if  $\Psi_n(t)$  is of the form

$$\Psi_n(t) = b_n t^2 + 2\pi f_n t ; \quad n = 0, 1, \dots, N-1, \quad (6.4-46)$$

then, from Equations (6.4-42) and (6.4-43), one can see that:

$$c_{mn} \equiv c_{mn}(\tau, \phi, b_m, f_m, b_n, f_n) \quad (6.4-47)$$

and

$$d_{mn} \equiv d_{mn}(\tau, \phi, b_m, f_m, b_n, f_n) . \quad (6.4-48)$$

Since it was assumed that  $\tilde{w} = \tilde{u}$ , where  $\tilde{u}$  is given, then from Equation (6.4-16), one can write

$$\tilde{w}_i = \tilde{u}_i = a_i + jb_i ; \quad i = 0, 1, \dots, N-1 , \quad (6.4-49)$$

where the  $a_i$ 's and  $b_i$ 's are real, known constants. Also, since  $\tilde{u}^\dagger \underline{C}_T(\tilde{u})\tilde{u} = \tilde{w}^\dagger \underline{C}_T(\tilde{u})\tilde{w}$  and  $\tilde{u}^\dagger \underline{C}_R(\tilde{u})\tilde{u} = \tilde{w}^\dagger \underline{C}_R(\tilde{u})\tilde{w}$ , then Equations (6.4-39) and (6.4-40) can be replaced by Equations (6.4-19) and (6.4-17), respectively.

Assume for simplicity that the transmit weighting vector is real, i.e., only uniform amplitude weighting is done. Therefore, under these assumptions and since  $|\tilde{u}|^2 = 1$ ,

$$a_i = \frac{1}{\sqrt{N}} ; i = 0, 1, \dots, N-1$$

and

(6.4-50)

$$b_i = 0 ; i = 0, 1, \dots, N-1$$

Upon substituting Equation (6.4-50) into Equations (6.4-19) and (6.4-17), Equations (6.4-39) and (6.4-40) can be expressed as:

$$-\tilde{u}^{\dagger} \underline{C}_T (\tilde{u}) \tilde{u} \equiv -\frac{1}{N} \sum_{k=1}^N \alpha_{kk} - \frac{2}{N} \sum_{\ell=2}^N \sum_{m=0}^{N-2} \alpha_{(\ell-1)(m+2)} \quad -\infty < \ell-m \leq +2 \quad (6.4-51)$$

and

$$\tilde{u}^{\dagger} \underline{C}_R (\tilde{u}) \tilde{u} \equiv \frac{1}{N} \sum_{k=1}^N x_{kk} + \frac{2}{N} \sum_{\ell=2}^N \sum_{m=0}^{N-2} x_{(\ell-1)(m+2)} \leq K \leq 0 \quad -\infty < \ell-m \leq +2 \quad (6.4-52)$$

respectively, where

$$\alpha_{ij} = \operatorname{Re}\{\tilde{t}_{ij}\} \quad (6.4-53)$$

or

$$\alpha_{ij} = \frac{1}{N} \sum_{\ell=0}^{N-1} \sum_{m=0}^{N-1} \int_{-\infty}^{\infty} \int \sigma(\tau, \phi) \left[ c_{(i-1)\ell} c_{(j-1)m} \right]_{\text{TRGT}} +$$

$$d_{(i-1)\ell} d_{(j-1)m} \big] d\tau d\phi ; i, j = 1, 2, \dots, N \quad (6.4-54)$$

and

$$x_{ij} = \operatorname{Re}\{\tilde{r}_{ij}\} \quad (6.4-55)$$

or

$$x_{ij} = \frac{1}{N} \sum_{\ell=0}^{N-1} \sum_{m=0}^{N-1} \int_{-\infty}^{\infty} \sigma_{\text{REV}}(\tau, \phi) [c_{(i-1)\ell} c_{(j-1)m} + d_{(i-1)\ell} d_{(j-1)m}] d\tau d\phi ; \quad i, j = 1, 2, \dots, N \quad .$$

(6.4-56)

As a result of the above analysis, our problem in nonlinear programming can be stated as follows: minimize the nonlinear objective function given by Equation (6.4-51) with respect to the parameters of the  $N$  subpulses, where  $\alpha_{ij}$  is given by Equation (6.4-54) and  $c_{ij}$  and  $d_{ij}$  are given by Equations (6.4-42) and (6.4-43), respectively. For example, if the instantaneous phase function of the  $n^{\text{th}}$  subpulse is given by Equation (6.4-46), one may choose to minimize with respect to either the frequency deviation parameters

$$f_n ; \quad n = 0, 1, \dots, N - 1$$

or the frequency sweep parameters

$$b_n ; \quad n = 0, 1, \dots, N - 1$$

or both. The minimization is to be performed subject to both the nonlinear constraint given by Equation (6.4-52), where  $x_{ij}$  is given by Equation (6.4-56), and suitably defined constraints on the subpulse parameters. For example,

$$-f_{\text{MAX}} \leq f_n \leq f_{\text{MAX}} ; \quad n = 0, 1, \dots, N - 1$$

and

$$-b_{\text{MAX}} \leq b_n \leq b_{\text{MAX}} ; \quad n = 0, 1, \dots, N - 1 .$$

(6.4-57)



Of the three optimization problems discussed concerning the doubly spread target, maximization with respect to the subpulse parameters is the most significant one. By closely inspecting Equations (6.4-51) through (6.4-57) and Equations (6.4-42) and (6.4-43), one can easily see that this rather general formulation is a very complex numerical problem. Let us investigate next the extent to which this important problem can be simplified, specifically the expressions for  $\alpha_{ij}$  and  $x_{ij}$  as given by Equations (6.4-54) and (6.4-56), respectively.

If the relatively simple target scattering function derived in Chapter IV [see Equations (4.3-8) through (4.3-12)] is normalized according to Equation (6.2-7) and then substituted into Equation (6.4-54), one obtains:

$$\alpha_{ij} = \left\{ \frac{1}{N\sigma_{\text{TRGT}}} \right\} \sum_{l=0}^{N-1} \sum_{m=0}^{N-1} \sum_{n=1}^{NH} \left\{ \left[ \left( 2 - [\phi_{\text{DET}_n} / f_c] \right) / (c\tau_n) \right]^2 \cdot \right. \\ \left. \exp \left\{ -4\alpha(f_c) \left[ (c\tau_n) / \left( 2 - [\phi_{\text{DET}_n} / f_c] \right) \right] \right\} \right\} \cdot \\ E\{|F_n(f_c)|^2\}(\sin\theta_n) \cdot \\ \left\{ \begin{array}{l} c[\tau_n, -\phi_{\text{DET}_n}, \dots]_{(i-1)l} c[\tau_n, -\phi_{\text{DET}_n}, \dots]_{(j-1)m} + \\ d[\tau_n, -\phi_{\text{DET}_n}, \dots]_{(i-1)l} d[\tau_n, -\phi_{\text{DET}_n}, \dots]_{(j-1)m} \end{array} \right\} ; \\ i, j = 1, 2, \dots, N, \quad (6.4-58)$$

where

$$\sigma_{\text{TRGT}} = \sum_{n=1}^{NH} \left[ \left( 2 - [\phi_{\text{DET}_n} / f_c] \right) / (c\tau_n) \right]^2 \cdot \exp \left\{ -4\alpha(f_c) \left[ (c\tau_n) / \left( 2 - [\phi_{\text{DET}_n} / f_c] \right) \right] \right\} \cdot E\{|F_n(f_c)|^2\} \sin\theta_n \quad (6.4-59)$$

and  $NH$  is the number of discrete point highlights along the target. The double integral originally appearing in Equation (6.4-54) has now been replaced by a single summation due to the presence of the target scattering function's Dirac delta functions in  $\tau$  and  $\phi$ . Note that  $c_{ij}$  and  $d_{ij}$  are functions of  $\tau_n$  and  $-\phi_{\text{DET}_n}$  plus the parameters of the instantaneous phase function [see Equations (6.4-42) and (6.4-43), respectively]. Although Equation (6.4-58) is a simplified version of Equation (6.4-54), it is still not trivial. In order to evaluate  $\alpha_{ij}$  for just one pair of values for  $(i,j)$ , a double summation over all  $N$  subpulses must be performed followed by a summation over all  $NH$  highlights of the target. In addition, each  $c_{(i-1)l}$ ,  $c_{(j-1)m}$ ,  $d_{(i-1)l}$ , and  $d_{(j-1)m}$  is an integral with respect to time  $t$ .

The expression for  $x_{ij}$  as given by Equation (6.4-56) can also be simplified somewhat by judiciously specifying the normalized reverberation scattering function  $\sigma(\tau, \phi)$ . A common simplification is to assume that the scattering function  $R_{S, \text{REV}}(\tau, \phi)$  is a function of

$\phi$  only, i.e.,  $R_{S_{REV}}(\tau, \phi) = R_{S_{REV}}(\phi)$ . Van Trees<sup>12</sup> refers to  $R_{S_{REV}}(\phi)$  as the Doppler scattering function. However, even with this simplification, the integration with respect to  $\tau$  remains in Equation (6.4-56) since  $c_{(i-1)l}$ ,  $c_{(j-1)m}$ ,  $d_{(i-1)l}$ , and  $d_{(j-1)m}$  are functions of  $\tau$ . Thus,  $x_{ij}$  remains a very complicated expression. In order to evaluate  $x_{ij}$  for just one pair of values for  $(i, j)$ , a double summation of a double integration with respect to  $\tau$  and  $\phi$ , in addition to integrations with respect to time  $t$ , must be performed over all  $N$  subpulses.

Therefore, in conclusion, even with the above simplifications, the important problem of maximization with respect to subpulse parameters remains a difficult nonlinear programming problem.

## CHAPTER VII

### SUMMARY AND CONCLUSIONS

This dissertation was concerned with the problem of detecting a doubly spread target return in the presence of reverberation and noise via maximization of the signal-to-interference ratio (SIR) by signal design. Previous research efforts have been devoted mainly to either the slowly fluctuating point target or singly spread target problems. The basic philosophy that was adopted in this dissertation was to treat both the ocean medium and the target as linear, time-varying, random filters. Accordingly, this dissertation began with a discussion on the fundamentals of linear, time-varying, deterministic and random filters in Chapter II. This chapter presented some of the basic mathematical relationships, terminology, and concepts that are part of linear, time-varying filter theory.

The four system functions which are used to characterize linear, time-varying filters were discussed. These functions are (1) the time-varying impulse response, (2) the time-varying frequency response or transfer function, (3) the spreading function, and (4) the bi-frequency function. It was shown that these four system functions and their corresponding autocorrelation functions are related to one another via Fourier transformations. In addition to various input-output relationships, expressions for the output power spectrum for both deterministic and random systems were derived. These expressions demonstrated the frequency spreading property of linear, time-varying filters. The

discussion on the important channel property of uncorrelated spreading introduced the concepts of the wide-sense stationary uncorrelated spreading (WSSUS) channel and the scattering function along with its various Fourier transforms.

Chapter II concluded with a brief discussion of two different ways of characterizing a time-varying channel via its scattering function. The first method involved interpreting the scattering function as a joint density function since it is real, non-negative, and can be normalized to integrate to unity. Thus, first and second order moments of the round-trip time delay (range) and frequency spread can be computed. The second method was concerned with the finite extent of the scattering function in the range-frequency plane. As a result of this approach, the concepts of an underspread and an over-spread channel were defined. Criteria for avoiding spreading in range and/or frequency were formulated in terms of the duration and bandwidth of the transmit signal and the extent of the scattering function in the range-frequency plane. It was concluded that both range and frequency spreading could be avoided only for underspread channels. For over-spread channels, one can choose a transmit signal such that either range or frequency spreading is avoided, but not both.

Chapter III introduced the problem of detecting a doubly spread target return in the presence of reverberation and noise. This chapter began with a brief discussion of the complex envelope notation for bandpass signals since the binary hypothesis testing problem was formulated in terms of the complex envelopes of the target, reverberation, and noise signals. Two different relationships between the input and output complex envelopes of a linear, time-varying filter

were derived. The first relationship was shown to be approximate and was based upon a narrowband assumption. However, the second relationship was shown to be exact and is valid for broadband as well as narrowband bandpass signals. Both the target and reverberation returns were modelled as the outputs from linear, time-varying, random filters which were assumed to be WSSUS communication channels.

The particular receiver structure used was a correlator followed by a magnitude squared operation. The magnitude squared output from the correlator was tested against a threshold determined from a probability of false alarm constraint in a Neyman-Pearson test.

Having specified both the binary hypothesis testing problem and the receiver, the signal-to-interference ratio (SIR) for a doubly spread target was derived. It was shown to be dependent upon the target and reverberation scattering functions and the cross-ambiguity function of the transmit signal and processing waveform. It was also demonstrated that the more familiar SIR expression for a slowly fluctuating point target could be obtained from the general SIR expression for a doubly spread target.

The final discussion in Chapter III was devoted to the question of receiver optimality. Although the chosen receiver structure can be an optimum receiver for detecting a slowly fluctuating point target, it is sub-optimum for detecting a doubly spread target. However, it was concluded that the use of a sub-optimum receiver is not necessarily a hindrance since the SIR can still be maximized by proper design of both the transmit and processing waveforms. And in the important case of Gaussian statistics, maximizing the SIR is equivalent to maximizing the probability of detection for a given probability of false alarm

(i.e., the Neyman-Pearson criterion). In order to maximize the SIR for a doubly spread target via signal design, one must be able to specify both the target and reverberation scattering functions. In general, the reverberation return is a composite of volume, surface, and bottom reverberation returns. However, only volume and surface reverberation were considered.

Both a volume reverberation and a target scattering function were derived in Chapter IV. In the past, assumed functional forms for the reverberation (clutter) scattering function were used in order to calculate the SIR.

Volume reverberation was modelled as the scattered acoustic pressure field from randomly distributed discrete point scatterers in deterministic plus random translational motion. The point scatterers were distributed in space according to an arbitrary volume density function with dimensions of number of scatterers per unit volume.

The two-frequency correlation function representing the volume reverberation communication channel was derived for a bistatic transmit/receive planar array geometry. A single scattering approximation was used and frequency dependent attenuation of sound pressure amplitude due to absorption was included. The scattered fields from different regions within the scattering volume were assumed to be uncorrelated. It was noted that the coherence time and coherence bandwidth can be computed from the two-frequency correlation function. The reciprocals of the coherence time and the coherence bandwidth are equal to the spectrum broadening and time broadening, respectively, that a wave will undergo as it propagates through a random, time-varying medium. The

volume reverberation scattering function was obtained from the two-frequency correlation function via a two-dimensional Fourier transformation and was shown to include explicitly all the important system functions and physical parameters as opposed to having them lumped together and accounted for by a single random variable as has been done in the past. A probability density function of random Doppler shift due to the random motion of the scatterers was also derived. In addition, the average received energy from volume reverberation was computed from the volume reverberation scattering function. Using several simplifying assumptions, it was shown to reduce to the sonar equation for reverberation level.

The doubly spread target was modelled as a linear array of discrete highlights in deterministic translational motion. The target scattering function was obtained from the monostatic form of the volume reverberation scattering function by appropriately specifying the volume density function of the highlights.

Computer simulation results for both the volume reverberation and target scattering functions were presented as examples involving a monostatic transmit/receive array geometry. The volume reverberation scattering function predicted frequency spreading as a function of both beam tilt angle and random motion of the discrete point scatterers. As one might expect, frequency spread increased as both beam tilt angle and random motion increased. Also predicted was time spread and/or contraction as a function of Doppler shift. Similarly, the target scattering function predicted a spread in Doppler values and a time spread and/or contraction as a function of Doppler shift. Computer



plots of the probability density function of the random Doppler shift were also presented for a monostatic geometry as a function of the standard deviation of the random motion of the scatterers.

A surface reverberation scattering function was derived in Chapter V. The underwater acoustic propagation path between transmit and receive planar arrays via the surface of the ocean was treated as a linear, time-varying, random WSSUS communication channel. The random, time-varying, surface reverberation transfer function was derived for a general bistatic geometry using a generalized Kirchhoff approach. The generalized Kirchhoff approach included a Fresnel corrected Kirchhoff integral and the Rayleigh hypothesis that the scattered acoustic pressure field can be represented as a sum of plane waves travelling in many different directions. Also, no small slope approximation was made.

The following important observations were made in deriving the surface reverberation transfer function: (1) Generally speaking, the validity of the transfer function is restricted to that region of the ocean surface which corresponds to the intersection of the transmit and receive projected beamwidths, especially if the beam patterns have significant sidelobes. (2) The binomial expansion becomes a less reliable approximation as the grazing angle approaches zero degrees and/or the beamwidths of the directivity functions increase. For some combinations of grazing angle and beamwidth, the binomial expansion is invalid. (3) Assuming that the functional form of the projected transmit and receive beam patterns is Gaussian leads to a major source of error when comparing theoretical predictions with experimental results. As a

result, the transmit and receive directivity functions included in the derivation of the transfer function in Chapter V were kept as general, frequency dependent expressions. The necessary transformation equations which will project both directivity functions exactly were provided.

(4) And when the transfer function derived in Chapter V was compared with previously published expressions for the scattered acoustic pressure obtained from a classical Kirchhoff approach, it was shown to contain additional "correction" terms which increase its magnitude, especially for the backscatter and specular geometries. This is encouraging since results based upon a classical Kirchhoff approach have predicted values for the scattering coefficient that were smaller than experimental values.

Two second order functions were derived from the surface reverberation transfer function by assuming that the randomly rough, time-varying ocean surface was a zero mean, wide-sense stationary, Gaussian random process. These included the two-frequency correlation function and the surface reverberation scattering function. The second order functions were shown to be dependent upon the directional wave number spectrum of the ocean surface. The surface reverberation scattering function predicted both a spread in round-trip time delay and in frequency. Previously published expressions for the ocean surface reverberation scattering function were based upon a Fresnel corrected Kirchhoff integral and a small slope approximation. They pertained only to a specular geometry. In addition, these expressions did not include a receive directivity function and a Gaussian functional form for the projected transmit beam pattern was assumed. And furthermore, very specific models for the ocean surface were used rather than

the general form of the directional wave number spectrum. These specific models are nothing more than special cases of the general form of the directional wave number spectrum.

Having derived the various scattering functions, the last major topic then was the optimization problem of maximizing the SIR for a doubly spread target via signal design. This problem was considered in Chapter VI. Both the transmit and processing waveforms were restricted to be pulse trains. Each subpulse of the transmit pulse train was allowed to be arbitrary in shape and could occupy the entire interpulse spacing interval if desired. This represents a generalization of earlier approaches. The optimum processing waveform was approximated by a time and frequency shifted replica of the transmit pulse train. Each subpulse of both the transmit and processing pulse trains were allowed to be complex weighted. Restricting the transmit and processing waveforms to be complex weighted pulse trains allowed the integral expression of the SIR to be transformed into an equivalent vector-matrix form. And the fact that each subpulse of the transmit pulse train was arbitrary in shape made this approach analogous to the Rayleigh-Ritz technique. Thus, the original problem of finding the optimum time functions was transformed into a parameter optimization problem.

Although the slowly fluctuating point target problem was not of primary concern in Chapter VI, it is an important and interesting problem in its own right and was included for completeness since substantial research effort has been devoted to it in the past. Two different optimization problems concerning the maximization of the SIR

for a slowly fluctuating point target were discussed. The first problem was to find the optimum, unit-energy, complex processing weighting vector that would maximize the SIR when the complex transmit weighting vector and the parameters of the subpulses were given. The second problem was to find the optimum, transmit-processing, complex weighting vector pair that would maximize the SIR when the parameters of the subpulses were given. The maximization was subject to unit-energy constraints on both the transmit and processing waveforms.

Three different optimization problems concerning the maximization of the SIR for a doubly spread target were discussed. The first problem was to find the optimum complex processing weighting vector that would maximize the SIR when the complex transmit weighting vector and the parameters of the subpulses were given. The maximization was subject to a unit-energy constraint on the processing weighting vector and a constraint on the desired amount of reverberation to be removed by the processing weighting vector. The second problem was to find the optimum, transmit-processing, complex weighting vector pair that would maximize the SIR when the parameters of the subpulses were given. The maximization was subject to a dynamic range constraint on the transmit weighting vector, a unit-energy constraint on the processing weighting vector, and a constraint on the desired amount of reverberation to be removed by the processing weighting vector.

And finally, the third problem was to maximize the SIR for a doubly spread target with respect to the parameters of the subpulses. For this particular optimization problem, it was assumed that both the transmit and processing weighting vectors were equal and given, and

that the maximization was subject to a constraint on the desired amount of reverberation to be removed by the processing waveform and constraints on the subpulse parameters themselves.

Since all three optimization problems for the doubly spread target were originally defined on a complex space, the approach taken in Chapter VI was to formulate the optimization problems into equivalent nonlinear programming problems defined on a real space. As a result, one need not develop algorithms to solve these problems, but rather, one can simply use standard computer programs or methods which are available for solving nonlinear programming problems.<sup>67,72,73</sup>

Of the three optimization problems discussed concerning the maximization of the SIR for a doubly spread target, maximization with respect to the subpulse parameters is the most interesting and significant one. However, even with several simplifying assumptions, it was shown to be a difficult nonlinear programming problem.

Therefore, in conclusion, all the information required to solve the problem of detecting a doubly spread target return in the presence of reverberation and noise by maximizing the SIR via signal design has been furnished; namely, the receiver structure; target, volume reverberation, and surface reverberation scattering functions; and the formulation of the various SIR optimization problems into equivalent nonlinear programming problems defined on a real space.

## CHAPTER VIII

### RECOMMENDATIONS FOR FUTURE RESEARCH

Although the volume reverberation model that was used in this dissertation was based upon classical assumptions, the derivation of the volume reverberation scattering function was nonetheless tedious, instructive, and did demonstrate some basic phenomena. For example, the volume reverberation scattering function predicted frequency spreading as a function of both beam tilt angle and random motion of the discrete point scatterers. Also predicted was time spread and/or contraction as a function of Doppler shift. However, it is recommended that more realistic models of the ocean medium be studied. For example, an investigation as to whether or not a volume reverberation scattering function could be derived for an ocean medium with a variable sound speed profile would be interesting. In addition, one could include scattering from internal waves along with incorporating more sophisticated target models.

Since the two-frequency correlation function is one of the fundamental expressions required in order to study wave propagation in a random medium, it is recommended that experimental values for both the target and volume reverberation two-frequency correlation functions be collected. The experimental values and theoretical predictions for frequency and time spreading could then be compared. On the basis of these comparisons, the validity of various mathematical models could be established; for example, the discrete point scatterer model used for

volume reverberation and the extended target and the WSSUS assumption required for scattering function calculations.

It was demonstrated in this dissertation that an ocean surface reverberation scattering function could be derived by using a generalized Kirchhoff approach. Since the validity of the Kirchhoff approach is dependent upon a radius of curvature restriction (which is based upon a sinusoidal ocean surface model), it is recommended to investigate a surface reverberation scattering function derivation based upon alternate approaches; for example, stochastic operator techniques<sup>74-76</sup> or applicable perturbation methods.<sup>48</sup> While a perturbation method is not dependent upon a radius of curvature restriction, it is dependent upon a restriction on the slope of the surface.<sup>48</sup> A composite surface roughness model--high spatial frequency waves (capillary waves) superimposed upon low spatial frequency sinusoidal waves (gravity waves)--should also be investigated.

Since the treatment of surface reverberation was entirely analytical in this dissertation, much computer simulation work with the equations could be done. For example, it is recommended that computation of the surface reverberation scattering function be performed for both specular and backscatter geometries and compared with the results from previously published expressions. The scattering function calculations should incorporate the directional wave number spectrum. For example, one could use the Neumann-Pierson spectrum, the Pierson-Moskowitz spectrum, and other special cases. Shallow grazing angles could especially be investigated in the backscatter case.

Besides computer simulation work, an experimental program should be conducted to determine the quality of agreement between experimental

values and theoretical predictions of the surface reverberation two-frequency correlation function. Both experimental and theoretical values for frequency and time spreading could be computed and compared.

Of the three optimization problems discussed concerning the maximization of the SIR for a doubly spread target, maximization with respect to the subpulse parameters is the most interesting and significant one. For example, this particular problem formulation allows one to find optimum frequency hop codes.<sup>77-79</sup> Although maximization with respect to the subpulse parameters is a difficult nonlinear programming problem, it is recommended that future research efforts be devoted to investigating valid simplifications and efficient methods for its solution so that meaningful example problems can be solved.



## REFERENCES

1. Zadeh, L. A. Frequency Analysis of Variable Networks. Proc. IRE, 1950, 38, 291-299.
2. Zadeh, L. A., & Desoer, C. A. Linear System Theory. New York: McGraw-Hill, 1963.
3. Kailath, T. Channel Characterization: Time-Variant Dispersive Channels. In E. J. Baghdady (Ed.), Lectures on Communication System Theory. New York: McGraw-Hill, 1961.
4. Ellinthorpe, A. W., & Nuttall, A. H. Theoretical and Empirical Results on the Characterization of Undersea Acoustic Channels. IEEE First Annual Communication Convention. 1965.
5. Sostrand, K. A. Mathematics of the Time-Varying Channel. Proceedings of NATO Advanced Study Institute on Signal Processing with emphasis on underwater acoustics. (Vol. II). Enschede, The Netherlands: 1968.
6. Johnsen, J. Spectrum Analysis of Reverberations. In J. W. R. Griffiths, P. L. Stocklin, & C. Van Schooneveld (Eds.), Signal Processing. New York: Academic Press, 1973.
7. Laval, R. Sound Propagation Effects on Signal Processing. In J. W. R. Griffiths, P. L. Stocklin, & C. Van Schooneveld (Eds.), Signal Processing. New York: Academic Press, 1973.
8. Bello, P. A. Characterization of Randomly Time-Variant Linear Channels. IEEE Trans. Commun. Systems, 1963, 11, 360-393.
9. Papoulis, A. Signal Analysis. New York: McGraw-Hill, 1977.
10. Ishimaru, A. Wave Propagation and Scattering in Random Media (Vol. I). New York: Academic Press, 1978.
11. Kennedy, R. S. Fading Dispersive Communication Channels. New York: Wiley-Interscience, 1969.
12. Van Trees, H. L. Detection, Estimation and Modulation Theory (Part III). New York: John Wiley and Sons, 1971.
13. Zadeh, L. A. Correlation Functions and Power Spectra in Variable Networks. Proc. IRE, 1950, 38, 1342-1345.
14. McDonald, J. F., & Spindel, R. C. Implications of Fresnel Corrections in a Non-Gaussian Surface Scatter Channel. J. Acoust. Soc. Am., 1971, 50, 746-757.

15. Green, P. E., Jr. Radar Measurements of Target Scattering Properties. In J. V. Evans & T. Hagfors (Eds.), Radar Astronomy. New York: McGraw-Hill, 1968.
16. Whalen, A. D. Detection of Signals in Noise. New York: Academic Press, 1971.
17. Moose, P. H. Signal Processing in Reverberant Environments. In J. W. R. Griffiths, P. L. Stocklin, & C. Van Schooneveld (Eds.), Signal Processing. New York: Academic Press, 1973.
18. Laval, R. Time-Frequency-Space Generalized Coherence and Scattering Functions. In G. Tacconi (Ed.), Aspects of Signal Processing. (Part I). Dordrecht, Holland: D. Reidel Publishing Company, 1977.
19. DeLong, D. F., Jr., & Hofstetter, E. M. On the Design of Optimum Radar Waveforms for Clutter Rejection. IEEE Trans. Inform. Theory, 1967, 13, 454-463.
20. Spafford, L. J. Optimum Radar Signal Processing in Clutter. IEEE Trans. Inform. Theory, 1968, 14, 734-743.
21. Price, R. Detectors for Radar Astronomy. In J. V. Evans & T. Hagfors (Eds.), Radar Astronomy. New York: McGraw-Hill, 1968.
22. Faure, P. Theoretical Model of Reverberation Noise. J. Acoust. Soc. Am., 1964, 36, 259-266.
23. Morse, P. M., & Ingard, K. U. Theoretical Acoustics. New York: McGraw-Hill, 1968.
24. Steinberg, B. D. Principles of Aperture and Array System Design. New York: Wiley-Interscience, 1976.
25. Papoulis, A. Systems and Transforms with Applications in Optics. New York: McGraw-Hill, 1968.
26. Goodman, J. W. Introduction to Fourier Optics. New York: McGraw-Hill, 1968.
27. Gassner, R. L., & Cooper, G. R. Note on a Generalized Ambiguity Function. IEEE Trans. Inform. Theory, 1967, 13, 126.
28. Purdy, R. J., & Cooper, G. R. A Note on the Volume of Generalized Ambiguity Functions. IEEE Trans. Inform. Theory, 1968, 14, 153-154.

29. Kelley, E. J., & Wishner, R. P. Matched-Filter Theory for High-Velocity, Accelerating Targets. IEEE Trans. Military Electronics, 1965, 9, 56-69.
30. Ziemer, R. E., & Tranter, W. H. Principles of Communications. Boston: Houghton Mifflin Company, 1976.
31. Davenport, W. B., Jr. Probability and Random Processes. New York: McGraw-Hill, 1970.
32. Papoulis, A. Probability, Random Variables, and Stochastic Processes. New York: McGraw-Hill, 1965.
33. Urlick, R. J. Principles of Underwater Sound. New York: McGraw-Hill, 1975 (2nd edition).
34. Clay, C. S., & Medwin, H. Acoustical Oceanography: Principles and Applications. New York: Wiley-Interscience, 1977.
35. Middleton, D. A Statistical Theory of Reverberation and Similar First-Order Scattered Fields. Part I: Waveforms and the General Process. IEEE Trans. Inform. Theory, 1967, 13, 372-392.
36. Ol'shevskii, V. V. Characteristics of Sea Reverberation. New York: Consultants Bureau, 1967.
37. Fortuin, L. The Sea Surface as a Random Filter for Underwater Sound Waves. J. Acoust. Soc. Am., 1972, 52, 302-315.
38. Eckart, C. The Scattering of Sound from the Sea Surface. J. Acoust. Soc. Am., 1953, 25, 566-570.
39. Gulin, E. P. Amplitude and Phase Fluctuations of a Sound Wave Reflected from a Sinusoidal Surface. Sov. Phys. Acoust., 1963, 8, 223-227.
40. Melton, D. R., & Horton, C. W., Sr. Importance of the Fresnel Correction in Scattering from a Rough Surface. I. Phase and Amplitude Fluctuations. J. Acoust. Soc. Am., 1970, 47, 290-298.
41. Horton, C. W., Sr., & Melton, D. R. Importance of the Fresnel Correction in Scattering from a Rough Surface. II. Scattering Coefficient. J. Acoust. Soc. Am., 1970, 47, 299-303.
42. Venetsanopoulos, A. N., & Tuteur, F. B. Stochastic Filter Modeling for the Sea-Surface Scattering Channel. J. Acoust. Soc. Am., 1971, 49, 1100-1107.

43. McDonald, J. F. Fresnel-Corrected Second-Order Interfrequency Correlations for a Surface-Scatter Channel. IEEE Trans. Commun., 1974, 22, 138-145.
44. McDonald, J. F., & Tuteur, F. B. Calculation of the Range-Doppler Plot for a Doubly Spread Surface-Scatter Channel at High Rayleigh Parameters. J. Acoust. Soc. Am., 1975, 57, 1025-1029.
45. Tuteur, F. B., McDonald, J. F., & Tung, H. Second-Order Statistical Moments of a Surface Scatter Channel with Multiple Wave Direction and Dispersion. IEEE Trans. Commun., 1976, 24, 820-831.
46. Beckmann, P., & Spizzichino, A. The Scattering of Electromagnetic Waves from Rough Surfaces. New York: The MacMillan Co., 1963.
47. Parkins, B. E. Scattering from the Time-Varying Surface of the Ocean. J. Acoust. Soc. Am., 1967, 42, 1262-1267.
48. Ishimaru, A. Wave Propagation and Scattering in Random Media (Vol. II). New York: Academic Press, 1978.
49. Tolstoy, I., & Clay, C. S. Ocean Acoustics. New York: McGraw-Hill, 1966.
50. Kinsman, B. Wind Waves, Their Generation and Propagation on the Ocean Surface. Englewood Cliffs, New Jersey: Prentice-Hall, 1965.
51. Hildebrand, F. B. Advanced Calculus for Applications. Englewood Cliffs, New Jersey: Prentice-Hall, 1962.
52. Klein, M. V. Optics. New York: John Wiley and Sons, 1970.
53. Tolstoy, I. Wave Propagation. New York: McGraw-Hill, 1973.
54. Butkov, E. Mathematical Physics. Reading, Massachusetts: Addison-Wesley, 1968.
55. Zornig, J. G., & McDonald, J. F. Experimental Measurement of the Second-Order Interfrequency Correlation Function of the Random Surface Scatter Channel. IEEE Trans. Commun., 1975, 23, 341-347.
56. Stutt, C. A., & Spafford, L. J. A Best Mismatched Filter Response for Radar Clutter Discrimination. IEEE Trans. Inform. Theory, 1968, 14, 280-287.

57. Rummler, W. D. Clutter Suppression by Complex Weighting of Coherent Pulse Trains. IEEE Trans. Aerospace Electron. Systems, 1966, 2, 689-699.
58. DeLong, D. F., Jr., & Hofstetter, E. M. The Design of Clutter-Resistant Radar Waveforms with Limited Dynamic Range. IEEE Trans. Inform. Theory, 1969, 15, 376-385.
59. Rummler, W. D. A Technique for Improving the Clutter Performance of Coherent Pulse Train Signals. IEEE Trans. Aerospace Electron. Systems, 1967, 3, 898-906.
60. Thompson, J. S., & Titlebaum, E. L. The Design of Optimal Radar Waveforms for Clutter Rejection Using the Maximum Principle. Supplement to IEEE Trans. Aerospace Electron. Systems, 1967, 3(6), 581-589.
61. Sibul, L. H., & Titlebaum, E. L. Signal Design for Detection of Targets in Clutter. Proc. IEEE, 1981, 69, 481-482.
62. Kooij, T. Optimum Signals in Noise and Reverberation. Proceedings of NATO Advanced Study Institute on Signal Processing with emphasis on underwater acoustics. (Vol. I). Enschede, the Netherlands: 1968.
63. Rosen, J. B. The Gradient Projection Method for Nonlinear Programming: Part I, Linear Constraints. J. Soc. Indust. Appl. Math., 1960, 8, 181-217.
64. Rosen, J. B. The Gradient Projection Method for Nonlinear Programming: Part II, Nonlinear Constraints. J. Soc. Indust. Appl. Math., 1961, 9, 514-532.
65. Cook, C. W., & Bernfeld, M. Radar Signals. New York: Academic Press, 1967.
66. Burley, D. M. Studies in Optimization. New York: Halsted Press, 1974.
67. Kuester, J. L., & Mize, J. H. Optimization Techniques with FORTRAN. New York: McGraw-Hill, 1973.
68. Ogata, K. State Space Analysis of Control Systems. Englewood Cliffs, New Jersey: Prentice-Hall, 1967.
69. Kirk, D. E. Optimal Control Theory. Englewood Cliffs, New Jersey: Prentice-Hall, 1970.

70. Wiberg, D. M. State Space and Linear Systems. New York: McGraw-Hill, 1971.
71. Luenberger, D. G. Optimization by Vector Space Methods. New York: John Wiley and Sons, 1969.
72. Avriel, M. Nonlinear Programming. Analysis and Methods. Englewood Cliffs, New Jersey: Prentice-Hall, 1976.
73. Bazaraa, M. S., & Shetty, C. M. Nonlinear Programming. Theory and Algorithms. New York: John Wiley and Sons, 1979.
74. Sibul, L. H. Application of Linear Stochastic Operator Theory (Doctoral dissertation, The Pennsylvania State University, 1968). Dissertation Abstracts International, 1969, 30, 1250. (University Microfilms No. 69-14, 569)
75. Adomian, G. Random Operator Equations in Mathematical Physics I. J. Math. Phys., 1970, 11, 1069-1084.
76. Middleton, D. Channel Characterization and Threshold Reception for Complex Underwater Acoustic Media. EASCON. Arlington, VA.: IEEE, 1980.
77. Titlebaum, E. L. Time-Frequency Hop Signals Part I: Coding Based Upon the Theory of Linear Congruences. IEEE Trans. Aerospace Electron. Systems, 1981, 17, 490-493.
78. Titlebaum, E. L., & Sibul, L. H. Time-Frequency Hop Signals Part II: Coding Based Upon Quadratic Congruences. IEEE Trans. Aerospace Electron. Systems, 1981, 17, 494-500.
79. Mersereau, R. M., & Seay, T. S. Multiple Access Frequency Hopping Patterns with Low Ambiguity. IEEE Trans. Aerospace Electron. Systems, 1981, 17, 571-578.

## APPENDIX A

### DERIVATION OF THE RETURN SIGNAL FROM A SLOWLY FLUCTUATING POINT TARGET

If one considers a slowly fluctuating point target to be in relative motion and in the far-field with respect to a bistatic transmit/receive array geometry, then it can be shown that the transfer function which corresponds to this physical situation is given by [see Equation (4.2-14) and Figure 7]:

$$H(f, t) = \frac{F(f)}{R_{o_T} R_{o_R}} \exp\{-jk[R_{o_T} + R_{o_R} + (\hat{n}_T - \hat{n}_R) \cdot \vec{V}t']\} , \quad (A1)$$

where

$$F(f) = D_T(ku_T, kv_T) g(\hat{n}_R, \hat{n}_T, f) D_R(ku_R, kv_R) , \quad (A2)$$

$$u_T = \sin\theta_T \cos\psi_T , \quad (A3)$$

$$v_T = \sin\theta_T \sin\psi_T , \quad (A4)$$

$$u_R = \sin\theta_R \cos\psi_R , \quad (A5)$$

$$v_R = \sin\theta_R \sin\psi_R , \quad (A6)$$

$$t' = \frac{t - \frac{R_{o_R}}{c}}{1 - \frac{\vec{V} \cdot \hat{n}_R}{c}} \quad (A7)$$

and  $k = \frac{2\pi f}{c}$  is the wave number, where  $c$  is the speed of sound in the ocean medium. The expressions  $D_T$  and  $D_R$  are the far-field directivity

patterns of the transmit and receive arrays, respectively. The function  $g(\hat{n}_R, \hat{n}_T, f)$  is the scattering amplitude function. It represents the random, far-field amplitude of the scattered wave in the direction  $\hat{n}_R$  when the point target is insonified by a unit amplitude plane wave propagating in the direction  $\hat{n}_T$ . Both  $\hat{n}_T$  and  $\hat{n}_R$  are unit vectors. The spherical angles  $(\theta_T, \psi_T)$  and  $(\theta_R, \psi_R)$  are measured with respect to the transmit and receive arrays, respectively. The velocity of the target  $\vec{V}$  is assumed to be constant, and  $R_{o_T}$  and  $R_{o_R}$  are the initial ranges of the target from the transmit and receive arrays, in the directions  $\hat{n}_T$  and  $(-\hat{n}_R)$ , respectively. The retarded time  $t'$  is given by Equation (A7).

Upon substituting Equations (A1) and (A7) into Equation (3.2-15), one obtains:

$$\begin{aligned} \tilde{y}(t) = & \frac{F(f_c)}{R_{o_T} R_{o_R}} \tilde{x} \left\{ s \left[ t - \frac{\tau(s)}{s} \right] \right\} \exp[-j2\pi f_c (1-s)t] \\ & \exp \left\{ -j2\pi f_c s \left[ \frac{\tau(s)}{s} \right] \right\} \end{aligned} \quad (A8)$$

which is the complex envelope of the return signal from a slowly fluctuating point target where it was assumed that  $|f_c| \gg |f|$  so that  $F(f + f_c) \approx F(f_c)$ . The time compression/stretch factor  $s$  is defined as:

$$s \triangleq \frac{1 - \frac{\hat{n}_T \cdot \vec{V}}{c}}{1 - \frac{\hat{n}_R \cdot \vec{V}}{c}} \quad ; \quad (A9)$$



the expression  $\tau(s)/s$  is defined as the round-trip time delay in seconds where

$$\tau(s) \triangleq \tau_o - (1-s) \frac{R_{oR}}{c} \quad (A10)$$

and

$$\tau_o \triangleq \frac{R_{oT} + R_{oR}}{c} ; \quad (A11)$$

and the Doppler shift factor  $(1-s)$  is defined as:

$$(1-s) \triangleq \frac{(\hat{n}_T - \hat{n}_R) \cdot \vec{V}}{c \left( 1 - \frac{\vec{V} \cdot \hat{n}_R}{c} \right)} \quad (A12)$$

or

$$(1-s) \approx \frac{(\hat{n}_T - \hat{n}_R) \cdot \vec{V}}{c} \quad (A13)$$

if one assumes that

$$\frac{|\vec{V}|}{c} \ll 1 \quad (A14)$$

Note that  $\tau(s)$  by itself is not the round-trip time delay.

For the more familiar monostatic or backscatter geometry,

$\hat{n}_R = -\hat{n}_T$ ,  $R_{oT} = R_{oR} = R_o$  and, therefore,

$$s = \frac{1 - \frac{\hat{n}_T \cdot \vec{V}}{c}}{1 + \frac{\hat{n}_T \cdot \vec{V}}{c}} \quad (A15)$$

and

$$\tau(s) = \tau_o \frac{(s+1)}{2} , \quad (A16)$$

where

$$\tau_o = \frac{2R_o}{c} \quad , \quad (A17)$$

and

$$(1 - s) = 2 \frac{\hat{n}_T \cdot \vec{V}}{c \left( 1 + \frac{\hat{n}_T \cdot \vec{V}}{c} \right)} \quad (A18)$$

or

$$(1 - s) \approx 2 \frac{\hat{n}_T \cdot \vec{V}}{c} \quad . \quad (A19)$$

When the velocity of the target  $\vec{V} = 0$ , note that both Equations (A9) and (A15) reduce to  $s = 1$  and, therefore, the round-trip time delays  $\left. \frac{\tau(s)}{s} \right|_{s=1}$ , for the bistatic and monostatic cases reduce to Equations (A11) and (A17), respectively, as would be expected. In addition, it is instructive to consider the backscatter case and assume that a point target is moving away from the observer. Therefore, the radial velocity  $\hat{n}_T \cdot \vec{V} > 0$  in Equation (A15) and, as a result,  $s < 1$ . With  $s < 1$ ,  $(1 - s) > 0$  and the complex exponential  $\exp\{-j2\pi f_c(1-s)t\}$  in Equation (A8) corresponds to a negative Doppler shift which is physically correct. The backscattered signal begins to appear at the output of the receiver at time [see Equations (A8) and (A16)]

$$\frac{\tau(s)}{s} = \frac{2R_o}{c} \left( \frac{1 + \frac{1}{s}}{2} \right) \quad (A20)$$

and with  $s < 1$ ,  $\frac{\tau(s)}{s} > 2R_o/c$  sec which is also physically correct. Similarly, if the point target is moving toward the observer, then  $\hat{n}_T \cdot \vec{V} < 0$ ,  $s > 1$ ,  $(1 - s) < 0$ ,  $\exp\{-j2\pi f_c(1-s)t\}$  corresponds to

a positive Doppler shift, and  $\frac{\tau(s)}{s} < 2R_0/c$  sec.

Equation (A8) represents the complex envelope of the return signal. If one calculates the pre-envelope or analytic signal<sup>16</sup> of  $y(t)$ ,  $Z_y(t)$ , one obtains:

$$Z_y(t) = \tilde{y}(t) \exp(+j2\pi f_c t) \quad (A21)$$

$$= \tilde{x} \left\{ s \left[ t - \frac{\tau(s)}{s} \right] \right\} \exp \left\{ +j2\pi f_c \left[ s \left[ t - \frac{\tau(s)}{s} \right] \right] \right\} \quad (A22)$$

$$= Z_x \left\{ s \left[ t - \frac{\tau(s)}{s} \right] \right\}, \quad (A23)$$

where the amplitude terms of Equation (A8) were dropped and  $Z_x(\cdot)$  is the analytic signal of  $x(t)$ .

With the exception of a multiplying amplitude factor, Equation (A22) is identical in form with the model of the return signal specified by Equation (1) in Gassner and Cooper.<sup>27</sup> Indeed, for the backscatter case,  $s$  and  $\tau(s)$  as given by Equations (A15) and (A16), respectively, are equal to the expressions  $\beta_0$  and  $\tau_0$ , respectively, as defined by Equations (3) and (4) in Gassner and Cooper.<sup>27</sup> The parameter  $\tau_0$  is referred to as being a suitably defined delay time<sup>28</sup> and is not referred to as being the round-trip time delay.<sup>27,28</sup>

Kelley and Wishner<sup>29</sup> model the backscattered echo corresponding to the transmission  $f(t)$  as:

$$f[x(t - s)] \quad (A24)$$

for a constant velocity target, where their "Doppler stretch factor"  $x$  is equal to our  $s$  as given by Equation (A15), and their  $s$  is defined

as round-trip time delay. More specifically, referring to Equation (5) of Kelley and Wishner<sup>29</sup>:

$$s = \frac{2}{c} r(t) \Big|_{t=\frac{s}{2}} = \frac{2}{c} r\left(\frac{s}{2}\right), \quad (\text{A25})$$

where  $t = s/2$  is the time at which a photon, having left the transmitter at  $t = 0$ , is reflected by the target, and  $r(s/2)$  is the target's range from the transmitter when the reflection occurred. Therefore,  $s$  is the round-trip time delay or, as Kelley and Wishner<sup>29</sup> state, "...the delay of a photon arriving at  $s$  is just  $s$ ." Thus, by comparing Equations (A23) and (A24), it can be seen that their round-trip time delay  $s$  is equivalent to our round-trip time delay  $\tau(s)/s$ , with the notable exception that our round-trip time delay [see Equation (A20)] is explicitly shown to be a function of the Doppler shift factor.

The round-trip time delay  $\tau(s)/s$  can also be expressed in another way. If one defines the Doppler shift  $\phi$  (in Hz) as:

$$\phi \triangleq - (1 - s)f_c, \quad (\text{A26})$$

then the time compression/stretch factor  $s$  is given by:

$$s = 1 + (\phi/f_c). \quad (\text{A27})$$

Therefore, with the use of Equation (A26), the general bistatic expression for  $\tau(s)$  as given by Equation (A10) can be written as:

$$\tau(s) \rightarrow \tau(\phi) \triangleq \tau_o + [(\phi R_{o_R})/(f_c c)], \quad (\text{A28})$$

where

$$\tau_o \triangleq (R_{o_T} + R_{o_R})/c \quad . \quad (A29)$$

Thus, from Equations (A27) and (A28), the round-trip time delay  $\tau(s)/s$  can also be expressed as  $\tau(\phi)/[1 + (\phi/f_c)]$  .

## APPENDIX B

### DERIVATION OF THE PROBABILITY DENSITY FUNCTION OF THE RANDOM DOPPLER SHIFT $\phi_{\text{RND}}$

Consider the random variable

$$\phi_{\text{RND}} \triangleq f_c (\hat{n}_T - \hat{n}_R) \cdot \vec{V}_f / c = f_c |\hat{n}_T - \hat{n}_R| |\vec{V}_f| \cos \xi / c, \quad (4.2-48)$$

where it is assumed that  $|\vec{V}_f|$  is Maxwell distributed, the angle  $\xi$  is uniformly distributed, and that the random variables  $|\vec{V}_f|$  and  $\cos \xi$  are statistically independent. In order for  $|\vec{V}_f| = (v_{fx}^2 + v_{fy}^2 + v_{fz}^2)^{1/2}$  to be Maxwell distributed, the three components  $v_{fx}$ ,  $v_{fy}$ , and  $v_{fz}$  must be statistically independent Gaussian random variables, each with zero mean and variance  $\sigma^2$  (e.g., see Papoulis<sup>32</sup>).

In order to derive the probability density function of  $\phi_{\text{RND}}$ , first rewrite Equation (4.2-48) as:

$$\phi_{\text{RND}} = XY, \quad (B1)$$

where

$$X = a |\vec{V}_f|, \quad (B2)$$

$$Y = \cos \xi \quad (B3)$$

and

$$a = f_c |\hat{n}_T - \hat{n}_R| / c. \quad (B4)$$

Note that  $E\{\phi_{\text{RND}}\} = E\{X\}E\{Y\} = 0$  since  $E\{\cos \xi\} = 0$  when  $\xi$  is uniformly distributed.<sup>30</sup> Since  $X$  and  $Y$  are statistically

independent random variables, the probability density function of  $\phi_{\text{RND}}$  is given by:<sup>31,32</sup>

$$p_{\phi_{\text{RND}}}(\phi) = \int_{-\infty}^{\infty} \frac{1}{|x|} p_X(x) p_Y(\phi/x) dx, \quad (\text{B5})$$

where<sup>32</sup>

$$p_X(x) = \frac{1}{|a|} \frac{p_{\vec{v}_f}(x/a)}{|\vec{v}_f|}, \quad (\text{B6})$$

$$p_{\vec{v}_f}(x/a) = \begin{cases} (2/\pi)^{1/2} (1/\sigma^3) (x/a)^2 \exp[-(1/2)(x/[a\sigma])^2] ; & x \geq 0 \\ 0 ; & x < 0 \end{cases} \quad (\text{B7})$$

and<sup>30,32</sup>

$$p_Y(\phi/x) = \begin{cases} 1/[\pi(1 - (\phi/x)^2)^{1/2}] & ; |\phi/x| < 1 \\ 0 & ; |\phi/x| > 1 \end{cases} \quad (\text{B8})$$

Note that the probability that  $(\phi/x) = \pm 1$  is zero.<sup>32</sup> Substituting Equations (B6) through (B8) into Equation (B5) yields:

$$p_{\phi_{\text{RND}}}(\phi) = (c/[|\hat{n}_T - \hat{n}_R| f_c \sigma])^3 (\sqrt{2} / [\pi \sqrt{\pi}]) \cdot$$

$$\int_{-\infty}^{\infty} (1/|x|) (1/[1 - (\phi/x)^2]^{1/2}) x^2 \cdot$$

$$\exp\{-(1/2)(c/[|\hat{n}_T - \hat{n}_R| f_c \sigma])^2 x^2\} dx ;$$

$$x \geq 0, \quad |\phi/x| < 1 \quad (\text{B9})$$

or

$$p_{\phi_{\text{RND}}}(\phi) = (c/[|\hat{n}_T - \hat{n}_R| f_c \sigma])^3 (\sqrt{2} / [\pi \sqrt{\pi}]) \cdot$$

$$\int_{|\phi|}^{\infty} (x^2/[x^2 - \phi^2]^{1/2}) \cdot$$

$$\exp\{-(1/2)(c/[|\hat{n}_T - \hat{n}_R| f_c \sigma])^2 x^2\} dx ;$$

$$|\phi| < x < \infty \quad (\text{B10})$$

which is the probability density function of the random Doppler shift  $\phi_{\text{RND}}$  as given by Equation (4.2-48).



## APPENDIX C

### DERIVATION OF THE NORMAL PARTIAL DERIVATIVE OF THE TOTAL ACOUSTIC PRESSURE FIELD ON THE OCEAN SURFACE

The total acoustic pressure field on the ocean surface at  $\vec{r}(t'_1)$  is defined by Equation (5.2-18), i.e.,

$$p[\vec{r}(t'_1)] \triangleq p_I[\vec{r}(t'_1)] + p_S[\vec{r}(t'_1)] \quad , \quad (5.2-18)$$

so that

$$\frac{\partial}{\partial n} p[\vec{r}(t'_1)] = \frac{\partial}{\partial n} p_I[\vec{r}(t'_1)] + \frac{\partial}{\partial n} p_S[\vec{r}(t'_1)] \quad , \quad (C1)$$

where<sup>51</sup>

$$\frac{\partial}{\partial n} p_I[\vec{r}(t'_1)] = \hat{n} \cdot \nabla p_I[\vec{r}(t'_1)] \quad (C2)$$

and

$$\frac{\partial}{\partial n} p_S[\vec{r}(t'_1)] = \hat{n} \cdot \nabla p_S[\vec{r}(t'_1)] \quad . \quad (C3)$$

Upon substituting Equation (5.2-28) into the right-hand side of Equation (C2) and then evaluating the gradient, one obtains:

$$\begin{aligned} \frac{\partial}{\partial n} p_I[\vec{r}(t'_1)] = & - (\hat{n} \cdot \hat{n}_T) j k_{EFF} p_I[\vec{r}(t'_1)] \cdot \\ & \left\{ 1 - j \left[ \frac{1}{k_{EFF} R_T(t'_1)} - \frac{\hat{n} \cdot \nabla D_T[k, \vec{r}(t'_1)]}{(\hat{n} \cdot \hat{n}_T) k_{EFF} D_T[k, \vec{r}(t'_1)]} \right] \right\} \quad (C4) \end{aligned}$$

since (e.g., see References 26, 46, or 52):

$$\nabla \left\{ \frac{\exp[-jk_{\text{EFF}} R_T(t'_1)]}{R_T(t'_1)} \right\} = \frac{\partial}{\partial R_T(t'_1)} \left\{ \frac{\exp[-jk_{\text{EFF}} R_T(t'_1)]}{R_T(t'_1)} \right\} \hat{n}_T. \quad (\text{C5})$$

Now if one assumes that

$$|k_{\text{EFF}} R_T(t'_1)| \gg 1 \quad (\text{C6})$$

and that

$$\frac{|\hat{n} \cdot \nabla D_T[k, \vec{r}(t'_1)]|}{|(\hat{n} \cdot \hat{n}_T) k_{\text{EFF}} D_T[k, \vec{r}(t'_1)]|} \ll 1, \quad (\text{C7})$$

then Equation (C4) simplifies to:

$$\frac{\partial}{\partial n} p_I[\vec{r}(t'_1)] \approx -(\hat{n} \cdot \hat{n}_T) j k_{\text{EFF}} p_I[\vec{r}(t'_1)]. \quad (\text{C8})$$

Equation (C3) will be evaluated next. Following the Kirchhoff approximation, the amplitude of the scattered acoustic pressure field on the ocean surface at  $\vec{r}(t'_1)$  is approximated by:

$$p_S[\vec{r}(t'_1)] \approx C_{\text{REF}} p_I[\vec{r}(t'_1)], \quad (\text{C9})$$

where the reflection coefficient  $C_{\text{REF}}$  is assumed to be a constant. The direction of  $p_S(\cdot)$  is specified by the unit vector  $\hat{n}_S$  (see Figure C1). Substituting Equation (C9) into Equation (C3) yields:

$$\frac{\partial}{\partial n} p_S[\vec{r}(t'_1)] \approx C_{\text{REF}} \hat{n} \cdot \nabla p_I[\vec{r}(t'_1)] \quad (\text{C10})$$

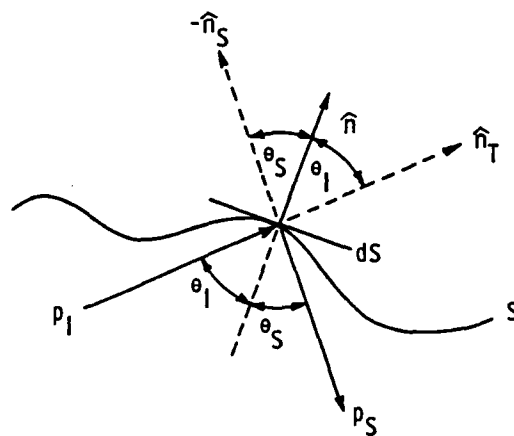


Figure C1. Scatter geometry for locally plane surface area element  $dS$ .

or, from Equation (C2),

$$\frac{\partial}{\partial n} p_S[\vec{r}(t'_1)] \approx c_{REF} \frac{\partial}{\partial n} p_I[\vec{r}(t'_1)] , \quad (C11)$$

where

$$\nabla \left\{ \frac{\exp[-jk_{EFF} R_T(t'_1)]}{R_T(t'_1)} \right\} = \frac{\partial}{\partial R_T(t'_1)} \left\{ \frac{\exp[-jk_{EFF} R_T(t'_1)]}{R_T(t'_1)} \right\} \hat{n}_S. \quad (C12)$$

Note that the unit vector appearing in Equation (C12) is  $\hat{n}_S$  and not  $\hat{n}_T$ . Therefore, by replacing  $\hat{n}_T$  in Equation (C8) with  $\hat{n}_S$ , Equation (C11) becomes:

$$\frac{\partial}{\partial n} p_S[\vec{r}(t'_1)] \approx - (\hat{n} \cdot \hat{n}_S) c_{REF} jk_{EFF} p_I[\vec{r}(t'_1)] . \quad (C13)$$

Consistent with the Kirchhoff approximation, the infinitesimal surface area element  $dS$  associated with the position vector  $\vec{r}(t'_1)$  is assumed to be locally plane as is illustrated in Figure C1. Since for a plane wave incident upon a plane boundary, the angles  $\theta_I$  and  $\theta_S$  are equal, then from Figure C1, it can be seen that:

$$\hat{n} \cdot \hat{n}_T = \cos\theta_I = \hat{n} \cdot (-\hat{n}_S) = \cos\theta_S . \quad (C14)$$

With the use of Equation (C14), Equation (C13) can be rewritten as:

$$\frac{\partial}{\partial n} p_S[\vec{r}(t'_1)] \approx + (\hat{n} \cdot \hat{n}_T) c_{REF} jk_{EFF} p_I[\vec{r}(t'_1)] , \quad (C15)$$

and upon substituting Equations (C8) and (C15) into Equation (C1), one obtains the desired result:

$$\frac{\partial}{\partial n} p[\vec{r}(t_1')] \approx - (\hat{n} \cdot \hat{n}_T) [1 - C_{REF}] j k_{EFF} p_I[\vec{r}(t_1')] , \quad (C16)$$

which is the normal partial derivative of the total acoustic pressure field on the ocean surface at  $\vec{r}(t_1')$  .

## APPENDIX D

### FUNCTIONAL DEPENDENCE OF THE TRANSMIT AND RECEIVE

#### DIRECTIVITY FUNCTIONS AND VECTORS $\vec{a}(x,y)$

#### AND $\vec{b}(x,y)$ ON THE $(x,y)$ COORDINATES

In order to obtain the functional dependence of the  $(a_x, a_y, a_z)$  and  $(b_x, b_y, b_z)$  terms on the  $(x,y)$  coordinates, one must first obtain expressions for  $\hat{n}_T(x,y)$  and  $\hat{n}_R(x,y)$ . Refer back to Figure 17 and note that:

$$\hat{n}_T = u_T \hat{x}_T + v_T \hat{y}_T + w_T \hat{z}_T, \quad (D1)$$

where

$$\begin{aligned} u_T &\triangleq \sin\theta_T \cos\psi_T, \\ v_T &\triangleq \sin\theta_T \sin\psi_T \end{aligned} \quad (D2)$$

and

$$w_T \triangleq \cos\theta_T$$

are the direction cosines of  $\hat{n}_T$  with respect to the  $X_T Y_T Z_T$  coordinate system. The spherical angles  $\theta_T$  and  $\psi_T$  are also measured with respect to the  $X_T Y_T Z_T$  coordinate system. Now let us assume that the  $Y_T$  and  $Y$  axes are parallel to one another so that  $\hat{y}_T = \hat{y}$ . If the  $X_T Y_T Z_T$  coordinate system is then rotated by an angle  $\beta_T$  in a clockwise direction with respect to the  $XYZ$  coordinate system, and recalling that  $\psi_1 = \pi$ , we obtain [see Figure D1 and, for example, Butkov<sup>54</sup>):

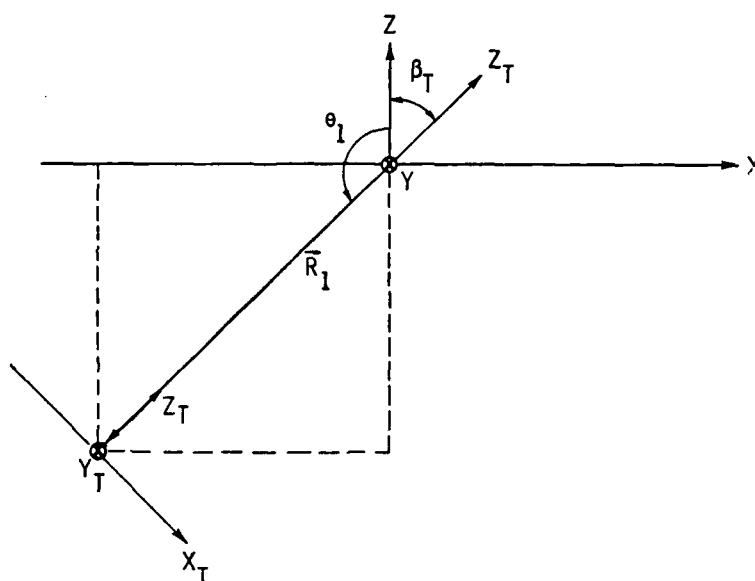


Figure D1. Orientation of the  $X_T Y_T Z_T$  coordinate system with respect to the  $XYZ$  reference coordinate system.

AD-A105 593

PENNSYLVANIA STATE UNIV UNIVERSITY PARK APPLIED RESE--ETC F/6 20/1  
A SCATTERING FUNCTION APPROACH TO UNDERWATER ACOUSTIC DETECTION--ETC(U)  
OCT 81 L J ZIOMEK N00024-79-C-6043  
ARL/PSU/TM-81-144 NL

UNCLASSIFIED

4 - 4

4 - 4

4 - 4



END

DATE

FILED

81

DTIQ



$$\begin{aligned}\hat{n}_T(x,y) = & [u_T(x,y)\cos\beta_T + w_T(x,y)\sin\beta_T]\hat{x} + \\ & v_T(x,y)\hat{y} + [w_T(x,y)\cos\beta_T - u_T(x,y)\sin\beta_T]\hat{z} \quad ,\end{aligned}\quad (D3)$$

where

$$u_T(x,y) = \frac{[x + (\cos\theta_1 \tan\beta_T + \sin\theta_1)R_1]\cos\beta_T}{R_T(x,y)} \quad ,$$

$$v_T(x,y) = y/R_T(x,y) \quad (D4)$$

and

$$w_T(x,y) = \pm \sqrt{1 - u_T^2(x,y) - v_T^2(x,y)} \quad ,$$

and

$$R_T(x,y) = \sqrt{x^2 + y^2 + 2R_1 x \sin\theta_1 + R_1^2} \quad . \quad (D5)$$

Although Figure D1 shows  $\vec{R}_1$  and the  $Z_T$  axis to be colinear, this may not be true in general. For example, if the transmit beam pattern were to be tilted in the  $X_T Z_T$  plane,  $\vec{R}_1$  and the  $Z_T$  axis would no longer be colinear. However,  $\vec{R}_1$  is always chosen to be colinear with the axis of the main lobe of the transmit beam pattern. Whether the transmit beam pattern is tilted or untilted in the  $X_T Z_T$  plane, the rotation angle  $\beta_T$  is still defined as the angle between the  $Z$  and  $Z_T$  axes as shown in Figure D1.

Equation (D4) can also be used to project the far-field transmit directivity function  $D_T(k_{x_T}, k_{y_T})$  onto the  $XY$  plane. It has already been stated in Chapter IV that  $D_T(k_{x_T}, k_{y_T})$  is given by the two-dimensional Fourier transform of the spatial distribution of normal driving velocity, say  $q_T(x_T, y_T)$ ; i.e.,

$$D_T(k_{x_T}, k_{y_T}) = \iint_R q_T(x_T, y_T) \exp[+j(k_{x_T} x_T + k_{y_T} y_T)] dx_T dy_T \quad (D6)$$

when the baffle surrounding the active region  $R$  of the array is assumed to be rigid [see Equation (4.2-7)]. The  $x_T$  and  $y_T$  components of the wave number  $k$  are given by:

$$k_{x_T} = k u_T = k \sin \theta_T \cos \psi_T \quad (D7)$$

and

$$k_{y_T} = k v_T = k \sin \theta_T \sin \psi_T ,$$

where  $u_T$  and  $v_T$  are defined in Equation (D2) and  $k = (2\pi f)/c = (2\pi)/\lambda$ . Replacing  $u_T = \sin \theta_T \cos \psi_T$  and  $v_T = \sin \theta_T \sin \psi_T$  with  $u_T(x, y)$  and  $v_T(x, y)$  as given in Equation (D4), respectively, yields the desired transformation

$$D_T(k_{x_T}, k_{y_T}) \rightarrow D_T(k, x, y) . \quad (D8)$$

The next piece of information required is an expression for  $\hat{n}_R(x, y)$ . Instead of working with  $\hat{n}_R$  directly, let us work with  $\hat{n}'_R$  which is defined as:

$$\hat{n}'_R \triangleq -\hat{n}_R = u_R \hat{x}_R + v_R \hat{y}_R + w_R \hat{z}_R , \quad (D9)$$

where

$$u_R \triangleq \sin \theta_R \cos \psi_R ,$$

$$v_R \triangleq \sin \theta_R \sin \psi_R \quad (D10)$$

and

$$w_R \triangleq \cos \theta_R$$

are the direction cosines of  $\hat{n}'_R$  with respect to the  $X_R Y_R Z_R$  coordinate system. The spherical angles  $\theta_R$  and  $\psi_R$  are also measured with respect to the  $X_R Y_R Z_R$  coordinate system. From Figure D2, it can be seen that the  $XY$  plane and  $Y_R$  axis are parallel to one another with the  $Y_R$  axis rotated through an angle  $\alpha_R$  with respect to the  $Y$  axis, and the  $Z_R$  axis rotated through an angle  $\beta_R$  with respect to the  $Z$  axis. Therefore,

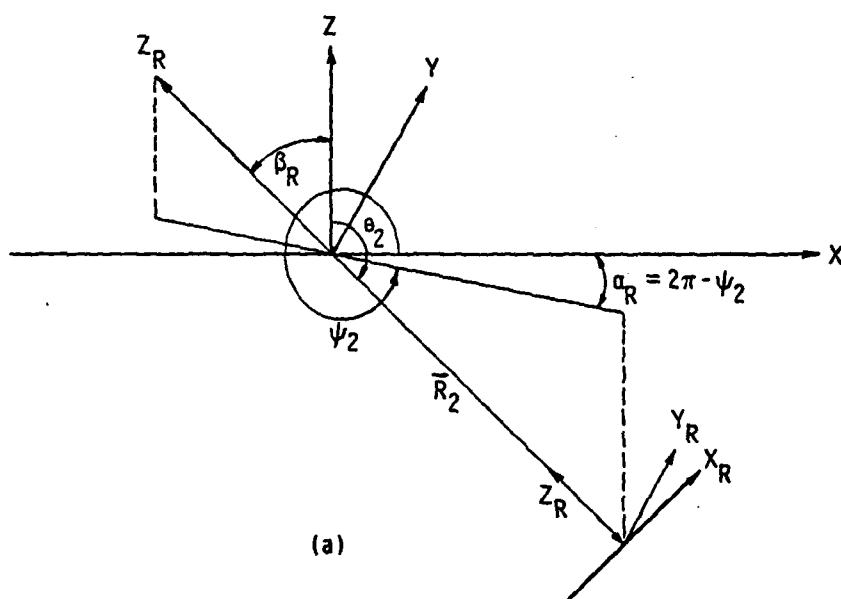
$$\begin{aligned}\hat{n}'_R(x,y) = & [u_R(x,y)\cos\alpha_R\cos\beta_R + v_R(x,y)\sin\alpha_R - \\ & w_R(x,y)\sin\beta_R\cos\alpha_R]\hat{x} + \\ & [v_R(x,y)\cos\alpha_R - u_R(x,y)\sin\alpha_R\cos\beta_R + \\ & w_R(x,y)\sin\alpha_R\sin\beta_R]\hat{y} + \\ & [u_R(x,y)\sin\beta_R + w_R(x,y)\cos\beta_R]\hat{z} \quad , \quad (D11)\end{aligned}$$

where

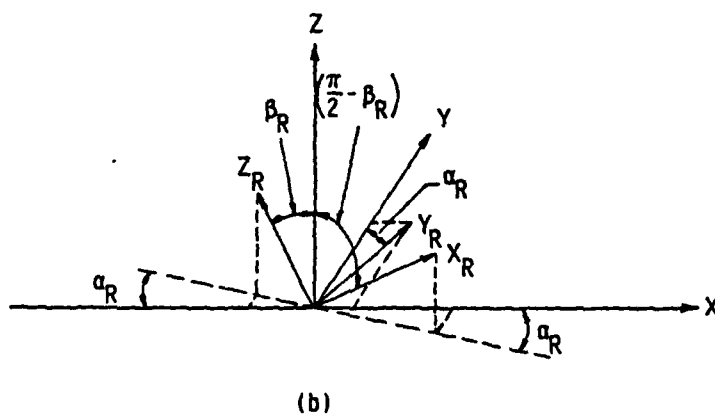
$$\begin{aligned}u_R(x,y) = & \frac{[(x-R_2u_2)-(y-R_2v_2)\tan\alpha_R]\cos\alpha_R\cos\beta_R - R_2w_2\sin\beta_R}{R_R(x,y)} \\ v_R(x,y) = & \frac{(x-R_2u_2)\sin\alpha_R + (y-R_2v_2)\cos\alpha_R}{R_R(x,y)} \quad (D12)\end{aligned}$$

and

$$\begin{aligned}w_R(x,y) = & \pm \sqrt{1 - u_R^2(x,y) - v_R^2(x,y)} \quad , \\ R_R(x,y) = & \sqrt{x^2 + y^2 - 2R_2(u_2x + v_2y) + R_2^2} \quad , \quad (D13)\end{aligned}$$



Actual physical separation between the  $X_R Y_R Z_R$  and  $XYZ$  coordinate system.



$X_R Y_R Z_R$  coordinate system superimposed upon the  $XYZ$  coordinate system.

Figure D2. Orientation of the  $X_R Y_R Z_R$  coordinate system with respect to the  $XYZ$  reference coordinate system.

and

$$\begin{aligned} u_2 &= \sin\theta_2 \cos\psi_2, \\ v_2 &= \sin\theta_2 \sin\psi_2 \end{aligned} \quad (D14)$$

and

$$w_2 = \cos\theta_2.$$

Although Figure D2 shows  $\vec{R}_2$  and the  $Z_R$  axis to be colinear, this may not be true in general. For example, if the receive beam pattern were to be tilted in the  $X_R Z_R$  plane,  $\vec{R}_2$  and the  $Z_R$  axis would no longer be colinear. However,  $\vec{R}_2$  is always chosen to be colinear with the axis of the main lobe of the receive beam pattern. Whether the receive beam pattern is tilted or untilted in the  $X_R Z_R$  plane, the rotation angle  $\beta_R$  is still defined as the angle between the  $Z$  and  $Z_R$  axes as shown in Figure D2.

With the use of Equation (D12), the receive directivity function  $D_R(k_{x_R}, k_{y_R})$  can also be projected onto the  $XY$  plane as was done for  $D_T(k_{x_T}, k_{y_T})$ . That is, we know that

$$k_{x_R} = ku_R = k\sin\theta_R \cos\psi_R$$

(D15)

and

$$k_{y_R} = kv_R = k\sin\theta_R \sin\psi_R,$$

where  $u_R$  and  $v_R$  are defined in Equation (D10). Replacing  $u_R = \sin\theta_R \cos\psi_R$  and  $v_R = \sin\theta_R \sin\psi_R$  with  $u_R(x,y)$  and  $v_R(x,y)$  as given in Equation (D12), respectively, yields the desired transformation:

$$D_R(k_{x_R}, k_{y_R}) \rightarrow D_R(k, x, y) \quad (D16)$$

We are now in a position to calculate the functional dependence of the  $(a_x, a_y, a_z)$  and  $(b_x, b_y, b_z)$  terms on the  $(x, y)$  coordinates. From Equations (5.2-75), (D3), (D9), and (D11), we obtain:

$$a_x(x, y) = u_T(x, y) \cos \beta_T + u_R(x, y) \cos \alpha_R \cos \beta_R + \\ v_R(x, y) \sin \alpha_R + w_T(x, y) \sin \beta_T - \\ w_R(x, y) \sin \beta_R \cos \alpha_R ,$$

$$a_y(x, y) = -u_R(x, y) \sin \alpha_R \cos \beta_R + v_T(x, y) + \\ v_R(x, y) \cos \alpha_R + w_R(x, y) \sin \alpha_R \sin \beta_R$$

and

(D17)

$$a_z(x, y) = -u_T(x, y) \sin \beta_T + u_R(x, y) \sin \beta_R + \\ w_T(x, y) \cos \beta_T + w_R(x, y) \cos \beta_R ,$$

and from Equations (5.2-76), (D3), (D9), and (D11), we obtain:

$$b_x(x, y) = u_T(x, y) \cos \beta_T + w_T(x, y) \sin \beta_T - \\ u_R(x, y) \cos \alpha_R \cos \beta_R - v_R(x, y) \sin \alpha_R + \\ w_R(x, y) \sin \beta_R \cos \alpha_R ,$$

$$b_y(x, y) = v_T(x, y) - v_R(x, y) \cos \alpha_R + u_R(x, y) \sin \alpha_R \cos \beta_R - \\ w_R(x, y) \sin \alpha_R \sin \beta_R$$

and

(D18)

$$b_z(x, y) = w_T(x, y) \cos \beta_T - u_T(x, y) \sin \beta_T - \\ u_R(x, y) \sin \beta_R - w_R(x, y) \cos \beta_R .$$

## APPENDIX E

### THE RELATIONSHIP BETWEEN $R_{\xi}(\Delta x, \Delta y, \Delta t')$ , $R_{\xi}(\Delta x, \Delta y, \Delta t)$ AND THE DIRECTIONAL WAVE NUMBER SPECTRUM OF THE OCEAN SURFACE

Let us examine the retarded time

$$\begin{aligned}
 t'_1 = t_1 - \frac{R_2}{c} \left\{ 1 - \left[ \frac{\sin \theta_2 \cos \psi_2}{R_2} x + \right. \right. \\
 \left. \left. \frac{\sin \theta_2 \sin \psi_2}{R_2} y + \frac{\cos \theta_2}{R_2} \xi(x, y, t'_1) \right] + \right. \\
 \left. \frac{(1 - \sin^2 \theta_2 \cos^2 \psi_2)}{2R_2^2} x^2 + \right. \\
 \left. \frac{(1 - \sin^2 \theta_2 \sin^2 \psi_2)}{2R_2^2} y^2 \right\}, \quad (E1)
 \end{aligned}$$

where Equation (E1) was obtained by substituting Equation (5.2-66) into Equation (5.2-19). Note that  $t'_1$ , as given by Equation (E1), is a random variable since  $\xi(x, y, t'_1)$  is random. Since

$$\left| \frac{\cos \theta_2}{R_2} \sigma_{\xi} \right| \ll 1 \quad (E2)$$

and assuming that

$$\left| \frac{x}{R_2} \right| < 1 \quad \text{and} \quad \left| \frac{y}{R_2} \right| < 1, \quad (E3)$$

Equation (E1) can be approximated by:

$$t'_1 = t_1 - \frac{R_2}{c} \left\{ 1 - \left[ \frac{\sin\theta_2 \cos\psi_2}{R_2} x + \frac{\sin\theta_2 \sin\psi_2}{R_2} y \right] \right\} \quad (E4)$$

which is now a deterministic quantity.

Referring back to Equation (5.3-18), it can be seen that  $t'_1$  is associated with the spatial coordinates  $(x + \Delta x)$  and  $(y + \Delta y)$  and that  $t'_2$  is associated with  $x$  and  $y$ . Therefore, using the form of Equation (E4),  $t'_1$  and  $t'_2$  can be written as:

$$t'_1 = t_1 - \frac{R_2}{c} \left\{ 1 - \left[ \frac{\sin\theta_2 \cos\psi_2}{R_2} (x + \Delta x) + \frac{\sin\theta_2 \sin\psi_2}{R_2} (y + \Delta y) \right] \right\} \quad (E5)$$

and

$$t'_2 = t_2 - \frac{R_2}{c} \left\{ 1 - \left[ \frac{\sin\theta_2 \cos\psi_2}{R_2} x + \frac{\sin\theta_2 \sin\psi_2}{R_2} y \right] \right\}. \quad (E6)$$

By subtracting Equation (E6) from Equation (E5), one obtains:

$$\Delta t' = \Delta t + \frac{1}{c} [\sin\theta_2 \cos\psi_2 \Delta x + \sin\theta_2 \sin\psi_2 \Delta y], \quad (E7)$$

where  $\Delta t = t_1 - t_2$ . Thus, from Equation (E7), it can be seen that  $\Delta t'$  is a function of  $\Delta x$ ,  $\Delta y$ , and  $\Delta t$ . Using the two-dimensional Fourier transform relationship<sup>48</sup>



$$R_{\xi}(\Delta x, \Delta y, \Delta t') = \left(\frac{1}{4}\right) \int_{-\infty}^{\infty} \int_{-\infty}^{\infty} W(p, q) \cdot \exp[-jp\Delta x - jq\Delta y + j\omega(p, q)\Delta t'] dp dq \quad (E8)$$

and substituting Equation (E7) into Equation (E8), one obtains:

$$R_{\xi}(\Delta x, \Delta y, \Delta t') \equiv R_{\xi}(\Delta x, \Delta y, \Delta t) \quad , \quad (E9)$$

where

$$R_{\xi}(\Delta x, \Delta y, \Delta t) = \left(\frac{1}{4}\right) \int_{-\infty}^{\infty} \int_{-\infty}^{\infty} W(p, q) \exp[+j\omega(p, q)\Delta t] \cdot \exp \left\{ -j \left[ p - \omega(p, q) \frac{\sin\theta_2 \cos\psi_2}{c} \right] \Delta x \right\} \cdot \exp \left\{ -j \left[ q - \omega(p, q) \frac{\sin\theta_2 \sin\psi_2}{c} \right] \Delta y \right\} \cdot dp dq \quad (E10)$$

The expression  $W(p, q)$  is the directional wave number spectrum of the ocean surface, where  $W(p, q)dpdq$  is the amount of the component of the rough surface having the spatial wave number between  $p$  and  $p + dp$  in the  $x$  direction and between  $q$  and  $q + dq$  in the  $y$  direction. The corresponding angular frequency (in rad/sec) is given by:

$$\omega(p, q) = \pm \left[ g(p^2 + q^2)^{1/2} \right]^{1/2} \quad , \quad (E11)$$

where  $g$  is the acceleration due to gravity.<sup>48</sup> The spectral density  $W(p,q)$  is a real positive function of  $p$  and  $q$  and since  $\xi(x,y,t)$  is real,  $W(p,q)$  is an even function of  $p$  and  $q$ , i.e.,  $W(-p,-q) = W(p,q)$ . Equation (E11) is applicable to deep-water ocean surface waves and it is an odd function of  $p$  and  $q$ , i.e.,  $\omega(-p,-q) = -\omega(p,q)$ . The choice of sign in Equation (E11) depends upon the motion of the surface.<sup>48</sup> For example, consider the backscatter case where both the transmit and receive array are located at  $\psi_1 = \psi_2 = \pi$ ,  $\theta_1 = \theta_2$ , and  $R_1 = R_2$  (see Figure 20). If the surface wave motion is in the positive  $x$  direction, choose the negative sign in Equation (E11) since

$$\exp[+j\omega(p,q)\Delta t] = \exp \left\{ -j[g(p^2 + q^2)^{1/2}]^{1/2}\Delta t \right\} \quad (E12)$$

will then correspond to a downward shift in frequency from the carrier, i.e., a negative Doppler shift. This makes physical sense because the surface waves are moving away from the receive array. Similarly, if the surface wave motion is in the negative  $x$  direction, choose the positive sign in Equation (E11) since

$$\exp[+j\omega(p,q)\Delta t] = \exp \left\{ +j[g(p^2 + q^2)^{1/2}]^{1/2}\Delta t \right\} \quad (E13)$$

will then correspond to an upward shift in frequency from the carrier, i.e., a positive Doppler shift. This also makes physical sense because the surface waves are moving toward the receive array.

## VITA

Lawrence J. Ziomek was born in Chicago, Illinois, on August 8, 1949. He attended Gordon Technical High School in Chicago where he graduated in June 1967. He received a B.E. degree in electrical engineering from Villanova University, Villanova, Pennsylvania, in May 1971, and a M.S.E.E. degree from the University of Rhode Island, Kingston, Rhode Island, in January 1974. He then went to work for TRW Systems Group, Redondo Beach, California, as a member of the technical staff from October 1973 until May 1976. While at TRW, he worked in the area of radar signal processing. He also attended night school at U.C.L.A. and Loyola Marymount University, Los Angeles, California, taking additional graduate level courses in electrical engineering. Since September 1976, he has been a full time research assistant at the Applied Research Laboratory of The Pennsylvania State University and a part-time Ph.D. graduate student in Acoustics. Lawrence J. Ziomek is a member of Eta Kappa Nu, Tau Beta Pi, Sigma Xi, and Phi Kappa Phi.

DISTRIBUTION LIST FOR TM

Commander (NSEA 0342)  
Naval Sea Systems Command  
Department of the Navy  
Washington, DC 20362

Copies 1 and 2

Commander (NSEA 9961)  
Naval Sea Systems Command  
Department of the Navy  
Washington, DC 20362

Copies 3 and 4

Defense Technical Information Center  
5010 Duke Street  
Cameron Station  
Alexandria, VA 22314

Copies 5 through 10

**DAT  
FILM**